Imperial College London
Department of Electrical and Electronic Engineering

Resilience-driven planning and operation of networked microgrids featuring decentralisation and flexibility

Yi Wang

Supervisor: Prof. Goran Strbac

This dissertation is submitted for the degree of
Doctor of Philosophy in Imperial College London, September 2022

Declaration of Originality

As required by the college, I hereby declare that this thesis and the work described in it are my own work. Any ideas or quotations from the work of other people, published or otherwise, are fully acknowledged through standard referencing practices of the discipline. No portion of the work referred to in this thesis has been submitted in support of an application for another degree or qualification of this or any other university or other institute of learning.

Yi Wang

September 2022

Copyright Declaration

Yi Wang

September 2022

Acknowledgements

Firstly, I would like to thank my supervisor, Professor Goran Strbac, for his continuous support, patience, and guidance over the last few years. It is his rigorous attitude and extensive professional knowledge that encouraged me to positively face all the challenges and insist on pursuing novel research. I deeply appreciate his help and the last few years have definitely been an enjoyable experience in all aspects.

I would like to express my gratitude to my examiners, Professor Richard Vinter and Dr. Panagiotis Papadopoulos, for the highly interesting and in-depth discussion during the viva examination and for their valuable comments on my thesis.

I would also like to thank my colleagues, Dr. Anastasios Oulis Rousis and Dr. Dawei Qiu, for giving me valuable suggestions about my research, which help me gain a deeper understanding of my research topic and grasp the key points of this work. We have built a close collaboration in the last few years through numerous discussions and meetings. Their recognition of my work is important to me.

I would like to thank Dr. Jochen Cremer, Dr. Yonghua Yin and Yuancheng Guo. When I was experiencing setbacks, they used their patience and knowledge to guide and encourage me to regain confidence and keep working.

Finally, I thank my parents Jianmei Li and Kefu Wang from the bottom of my heart for their continued support and encouragement that give me great confidence to pursue my dreams. I am deeply grateful to my wife Run Yang for her patience, encouragement, and unconditional love. This Ph.D. study would not have been possible without them.

Abstract

High-impact and low-probability extreme events including both man-made events and natural weather events can cause severe damage to power systems. These events are typically rare but featured in long duration and large scale. Many research efforts have been conducted on the resilience enhancement of modern power systems. In recent years, microgrids (MGs) with distributed energy resources (DERs) including both conventional generation resources and renewable energy sources provide a viable solution for the resilience enhancement of such multi-energy systems during extreme events. More specifically, several islanded MGs after extreme events can be connected with each other as a cluster, which has the advantage of significantly reducing load shedding through energy sharing among them. On the other hand, mobile power sources (MPSs) such as mobile energy storage systems (MESSs), electric vehicles (EVs), and mobile emergency generators (MEGs) have been gradually deployed in current energy systems for resilience enhancement due to their significant advantages on mobility and flexibility.

Given such a context, a literature review on resilience-driven planning and operation problems featuring MGs is presented in detail, while research limitations are summarised briefly. Then, this thesis investigates how to develop appropriate planning and operation models for the resilience enhancement of networked MGs via different types of DERs (e.g., MGs, ESSs, EVs, MESSs, etc.). This research is conducted in the following application scenarios:

- This thesis proposes novel operation strategies for hybrid AC/DC MGs and networked MGs towards resilience enhancement. Three modelling approaches including centralised control, hierarchical control, and distributed control have been applied to formulate the proposed operation problems. A detailed non-linear AC OPF algorithm is employed to model each MG capturing all the network and technical constraints relating to stability properties (e.g., voltage limits, active and reactive power flow limits, and power losses), while uncertainties associated with renewable energy sources and load profiles are incorporated into the proposed models via stochastic programming. Impacts of limited generation resources, load distinction intro critical and non-critical, and severe contingencies (e.g., multiple line outages) are appropriately captured to mimic a realistic scenario.

- This thesis introduces MPSs (e.g., EVs and MESSs) into the suggested networked MGs against the severe contingencies caused by extreme events. Specifically, time-coupled routing and scheduling characteristics of MPSs inside each MG are modelled to reduce load shedding when large damage is caused to each MG during extreme events. Both transportation networks and

power networks are considered in the proposed models, while transporting time of MPSs between different transportation nodes is also appropriately captured.

- This thesis focuses on developing realistic planning models for the optimal sizing problem of networked MGs capturing a trade-off between resilience and cost, while both internal uncertainties and external contingencies are considered in the suggested three-level planning model. Additionally, a resilience-driven planning model is developed to solve the coupled optimal sizing and pre-positioning problem of MESSs in the context of decentralised networked MGs. Internal uncertainties are captured in the model via stochastic programming, while external contingencies are included through the three-level structure.

- This thesis investigates the application of artificial intelligence techniques to power system operations. Specifically, a model-free multi-agent reinforcement learning (MARL) approach is proposed for the coordinated routing and scheduling problem of multiple MESSs towards resilience enhancement. The parameterized double deep Q-network method (P-DDQN) is employed to capture a hybrid policy including both discrete and continuous actions. A coupled power-transportation network featuring a linearised AC OPF algorithm is realised as the environment, while uncertainties associated with renewable energy sources, load profiles, line outages, and traffic volumes are incorporated into the proposed data-driven approach through the learning procedure.

Contents

List of Tables

List of Figures

Nomenclature

A. Abbreviations

MG Microgrid

DG Diesel generator

DER Distributed energy resource

MPS Mobile power sources

OPF Optimal power flow

EMS Energy management system

RES Renewable energy resource

PV Photovoltaic

WT Wind turbine

BESS Battery energy storage system

MESS Mobile energy storage system

EV Electric vehicle

P. Parameters

Δt Time interval

η^c Efficiency of storage device(s) during charging

η^d Efficiency of storage device(s) during discharging

B_{bp} Susceptance of branch connecting AC buses b, p

G_{bp} Conductance of branch connecting AC buses b, p

c^{ls} Cost associated with load shedding

c^{sho} Penalty coefficient associated with power shortage

c^{sur} Reward coefficient associated with power surplus

c^{e} Power exchange cost between MGs

ES_b^{max} Maximum state of charge

ES_b^{min} Maximum depth of discharge

EV_k^{max} Maximum state of charge in EV fleet k

EV_k^{min} Maximum depth of discharge in EV fleet k

EV_k^{tar} Minimum energy storage level of EV fleet k

GS_g^{Ini} Initial state of generation resources during extreme events

GS_g^{min} Minimum energy reserve during extreme events

P_g^{max} Maximum power of a generator g (active)

P_g^{min} Minimum stable generation of a generator g (active)

P_k^{max} Maximum storage power of EV fleet k

Q_g^{max} Maximum power of a generator g (reactive)

Q_g^{min} Minimum stable generation of a generator g (reactive)

S^{max} Maximum storage power

T Time scheduling horizon

T_{ev} EV shceduling horizon

T_{mes} MESS shceduling horizon

T_{ij}^{max} Tie-line capacity between MG i and MG j

V^{max} Maximum permissible voltage

V^{min} Minimum permissible voltage

T_{bp}^{trl} The travelling time of mobile unit k from bus b to bus p

S_i^{lim} Capacity limit of branch i

δ_{bp}^{lim} Maximum permissible voltage angle variation between bus b and bus p

S. Sets

G_{bus} Total number of generator buses, $G_{bus} \subset N_{bus}$

L_{bus} Total number of load buses, $L_{bus} \subset N_{bus}$

N_{br} Total number of branches

N_{bus} Total number of buses

N_g Total number of generators in a MG

S_{bus} Total number of buses with storage device(s), $S_{bus} \subset N_{bus}$

N_{ev} Total number of EV fleets

N_{mes} Total number of MESSs

M Total number of connected microgrids

V. Variables

$\delta_{b,t,s}$ Voltage angle of bus b at time t under scenario s

$\delta_{p,t,s}$ Voltage angle of bus p at time t under scenario s

$\delta_{bp,t,s}$ Voltage angle difference between buses b, p at time t under scenario s

$ES_{b,t,s}$ Energy content in storage in bus b at the end of current time step t under scenario s

$GS_{g,t,s}$ Energy reserve of generator g in a MG at the end of current time step t under scenario s

$P_{g,t,s}$ Active power generation of generator g at time t under scenario s

$P_{b,t,s}^{ex}$ Active power exchange between considered bus b and other buses at time t under scenario s

$P_{b,t,s}^{ls}$ Involuntary loss of active AC load at bus b at time t under scenario s

$P^{l}_{b,t,s}$ Active AC load at bus b at time t under scenario s

$Q_{g,t,s}$ Reactive power generation of generator g at time t under scenario s

$Q^{es}_{b,t,s}$ Reactive power exchange between bus b and other buses at time t under scenario s

$Q^{ls}_{b,t,s}$ Involuntary loss of reactive AC load at bus b at time t under scenario s

$Q^{l}_{b,t,s}$ Reactive AC load at bus b at time t under scenario s

$S_{i,t,s}$ Apparent power of branch i at time t under scenario s

$P^{c}_{b,t,s}$ Storage charging into bus b at time t under scenario s

$P^{d}_{b,t,s}$ Storage discharging from bus b at time t under scenario s

$V_{b,t,s}$ Voltage at bus b at time t under scenario s

$V_{p,t,s}$ Voltage at bus p at time t under scenario s

$u_{b,k,t,s}$ Integer variable that shows the status of EV fleet k in bus b at time t under scenario s

$P^{ev,c}_{b,k,t,s}$ Charging of EV fleet k into bus b at time t under scenario s

$P^{ev,d}_{b,k,t,s}$ Discharging of EV fleet k into bus b at time t under scenario s

$P^{mes,c}_{b,k,t,s}$ Charging of MESS k into bus b at time t under scenario s

$P^{mes,d}_{b,k,t,s}$ Discharging of MESS k into bus b at time t under scenario s

$EV_{k,t,s}$ Energy content of EV fleet k at time t under scenario s

$P^{buy}_{ij,t}$ Active power bought from MG j to MG i at time t

$P^{sell}_{ij,t}$ Active power sold from MG i to MG j at time t

$P^{fsho}_{i,t}$ The final power shortage of MG i at time t

$P^{fsur}_{i,t}$ The final power surplus of MG i at time t

Chapter 1

Introduction

1.1 Context

Extreme natural disasters, such as flooding, earthquakes, and hurricanes, can affect the status of components in power systems (e.g., power plants, substations, and cables) and cause severe power outages. According to [6], seven of ten major storms during the last four decades have occurred in the last 10 years and each event caused the huge economic loss (over 1 billion dollars). Such events are typically rare and therefore not anticipated, while their impact on power systems is immense. In order to deal with these so-called high-impact low-probability (HILP) events, the concept of "resilience" is introduced in power systems. Resilience etymologically comes from the Latin word "resilio" and refers to "the ability of a system to anticipate and withstand external shocks, bounce back to its pre-shock state as quickly as possible and adapt to be better prepared to future catastrophic events" [7]. In [8], the difference between reliability and resilience is discussed and resilience is regarded as a compromise and necessary component of reliability. In [4], resilience is defined as a dynamic and ongoing procedure for improving robustness and operational flexibility to deal with uncertainties, compared with reliability normally considered as a static concept. More differences between typical outages and natural-disaster induced outages can be found in [1]. Considering the large disruptions caused by extreme events, the main task for a resilient power system is to maintain the continuity of power services to critical loads (e.g., hospitals, police stations, and data centres).

Decentralisation and digitalisation are rapidly transforming the energy sector, as illustrated in Figure 1.1. Increasingly popular, distributed energy resources (DERs), including diesel generators (DGs), photovoltaic (PV) plants, wind turbines (WTs), and energy storage systems (ESSs), are disrupting the traditional top-down philosophy of power systems [9]. Particularly, energy systems are experiencing an unprecedented shift from a centralised to a decentralised operation paradigm featuring networked MGs and other local energy networks, which can introduce benefits concerning cost reduction, resilience enhancement, and security performance. Additionally, mobile power sources (MPSs) have been gradually deployed in current energy systems for resilience enhancement due to their significant advantages in mobility and flexibility. The importance of networked MGs and the locality in general within the undergoing energy transition is schematically represented in Figure 1.1.

Microgrids (MGs) are regarded as localised small power systems, which have two operational modes: grid-connected mode and islanded mode [10]. Controllability is the biggest difference between an MG and a distribution system, and voltage control and frequency/load-generation balance are two basic problems in the operation of an MG under grid-connected mode and islanding mode respectively [11]. According to [12], MGs can provide higher load reliability compared to bulk power systems. In [13], the feasibility of MGs as a local resource, a community resource, and a black start resource is analysed. DERs in MGs, such as DGs, WTs, and PVs, can restore local loads via islanding schemes or restore global critical loads via dynamic boundaries and formation, if the utility power supply is entirely or partially interrupted during extreme events. As such, this thesis particularly deals with the problem of optimal planning and operation for networked MGs in resilience enhancement scenarios (i.e., in the presence of extreme events) focusing on appropriate operation strategies for DERs, including both static and mobile, towards increasing security of supply.

1.2 Motivation and Objectives

In recent years, much research has been conducted on utilising MGs to enhance the resilience of power systems, especially for distribution systems, e.g., using MGs as virtual feeders, dynamical MG formations, islanding schemes of MGs, and networked MGs. In general, some papers regard MGs as one type of DERs and use them to enhance the resilience of upper-level systems, while others focus on enhancing the resilience of MGs through appropriate planning or operational strategies. Detailed information about these different categories can be found in the next chapter. To summarise, all of these exhibit some fundamental limitations as follows:

Most research chooses simplified modelling approaches for resilience-driven planning and operational problems of MGs (e.g., energy management systems (EMSs), DC OPF, or linearised Distflow),

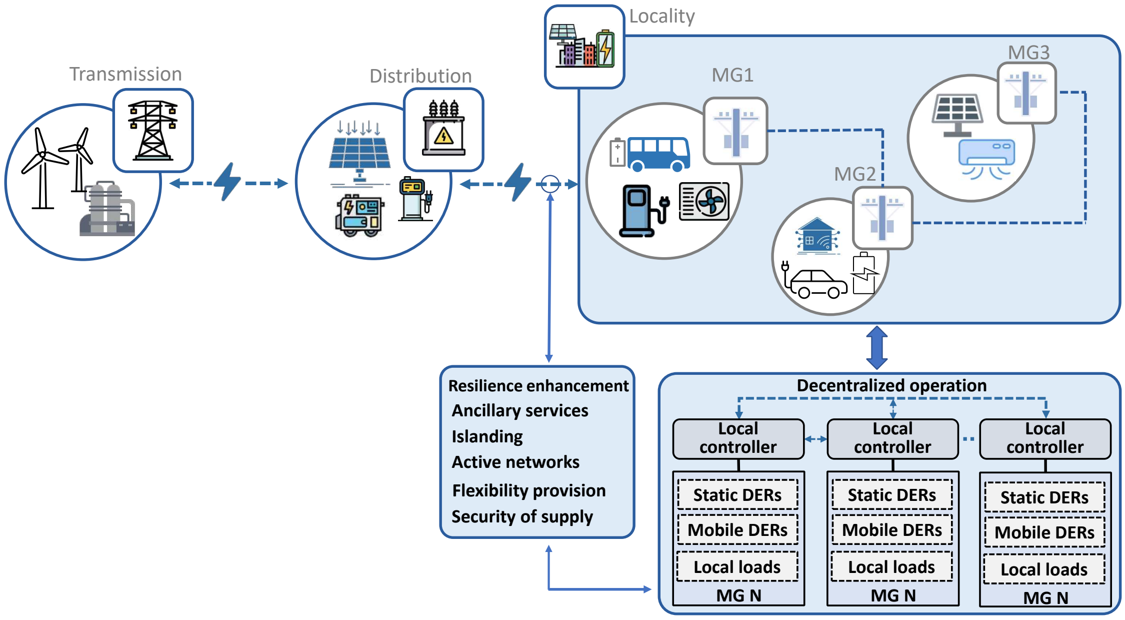

Figure 1.1: Importance of networked MGs in the undergoing energy transition.

which cannot effectively capture all the network and technical constraints related to stability properties, e.g., voltage limits, power losses, line capacity limits, etc. Note that MGs may reach their operation limits more frequently and the risk of system failure is increased, when severe contingencies are caused by extreme events. These highlight the importance of capturing all the operational constraints and considering power dynamics in a resilience scenario.

Internal uncertainties and external contingencies occur due to the high-impact nature of extreme events. However, most resilience-driven operational models fail to comprehensively consider the influence of these uncertain parameters on final optimal results. As mentioned before, power systems are undergoing a significant transition from fossil fuel resources to the decarbonlisation of renewable energy resources (RESs), promising to address the environmental concerns [11]. The prediction of renewable energy sources under extreme weather events can have large fluctuations, which shall be appropriately considered in resilience-driven system operations.

There has been a large amount of research focusing on developing planning models for MGs or networked MGs, e.g., optimal sizing, optimal positioning, and topology design. On the other hand, research on resilience-driven planning problems is very limited, since the low-probability nature of extreme events and the high modelling complexity of uncertainties and contingencies. However, the high-impact nature of extreme events and the relatively higher frequency of occurrence are gradually making it a necessity to capture resilience at the planning level.

Networked MGs can provide more benefits in reducing operational costs and restoring loads than a single MG through the power sharing between MGs. Three approaches have been proposed to model the operation of networked MGs: centralised control, hierarchical control, and distributed control. However, centralised control approaches normally suffer from the large computational burden, especially with the increase of the number of MGs in the cluster, while privacy issues might be caused due to the large scale of information sharing in local MGs. Additionally, both centralised control and hierarchical control require a central controller to manage the operation of the MG cluster, which might be unavailable during extreme events. Compared to centralised control, control approaches featuring decentralisation are appropriate in the context of resilience enhancement.

As discussed above, a large number of DERs have been deployed in modern power networks, including DGs, PVs, WTs, and ESSs. Most existing research on resilience-driven planning and operation is based on these static DERs, which might not be enough to deal with the severe contingencies caused by extreme events. As such, it is necessary to develop effective combinatorial strategies considering both static DERs and mobile DERs for resilience enhancement, due to the high flexibility and mobility provided by MPSs. Additionally, large computational burden might be caused due to the involvement of MPSs (e.g., a large number of integer variables), which motivates researchers to develop more efficient operational strategies for MPS scheduling problems.

To summarise, this thesis will deeply analyse the benefits of MGs, appropriate modelling approaches, demand-side response led by MPSs, and decentralised approaches on the resilience enhancement of distribution systems. In more detail, the work will try to give answers to the questions below:

- How to select and develop appropriate modelling approaches capturing detailed network and operational constraints for MG planning and operation problems towards resilience enhancement?
- How to comprehensively consider the influence of internal uncertainties associated with renewable energy sources and load profiles as well as external contingencies including multiple line outages on optimal solutions?
- How to develop a comprehensive planning model for the optimal sizing problem of DGs and ESSs in the context of networked MGs, which can capture the trade-off between resilience and cost?

- How to model the connection among MGs and develop appropriate strategies featuring decentralisation to manage the power sharing among MGs towards load restoration after extreme events?
- What would be the value of MPSs such as MESSs and flexible technologies such as demand shifting, etc. in enhancing the resilience of power networks?
- How to apply model-free approaches such as reinforcement learning in coordinated operational problems of multiple MESSs towards resilience enhancement?

1.3 Contributions

It can be envisioned that building-scale and local-aggregator MGs will become common in the coming decades. Apart from distribution systems, MGs can potentially be applied to transmission systems for resilience purposes and even to account for the connections between transmission systems and distribution systems for resource sharing (e.g., MGs, DGs, MPSs, and battery units) to reduce system costs and increase stability. As such, this work intends to analyse the impacts of regional MGs on resilience enhancement.

The main contribution of this work is to model and analyse in depth the coordination of MGs, MPSs (e.g., MESSs), and demand-side techniques towards resilience enhancement. Effective control strategies for networked MGs (e.g., hierarchical control and distributed control) will be developed to make decisions about power sharing among MGs during extreme events. Additionally, comprehensive planning models for the optimal sizing problems of networked MGs, DGs, and battery units are developed to balance investment costs and resilience. In more detail, the contributions of this research are listed hereafter:

- Existing literature on resilience-driven planning and operational strategies associated with MGs is comprehensively reviewed across four distinct dimensions, i) modelling objectives and metrics, ii) resilience scenarios, iii) modelling approaches, and iv) strategies and topologies. Research limitations and future directions are briefly summarised.
- A resilience-driven operational strategy considering both the preventive stage and corrective stage is developed for the resilience enhancement of a hybrid AC/DC MG. Preventive power importing is used in the preventive stage for better preparedness before events occur, while demand shifting is employed in the corrective stage to reduce load shedding.

- A stochastic hierarchical control approach capturing EV routing and scheduling is developed for the load restoration problem of networked MGs after an extreme event. Internal uncertainties associated with renewable energy sources and load profiles as well as external contingencies including multiple line outages are appropriately captured via stochastic programming.

- A stochastic distributed control approach is proposed for the resilience-driven operation of networked MGs incorporated with the routing and charging/discharging characteristics of MESSs, while a roll optimisation method is utilised to capture the flexibility of storage units and power exchange. Uncertainties related to renewable energy sources and loads are considered via stochastic programming.

- A three-level defender-attacker-defender model is suggested to solve the optimal sizing problem of networked MGs considering a trade-off between resilience and cost. A non-linear AC OPF algorithm is employed for the modelling of each MG capturing all the technical constraints related to stability properties (e.g., voltage limits, active and reactive power flow limits, and power losses), while an adaptive genetic algorithm (GA) is proposed to handle the influence of internal uncertainties and external contingencies.

- A resilience-driven planning model is proposed to solve the optimal sizing and pre-positioning problem of MESSs in the context of decentralised networked MGs. Internal uncertainties associated with renewable energy sources and load profiles are modelled via a stochastic programming approach, while external contingencies including multiple line outages are captured through the defender-attacker-defender structure.

- A resilience-driven multi-agent reinforcement learning (MARL) approach featuring parameterized double deep Q-networks is developed for the coordinated routing and scheduling problem of MESSs, which is reformulated as a Partially Observable Markov Game (POMG). Various uncertainties including renewable energy sources, load profiles, line outages, and traffic volumes are captured in the MARL training procedure, while a coupled power-transportation network is realised as the environment.

1.4 Thesis outline

The remainder of this thesis is organised as follows:

Chapter 2 comprehensively reviews existing research on resilience-driven planning and operation strategies associated with MGs, i.e., using MGs as resilience resources and enhancing the resilience of MGs. Following this pattern, four different types of operational strategies for MGs are illustrated: a) using MGs as virtual feeders, b) dynamic MG formation, c) islanding schemes of MGs, and d) networked MGs. From the view of resilience modelling, commonly-used objective functions, metrics, and modelling approaches are summarised to present a detailed operational scheme of MGs in the context of resilience. More specifically, different types of MGs, control approaches for MG clusters, and modelling approaches are listed and compared to show their advantages and disadvantages and how they can be appropriately used for resilience-driven modelling.

Chapter 3 aims to provide a detailed operational model for a hybrid AC/DC MG towards resilience enhancement in the presence of extreme weather events. Specifically, both the preventive stage and corrective stage are considered, where preventive power importing is proposed to inject as much energy as possible into battery units for better preparedness, and demand shifting is used in the corrective stage to reduce emergency load shedding. A detailed AC OPF algorithm capturing all the technical constraints relating to voltage, angle, and power losses is employed to model MG operations, where load distinction into essential and non-essential, limited generation resources, and severe contingencies are incorporated into the model for realistic decision making.

Chapter 4 focuses on a novel three-stage hierarchical control strategy for the resilience enhancement of networked MGs. In the first and third stages, several local MGs can run their own AC OPF algorithm in parallel; thus, the computing time can be significantly reduced compared to approaches related to centralised control. To capture the high-impact and low-probability nature of extreme events, both internal uncertainties and external contingencies are captured in the proposed model via a stochastic programming approach. Additionally, the routing and scheduling characteristics of EV fleets are involved in this work for load restoration due to their mobility and flexibility. Extensive case studies have shown that mobile EVs can obtain a much higher resilience level than static EVs.

Chapter 5 proposes a distributed control approach featuring rolling optimisation towards the load restoration problem of networked MGs after extreme events. Compared to the approach suggested in Chapter 4, this method can both ensure fast response and realistic decision making due to the utilisation of a linearised AC OPF algorithm, while it can capture the flexibility of both storage systems and power exchange, and handle potential cascaded damage caused by extreme events due to the utilisation of rolling optimisation. Additionally, the scheduling and routing characteristics of MESSs are introduced into the resilience-driven formulation of MG clusters for load restoration. Uncertainties associated with renewable energy sources and load profiles are captured via stochastic programming.

Chapter 6 suggests a three-level defender-attacker-defender (DAD) model for the optimal sizing problem of networked MGs capturing a trade-off between cost and resilience. Both the capacities of distributed generators and ESSs are considered in the proposed planning model, while both internal uncertainties associated with load profiles and external contingencies including both line faults and generator outages are captured through the robust-based three-level structure. A detailed AC OPF algorithm is utilised at the operation level to ensure secure system operations and accurate optimisation results. Simulations considering meshed networks and load distinction into critical and non-critical are developed to demonstrate algorithm effectiveness in capturing resilience at the planning stage and optimally sizing multiple parameters. The results indicate that higher resilience levels lead to higher investment costs, while sizing networked MGs leads to decreased investment in comparison with stand-alone MGs sizing.

Chapter 7 focuses on utilising the three-level defender-attacker-defender formulation to solve resilience-driven optimal sizing and pre-positioning problems of MESSs in networked MGs with distributed control. The upper-level problem is formulated as the master problem to obtain optimisation results against a certain contingency, while the middle-level problem and the lower-level problem are merged as a subproblem to select a contingency that can cause the most severe damage. An adaptive GA is employed to search for sizing and positioning decisions and capture various potential attack actions, while a distributed control approach based on the consensus algorithm and linearised AC optimal power flow is utilised to model MG operations and capture technical constraints relating to voltage and power loss. Uncertainties relating to renewable energy sources and load profiles are incorporated into the model via stochastic programming. Extensive case studies considering meshed networks and load discrimination into essential/non-essential are developed to demonstrate the effectiveness of the proposed model on accurate decision making of MESS capacities and initial locations.

Chapter 8 develops a novel MARL approach for the real-time automatic routing and scheduling problem of multiple coordinated MESSs towards resilience enhancement after extreme events. A parameterized multi-agent double deep Q-network capable of handling a hybrid continuous-discrete action space is proposed to output MESSs routing and scheduling decisions, while uncertainties associated with renewable energy sources, load profiles, line outages, and traffic volumes are captured through the training process of the proposed MARL method. The MESSs routing and scheduling problem is reformulated as a POMG, including detailed settings of state, observation, action, reward, and state transition. Both transportation and power networks are examined in the test system, while a linearised AC-OPF algorithm is employed to capture all the technical constraints related to stability properties, which is realised as the environment of the suggested MARL method. Extensive case studies in the context of both 6- and 33-bus power networks have been developed to testify the effectiveness and robustness of the proposed method in addressing such coordinated MESSs routing and scheduling problems.

Chapter 9 concludes this thesis by summarising the main contributions of this research and discussing potential directions for future work.

1.5 Statement of Originality

This is to certify that to the best of my knowledge, the content of this thesis is my own work. This thesis has not been submitted for any degree or other purposes.

1.6 Publications

Some ideas and figures will appear in the following publications:

1. **Y. Wang** and A. Oulis Rousis and G. Strbac. *On microgrids and resilience: A comprehensive review on modeling and operational strategies.* Renewable & Sustainable Energy Reviews, 134:110313, Dec. 2020.

2. **Y. Wang** and A. Oulis Rousis and G. Strbac. *Resilience-Driven Modeling, Operation and Assessment for a Hybrid AC/DC Microgrid.* IEEE Access, 8:139756-139770, Aug. 2020.

3. **Y. Wang** and A. Oulis Rousis and G. Strbac. *A resilience enhancement strategy for networked MGs incorporating electricity and transport and utilizing a stochastic hierarchical control approach.* Sustainable Energy, Grids and Networks, 26:100464, Jun. 2021.

4. **Y. Wang** and A. Oulis Rousis and G. Strbac. *A three-level planning model for optimal sizing of networked microgrids considering a trade-off between resilience and cost.* IEEE Transactions on Power Systems, 36(6):5657-5669, Nov. 2021.

5. **Y. Wang** and A. Oulis Rousis and G. Strbac. *Resilience-driven optimal sizing and pre-positioning of mobile energy storage systems in decentralized networked microgrids.* Applied Energy, 305:117921, Jan. 2022.

6. **Y. Wang** and A. Oulis Rousis and G. Strbac. *A stochastic decentralized control approach for resilience enhancement of networked microgrids based on rolling optimization.* IEEE Transactions on Smart Grid. (Under Review)

7. **Y. Wang** and D. Qiu and G. Strbac. *Multi-agent deep reinforcement learning for resilience-driven routing and scheduling of mobile energy storage systems.* Applied Energy, 310:118575, March. 2022.

8. **Y. Wang**, D. Qiu, F. Teng and G. Strbac. *Towards Microgrid Resilience Enhancement via Hierarchical Multi-Agent Reinforcement Learning.* IEEE Transactions on Power Systems. (Under Review)

9. **Y. Wang**, D. Qiu, G. Strbac and Z. Gao. *Coordinated Electric Vehicle Active and Reactive Power Control for Active Distribution Networks.* IEEE Transactions on Industrial Informatics. (accepted)

10. **Y. Wang**, D. Qiu, G. Strbac and Z. Gao. *Decarbonize transportation and power systems by integration of electric vehicles: a joint route selection and power scheduling strategy.* IEEE Transactions on Industrial Informatics. (Under Review)

11. **Y. Wang**. *G-networks and the optimization of supply chains.* Probability in the Engineering and Informational Sciences, 35(1):62-74, Jan. 2021.

Other publications:

1. D. Qiu, **Y. Wang**, T. Zhang, M. Sun and G. Strbac. *Hybrid Multi-Agent Reinforcement Learning for Electric Vehicle Resilience Control Towards a Low-Carbon Transition.* IEEE Transactions on Industrial Informatics. (accepted)

2. D. Qiu, **Y. Wang**, M. Sun and G. Strbac. *Multi-service provision for electric vehicles in power-transportation networks: a hierarchical and hybrid multi-agent reinforcement learning approach.* Applied Energy, 313:118790, May 2022.

3. D. Qiu, **Y. Wang**, T. Zhang, M. Sun and G. Strbac. *Hierarchical multi-agent reinforcement learning for repair crews dispatch control towards multi-energy microgrid resilience.* Applied Energy. (Under Review)

4. E.Gelenbe and **Y. Wang**, *Supply chains for perishable goods and g-networks.* IEEE Conference on Industrial Electronics and Applications, Xi'an, China, 2019.

Chapter 2

Background Theory

2.1 Resilience and reliability

Both resilience and reliability are very important concepts in the context of power grids. Reliability is defined as the ability of power grids to deliver electricity in the quantity and with the quality demanded by users, which focuses on ensuring the lights on and is regarded as the end goal of a power system [8]. On the other hand, a resilient power grid shall be designed to be capable of withstanding external shocks and bounce back quickly when extreme events occur. More specifically, strong adaptation is extremely critical when power grids aim to enhance resilience against various extreme events including both natural disasters and man-made events, given their HILP nature. As such, compared to reliability, resilience refers not only to withstand an event, but also to focus on how to adapt and respond to this event, especially for HILP events.

From the perspective of contingencies, the concept of reliability with various interruption indices is mainly applied to deal with typical outages, while resilience-driven approaches focus on severe line outages caused by extreme events [1]. Detailed information about typical outages and severe outages can be found in Table. 2.1. In this context, conventional planning and operational strategies developed for power systems towards typical outages might not be enough for the power system recovery from severe damages caused by extreme events. To deal with these challenges, advanced technologies based on various types of DERs featuring decentralisation, flexibility and mobility may be capable of providing reasonable solutions for the resilience enhancement of modern power grids. In recent years, much research has focused on proposing resilience-driven planning and operational models, e.g., using MGs for power system restoration after extreme events, which is described in

Table 2.1: Differences between typical outages and severe outages caused by extreme events [1].

No.	Typical outages	Outages caused by extreme events
1	One component failure	Multiple faults (e.g., line outages)
2	No stochastic characteristic	High degree of uncertainty
3	No spatiotemporal correlation for the failure	Spatiotemporal correlation for the faults
4	Most DERs stay connected	Some DERs may be out of service
5	Power networks remain intact	Power networks may be damaged
6	Mainly involve power networks	Influence other infrastructures
7	Quick restoration	Difficult restoration

the following sections from the modelling perspective in more detail.

2.2 Resilience modelling objectives and metrics

Basic modelling objectives used in existing literature can be found in Table 2.2. There are many papers using only load survivability or load restoration as modelling objectives, which assumes that loads have a much higher priority than operational cost in emergency situations [14, 15], while operational costs are also considered in [3, 16–21] as part of the modelling objectives because of large pre-allocation cost or generation cost. To reduce frequency and voltage deviations is a commonly utilised objective in transient modelling, which can be achieved by adjusting loads or scheduling DG resources. Furthermore, there are papers considering both operational- and infrastructure-oriented objectives, e.g., the failure rate of distribution system equipment [22] and the number of failed lines [23].

Table 2.2: Resilience-oriented modelling objectives

	Objective functions	References
Load	Maximise load survivability or restoration (critical and non-critical loads)	[14, 15, 24–28]
Cost	Minimise generation cost, pre-allocation cost or load shedding cost	[3, 16–21]
Transient	Reduce frequency and voltage deviations, minimise power mismatch	[29–35]

To assess the resilience of the utilised networks and satisfy the aforementioned objectives, a great deal of research has developed metrics as better summarised in Table 2.3. For instance, the work presented in [22] adopts an analytical hierarchical process and percolation theory to assess topological resilience and composite resilience. In [36], a probabilistic framework is proposed to assess the resilience of distribution networks in four dimensions (technical, organisational, social and economic). Among these studies, a multi-phase resilience trapezoid model and related resilience metrics have been developed and widely used to assess different resilience-oriented strategies [4, 7, 37, 38]; the multiple-phase resilience curve is illustrated in Figure 2.1. Operational-oriented resilience and infrastructure-oriented resilience are evaluated via different metrics. However, the work presented in [7] does not involve concensus around how to assess the coordination effects of infrastructure-oriented strategies and operational strategies.

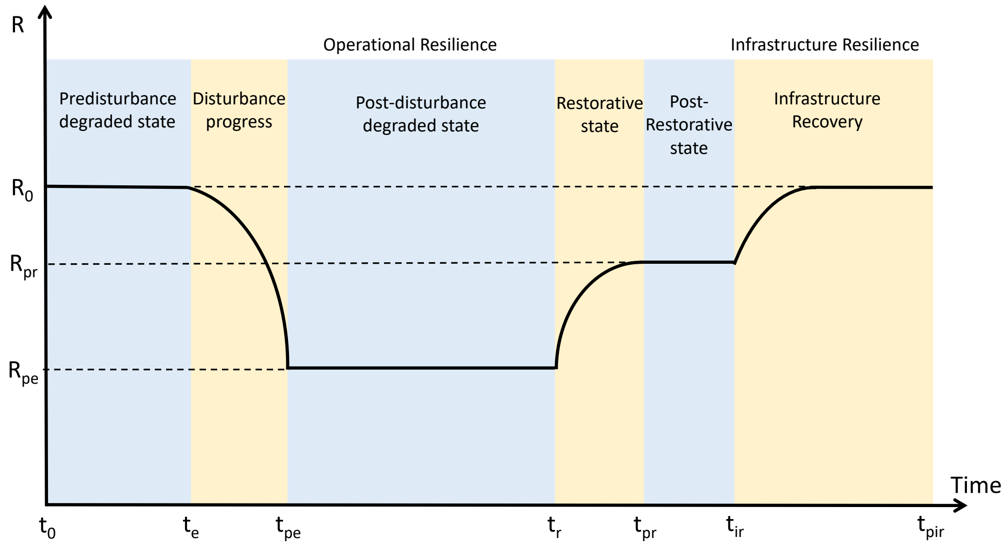

Figure 2.1: Multi-phase resilience curve [4]

Most resilience metrics presented in Table 2.3 are based on minimisation of load shedding. On the one hand, metrics used in [39–42] are based on load survivability and focus on disturbance progress and post-disturbance states. On the other hand, resilience metrics used in [15, 17, 19, 43, 44] are concerned with critical load restoration, since the main objective and focus is on restorative and post-restorative phases. Reference [17] develops four indices to capture both infrastructure and operational resilience. Furthermore, several papers capture the whole process of extreme events (disturbance progress state, post-disturbance degraded state and restoration state) and consider both load survivability and restoration [45, 46].

To summarise, a lot of resilience-related research on microgrids utilizes the multi-phase resilience curve suggested by [4] to assess the impact of microgrids on system resilience. These studies are mainly based on two assumptions: (1) unlimited energy supply during extreme events (e.g., unlimited fuels, abundance of solar irradiation, wind, etc.); (2) the time and duration of an outage can be predicted. These two assumptions guarantee the perfect combination between post-restorative

Table 2.3: Literature review on metrics used for resilience assessment

References	Main considerations	Related metrics
[22]	Composite resiliency and topological resiliency.	Load Not Lost Factor, Power flow feasibility, Failure rate of distribution system equipment, intensity of the unfavorable event, Topological metrics
[36]	Technical, organisational, social and economic.	The percentage of energised substations, distribution nodes with power,critical facilities with power,customers with power and economic loss.
[7, 37]	Infrastructure and operation. A multi-phase trapezoid curve.	$\Phi\Lambda E\Pi$ resilience metrics and an area metric.
[38]	Resistance, reaction, restoration and temporal behaviours.	A normalised degradation index, a restoration efficiency index and a resilience index.
[39]	Preventive state.	The sum of electric and thermal storage at the event onset
[40]	Preventive stage.	The disruption cost caused by cyber-attacks
[41, 42]	Disturbance progress and post-disturbance states.	The survivability of loads with different priorities
[15, 19, 43]	Restorative and post-restorative states.	The percentage of restored critical loads.
[44]	Restorative and post-restorative states.	The percentage of the performance loss, such as unrestored loads.
[17]	Infrastructure and operation. Restorative and post-restorative states.	the average number of line trips, connectivity losses, load curtailments and the grid recovery index
[45]	Resistance, recovery and resilience.	The percentage of uninterrupted load and restored load
[46]	Disturbance progress, post-disturbance degradedand restorative states.	A resilience index based on social welfare.
[23]	Infrastructure and operation.Redundancy, robustness and responsiveness.	Loss of Load Frequency and Expected Energy Not Supplied, offline generation capacity and the number of failed lines

state and infrastructure recovery state. However, natural disasters can cause the disconnection of a distribution network and the transmission grid leading to unavailable utility power supply. Extreme events can cause severe damage on energy supply chains, such as gas networks and fuel networks, which leads to limited generation resources in islanded distribution networks. The highly uncertain feature of extreme events (severe damage and large geographical scope) also makes it hard to accurately predict the outage duration, which means it may be difficult to schedule planned optimal strategies according to a clear blackout interval. If MGs or DERs are used to supply loads over a specific period, they may fail to operate (e.g., due to fuel shortage) and the performance curve (e.g., the restored load or frequency) will drop again during the post-restorative phase. Additionally, subsequent damage from extended events may introduce further performance degradation to distribution networks [31, 47, 48]. In these situations, the multi-phase resilience curve suggested by [4] may not accurately capture the operation state of distribution networks.

2.3 Resilience-oriented modelling scenarios

Uncertainties, multiple contingencies and interdependencies are main features of outages due to natural disasters [1]. An indicative timeline of a MG-based response in power systems capturing these features and correlating them to resilience-proofing is illustrated in Figure 2.2. Essentially, the timeline indicates how these features feed in the resilience process of power systems and responds to the fundamental question of whether resilience is delivered by design or by operation. It is shown that resilience, being such a complicated theme, is correlated to various phases of a power system from the planning stage to operational stages in an iterative way (e.g., operational aspects continuously affecting design stages). Thus, these features appear to be investigated in the literature (partially or holistically) and the next sections highlight the various aspects relating to them. More details can be found in Table 2.4.

2.3.1 The uncertain nature of information

There are several types of uncertainties considered in literature: renewable energy resources, load profiles, network topologies, energy market prices, and time and duration of extreme events. On the one hand, extreme events can lead to uncertain weather conditions and human activities, which introduce more stochastic features in energy market price, renewable energy sources and load profiles. On the other hand, the damage caused by natural disasters is normally deeply severe and uncertain (e.g., multiple faults or power interruption). Due to extreme events, outage duration and repair time may take from hours to several days or even weeks [49], which introduces the necessary uncertainties surrounding time and duration of outages. Robust optimisation and stochastic methods are two basic ways tackling uncertainties relating to natural disasters. In comparison with scenario-based methods, robust optimisation can provide a guaranteed immunity against worst-case realisation and with a relatively low computation burden [50]. However, inherent conservativeness is a problem of robust optimisation.

In addition to stochastic method and robust optimisation, risk-based methods [51–53] and data-driven methods [41] have been used to handle uncertainties relating to renewable generation resources. Although the methods suggested by [41,53] are verified to be more effective than stochastic method and robust optimisation methods, they both ignore interdependencies between different uncertainties. Future research should focus on developing more valid methods to tackle multiple uncertainties and their interdependencies caused by extreme events.

2.3.2 Multiple contingencies

There are mainly three types of contingencies considered in literature: multiple line faults, power source damage and cascading failures. Except for [20, 43, 54–58] (which consider single line fault or no line faults), the rest of the papers introduce multiple line faults to mimic a realistic scenario, while references [15, 16, 19, 24, 25, 29, 31–34, 55, 56, 59] introduce power source damage as part of the considered contingencies. However, there is limited research capturing these two types of contingencies in parallel.

Cascading failures occur if the failure of one component causes one or more components to fail [60], which shows the spatiotemporal correlation of the faults happening due to extreme events. Except for [61] and [62], there is little research focusing on handling cascading faults through MG-based operations. It is also worth noting that MGs can equally be damaged from natural disasters. However, most existing literature on islanding schemes assumes that the structure of MGs remains intact after extreme events [3, 51, 63–66]. As such, it appears that there is a need for resilience-oriented modelling problems to comprehensively and appropriately incorporate all possible contingencies towards reflecting realistic scenarios.

2.3.3 Interdependencies of different distribution networks

The interdependencies between distribution networks and other network infrastructures, such as gas networks, water supply networks, transportation networks and communication networks, introduce more challenges for load restoration process. In [39, 40], the interdependency between natural gas networks and electricity infrastructures is presented via electrical power flow, thermal power flow and natural gas flow, while the interdependency between power networks and water networks is considered in [25, 46].

Conventional restoration process has to be delayed until damaged components are accordingly repaired, while rapid restoration processes can be achieved by deploying MPSs utilising intact transportation networks. In [19, 62, 67–69], both transportation networks and distribution networks are considered to present flexibility and advantages of MPSs. Specifically, the influence of road damage on delivering MPSs is studied in [62, 67], which indicates that a longer travelling time (caused by road damage) adversely impacts the objective function. Much research focuses on the effectiveness of EVs on resilience enhancement [16, 29, 41, 56, 59, 63, 70–73]. However, these papers all ignore the influence of transportation networks on EVs.

Overall, the interdependencies among different networks have significant impacts on optimal operational strategies and introduce certain challenges to resilience enhancement. Future resilience-oriented research may focus on how to appropriately model these interdependencies in order to obtain more realistic solutions.

2.3.4 Technology of generation resources

Except for conventional distributed generators (e.g., diesel generators, micro-turbines, etc.), there are several other types of generation resources utilised to enhance resilience, such as non-dispatchable generators (e.g., WTs, PVs, etc.), battery energy storage systems (BESSs), EVs and MPSs. Wind, PV and BESS devices are three widely-used generation resources in resilience studies and the existence of BESSs can handle the stochasticity introduced by renewable energy sources. Future research may focus on developing appropriate models to tackle uncertainties and frequency/voltage deviations caused by renewable energy sources. In addition, there are multiple papers considering the application of MPSs and EVs on load restoration problems, which introduces challenges for primary and secondary control of power systems.

Table 2.4: Literature review on resilience modelling scenarios

Category	Subcategory	References
Distributed generation	Battery energy storage system (BESS)	[3, 25, 29, 30, 32, 45, 51, 53–55, 63–67, 71, 74, 75], [15, 21, 24, 25, 38, 39, 41–43, 52, 70, 73, 76–85]
	Photovoltaic (PV)	[3, 25, 27, 43, 51, 54, 55, 57, 64–66, 74, 75, 84–87], [21, 24, 29–31, 35, 41, 42, 52, 71–73, 76, 78, 79, 82, 88, 89]
	Wind turbine (WT)	[3, 25, 43, 45, 51, 54, 63, 65, 66, 74, 82–85, 87, 88], [15, 29, 30, 32, 38, 41, 53, 55, 70, 71, 73, 76, 78, 80]
	Electric vehicles (EV)	[29, 38, 56, 59, 63, 70–73]
	Mobile emergency resources (MER)	[16, 18, 19, 48, 59, 62, 67–69]
	Combined heat and power (CHP)	[21, 53, 56]
Uncertainties	Event time and duration	[41, 46, 70, 78, 79, 81–85]
	Event damage	[16, 20, 38, 46, 53, 59, 61, 62, 69, 90, 91]
	Renewable generation	[15, 25, 45, 51, 53, 63, 64, 70, 74, 75, 88], [41, 43, 52, 73, 76, 78, 80, 81, 83–85]
	Load profiles	[15, 21, 25, 46, 54, 62, 63, 67, 74, 75], [41, 43, 53, 73, 76, 78, 80, 83–85, 88]
	Energy market price	[21, 41, 52, 56, 70, 81, 84]
Contingencies	Multiple line faults	[15–19, 24–28, 45, 46, 60, 62, 68, 69, 90–94], [14, 38, 40, 48, 53, 59, 61, 66, 67, 72, 74, 75, 95, 96]
	Power source faults	[15, 16, 19, 25, 29, 31–34, 53, 55, 56, 59, 86, 97]
	Single or no line fault	[20, 43, 54, 55, 57, 58]
	Cascading faults	[61, 62]
Interdependencies	With transportation networks	[19, 62, 67–69]
	With water networks	[25, 46]
	With gas networks	[39, 40]

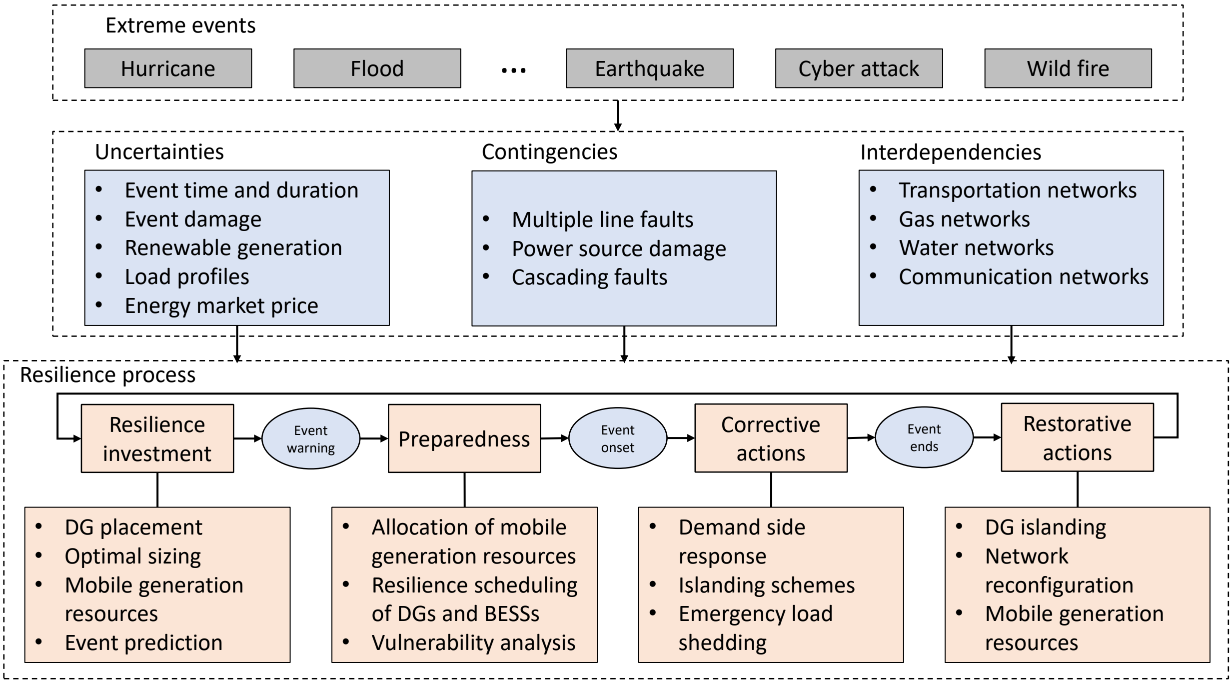

Figure 2.2: Timeline of the MG-based response in power systems

2.4 Resilience-oriented modelling methods

Optimal power flow (OPF) algorithms and energy management systems (EMSs) are two basic ways towards modelling the static behaviours of power systems. OPF models can capture voltage, angle variation, and power losses in addition to power balance, while EMS models typically consider the power balance equation along with high-level operational constraints of each resource. The conventional OPF models can further incorporate differential equations as transient stability-constrained OPF (TSC-OPF) to capture the dynamic characteristics of frequency and voltage deviations.

Constraints considered in OPF and EMS models can be found in Figure 2.3. Voltage and frequency characteristics of the networks can facilitate enhanced monitoring of their stability indices and eventually lead to increased resilience and security of supply, even under contingencies. Additionally, severe damage caused by extreme events makes power systems prone to voltage and frequency limits violation. In such situations, optimal strategies based on EMS models may lead to inaccurate solutions [98]. However, conventional OPF algorithms (that are considered to be an appropriate dispatch tool) do not consider transient stability, unit commitment and ramping rates of generators [7].

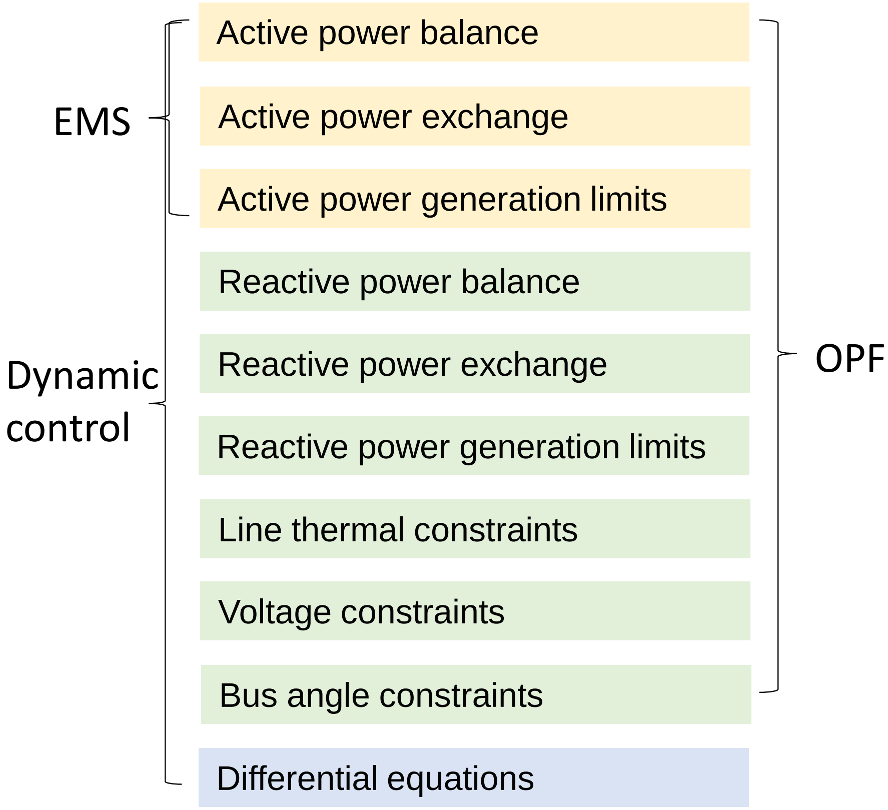

Figure 2.3: Constraints incorporated in OPF, EMS and dynamic control models

2.4.1 Classical AC OPF algorithms

AC OPF related approaches can be further divided into three categories: a) the non-linear AC OPF algorithm, b) OPF approaches after convex relaxation and c) linearised AC OPF algorithms with simplified network constraints. On the one hand, these methods are capable of taking reactive power and voltage into account; on the other hand, these approaches can be utilised for both meshed and radial networks and effectively capture power losses through loss factors. Among these, only the non-linear OPF is capable of obtaining solutions strictly subject to all the operational limits and power flow equations, although the solution might be a local minimum. The most common formulation of the objective function can be found in (2.1), aiming at the minimisation of the operational costs [99]. On the other hand, there are some other widely-used objective functions towards different purposes, including the minimisation of losses, constraint violations and the number of control actions [2]. Specifically, the objective function shall focus on the restoration of essential demand when resilience-driven operations are required. More details about this topic can be found in the next chapter.

$$\min_{P_g, Q_g, v, \theta} f(P_g, Q_g, v, \theta) \tag{2.1}$$

Constraints of the classical OPF algorithm include both power flow equations and operational limits, which are detailed in the following. Power flow equations set the basic rule for safe power transmission. The apparent power flow on branch (i, j) is shown in Eq. (2.2), where V, I, S and Y refer to voltage, current, apparent power and network parameter coupled by the Ohms law and Kirchhoff law respectively. According to the polar coordinate of voltage V, Eq. (2.2) can be further decoupled into Eqs. (2.3) and (2.4), corresponding to the active and reactive power flow on branch (i, j) [100]. As an explicit expression of Eq. (2.2), this is commonly used in various OPF-based models. Note that both of these formulations involve high non-linear features, which may cause large computational burden [101]. Following this decoupled fashion, the nodal power balance equation can be given as Eq. (2.5). Furthermore, the operational limits associated with branch flow, power generation, voltage and angle difference, given in Eqs. (2.6)-(2.8).

$$S_{ij} = V_i I_{ij}^* = Y_{ij}^* V_i (V_i^* - V_j^*) \tag{2.2}$$

$$P_{ij} = g_{ij}(v_i^2 - v_i v_j \cos\theta_{ij}) - b_{ij} v_i v_j \sin\theta_{ij} \tag{2.3}$$

$$Q_{ij} = -b_{ij}(v_i^2 - v_i v_j \cos\theta_{ij}) - g_{ij} v_i v_j \sin\theta_{ij} \tag{2.4}$$

$$\sum_{g \in B_G} P_g - P_{d,i} = \sum_{(i,j)\in L} P_{ij}, \ \sum_{g \in B_G} Q_g - Q_{d,i} = \sum_{(i,j)\in L} Q_{ij} \tag{2.5}$$

$$P_{ij}^2 + Q_{ij}^2 \le (S_{ij}^{max})^2 \tag{2.6}$$

$$P_g^{min} \le P_g \le P_g^{max}, \ Q_g^{min} \le Q_g \le Q_g^{max} \tag{2.7}$$

$$v^{min} \le v_i \le v^{max}, \ \theta_{ij}^{min} \le \theta_{ij} \le \theta_{ij}^{max} \tag{2.8}$$

Simplified AC OPF

As discussed above, the nonconvexity of the classical OPF is from Eqs. (2.3) and (2.4), where variables are coupled tightly and lead to a nonconvex surface. To address this issue, two types of approaches including OPF based on convex relaxation and OPF based on linearisation are developed for handling the non-linear power flow equations. Detailed comparison between these approaches can be found in Table. 2.5.

Regarding the OPF based on convex relaxation, power flow equations can be relaxed to inequalities ensuring a convex region and global optimum; nevertheless, obtained solutions may not

Table 2.5: Comparison of the Different Categories of OPF Methods [2]

Properties	Computational difficulty	Convergence	Solution quality
OPF with strict network model	NP hard problem	Not guaranteed	Ensure stability properties but may be a local optimum
OPF with convex relaxation	Terminate in a polynomial time (SOCP<QP<SDP)	Guaranteed	When relaxations are inexact, no clear physical meaning.
OPF with linearised network models	Terminate in a polynomial time	Guaranteed	Not strictly subject to power flow, but are close to be AC feasible

be able to clarify their physical meanings if the relaxation is inexact, which limits its application on practical operations [2]. Specifically, the power flow Eq. (2.2) can be reformulated in Eqs. (2.9) and (2.10). Eq. (2.9) is linearised by treating W_{ij} as a variable and Eq. (2.10) can be transferred to Eq. (2.11), indicating the matrix $W_{n\times n}$ is semidefinite with Rank 1 [102]. OPF algorithms based on convex relaxation mainly include three formulations, i.e., second-order cone programming (SOCP) relaxation, semidefinite programming (SDP) relaxation and quadratic programming (QP) relaxation. More details about these formulations can be found in [2].

$$S_{ij} = Y_{ij}^{*} W_{ii} - Y_{ij}^{*} W_{ij} \tag{2.9}$$

$$W_{ii} = V_i V_i^{*},\ W_{ij} = V_i V_j^{*} \tag{2.10}$$

$$W_{n\times n} \succeq 0,\ rank(W_{n\times n}) = 1 \tag{2.11}$$

On the other hand, the OPF methods with linearised network models linearise power flow equations, which can obtain optimal solutions very close to an AC feasible one if appropriate approximations are used. However, there still exists risk for the linearised OPF to obtain solutions that do not satisfy power flow equations, which may require a further verification of AC feasibility via power flow calculation. Linearised OPF approaches are used for current industrial practice of many system operation centres and international standards organisations due to their computing efficiency [2]. Among them, DC OPF is widely used for optimisation problems in market clearing, system operation and planning. The simplified DC network model is calculated in Eq. (2.12), neglecting reactive power and losses as well as assuming flat voltage profiles [103]. However, decision making obtained from DC OPF might be inappropriate due to these simplifications, especially under situations that power systems frequently reach their operation limits. In this case, advanced linearised AC OPF algorithms that can accurately capture both reactive power and power losses are required [104].

$$P_{ij} = b_{ij}\theta_{ij} = \theta_{ij}/x_{ij} \tag{2.12}$$

Transient Stability-Constrained OPF

Conventional OPF algorithms (that are considered to be an appropriate dispatch tool) do not consider transient stability, unit commitment and ramping rates of generators [7]. Modelling dynamic behaviours is becoming essential in the designing part of a distribution system for resilience purposes [13]. However, there is only limited research focusing on capturing dynamic control of MGs. In [14,29,32,48,86,96,97], load sharing, load shedding or load restoration strategies are suggested to maintain frequency and voltage excursions within admissible limits after extreme events. In [33,34], a decentralised event-triggered strategy and two distinct modes of networked MGs are considered to mitigate the system power imbalance caused by the failure of communication links (causing, for example, load disconnection or DG disconnection). In [31,35,89], advanced devices, such as electric springs, voltage control devices and grid-friendly appliance controllers, are employed to support the coordination of multiple MGs and mitigate the transients caused by fluctuating renewable energy sources and switching operations from grid-connected mode to islanded mode. In [30], the hierarchical control strategy of a DC MG including primary, secondary and tertiary controls is analysed to present the merits of DC MGs on resilience enhancement.

Even though dynamic performance based on droop characteristics is important for the resilience enhancement of power systems, it is worth noting that most research above uses dynamic simulations to present frequency and voltage characteristics rather than model-based optimisation approaches. As a model-based approach, transient stability-constrained OPF (TSC-OPF) algorithms can capture economic and secure power system operations. As explained in [105], TSC-OPF is formulated as a semi-infinite optimisation problem for preventive control of power systems, utilising differential-algebraic equations (DAEs) to model system stability properties. In general, this TSC-OPF problem can be described using Eqs. (2.13)-(2.17), while there are mainly three approaches available for solving this time-consuming optimisation problem, including numerical discretisation, generation rescheduling and artificial intelligence algorithms [105]. However, it is worth noting that the incorporation of large number of differential equations can cause large computational burden [106], which hasn't been handled appropriately and may be a problem for resilience-driven operations due to the requirement for fast response and close coordination. More advanced approaches are required to overcome this challenge before its application in real-world system operations.

$$\min C(x) \tag{2.13}$$

subject to

$$g(x) = 0 \tag{2.14}$$

$$h^{min} \leq h(x) \leq h^{max} \tag{2.15}$$

$$dx/dt = f(x) \tag{2.16}$$

$$x(t_0) = x_0 \tag{2.17}$$

2.4.2 OPF problems with uncertainties

As discussed above, it is necessary to consider the influence of various uncertainties from DERs (e.g., renewable energy sources and loads) on optimal results of OPF problems due to the high-impact nature of extreme events and the high penetration of renewable energy sources. In this subsection, important approaches on handling uncertainties are discussed in detail. In general, there are mainly five approaches used to deal with uncertainties in OPF problems: a) scenario-based stochastic optimisation, b) robust-based optimisation, c) risk-based optimisation, d) chance-constrained optimisation and e) artificial intelligence technologies [107]. However, it is worth noting that most of proposed OPF formulations in existing literature have been considerably complicated due to the incorporation of various constraints (e.g., power balance and operation limits) and the increase of network size. Thus, there is no doubt that capturing uncertainties in these models will further increase complexity and raise a larger computational burden. Details about these five approaches can be found hereafter:

Scenario-based optimisation has been widely used for various optimisation problems featuring EMS or OPF, which is normally realised as an optimisation problem including two stages, i.e., here-and-now and wait-and-see [108]. The here-and-now stage formulates the optimisation as a day-ahead structure across the whole uncertain set through the forecasting of uncertain parameters, while the wait-and-see stage realises the optimisation as a real-time management problem towards each scenario obeying a certain probability distribution. Afterwards, optimisation problems at these two stages are co-optimised and output final optimal solutions. Detailed formulation and solving procedure of this approach have been presented in some of this work. However, it is worth noting that scenario-based stochastic approaches may only be able to consider a small number of scenarios due to the large computing burden, especially when a large number of scenarios need to be involved. In this case, the limited number of scenarios may fail to represent the whole space of uncertain variables and parameters [109]. On the other hand, scenario generation requires the awareness of a certain probability distribution; nevertheless, the clear distribution of an uncertain parameter might be unavailable in real-world cases.

Regarding robust-based optimisation, the main idea is to search the worst case scenario, and then ensure that solutions do not violate the constraints of this scenario [110]. Because the only focus of these approaches is the worst case scenario, they usually provide very conservative solutions. On the one hand, these solutions can ensure secure system operations of power industries; on the other hand, the solutions may be not very economical [109]. It is worth noting that maintaining secure operations and ensuring the continuity of power supply to essential demand can be much more important than cost-effective schemes in resilience scenarios. In this case, robust optimisation might be a more appropriate method to capture the influence of uncertainties than scenario-based optimisation. To find the worst case scenario and then output solutions, bi-level or even three-level structure may be required, of which most are utilised for linearised DC network models [2]. As one of robust-based approaches, a defender-attacker-defender (DAD) model is formulated in this thesis to deal with resilience-driven planning problems of networked MGs. Novel features have been included to achieve a better trade-off between economics and conservation.

Chance-constrained optimisation uses probabilistic constraints to replace the original deterministic constraints, making sure that the probability of constraint violation is smaller than a certain threshold. In other words, it is allowed that decision making does not meet the constraints to a certain extent; nevertheless, the solution should guarantee that the probability within the constraint condition is not less than a certain confidence level. Normally, chance-constrained optimisation problems are intractable and difficult to solve [111]. To make a tractable representation of chance constraints, certain probability distribution of forecasting errors is assumed in some approaches, which is capable of achieving an analytical formulation, e.g., [112] and [113]. In [114], a sample average algorithm is proposed to generate the distribution of uncertain variables and parameters via the Monte Carlo simulation.

Additionally, risk-based approaches can be used to capture uncertainties in mathematical models through an additional risk term in the objective function. This term can be defined as the cost of risks across multiple scenarios with different occurrence probability. For instance, ref. [115] considers the wind curtailment and expected energy not served (EENS) as the risk term. Normally, the risk term is presented in a non-linear formulation, which can be linearised via some convex approaches [116].

Furthermore, compared to approaches featuring mathematical programming, RL [117], as a data-driven and model-free approach, is suitable for resilience-driven operations because of its ability to provide fast response and incorporate uncertainties and contingencies. RL-based approaches eliminate the need to solve an optimisation problem in a time-coupled fashion and enables the managed agents to provide an adaptive control scheme for various system dynamics and state conditions without the knowledge of uncertain parameters.

2.5 Microgrids: benefits and types

MGs, as localised small power systems, contain electric loads (controllable and uncontrollable) and DERs, e.g., conventional generation resources, renewable energy resources and even energy storage devices, while they can be managed in a coordinated way involving two operation mode: grid-connected mode when connected to the main grid and islanded mode when disconnected to the main grid intentionally or unintentionally [5]. Different than the integration of demand side or the interconnection of DGs, MGs have three fundamental features: a) intelligent control schemes, b) local load, c) local micro sources [5]. Additionally, MGs are capable of providing various carbon intensity services for the main grid through their high penetration of renewable energy resources (e.g., PV panels and wind turbines) and high flexibility of demand-side technologies [118].

2.5.1 Benefits of DERs in the context of MGs

It is worth noting that power systems are undergoing a significant transition from the fossil fuel resources to the decarbonlisation of renewable energy sources, promising to low-carbon future [119]. Moving towards low-carbon transition requires a significant increase in renewable energy sources. As efficient integration schemes, MGs are capable of unlocking the full benefits of DERs and further benefit threefolds, including: a) economic benefits or cost efficiency, b) environmental benefits, e.g., reducing carbon emissions, c) technical benefits, e.g., improving reliability and resilience of power systems [5]. Detailed benefits of DERs in the context of MGs have been schematically presented in Figure 2.4.

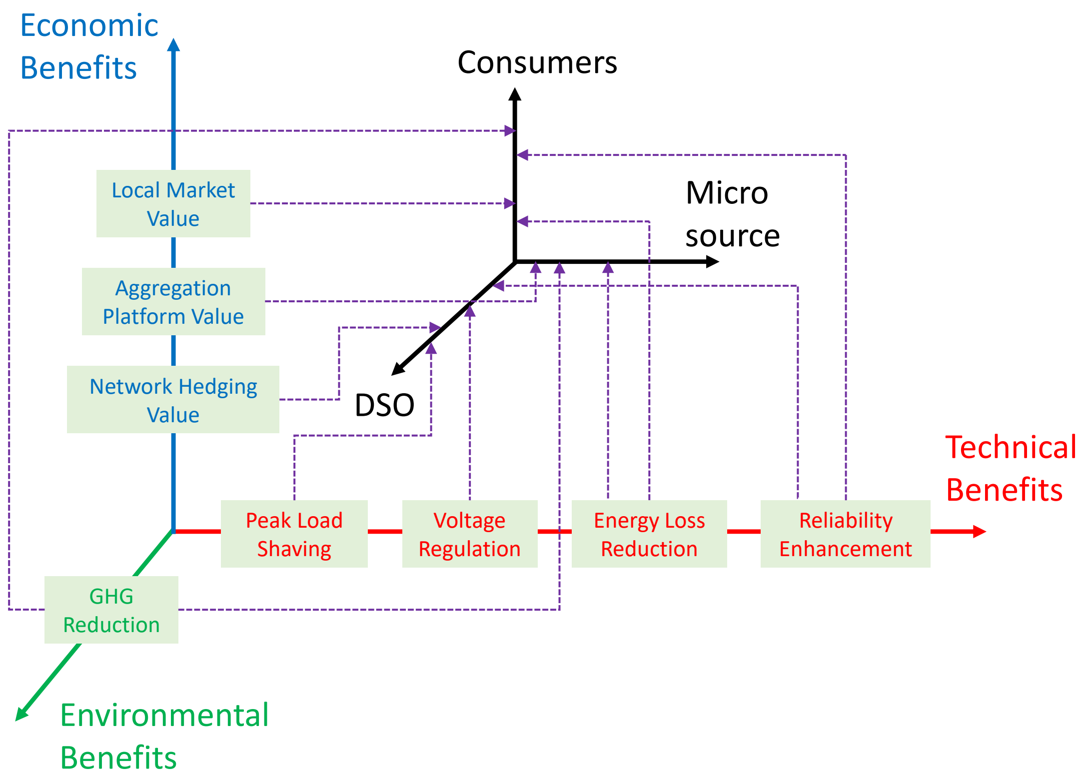

Figure 2.4: Benefits of local DERs categorised by criteria and stakeholders [5].

One element missed in the figure above is the benefit of DERs on resilience enhancement of power systems (e.g., maintaining power supply and reducing load shedding during extreme events), which has gradually become a fundamental requirement for system operations and is the main focus of this thesis. Nowadays, HILP events have happened more frequently than before partly because of the rapid climate change [120], which can cause severe damage to power systems. As local resources, MGs and DERs are capable of providing power supply for the damaged grid, enhancing the obstructed power flow and maintaining secure system operations. There has been much research on developing resilience-driven planning and operation strategies based on MGs for resilience enhancement. Detailed information can be found in the next section.

2.5.2 Types of MGs

Regarding the scale of MGs with applications, MGs vary significantly ranging from nano-scale (10-80 W) to mini-grids (100s of kW). According to the definition above, modern MGs mainly correspond to low voltage and small-scale power networks; nevertheless, a vast increase in MW-scale MGs has been seen recently, which can even connect to distribution systems (especially in large urban centres) [121]. More details are provided in this subsection for giving a picture on types of MGs depending on the technologies utilised and the power electronics deployed. Typical structures of AC MGs, DC MGs and AC/DC hybrid MGs have been better depicted in Figure 2.5. It can be found that MGs often contain local DERs such as microturbines and solar PV panels outputting AC power and DC power respectively, which requires the deployment of power electronics devices for the appropriate connection between DERs and the MG.

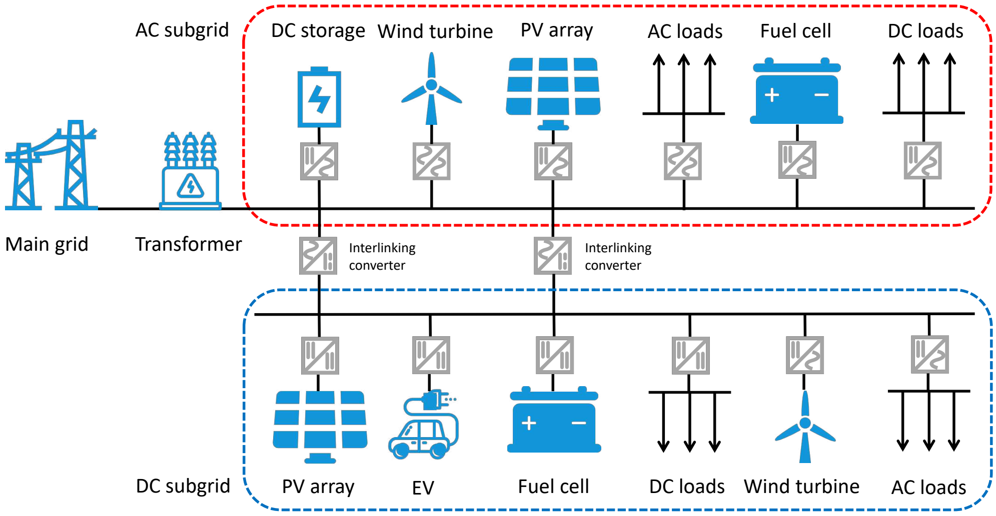

Figure 2.5: Three types of MGs: AC MGs, DC MGs and hybrid MGs.

AC MG structures have been widely applied to integrate DERs in current utility grid and no viability and security issues are raised since the involved technologies are mature and the modifications required are minor. More specifically, AC MG systems can easily modify their voltage levels via transformers and are equipped with various protection devices having high fault management capability for quick fault detections and clearings; nevertheless, power losses may be increased due to reactive power circulation or DG synchronisation.

To deal with these issues, DC MGs are introduced, reducing the need for power electronics device towards voltage level coordination. As illustrated in Figure 2.5, various DERs (e.g., fuel cells, battery storage systems and PV panels) and demand (e.g., ventilation, heating and lighting) output or accept DC power; thus, the utilisation of DC MGs can avoid power losses from power converting [122]. Since much less energy is dissipated as heat at the conversion stage, the requirement for ventilation and cooling systems can be reduced significantly, which is very important for applications with intense power usage, e.g., charging stations and data centres. [123]. Additionally, DC MGs can alleviate potential operation issues brought by reactive currents, synchronisation and harmonic distortion [30].

As a configuration combining both AC and DC MG architectures through bidirectional AC/DC interlinking converters, hybrid AC/DC MGs are utilised to increase the penetration of renewable energy sources, battery storage systems and various demand-side technologies with minor modifications and reduced investment cost [124]. The power sharing between AC subgrids and DC subgrids can better ensure power supply to demand and even reduce load shedding when a disturbance occurs; hence, the reliability and resilience of this power system can be largely enhanced, which is aligned with the main focus of this thesis. The typical network structure of an AC/DC MG is shown in Figure 2.5, including both AC-type units (e.g., WTs and AC loads) and DC type units (e.g., PV panels and DC loads).

2.6 Resilience-oriented strategies featuring MGs

Resilience-oriented strategies including operational and planning strategies are shown in Table 2.6. Among them, DG islanding and network reconfiguration are two widely used methods for grid load restoration, while feasible islanding is a valid way to guarantee resilience of a MG itself via islanding schemes. Most existing research considers DGs with black-start capabilities as main power resources of MGs. In addition, DG islanding, network reconfiguration and demand response are mainly applied in the corrective state or restorative state, while preventive allocation and optimal sizing belong to preventive planning strategies that normally consider both preventive and restorative states [125]. It is worth noting that feasible islanding and vulnerability-based line tripping are two preventive operations, which focus on how to achieve a stable islanded MG. The latter two methods tend to consider both preventive and corrective states rather than restorative state.

According to the roles of MGs and network topologies, the application of MGs can be categorised in four separate areas: i) MGs as virtual feeders for global resilience, ii) dynamic formation of MGs for global resilience, iii) islanded MGs for local resilience and iv) networked MGs for local resilience, which are shown in Figure 2.6. The solid black lines correspond to cable lines and the dotted red lines represent information flows between central controller and MGs. Types i) and ii) regard MGs as a type of generation resources, while types iii) and iv) mainly consider how to guarantee local load survivability of a MG itself. Note that type iv) in Figure 2.6 only represents the centralised control method and other control methods (e.g., decentralised control or hybrid control) are not shown here. A summary of literature about MGs as resilience resources for global and local resilience is presented in Table 2.7.

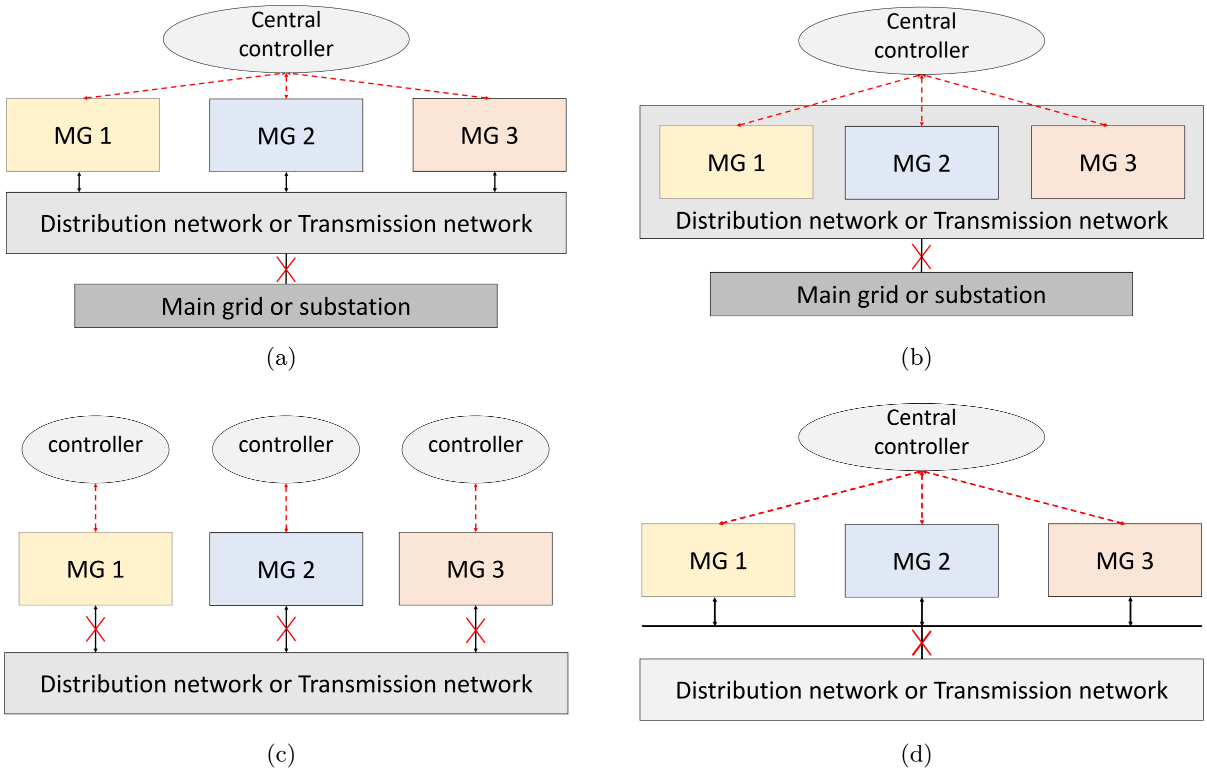

Figure 2.6: Network topologies used by four types of strategies: (a) MGs as virtual feeders for global resilience, (b) dynamic formation of MGs for global resilience, (c) islanded MGs for local resilience and (d) networked MGs for local resilience.

2.6.1 MGs for global resilience

In this subsection, literature adopting AC MGs to supply critical loads due to their network flexibility and service reliability is presented. When using MGs as virtual feeders, the limitation of generation resources is an important modelling factor. When several MGs are dynamically formulated, formatting principles (i.e., "one MG to one DG" or "one MG to multiple DGs") decide the number and network structures of MGs.

MGs as virtual feeders

This type of research assumes that the structure of existing MGs remains intact during extreme events. Limited generation resources in MGs and accurate prediction of extreme events are assumed to mimic a realistic scenario [17]. In [14, 15], service restoration strategies based on network reconfiguration and MGs are presented to restore critical loads. Both of them ignore non-critical loads

Table 2.6: Literature review on resilience-oriented strategies

Strategies	Classification	References
Operational strategies	Network reconfiguration	[18, 25–28, 45, 46, 48, 54, 57, 59, 60, 68, 69, 90, 91, 93, 94, 96]
		[14, 14–16, 19, 22, 24, 48, 62, 67, 72, 74, 75, 77, 92, 95, 96]
	DG islanding	[18, 26–28, 45, 46, 48, 54, 59, 60, 68, 69, 90, 91, 93, 94, 96]
	Feasible islanding	[39, 41, 42, 52, 70–72, 76–78, 81–84]
	Demand side response	[20, 25, 29, 45, 70, 72, 73, 75, 77, 84, 89]
	Vulnerability analysis	[40, 72, 77]
Planning Strategies	Preventive allocation	[16, 18, 25, 38, 46, 59, 61, 69, 91, 95]
	Optimal sizing	[64, 79]
	Line hardening	[25, 46, 61, 90, 91, 95]
	Repair crews	[68]

Table 2.7: Literature review on MGs for resilience enhancement

Category	Classification 1	Classification 2	References
MGs as virtual feeders	limited energy capacity	preventive and restorative states	[16, 25]
		only restorative state	[14, 15, 17, 19, 62]
	unlimited energy capacity	preventive and restorative states	[20, 21]
		only restorative state	[24, 55–58, 92]
Dynamic formation of MGs	One microgrid with one DG	preventive and restorative states	[18, 69, 91]
		only restorative state	[26, 27, 48, 94]
	One microgrid with multiple DGs	preventive and restorative states	[46, 59, 90]
		only restorative state	[28, 45, 54, 60, 68, 93, 96]
Islanding schemes for local resilience	AC MGs	Normal and emergency modes	[39, 42, 52, 70, 78, 79, 81, 84]
		Only islanded mode	[29, 32, 38, 72, 73, 77, 80, 83], [33, 40, 43, 61, 87]
	AC/DC hybrid microgrids	Normal and emergency modes	[41, 71, 76, 82]
		Only islanded mode	[85]
	DC microgrids	Normal and emergency modes	[30]
		Only islanded mode	[97]
Networked MGs for local resilience	Centralised control	Grid-connected and islanded modes	[22, 53, 64, 67, 86, 95]
		Only islanded mode	[31, 35, 51, 74, 75, 89]
	Decentralised control	Grid-connected and islanded modes	[88]
		Only islanded mode	[34, 66, 75]
	Hybrid control	Grid-connected and islanded modes	[3, 63]
		Only islanded mode	[65]

and operational costs (e.g., generation cost and allocation cost). In [25], both operation-oriented and infrastructure-oriented strategies including network reconfiguration, line hardening, upgrading energy storage size in MGs are applied to enhance resilience. There are several studies incorporating operational cost or allocation cost as part of objective functions [16,17,19,62]. A post-disaster joint restoration scheme based on MPSs and network reconfiguration is proposed in [19,62], while a pre-hurricane resource allocation strategy is suggested in [16] to provide proactive preparedness against natural disasters.

Many resilience-oriented studies assume unlimited generation resources in MGs during extreme events [20,21,24,55–58,92]. Restoration strategies based on unbalanced three-phase power flow and network reconfiguration are considered in [24,57,58,92] and EVs are employed in [56] for resilience enhancement, while reference [55] suggests a decentralised control method based on game theory to improve resilience and protect customer privacy. Proactive decisions (e.g., DG scheduling, energy reserve services and demand-side response) are made in [20, 21] in the presence of a progressing wildfire. Nevertheless, most of the above studies cannot entirely capture the features of extreme events. For instance, only single fault is considered in [20, 55] and no line faults are considered in [56, 57]. Reference [21] only differentiates resilience services from reliability ones according to service duration and ignores the difference in severity and frequency.

Overall, most of the above research assumes that MGs are intact during extreme events. However, the structure of MGs may be damaged because of the highly uncertain nature of extreme events. Ignoring the vulnerability of a MG itself may lead to unrealistic optimisation results and even cause more damage on the whole power system. Furthermore, MGs normally have fixed boundaries and self-controllability because of the considerations of customer privacy, load/power balance and frequency/voltage control. In existing literature, most research on dynamic boundaries of MGs assumes centralised control methods, which can be unrealistic in practice. Additional work is required to develop models based on decentralised MGs.

MG formation based on DG islanding

Technologies, such as smart switches and DGs with black-start capabilities, highlight the research relating to the dynamical formation of MGs for global resilience. In [26], a dynamic formation mechanism of MGs is firstly suggested to restore critical loads via distributed generators and remotely controlled switches. Radial constraints are incorporated into this model in [94] to reduce computational burden, while a master-slave control technique is proposed in [27] to control the formation of MGs. In [18, 69, 91], both infrastructure- and operation-based preventive strategies (e.g., pre-positioning and optimal dispatch of MPSs, line hardening, DG placement and network reconfiguration) are considered to dynamically formulate multiple MGs, while the optimal dispatch of MPSs based on minimum-scale MG principle and looped topologies is employed in [48] to generate MGs. The above indicated studies assume that each formulated MG can include only one distributed generator; in other words, the number of formulated MGs is pre-determined and fixed before optimisation. Except for [18, 48], the rest of the studies do not consider multi-period dynamic operation of MGs. Additionally, reference [91] assumes that a hardened line will no longer be damaged during extreme events, which can be considered unrealistic.

The dynamic formation of MGs with more than one distributed generators is considered in [28, 45, 46, 54, 59, 60, 68, 90, 93, 96]. In [28, 45, 54, 60, 93, 96], operational strategies (e.g., network reconfiguration, demand-side response and optimal management of DERs) are considered to dynamically formulate MGs, while both infrastructure- and operation-oriented preventive strategies (e.g., line hardening, DG placement and network reconfiguration) are suggested in [46, 90] to restore critical loads. Among these, both tie switches and sectionalizing switches are considered for network reconfiguration in [28, 45, 46, 60, 90, 93]. However, in addition to [28, 96], these studies belong to one-shot decisions and ignore the dynamic behaviours of loads and power output. Furthermore, the dynamic manner of MPS dispatch is considered in [59, 68] and the consideration of repair crews helps predict the duration of restoration process. Reference [59] considers both load survivability and restoration.

To summarise, the combination and interdependency between infrastructure-oriented strategies, such as line hardening [46, 90] and repair crews [68], and operational strategies, such as network reconfiguration and DG islanding [45, 93], can bring more benefits for resilience enhancement than a single strategy type. Strategies based on dynamic formation of MGs face two basic challenges. On the one hand, dynamic reconfiguration of power systems highly depends on their communication networks, of which the vulnerability (e.g., communication failures) during extreme events will influence the controllability of smart switches. On the other hand, smart network reconfiguration techniques require a large number of remotely controlled switches, which necessitates high investment. Even though there are studies considering the operational cost of switches as part of the objective function (e.g., [93]), the installation cost and maintenance cost of smart switches are ignored. Specifically, reference [48] points that dynamic formation of MGs based on "minimum-scale coverage" can improve the survivability of MGs because of the small modelling scale. Future research may focus on defining the optimal design scale of MGs (e.g., bus numbers and maximum power capacity) for resilience purposes.

2.6.2 MGs for local resilience

After distribution networks fail to operate during extreme events, a grid-connected MG can switch into islanded mode and provide power supply and emergency demand response for local loads [49]. Models based on different types of MGs (e.g., AC MGs, DC MGs, AC/DC hybrid MGs) and control methods (e.g., centralised control, decentralised control and hybrid control) have been developed. A summary of existing literature can be found in Table 2.7.

Islanding schemes for local resilience

Grid-connected mode is used to make preparations for upcoming events via battery management and generator pre-scheduling. In [39, 42, 52, 70, 78, 79, 81, 84], optimal strategies (e.g., vulnerability analysis, conservation voltage regulation, network reconfiguration, demand-side response, risk analysis, power importing in advance, and optimal sizing and operation of renewable energies with storage units) are suggested to improve the preparedness against extreme events. In [41, 71, 76, 82], both the feasible islanding of AC/DC hybrid MGs and load survivability are considered; nevertheless, these models on AC/DC hybrid MGs consider only power balance equations to control power flows. The omission of operational constraints relating to voltage, frequency and angle variation can lead to inaccurate solutions [98]. Much as [76], other papers assume unlimited energy supply during islanding mode. In [30], the hierarchical control strategy of a DC MG including primary, secondary and tertiary controls is analysed to present the merits of DC MGs on resilience enhancement.

There are several studies focusing only on the operations of islanded MGs. Proactive operational strategies based on network reconfiguration, DG allocation, demand-side response and vulnerability analysis are proposed in [40,61,72,77,91] to minimise load shedding, while references [29,32,33,43,73, 80,83,85,87,97] adopt corrective control actions (e.g., DG scheduling, demand-side response, energy storage management and load shedding strategies) to maximise economic performance and load survivability or minimise voltage and frequency deviations. Line hardening is employed in [38, 61] to enhance system resilience. Similarly to [91], these papers assume that a hardened line will no longer be damaged during extreme events.

Overall, there are several research limitations on the islanding schemes of MGs. Most literature assumes that there is unlimited energy supply during islanding mode and the occurrence time of extreme events can be predicted. Both can be considered unrealistic. Furthermore, most literature tends to consider an islanding period shorter than 24 hours. However, a MG may stay in islanding mode for a more extensive period of time, because of the difficulty to remove issues and reconnect the MG [52]. It is necessary to consider a much longer operating horizon (e.g., at least several representative days/weeks) to verify the effectiveness of proposed resilience strategies. It is also worth noting that AC MGs are widely used for modelling purposes, while only limited literature considers the benefits of AC/DC hybrid MGs and DC MGs on resilience enhancement [126].

Networked MGs for local resilience

Networked MGs can be used to decrease operational cost in grid-connected mode, while the energy sharing between networked MGs reduces load shedding in islanded mode [44, 63, 127]. Centralised control methods have been widely used to manage the power flow of networked MGs [53,95]. Strategies based on centralised control (e.g., optimal energy storage sizing [64], line hardening [95], redundancy [95], proactive resilient scheduling [53], the routing of MPSs and network reconfiguration [22, 67, 74, 95]) have been employed to restore loads. The above studies assume that the time and duration of extreme events can be accurately predicted, which is unrealistic. Frequency and voltage control strategies of networked MGs are employed in [31, 35, 86, 89] to enhance resilience.

Compared with centralised control, decentralised control methods may not guarantee a globally optimal solution but can better protect customer privacy, reduce computation burden and reduce the dependence of networked MGs on communication networks [66, 75]. Reference [88] considers both grid-connected mode and islanded mode according to different objectives: cost minimisation, and voltage stability and load survivability respectively. However, this paper does not consider relative preventive strategies in grid-connected mode. References [34, 66, 75] consider only islanded mode of networked MGs and employ operational strategies (e.g., flexible division and unification control, risk-based and self-healing strategies) to restore loads or reduce frequency deviations. Hierarchical control schemes are considered in [63, 65] to enhance the resilience of networked MGs. Reference [3] presents a nested energy management strategy for networked MGs to guarantee both network resilience and customer privacy. Overall, it can be highlighted that centralised energy management systems offer better solutions, while decentralised energy management systems lead to reduced operational costs and protected customer privacy. Typical network configurations of hierarchical control and decentralised control are presented in Figure 2.7, while detailed limitations of above control approaches can be found in Table. 2.8.

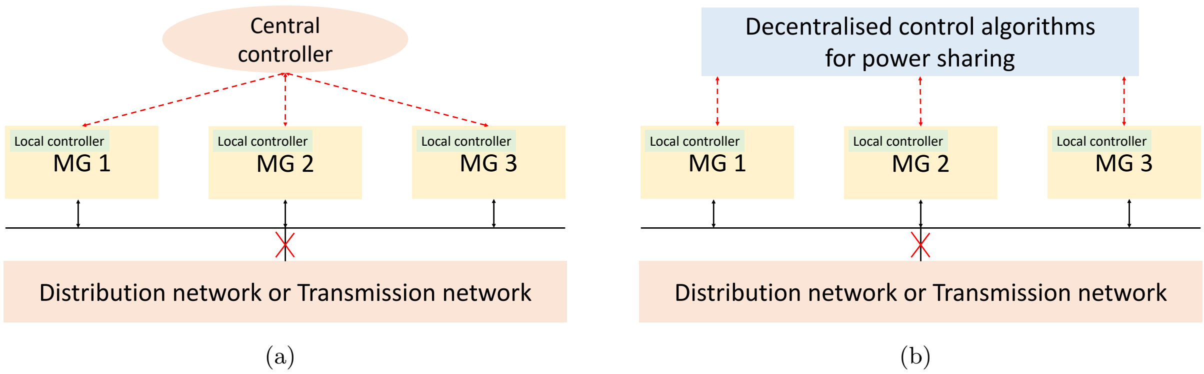

Figure 2.7: Network MGs based on different control approaches: (a) Hierarchical control, (b) decentralised control.

Table 2.8: Limitations of different control approaches in the context of networked MGs [3].

NO.	Type	Limitations
1	Centralised control	1.Raise large computational burden; 2.Fail to consider customer privacy; 3.Require expensive communication setup.
2	Decentralised control	1.Unaware of global system information; 2.Hard to reach optimum due to individual objectives.
3	Hybrid control	1.Depend on central controllers; 2.May lead to privacy issues.

Going further, most literature on networked MGs adopts AC MGs as basic units, except for references [3, 63] that consider AC/DC hybrid MGs. Optimal strategies of networked MGs based on DC MGs and hybrid MGs may be developed in the future. Much research cannot appropriately capture the main features of resilience-oriented modelling. For instance, except for [66, 67, 74, 75] (consider multiple line faults), other research assumes that the structure of networked MGs remains intact during extreme events. Except for [3, 63, 65, 67], the rest of the papers do not consider the contingency of interrupted interconnection between two networked MGs. Additionally, ancillary devices introduced in [31, 35, 89] may lead to cost problems. Furthermore, operations of networked MGs have a high requirement for communication systems so that communication failures may cause large damage on networked MGs.

Chapter 3

Resilience-driven operation of a hybrid AC/DC MG

3.1 Introduction

As discussed before, both centralised control and hierarchical control approaches require the involvement of central controllers for energy management between MGs. This chapter aims to propose novel mathematical models for the resilience-driven operation of networked MGs based on central controllers. As far as the resilience-driven modelling and operations of MGs are concerned, various techniques have recently been proposed for the resilience enhancement of traditional AC MGs featuring centralised control, since research in this area is a lot more mature. On the one hand, there is much research utilising the grid-connected mode of AC MGs to make preparations for upcoming events via battery management or generator pre-scheduling (e.g., [52, 78, 84]). On the other hand, there are several papers only focusing on the resilience-driven modelling and operations of AC MGs in islanded mode ([40, 72, 77]), e.g., demand-side response.

In comparison with AC MGs, hybrid AC/DC MGs or DC MGs have the advantages to incorporate these DC sources and loads, which is becoming more crucial because of the recent widespread of DC sources and loads [128]. In [126], future MGs are predicted to be hybrid AC/DC MGs. However, there is only limited research focusing on the development of resilience-driven operational strategies for AC/DC MGs or DC MGs. In [71, 76, 82], both feasible islanding and the survivability of critical loads are considered to enhance the resilience of a hybrid MG. Based on above research, a data-driven method is suggested in [41] to estimate the impact of dynamic uncertain

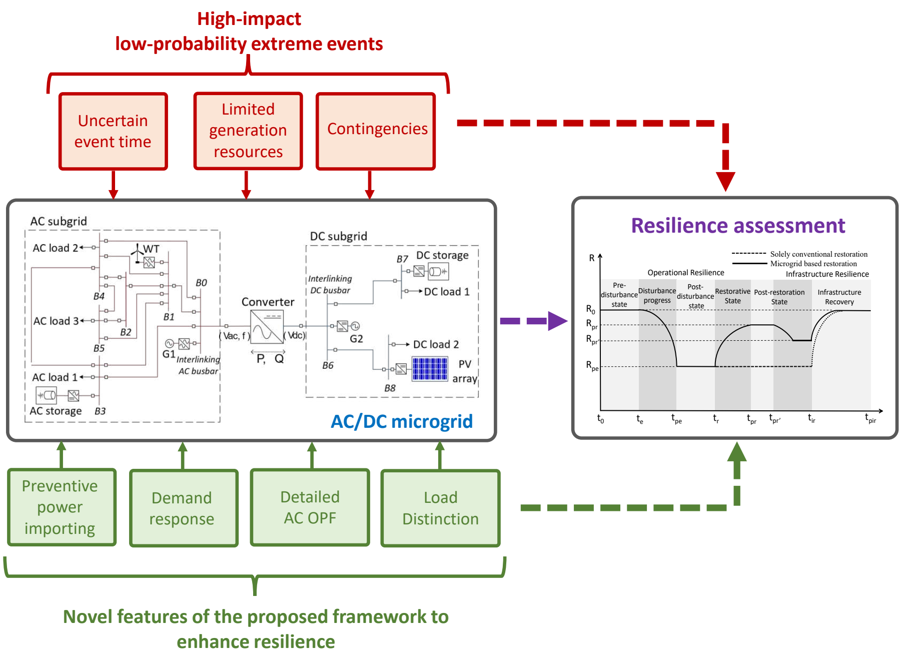

Figure 3.1: Schematic of the MG under consideration.

bounds on the resilient operation of hybrid MGs and a demand response program is considered to reduce load shedding during emergency period. In [85], a robust dispatching model is developed to obtain the robust plans in the worst scenario for a hybrid MG with the consideration of uncertain event occurrence time. In [97], a resilience analysis framework is put forward to study the fault ride-through capability of a DC MG against unknown cyber attacks. Note that these models on AC/DC hybrid MGs consider only power balance equations to control power flows. The omission of operational constraints relating to voltage, power loss and angle variation can lead to inaccurate solutions [129]. Additionally, except for [76], the rest of the papers all assume unlimited energy supply during islanded period.

To summarise, there is no significant research comprehensively considering main modelling details of a realistic resilience scenario, which shall definitely influence the accuracy and reality of optimal solutions. In this chapter, an as realistic as possible resilience-based scenario is considered for accurate optimal solutions. Within this context, limitation of generation resources, uncertain event occurrence time and two types of contingencies, including multiple line faults and the interrupted connection between two subgrids, are investigated capturing main features of extreme events (high uncertainty and severity) and further verifying the effectiveness of the proposed operational strategy. The distinction of critical loads and non-critical loads is also considered. Additionally, to clearly show the influence of limited generation resources, we investigate an islanding period lasting 48 hours after extreme events.

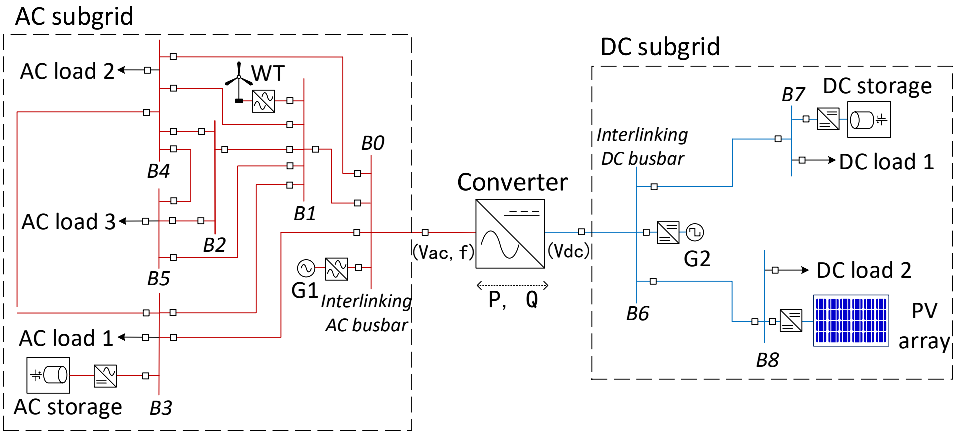

Figure 3.2: Schematic of the MG under consideration.

On the other hand, a comprehensive operational strategy considering both grid-connected mode and islanded mode is developed for the resilience enhancement of an AC/DC hybrid MG. In grid-connected mode, the objective is to minimise the operational cost and to import power from the main grid to be prepared for upcoming events, while the primary objective in islanded mode is to maximise load survivability. Day-ahead scheduling is used to appropriately demonstrate the benefits of BESSs and demand shifting on resilience enhancement. A detailed AC OPF algorithm is incorporated into the proposed model instead of a simple energy management strategy in order to yield more accurate solutions capturing critical operating characteristics, such as voltage profiles, active and reactive power flow, and power losses. Note that the dynamic characteristics related to frequency and voltage deviations require the incorporation of differential equations, which is not considered in the suggested AC OPF algorithm. The outline of the proposed resilience-driven operation strategy is illustrated in Figure 3.1.

3.2 Problem formulation

The structure of the utilised hybrid AC/DC MG is presented in Figure 3.2. AC and DC subgrids are linked through an interlinking converter. Both the AC and DC subgrids have a conventional generator (e.g., diesel generators in AC side and fuel cells in DC side) and an ESS. In the AC subgrid, a WT is installed as renewable energy resource, while a PV is used as renewable energy resource in the DC subgrid. Note that the voltage control capabilities of inverter-based renewable generators and storage units are not considered in the following case studies.

3.2.1 Resilience operation mode before event occurs

Before receiving the first alert signal, the objective is to minimise operational cost, while the main goal after the alert is to try to keep a high level of energy stored in ESS units as well as to reduce operational cost, which is given in (3.1). It is worth noting that the duration of the preventive stage after receiving the event warning is assumed to be deterministic (i.e., fixed duration), while a sensitivity analysis considering different event occurrence time and duration is conducted in case studies to capture the effect of the uncertainty surrounding event occurrence in a simple but rather effective way. In the future, a scenario-based stochastic model can be developed to capture the influence of uncertain event time and duration in a more realistic manner.

The operational cost includes the cost from power exchange with main grid, generation cost and load shedding cost. The first four terms refer to generation cost and load shedding cost in AC and DC subgrids respectively. The next term is the cost of power exchange with main grid, while the last two terms relate to the energy storage level of ESS units in AC and DC subgrids respectively. Because the occurrence time and duration of extreme events cannot be accurately predicted, the MG will start being prepared after receiving the first warning. In other words, the MG will try to keep a high energy storage level of ESS units in the whole preventive stage. Therefore, the values of coefficients α_{AC} and α_{DC} shall be larger than the generation and power exchange cost. It is worth noting that each storage unit may have a different coefficient at different time points according to their potential contributions on load survivability and the possibility of event occurrence. The risk preference of operators also influences the values of α^{AC} and α^{DC}. For instance, a large value of α may be chosen if the load survivability during events is highly valued by the operator, while the coefficients may have a small value if the operator has a high level of risk tolerance.

$$\begin{aligned} F_1 = & \sum_{t\in T}\sum_{g\in N_g^{AC}} c_g P_{g,t}^{AC} + \sum_{t\in T}\sum_{b\in L_{bus}^{AC}} c^{ls} P_{b,t}^{AC,ls} + \sum_{t\in T}\sum_{g\in N_g^{DC}} c_g P_{g,t}^{DC} + \sum_{t\in T}\sum_{b\in L_{bus}^{AC}} c_{ls} P_{b,t}^{DC,ls} \\ & + \sum_{t\in T} c^b P_t^{buy} - \sum_{t\in T} c^s P_t^{sell} - \sum_{t\in T}\sum_{b\in S_{bus}^{AC}} \alpha^{AC} ES_{b,t}^{AC} - \sum_{t\in T}\sum_{b\in S_{bus}^{DC}} \alpha^{DC} ES_{b,t}^{DC} \end{aligned} \tag{3.1}$$

The optimisation is posed as a minimisation problem, subject to the constraints represented by (3.2)-(3.21). Active and reactive power balance equations at each bus b are shown in (3.2) and (3.3), while the classical equations pertaining to power flow problems are presented in (3.4) and (3.5). Equation (3.6) shows the power buying and power selling cannot occur simultaneously and equation (3.7) corresponds to the power exchange limit between the MG and main grid.

$$P_t^{buy} - P_t^{sell} + P_{b,t}^{d} - P_{b,t}^{c} + \sum_{g \in NG_b} P_{g,t} + P_{b,t}^{ls} = P_{b,t}^{ex} + P_{b,t}^{l} + P_t^{ic},\ \forall t \in T,\ \forall b \in N_{bus} \tag{3.2}$$

$$\sum_{g \in NG_b} Q_{g,t} + Q_{b,t}^{ls} = Q_{b,t}^{ex} + Q_{b,t}^{l} + Q_t^{ic},\ \forall t \in T,\ \forall b \in N_{bus} \tag{3.3}$$

$$P_{b,t}^{ex} = \sum_{p \in N_{bus}} V_{b,t} V_{p,t} (G_{bp} cos\delta_{bp,t} + B_{bp} sin\delta_{bp,t}),\ \forall t \in T,\ \forall b \in N_{bus} \tag{3.4}$$

$$Q_{b,t}^{ex} = \sum_{p \in N_{bus}} V_{b,t}, V_{p,t} (G_{bp} sin\delta_{bp,t} - B_{bp} cos\delta_{bp,t}),\ \forall t \in T,\ \forall b \in N_{bus} \tag{3.5}$$

$$P_t^{buy} \cdot P_t^{sell} = 0, \forall t \in T \tag{3.6}$$

$$P_t^{buy}, P_t^{sell} \leq P^{max}, \forall t \in T \tag{3.7}$$

Note that P_t^{ic} and Q_t^{ic} in (3.2) and (3.3) represent the power flow through the interlinking converter connecting AC and DC grids. They are determined by (3.8) based on a droop control strategy, while power exchange limits can be found in (3.9). Δe represents the difference between the frequency and DC voltage, which can be found in (3.10). A normalisation procedure called 'feature scaling' in statistics is utilised to bring the measurements in a per unit basis as described by (3.11), where $\omega^{max}, \omega^{min}$ and $V_{DC}^{max}, V_{DC}^{min}$ correspond to the frequency and DC voltage operational limits, respectively. Therefore, the given dataset in values are converted within the range of [-1,1] to allow comparison of $\hat{\omega}$ and $\hat{V}_{DC}$ and then calculate Δe. This procedure effectively couples DC voltage and AC frequency and eventually obtains the resulting power sharing. More details about the implemented droop control strategy can be found in [129, 130]. However, it is worth noting that both active and reactive power in the employed droop control strategy are used in response to the same deviation Δe, which may be a lack of flexibility. In this context, more flexible control strategies can be utilised for more effective power sharing between AC and DC subgrids.

$$P^{ic} = -\frac{1}{\gamma_p} \Delta e,\ Q^{ic} = -\frac{1}{\gamma_q} \Delta e \tag{3.8}$$

$$\mid P_{ic} \mid \leq P_{ic}^{lim},\ \ \mid Q_{ic} \mid \leq Q_{ic}^{lim} \tag{3.9}$$

$$\Delta e = \hat{\omega} - \hat{V}_{DC} \tag{3.10}$$

$$\hat{\omega} = \frac{2 \cdot \omega - (\omega^{max} + \omega^{min})}{\omega^{max} - \omega^{min}},\ \hat{V}_{DC} = \frac{2 \cdot V_{DC} - (V_{DC}^{max} + V_{DC}^{min})}{V_{DC}^{max} - V_{DC}^{min}} \tag{3.11}$$

Equations (3.12)-(3.14) represent the operational constraints regarding voltage limits, line capacities and angle variation, while equations (3.15)-(3.16) correspond to the power generation limit of conventional generators. Given that a detailed AC OPF is employed to model a hybrid MG capturing voltage and frequency, ramp-up and ramp-down constraints have not been considered as no significant changes of generation would be allowed within one time interval.

$$V^{min} \leq V_{b,t} \leq V^{max},\ \forall t \in T,\ \forall b \in N_{bus} \tag{3.12}$$

$$S_{i,t} \leq S_i^{lim},\ \forall t \in T,\ \forall i \in N_{br} \tag{3.13}$$

$$|\delta_{b,t} - \delta_{p,t}| \leq \delta^{lim},\ \forall t \in T,\ \forall b, p \in N_{bus} \tag{3.14}$$

$$P_g^{min} \leq P_{g,t} \leq P_g^{max},\ \forall t \in T,\ \forall g \in N_g \tag{3.15}$$

$$Q_g^{min} \leq Q_{g,t} \leq Q_g^{max},\ \forall t \in T,\ \forall g \in N_g \tag{3.16}$$

Inequalities (3.17) and (3.18) denote the limits for the charging and discharging power of ESSs, while equation (3.19) ensures that charging and discharging cannot occur simultaneously. Equation (3.20) gives the limits for minimum and maximum energy storage, which can also be presented via the state-of-charge (SOC) level. The dependence of energy storage level at each time interval on the previous time step is introduced in equation (3.21). Note that these constraints only capture the features of the AC subgrid; therefore, equations (3.12), (3.13), (3.15) and (3.17)-(3.21) are duplicated in this model and accordingly modified to account for the DC subgrid. In other words, to simplify the model formulation, the DC subgrid model developed in this chapter follows similar principles as the AC subgrid without extra control strategies, where the detailed formulation of the DC subgrid can be found in [131].

$$0 \leq P_{b,t}^c \leq P_b^{max},\ \forall t \in T,\ \forall b \in S_{bus} \tag{3.17}$$

$$0 \leq P_{b,t}^d \leq P_b^{max},\ \forall t \in T,\ \forall b \in S_{bus} \tag{3.18}$$

$$P_{b,t}^c \cdot P_{b,t}^d = 0,\ \forall t \in T,\ \forall b \in S_{bus} \tag{3.19}$$

$$ES_b^{min} \leq ES_{b,t} \leq ES_b^{max}, \forall t \in T, \forall b \in S_{bus} \tag{3.20}$$

$$ES_{b,t} = ES_{b,t-1} + (\eta^c P_{b,t}^c - \eta^d P_{b,t}^d)\Delta t,\ \forall t \in T - \{1\},\ \forall b \in S_{bus} \tag{3.21}$$

3.2.2 Emergency operation mode during the event

In emergency mode, it is assumed that the hybrid MG will be disconnected from the main grid and severe line outages can happen inside the MG. However, note that it is also realistic to assume that MGs stay connected with the main grid during extreme events (e.g., supporting the critical load restoration in the main grid), which is not considered in this thesis. The objective for minimising operational cost would translate into maximisation of load survivability due to the emergency situation, given in (3.22). Note that load curtailment is coupled with a significantly high value of lost cost c_{ls}.

$$F_2 = \sum_{t \in T} \sum_{g \in N_g^{AC}} c_g P_{g,t}^{AC} + \sum_{t \in T} \sum_{b \in L_{bus}^{AC}} c^{ls} P_{b,t}^{AC,ls} + \sum_{t \in T} \sum_{g \in N_g^{DC}} c_g P_{g,t}^{DC} + \sum_{t \in T} \sum_{b \in L_{bus}^{AC}} c_{ls} P_{b,t}^{DC,ls} \tag{3.22}$$

In addition to equation (3.2), other constraints in this mode are same as those in resilience operation mode. Because power exchange is interrupted, the active power balance equation is modified as equation (3.23). Furthermore, it is assumed that the MG has limited generation resources in islanded mode, which accounts for equations (3.24) and (3.25). Note that constraints relating to limited generation resources also need to be duplicated and modified for the DC subgrid.

$$P_{b,t}^d - P_{b,t}^c + \sum_{g \in NG_b} P_{g,t} + P_{b,t}^{ls} = P_{b,t}^{ex} + P_{b,t}^l + P_t^{ic}, \ \forall t \in T, \ \forall b \in N_{bus} \tag{3.23}$$

$$GS_{g,t} = GS_{g,t-1} - P_{g,t}\Delta t, \ \forall t \in T_e/\{1\}, \forall g \in N_g \tag{3.24}$$

$$GS_g^{min} \leq GS_{b,t} \leq GS_g^{Ini}, \forall t \in T, \forall g \in N_g \tag{3.25}$$

Equations (3.26)-(3.28) correspond to the demand shift response in AC subgrid. As described in constraint (3.26), the ratio β_f ($0 \leq \beta_f \leq 1$) represents the maximum percentage of load type f for load shift and T_f is the acceptable shifting horizon for load type f. $\beta_f = 0$ implies that load f does not exhibit any time-shifting flexibility, while $\beta_f = 1$ implies that the whole demand can be shifted in acceptable time horizon. Constraint (3.27) ensures that load shifting is energy neutral for any types of loads within the operating horizon and load shifting does not involve energy losses. In equation (3.28), $P_{b,t}^{l,base}$ means the total base load without load shifting and $P_{b,t}^l$ exhibits the total load of bus b at time point t after load shifting. The constraints related to limited generation resources and demand shift also need to be duplicated and modified for the DC subgrid, i.e., with the DC notations.

$$-\beta_f P^l_{b,f,t} \leq P^{lsh}_{b,f,t} \leq \beta_f P^l_{b,f,t}, \forall t \in T_f, \forall f \in N_L, \forall b \in N_{bus} \tag{3.26}$$

$$\sum_{t \in T_f} P^{lsh}_{b,f,t} = 0, \forall f \in N_L, \forall b \in N_{bus} \tag{3.27}$$

$$P^l_{b,t} = P^{l,base}_{b,t} + \sum_{f \in N_L} P^{lsh}_{b,f,t}, \forall t \in T_f, \forall f \in N_L, \forall b \in N_{bus} \tag{3.28}$$

3.2.3 Resilience index

A resilience index (RI) (3.29) is used to evaluate the effects of MGs on load survivability, which corresponds to the percentage of total curtailed loads before infrastructure restoration starts (e.g., dispatch of repair crews). This metric will be 0 when a MG can entirely restore all the loads within this period, while a bigger RI is coupled with worse performance of MGs. In this chapter, the original performance $R_0(t)$ (i.e., pre-disturbance state) and the real-time performance $R(t)$ (i.e., performance across the event evolution) consider both critical loads and non-critical loads. As such, $R(t)$ can be calculated by the performance of critical loads $R^c(t)$ and non-critical loads $R^n(t)$, which are multiplied by different weighting factors w^c and w^n respectively. Note that selection of the weighting factors w^c and w^n indicates the significance of critical loads and non-critical loads ($w^c > w^n$).

$$RI = \frac{\int_0^T (R_0(t) - R(t))}{\int_0^T (R_0(t))}, \ where\ R_0(t) = w^c R^c_0(t) + w^n R^n_0(t),\ R(t) = w^c R^c(t) + w^n R^n(t). \tag{3.29}$$

3.3 Case studies

We assume that the first warning occurs at $t = 0$, and then the hybrid MG switches into resilience operation mode to import power from main grid and be prepared. When the extreme event occurs, the MG switches into islanded mode (the occurring time remains uncertain) to protect itself for at least two days. To appropriately present the advantages of ESS units on resilience enhancement, the day-ahead scheduling method is employed to run the AC OPF algorithm to make decisions about power output of generators, power exchange and battery energy management. WT and PV devices are considered as non-dispatchable generation resources and have a capacity of 100 kW and 50 kW respectively, while wind power, solar power and load profiles are extracted from [129] and can be found in Figure 3.3. The parameters associated with lines, generators and ESSs are specified in Table 3.1-3.3 respectively.

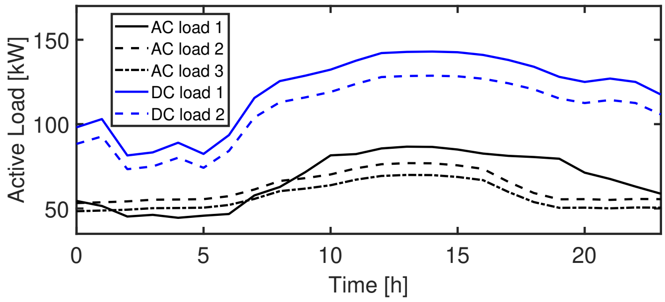

(a)

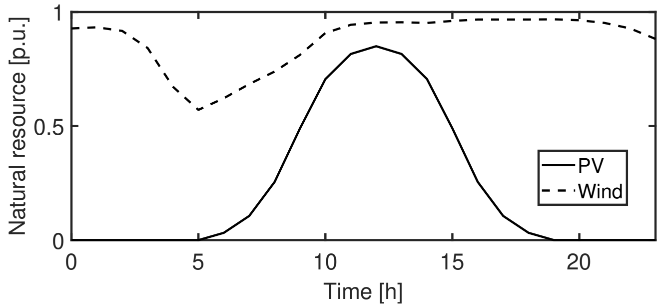

(b)

Figure 3.3: (a) Load profiles, (b) Wind profiles and PV profiles.

It is more realistic to assume that not all loads would be critical, hence this simulation extends the model by introducing discrimination of loads into critical and non-critical. For example, in a building-scale MG the critical loads could be lights and lift motors and the non-critical loads could be kitchen and toilet appliances [129]. Similar to [71], it is assumed that loads L_3 in bus 3 of AC subgrid (around 30% of total loads) and L_7 in bus 7 of DC subgrid (around 50% of total loads) are critical loads with high curtailment cost, while the rest of the loads are non-critical loads with relatively low curtailment cost. It is worth noting that there is no standard for the ratio of critical and non-critical loads in a power network, and the ratio and location of critical loads will affect the optimal scheduling results.

3.3.1 Simulation I - Effect of preventive power importing

We assume there are 15000 kWh energy reserve in AC subgrid and 6000 kWh energy reserve in DC subgrid. Note that, according to this assumption, the AC subgrid has enough energy to support itself for a long period, while the DC subgrid has a large risk of energy shortage. In the first

Table 3.1: Line data corresponding to the hybrid AC/DC MG of Figure 2

Line between bus i $\rightarrow$ j	Reactance ($X_{li}[p.u.]$)	Resistance ($R_{li}[p.u.]$)	Capacitance ($C_{li}[p.u.]$)	Maximum flow [kVA]
0 $\rightarrow$ 1	0.200	0.100	0.040	100
0 $\rightarrow$ 3	0.200	0.050	0.040	100
0 $\rightarrow$ 4	0.300	0.080	0.060	100
1 $\rightarrow$ 2	0.250	0.050	0.060	60
1 $\rightarrow$ 3	0.100	0.050	0.020	60
1 $\rightarrow$ 4	0.300	0.100	0.040	60
1 $\rightarrow$ 5	0.200	0.070	0.050	60
2 $\rightarrow$ 4	0.260	0.120	0.050	60
2 $\rightarrow$ 5	0.100	0.020	0.020	60
3 $\rightarrow$ 4	0.400	0.200	0.080	60
4 $\rightarrow$ 5	0.300	0.100	0.060	60
6 $\rightarrow$ 7	-	1.040	-	120
6 $\rightarrow$ 8	-	1.040	-	120

Table 3.2: Characteristics of generators in the hybrid MG

Type	Subgrid	Min-Max Capacity (kW)
Diesel generator	AC subgrid	0-150
Fuel cell	DC subgrid	0-150

Table 3.3: Characteristics of ESS units in the hybrid MG

Type	Subgrid	Min-Max SOC (kWh)	Power capacity (kW)	Initial SOC (kWh)
ESS	AC subgrid	0-200	50	100
ESS	DC subgrid	0-2000	100	100

investigated scenario, the hybrid MG needs to be prepared at every time point (from t = 0h to t = 11h) in the preventive stage. Note that a sensitivity analysis on different event occurrence time will be shown later to capture the influence of uncertain nature of an extreme event. A 48-hour islanding period is considered as the emergency situation to appropriately present the advantages of the proposed resilience strategy and the impacts of energy shortage. Furthermore, a strategy which does not consider preventive power importing (i.e., base case without resilience enhancement) is simulated for comparison. The objective function of the base case ignores the last two terms in equation (3.1), which means that no preventive power importing strategy is applied. Constraints in the base case are the same as those in the resilience case.

Figure 3.4(a) shows that the resilience strategy guarantees the survivability of critical loads in the first 24-hour islanding period, while the strategy without resilience causes 144.58 kWh load shedding of critical loads. Additionally, load shedding of non-critical loads is reduced from 422.43 kWh to 273.82 kWh. Figure 3.4(b) shows that load shedding occurs in both cases when the hybrid MG switches into islanded mode, because of the interrupted connection between the MG and main grid. Additionally, the proposed resilience strategy results in less load shedding in the first 24-hour islanded period than the strategy without resilience. The reason is that more energy is stored in ESS units through power importing in preventive stage. Figure 3.5(a)-3.5(b) indicate that storage units in both AC and DC sides charge in the preventive stage and keep a high state of energy. As one of the most common proactive ways to enhance resilience, the advantages of preventive power importing have been appropriately presented. However, in the second 24-hour period, both cases yield large load shedding, because of the deficiency of generation resources in DC subgrid. Figure 3.4(b) also illustrates that the proposed strategy only has a positive effect on load survivability in the first 24 hours of islanded mode. The reason is that imported power in the proposed strategy is not enough to support a longer islanding period, because of the limitation of battery capacity and the duration of preventive stage. The further load shedding primarily demonstrates the impact of energy deficiency on resilience.

With respect to the suggested resilience index, Table 3.4 shows that, the proposed strategy obtains a smaller RI value (0.0117) in the first 24 hours than the strategy without resilience (0.0427), while the same RI value is achieved in both cases during the last 24 hours because of the energy deficiency in DC subgrid. To summarise, with the consideration of preventive power importing, the resilience of the AC/DC hybrid MG (RI value from 0.1184 to 0.1028) is enhanced.

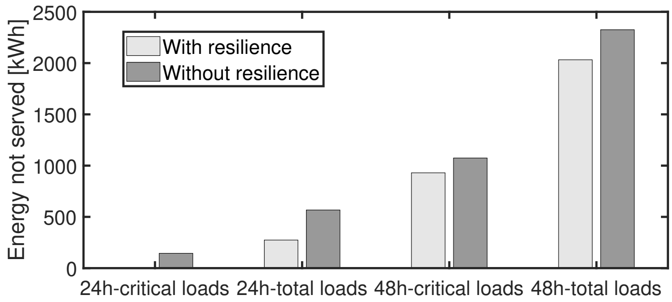

(a)

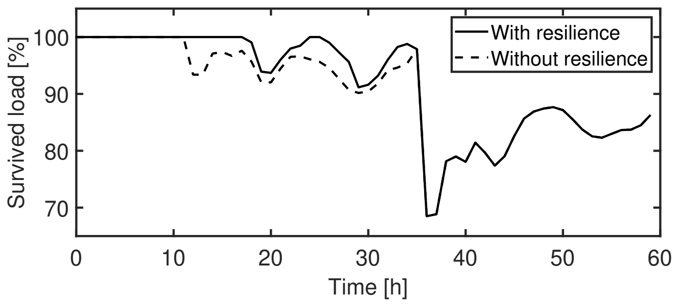

(b)

Figure 3.4: Simulation I: (a) Energy not served [kWh], (b) Percentage of survived load.

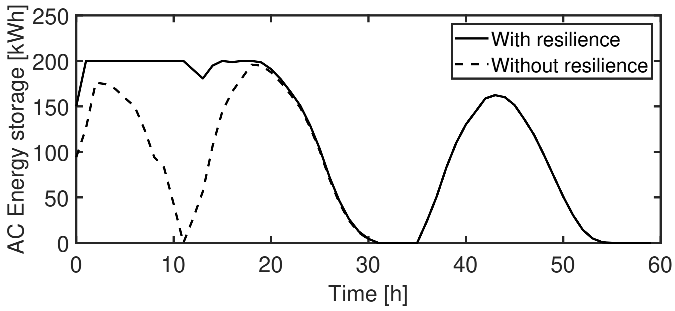

(a)

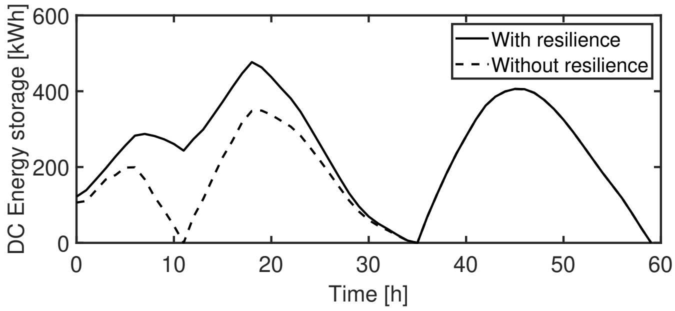

(b)

Figure 3.5: Simulation I: (a) Battery storage change in AC subgrid, (b) Battery storage change in DC subgrid.

Table 3.4: Resilience index in Simulation I

	No resilience	With resilience
RI (12-59h)	0.1184	0.1028
RI (12-35h)	0.0427	0.0117
RI (36-59h)	0.1940	0.1940

Furthermore, as depicted in Figure 3.4(a), both cases have a great deal of critical load shedding in DC subgrid in the second 24-hour islanding period. Note that the critical load shedding takes approximately 50% of total load shedding in the last 24 hours and all curtailed loads are from DC subgrid. In other words, the discrimination of critical and non-critical loads has no significant effects on reducing critical load shedding in the last 24 hours. A potential explanation to this would be the

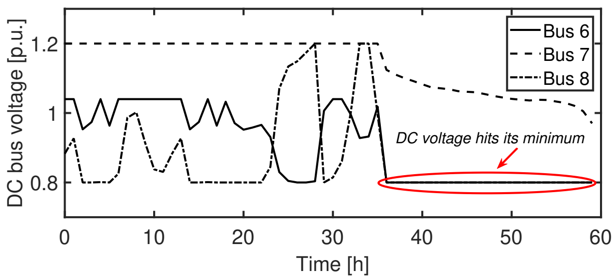

(a)

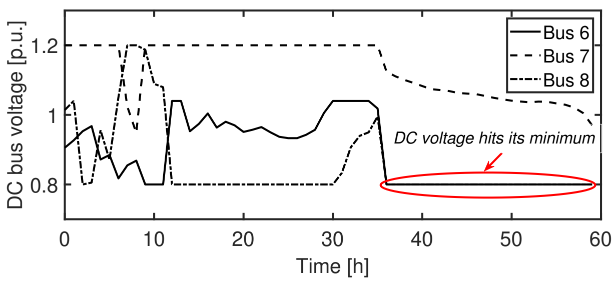

(b)

Figure 3.6: Simulation I: (a) Bus voltage in DC subgrid with resilience, (b) Bus voltage in DC subgrid without resilience.

fact that DC voltage in bus 8 (connecting non-critical loads) is reaching its minimum allowed value (i.e., 0.8 p.u.) avoiding more non-critical loads in bus 8 to be curtailed; this is illustrated in Figure 3.6. Because of the voltage constraints, the hybrid MG has to curtail critical loads to ensure power balance. Note that voltage at bus 6 connected with a conventional generator is also down to the minimum value, which means no more loads can be supplied in this period. This is an important aspect of the proposed model, as typical energy management systems found in the literature would neglect the influence of voltage and obtain less critical load shedding; this would lead to violation of technical requirements. Even though more load shedding is caused through the proposed AC OPF algorithm, the result ensures an intact power system with no violation of technical requirements; this would be increasingly important in larger-scale MGs, as more and more MGs are embedded into distribution networks.

Note that we also assume that the event may happen at any time point in the preventive stage because of its uncertain nature. In this scenario, the hybrid MG needs to be prepared at every time point from receiving the first warning about an event to event occurrence. To entirely present the effects of preventive power importing on resilience enhancement, a sensitivity analysis on different event occurrence time is done and the results can be seen as follows. Figure 3.7 shows that the case with resilience obtained less load shedding than the case without resilience for all the different time points of event occurrence. It can also be concluded that a longer preventive stage allows more power injection and achieves more resilience.

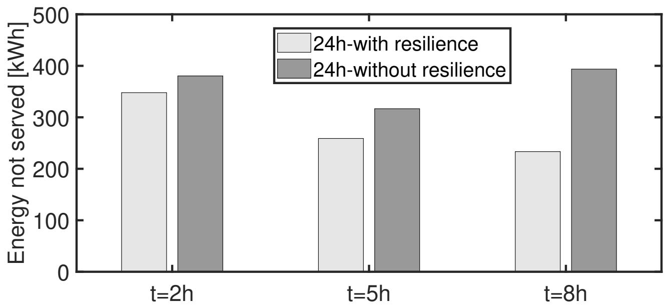

Figure 3.7: Simulation I: Sensitivity analysis on different event occurrence time points.

3.3.2 Simulation II - Effect of demand shifting

Demand shifting may be one of the most effective and economic ways to reduce load shedding during extreme events, compared with other strategies (such as MPSs or EVs). In this subsection, the effects of demand shifting on reducing load shedding and enhancing resilience are appropriately investigated. Preventive power importing and discrimination of loads into critical and non-critical are also considered. Note that the effect of limited generation resources has already been illustrated in Simulation I, so a 24-hour islanding period is considered to simplify this case. Additionally, we assume that shiftable loads can be shifted across the whole scheduling horizon.

Figure 3.8(a) shows that non-critical load shedding is gradually reduced as the percentage of shiftable loads increases; for clarity, no critical load shedding is caused when demand shifting is applied. However, when the percentage of shiftable loads is over 15%, demand shifting has no effects on load survivability. Figure 3.8(b) shows the change of resilience index RI, which is reduced with the increase of the percentage of shiftable loads. When the percentage of shiftable loads is over 15%, resilience index RI reaches the minimum value (0.0054).

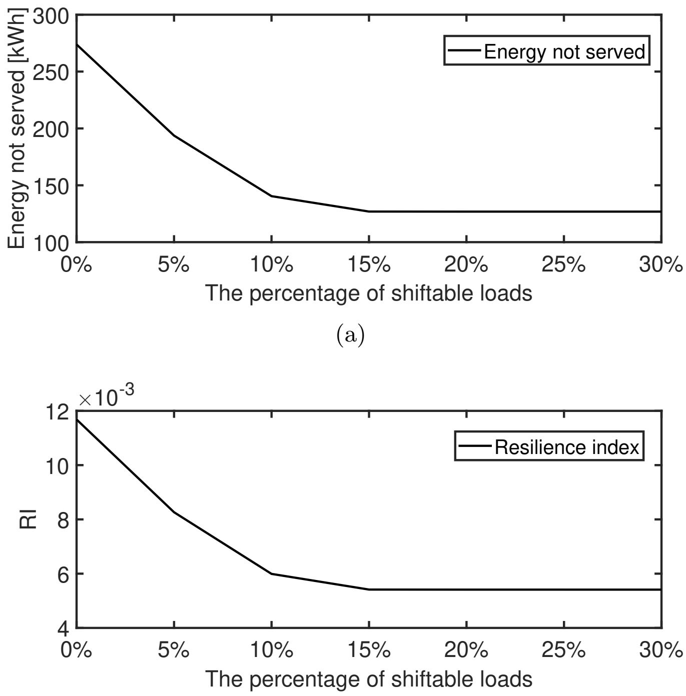

(b)

Figure 3.8: Simulation II: (a) Energy not served [kWh] for non-critical loads under different percentage of shiftable loads, (b) Change of RI with the percentage of shiftable loads.

3.3.3 Simulation III - Impact of contingencies

Most existing literature assumes that the structure of an islanded MG is intact during extreme events. However, a MG can be damaged because of the highly uncertain nature of extreme events. To account for such cases, two types of contingencies including multiple line faults (contingency 1) and interrupted connection between AC and DC subgrids (contingency 2) are considered here to appropriately mimic a realistic scenario and further highlight the advantages of the proposed resilience strategy. Both preventive power importing and demand shifting (15% shiftable loads) are considered. As far as multiple line faults are concerned, it is assumed that the line between bus 3 and bus 4 and the line between bus 4 and bus 5 are damaged during the investigated event. Figure 3.9(a) presents that the resilience strategy still obtains less load shedding than a strategy without resilience, while the proposed strategy successfully protects critical loads in the first 24 hours after extreme events. Tab. 3.5 shows that the resilience strategy also obtains a lower resilience index RI (0.0056) than a strategy without resilience (0.0431).

In the simulated case, the power transfer from the AC subgrid to the DC subgrid supports the latter to reduce its load shedding. However, this connection can be interrupted during extreme events, as is the case in this simulation. Specifically, an interruption between the two subgrids has been modelled for 10 hours. Figure 3.9(b) demonstrates that the proposed resilience strategy obtains much less critical load shedding (from 340.62 kWh to 68.37 kWh) and total load shedding (from 729.64 kWh to 336.09 kWh) than a strategy without resilience in the first 24 hour islanding period. Bus voltage changes in both cases are shown in Figure 3.10. When the connection between the AC and DC subgrids is interrupted, DC voltages in all three buses are reduced and particularly bus 6 and bus 8 are down to the minimum value; see red circles on Figure 3.10 indicating DC voltage reaching its minimum limit.

Table 3.5 shows that the resilience strategy also obtains a lower resilience index RI (0.0210) than a strategy without resilience (0.0747), because of the consideration of preventive power importing and demand shifting. Even with the consideration of contingencies, the advantages of the proposed strategy are clearly shown with these results.

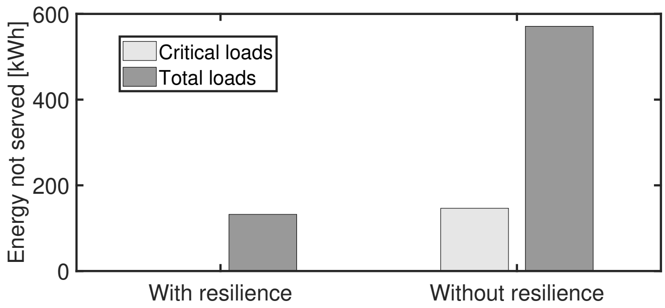

(a)

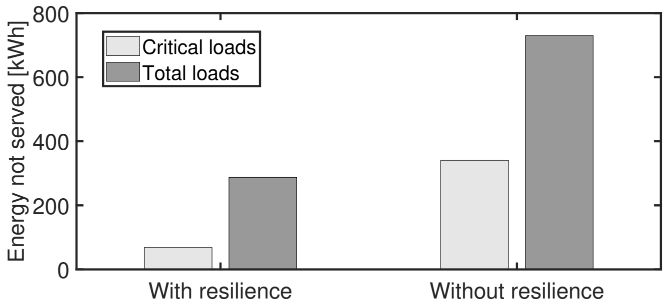

(b)

Figure 3.9: Simulation III: (a) Energy not served [kWh] under multiple line faults, (b) Energy not served [kWh] under interrupted connection.

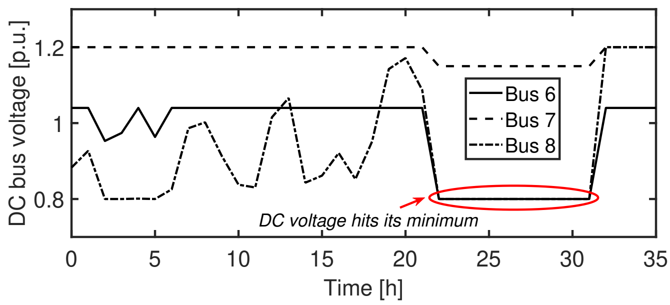

(a)

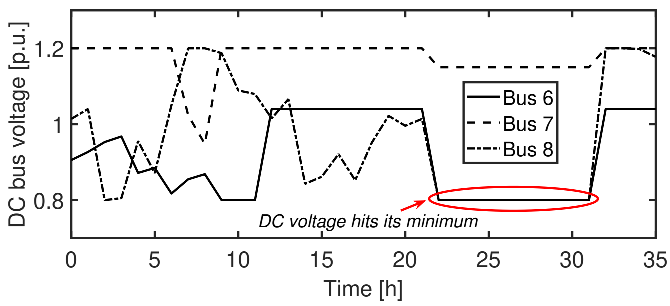

(b)

Figure 3.10: Simulation III: (a) Bus voltage in DC subgrid under interrupted connection [with resilience], (b) Bus voltage in DC subgrid under interrupted connection [without resilience].

3.4 Cost analysis

Extensive simulations considering different case studies have been presented to verify the effectiveness of the proposed resilience strategy. In all simulations, the proposed resilience strategy obtains better solutions (lower load shedding and a better *RI* value) than a strategy without resilience. In simulations I-III, the proposed resilience strategy successfully guarantees the survivability of critical loads in the first 24-hour period of the scheduling horizon. Table 3.6 shows that, even though power importing brings slightly higher operation cost in preventive stage, it is worth employing this strategy for resilience purposes, as load survivability is more important than economical profits during emergency situations; of course this is appropriately reflected in the total operation cost. It can be deducted that the proposed strategy would become more economical if the event occurrence time is accurately predicted, because it only needs to improve the storage level of ESSs in one specific time point rather than the whole preventive stage. Table 3.6 also shows that demand shifting is an effective way to balance load and power and reduce load shedding. With the increase of the percentage of shiftable loads, the total operational cost is gradually reduced and the generation cost of conventional generators is slightly increased, which means that the energy has been more effectively used for load survivability. Generally, the cost analysis presented in Table 3.6 is consistent with the results for resilience index shown in previous sections.

Table 3.5: Resilience index in Simulation III

	No resilience	With resilience
24h-RI (line faults)	0.0431	0.0056
24h-RI (interrupted connection)	0.0747	0.0210

Table 3.6: Comparison of costs between simulations I-III

	Preventive cost (£)	Generation cost (£)	Shedding cost (£)	Total cost (£)
S1 - Base case (without resilience)	423.16	943.18	50037.5	51403.84
S1 - Resilience case (no load shifting)	496.43	921.40	13691.40	15109.23
S2 - Resilience (5% shiftable loads)	496.43	933.42	9684.80	11114.65
S2 - Resilience (10% shiftable loads)	496.43	941.50	7022.10	8190.03
S2 - Resilience (15% shiftable loads)	496.43	943.52	6345.23	7785.18
S3 - Resilience and contingency 1	496.43	943.52	6609.67	8049.62

Chapter 4

A hierarchical control approach for networked MGs

4.1 Introduction

Recently, much research has focused on the benefits of networked MGs on resilience enhancement. Energy sharing between networked MGs is an effective way to reduce load shedding [44, 127]. In comparison with a single MG, networked MGs can provide operational flexibility and enhance resilience [132]. Centralised control, distributed control and hierarchical control are three basic approaches to operate networked MGs. Planning and operation strategies based on centralised control have been widely developed to enhance the resilience of networked MGs (e.g., [67, 74, 95, 133]. However, each MG normally has fixed boundaries and self-controllability due to customer privacy. The requirement of centralised control for high information sharing among MGs may introduce security problems.

A detailed survey about previous studies on networked MGs can be found in Table 4.1. It is shown that there is no significant amount of literature considering both networked MGs and mobile storage units. Additionally, most papers utilise linearised OPF or EMS to model power systems, which lead to inaccurate solutions [134]. In fact, only one reference ([74]) considers the utilisation of the entire AC OPF; nevertheless, this paper employs centralised control method for MG operation, which leads to large computing burden (the paper only considers a 2-hour scheduling horizon to reduce computing time). Furthermore, most papers tend to utilise radial networks for case studies. However, meshed networks may guarantee a higher resilience level than radial networks, when extreme events happen; needless to say that meshed networks are common in power systems across the globe. In this chapter, a hierarchical control approach incorporating uncertainties and contingencies based on a detailed AC OPF formulation is developed to model networked MGs, while both static storage units (e.g., batteries) and mobile storage units (e.g., EVs) are employed for load restoration.

4.2 Operation of networked MGs

Figure 4.1 illustrates that three MGs are connected with each other and are controlled by a central controller and multiple local controllers, where the central controller will only make decisions on the power exchange among MGs. There is no connection between the main grid and MGs during extreme events; nevertheless, a MG can utilise tie-lines or smart switches to be connected and exchange power with nearby MGs. The main task of MG operation during extreme events is to maintain the continuous supply of critical loads, reduce load shedding [15] or maximise the cumulative service time of MGs to loads [14]. As such, the final objective of each MG local controller in the network is to minimise load shedding cost including critical and non-critical load shedding, which can be found in (4.1). Multiple scenarios are simulated via stochastic programming to capture the uncertainties with renewable energy sources and loads and ensure the effectiveness of the proposed resilience strategy.

$$F = \sum_{s \in S} p_s \sum_{t \in T} \sum_{b \in L_{bus}} c^{ls} P^{ls}_{b,t,s} \tag{4.1}$$

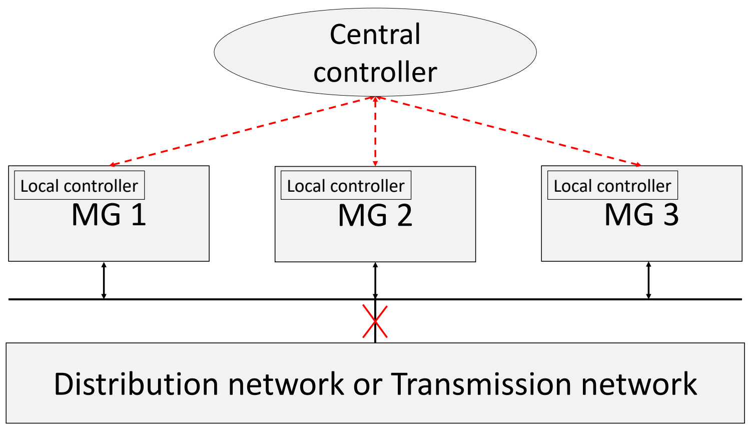

Figure 4.1: Networked MGs based on hierarchical control.

A flowchart of the proposed resilience enhancement strategy based on hierarchical control and

Table 4.1: Survey of previous studies.

Ref	Model	MG structure (radial/meshed)	Power Flow	Storage units	Control methods	Time horizon	Uncertainty	Contingencies
[64]	MILP	Both	EMS	ES	Centralised	yes	No	Islanding, single fault
[53]	MILP	Radial	Linearised OPF	ES	Centralised	yes	Load, RES	Islanding, multiple faults
[95]	MILP	Radial	Linearised OPF	No	Centralised	yes	No	Islanding, multiple faults
[74]	MINLP	Both	AC OPF	ES	Centralised	yes (2 h)	Load, RES	Islanding, multiple faults
[67]	MILP	Radial	Linearised OPF	ES, MER	Centralised	yes (5 h)	Load, RES	Islanding, multiple faults
[135]	MILP	Both	EMS	ES	Decentralised	yes	No	Islanded MG
[75]	MILP	Radial	distflow	ES	Decentralised	yes	Load, RES	Islanding, multiple faults
[66]	MILP	Radial	EMS	ES	Decentralised	no	No	Islanding, multiple faults
[88]	MILP	Radial	distflow	no	Decentralised	no	Load, RES	Islanded MG
[63]	MILP	Both	EMS	ES, static EV	Decentralised	yes	Load, RES	Islanded MG
[3]	MILP	Both	EMS	ES	Hierarchical	yes	No	Islanded MG
[65]	MILP	Both	EMS	ES	Hierarchical	yes	No	Islanded MG
[136]	MILP	Both	EMS	ES	Hierarchical	yes	Load, RES	No
[137]	MILP	Radial	distflow	ES	Hierarchical	yes	Load, RES	Islanded MG
Proposed method	MINLP	Both	AC OPF	ES, mobile EV	Hierarchical	yes	Load, RES	Islanding, multiple faults

EVs can be found in Figure 4.2. During an extreme event, each MG switches into islanded mode and runs its AC OPF algorithm via local controller to calculate their power surplus or power shortage for the next scheduling horizon (e.g., 24 hours). Voltage limitations and potential power loss through power flow are considered in the utilised AC OPF. The results will be reported to the central controller, which makes final decisions on the power exchange among MGs and then returns these decisions to each MG respectively. According to these decisions, each MG employs once again its local AC OPF algorithm (capturing EV routing) to eventually schedule its generation resources ensuring load survivability. Note that EVs are only used as back-up resources at the third stage due to potential privacy concerns. In other words, EV fleets will be employed for resilience enhancement only when there still exists load shedding at the third stage.

Going further, as suggested in [16,59], the proposed stochastic hierarchical control approach can choose to utilise utility-owned EV units for resilience enhancement. Note that EVs have been used for load restoration purposes; this extends to both research applications and real-world examples [16, 59]. Furthermore, it would be interesting to discuss the possibilities of utilising privately-owned EVs for resilience enhancement. Extreme events are characterised by high impact and low probability. The main task during extreme events is to maintain the continuity of supply to critical loads. In this context, resilient responses against extreme events may require coordinated efforts of different infrastructures and organizations. Thus, the utility may be able to obtain the temporary authority needed to use even privately-owned EVs for load restoration [59].

4.2.1 Hierarchical control for power sharing

After MGs switch into islanded mode, load shedding may be caused because of the loss of power support from the main grid and the potential limitation of available generation resources. To minimise load shedding, a hierarchical control approach is employed to make decisions on power exchange among MGs.

Stage 1 - calculate power shortage or power surplus

In the first stage, every MG runs AC OPF algorithm in the stand-alone condition and calculates power shortage or power surplus via a day-ahead scheduling method. These signals are sent to the central controller. The local objective function for each MG at stage 1 is given by (4.2), where the first two terms are related to the cost for power surplus and power shortage and the last term

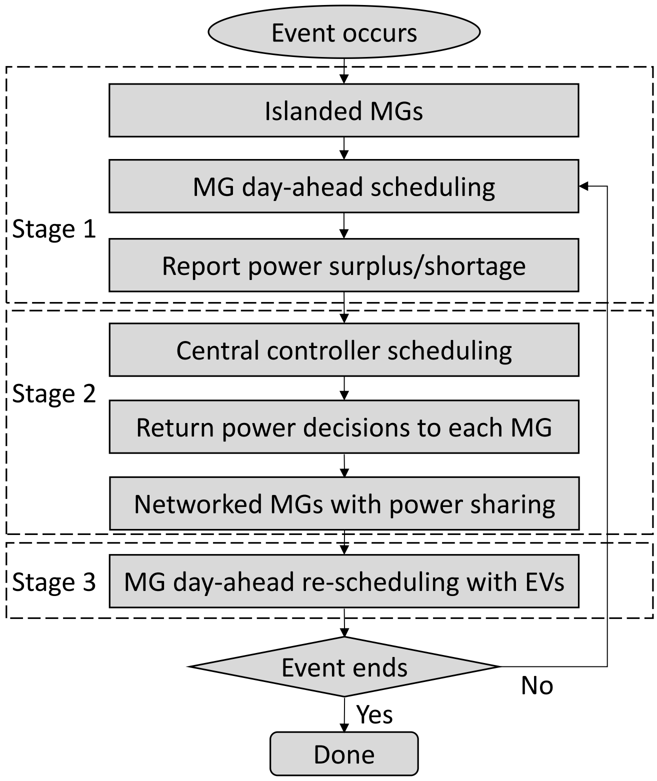

Figure 4.2: The proposed resilience strategy based on hierarchical control and EVs.

corresponds to the potential load shedding cost under different scenarios. Note that the process of calculating power shortage/surplus for each MG has been formulated as a stochastic problem in which decisions are made via a set of scenarios [138]. Variables of both here-and-now and wait-and-see type are included in equation (4.2), where variables on power exchange (i.e., the first two terms) are regarded as here-and-now decision variables and the others (e.g., load shedding or power output of generators) are wait-and-see variables depending on the realisation of each scenario.

$$F_1 = \sum_{t \in T} c^{sho} P_t^{sho} - \sum_{t \in T} c^{sur} P_t^{sur} + \sum_{s \in S} p_s \sum_{t \in T} \sum_{b \in L_{bus}} c^{ls} P_{b,t,s}^{ls} \tag{4.2}$$

The optimisation is posed as a minimisation problem, subject to typical AC OPF constraints. The active power balance equation at the exchange bus b is shown in (4.3), while the reactive power balance equation is shown in (4.4). Classical equations pertaining to power flow problems are presented in (4.5) and (4.6). Equation (4.7) shows that power shortage and power surplus cannot occur simultaneously, while equation (4.8) corresponds to the power exchange limit between the MG and nearby MGs. Note that T_{ij}^{max} means the tie-line capacity between two MGs (e.g., MG i and MG j). Furthermore, extreme events may cause potential damage on energy supply chains, such as gas networks and fuel networks, and therefore generation resources (e.g., fuel reserve) within one

MG may be limited [15]. It is, therefore, reasonable to assume that each MG has limited generation resources during extreme events, which accounts for equations (4.9) and (4.10). GS_g^{Ini} corresponds to the initial energy reserve of a MG when an event occurs and generator g will fail to operate when GS_g^{Ini} reaches its minimum value GS_g^{min}. ESS-related constraints and operational constraints on voltage limit, line capacity, angle and generator limits are all included into the model.

$$P_t^{sho} - P_t^{sur} + P_{b,t,s}^{d} - P_{b,t,s}^{c} + P_{b,t,s}^{ls} + \sum_{g \in NG_b} P_{g,t,s} = P_{b,t,s}^{ex} + P_{b,t,s}^{l},\ \forall t \in T,\ \forall b \in N_{bus},\ \forall s \in S \quad (4.3)$$

$$\sum_{g \in NG_b} Q_{g,t,s} + Q_{b,t,s}^{ls} = Q_{b,t,s}^{ex} + Q_{b,t,s}^{l},\ \forall t \in T,\ \forall b \in N_{bus},\ \forall s \in S \quad (4.4)$$

$$P_{b,t,s}^{ex} = \sum_{p \in N_{bus}} V_{b,t,s} V_{p,t,s} (G_{bp} cos\delta_{bp,t,s} + B_{bp} sin\delta_{bp,t,s}),\ \forall t \in T,\ \forall b \in N_{bus},\ \forall s \in S \quad (4.5)$$

$$Q_{b,t,s}^{ex} = \sum_{p \in N_{bus}} V_{b,t,s} V_{p,t,s} (G_{bp} sin\delta_{bp,t,s} - B_{bp} cos\delta_{bp,t,s}),\ \forall t \in T,\ \forall b \in N_{bus},\ \forall s \in S \quad (4.6)$$

$$P_{sho,t} \cdot P_{sur,t} = 0,\ \forall t \in T \quad (4.7)$$

$$P_{sho,t}, P_{sur,t} \leq T_{ij}^{max},\ \forall t \in T \quad (4.8)$$

$$GS_{g,t,s} = GS_{g,t-1,s} - P_{g,t,s} \Delta t\ \forall t \in T - \{1\},\ \forall g \in N_g \quad (4.9)$$

$$GS_g^{min} \leq GS_{b,t,s} \leq GS_g^{Ini},\ \forall t \in T,\ \forall g \in N_g,\ \forall s \in S \quad (4.10)$$

Stage 2 - make decisions on power exchange

In the second stage, the central controller makes decisions about the power exchange between MGs and then sends these decisions back to the local controller of each MG. The objective function of the central controller is captured in (4.11), which aims to minimise the total power shortage of networked MGs. Note that there exists a possibility that not every MG can get enough power to cover its shortage. In other words, load shedding may still exist after the power exchange between MGs.

$$F_2 = \sum_{t \in T} \sum_{i \in M} c_{sho} P_{fsho}(i,t) \quad (4.11)$$

The constraints of the second stage can be found in equations (4.12)-(4.16). Among these, equation (4.12) refers to the power balance, while constraints (4.13) and (4.14) refer to the limitations of extra generation and final power shortage. $P_{ij,t}^{buy}$ and $P_{ij,t}^{sell}$ correspond to active power bought and sold from MG j to MG i at time t respectively. Constraint (4.15) corresponds to the power exchange limitation of tie-lines and constraint (4.16) exhibits that power buying and power selling between MGs cannot occur simultaneously, where T_{ij}^{max} represents the tie-line capacity between MG i and MG j.

$$P_{i,t}^{fsur} + \sum_{j \in M/i} (P_{ij,t}^{buy} - P_{ij,t}^{sell}) = P_{i,t}^{sho} - P_{i,t}^{fsho} \tag{4.12}$$

$$0 \leq P_{i,t}^{fsur} \leq P_{i,t}^{sur}, \ \forall t \in T, \ \forall i \in M \tag{4.13}$$

$$0 \leq P_{i,t}^{fsho} \leq P_{i,t}^{sho}, \ \forall t \in T, \ \forall i \in M \tag{4.14}$$

$$P_{ij,t}^{buy} + P_{ij,t}^{sell} \leq T_{ij}^{max}, \forall t \in T, \ \forall i, j \in M \tag{4.15}$$

$$P_{ij,t}^{buy} \cdot P_{ij,t}^{sell} = 0, \ \forall t \in T, \ \forall i, j \in M \tag{4.16}$$

4.2.2 Stage 3 - Re-scheduling with EVs

In the third stage, each MG receives the decisions on power exchange and runs its own AC OPF again to obtain optimal solutions that ensure the decisions obtained by the central controller are respected, while mobile EV fleets are also incorporated into the model to tackle potential contingencies and ensure load survivability. Note that EVs are only allowed to move inside one MG, as typically MGs have fixed boundaries and self-controllability due to customer privacy concerns [135]. The objective function of each MG at stage 3 can be found in (4.1), which corresponds to minimise total load shedding under different scenarios. The active power balance in the exchange bus b is replaced by equation (4.17), where the first two terms correspond to power exchange between MG i and other connected MGs, followed by the charging/discharging patterns of batteries and EVs. The rest of the terms are as described earlier. Constraints (4.5)-(4.6) and (4.9)-(4.10) are also considered in this stage.

$$\begin{aligned} &\sum_{j \in M/i} (P_{ij,t}^{buy} - P_{ij,t}^{sell}) + P_{b,t,s}^{d} - P_{b,t,s}^{c} + \sum_{k \in N_{ev}} (P_{b,k,t,s}^{ev,d} - P_{b,k,t,s}^{ev,c}) + \\ &\sum_{g \in NG_b} P_{g,t,s} + P_{b,t,s}^{ls} = P_{b,t,s}^{ex} + P_{b,t,s}^{l}, \ \forall t \in T, \ \forall b \in N_{bus}, \ \forall s \in S \end{aligned} \tag{4.17}$$

EV-related constraints are shown in equations (4.18)-(4.24). To mimic a realistic situation, EV scheduling horizon is represented by T_{ev}, which may be different from the MG scheduling horizon T. At the end of the EV scheduling horizon, the storage level of EV fleets should be over or equal to a target value to make sure that EVs can continue being utilised by their owners for sufficient amount of time after extreme events, which is appropriately demonstrated by equation (4.24). Additionally, it is assumed that utilised EVs have bi-directionality capabilities and can move between different buses within each MG. Inequalities (4.18) and (4.19) refer to the limits of charging and discharging power for EV fleet k, where $P^{ev,c}_{b,k,t,s}$ and $P^{ev,d}_{b,k,t,s}$ correspond to charging and discharging behaviors of EV fleet k in bus b at time t under scenario s respectively. Integer variable $u_{b,k,t,s} = 0$ means that the EV fleet k does not connect with bus b at time t under scenario s and vice versa, while inequality (4.20) represents that EV fleet k can only connect with one bus b at time t. Constraint (4.21) corresponds to the transportation of EV fleet k within a MG, where T^{trl}_{bp} represents the travelling time of the EV fleet k from bus b to bus p [18]. Inequality (4.22) gives the limits with minimum energy storage and maximum energy storage of EV fleet k, while constraint (4.23) introduces the dependence of energy storage level at each time interval on the previous time step. Note that, due to the small scale of the MG and the assumption of EV fleets, the power consumption of EVs on the road is not considered, while one power loss term can also be added in constraint (4.23), as suggested in [59, 139].

The incorporation of technical constraints (e.g., (4.5)-(4.6)) and EV routing makes the model become a mixed-integer non-linear programming (MINLP) problem, which is normally difficult to solve with the consideration of time-coupled constraints. However, the suggested model is based on a hierarchical control approach and the model formulation of each MG at stage 3 can be solved via a distributed manner, which largely reduces the computation burden. As such, the suggested model can be solved by commercial solvers, such as BONMIN and DICOPT [140].

$$0 \leq P^{ev,c}_{b,k,t,s} \leq u_{b,k,t,s} \cdot P^{max}_{k},\ \forall b \in N_{bus},\ \forall k \in N_{ev},\ \forall s \in S \tag{4.18}$$

$$0 \leq P^{ev,d}_{b,k,t,s} \leq u_{b,k,t,s} \cdot P^{max}_{k},\ \forall b \in N_{bus},\ \forall k \in N_{ev}, \forall s \in S \tag{4.19}$$

$$\sum_{b \in N_{bus}} u_{b,k,t,s} \leq 1,\ \forall t \in T_{ev},\ \forall k \in N_{ev},\ \forall s \in S \tag{4.20}$$

$$\begin{gathered} u_{b,k,t,s} - u_{b,k,t+1,s} \leq 1 - u_{p,k,t+h,s},\ \forall t \in T_{ev} - \{1\},\ \forall k \in N_{ev}, \\ \forall b \neq p \in N_{bus}, \forall h \in [1, ..., min(T^{trl}_{bp}, T_{ev} - t)],\ \forall s \in S \end{gathered} \tag{4.21}$$

$$EV^{min}_{k} \leq EV_{k,t,s} \leq EV^{max}_{k},\ \forall t \in T_{ev},\ \forall k \in N_{ev},\ \forall s \in S \tag{4.22}$$

$$EV_{k,t,s} = EV_{k,t-1,s} + (\eta^c \sum_{b \in N_{bus}} P^{ev,c}_{b,k,t,s} - \eta^d \sum_{b \in N_{bus}} P^{ev,d}_{b,k,t,s})\Delta t,\ \forall t \in T_{ev} - \{1\},\ \forall k \in N_{ev},\ \forall s \in S \quad (4.23)$$

$$EV(k, T_{ev}, s) \geq EV^{tar}_k,\ \forall k \in N_{ev},\ \forall s \in S \quad (4.24)$$

4.2.3 Uncertainty modelling

Uncertainties relating to renewable energy sources and load profiles shall be considered to capture realistic fluctuations and output more realistic results. Firstly, this chapter utilises Monte-Carlo simulation to produce a large number of scenarios (e.g., 1000) initially based on a normal distribution function with 5% and 3% errors in PVs and load profiles respectively [138]. On one hand, it is worth noting that the scenario number shall be large enough to capture the fluctuating nature of renewable energy resources and load profiles; on the other hand, the distribution function is only used for scenario generation, while other distribution functions (e.g., *Beta* distributions) can also be employed for more realistic representation. Secondly, the agglomerative hierarchical clustering method (bottom-up approach) with Ward's linkage is employed to group and reduce the number of scenarios [141]. Finally, 10 scenarios are produced to represent the uncertainty set of renewable sources and loads. Hierarchical clustering can construct a hierarchy of clusters by employing a measure of similarity between groups of data points [142]. For clusters k_1 and k_2, the distance measure d_{k_1,k_2} can be calculated as follows:

$$d_{k_1,k_2} = \| \Gamma_{k_l} - \Gamma_{k_2} \|_2 \sqrt{2n_{k_1}n_{k_2}/(n_{k_1} + n_{k_2})} \quad (4.25)$$

where n_{k_1} and n_{k_2} are the numbers of scenarios in clusters k_1 and k_2, Γ_{k_l} and Γ_{k_2} represent the centroids of clusters k_1 and k_2, and $\| \cdot \|_2$ is Euclidean distance. After obtaining these clusters, medoid points of clusters are selected to represent final 10 scenarios. Given that initial 1000 scenarios have the same occurrence probability, the probability of each final scenario can be calculated as the ratio of the number of initial scenarios that belong to the cluster and the number of scenarios [141]. Additionally, it is worth noting that this method can also be used to cluster weighted scenarios with different occurrence probabilities, if appropriate variance reduction techniques are applied [143].

Regarding external contingencies, three levels of contingencies with different probabilities are considered to represent different damage levels of each MG caused by extreme events. For instance, single line fault for each MG will be the lowest level of damage, while three faulted lines correspond to the highest level of damage. Normally, the higher level of damage has lower probability of occurrence. In this chapter, the probability set [0.5, 0.3, 0.2] accounts for the occurrence probability of three levels of damage respectively. As such, a total of 30 scenarios are generated to represent the influence of uncertainties and contingencies.

4.2.4 Resilience index

The final objective function (4.1) is calculated in a decentralised way, which is not suitable for the performance evaluation of multiple MGs. Therefore, a resilience index (RI) is utilised in this chapter for better evaluation, which is shown in (4.26) and corresponds to the ratio of weighted load shedding and total weighted loads under event scenarios. This area metric will be 1 when a MG can fully restore all the loads within the period T, while a smaller RI corresponds to worse performance of MGs (i.e., larger load sheding). Note that the original performance $R_0(t)$ (i.e., the state before event occurs) and the real-time performance $R(t)$ (i.e., performance across the event evolution) consider load distinction. For instance, $R(t)$ can be calculated by the performance of critical loads $R^c(t)$ and non-critical loads $R^n(t)$, which are multiplied by different weighting factors w^c and w^n. Selection of the weighting factors w^c and w^n indicates the significance of critical loads and non-critical loads ($w^c > w^n$). It is worth noting that the RI suggested in this chapter is expressed via restored loads, while the RI suggested in the previous chapter corresponds to the ratio of the curtailed loads. In general, they focus on the same information in a similar manner.

$$RI = \frac{\int_{t_0}^{T} R(t)}{\int_{t_0}^{T} R_0(t)},\ R_0(t) = w^c R_0^c(t) + w^n R_0^n(t),\ R(t) = w^c R^c(t) + w^n R^n(t). \tag{4.26}$$

4.3 Comparative case studies

The structure of an AC MG is presented in Figure 4.3, where a diesel generator and a PV plant are installed as conventional energy sources and renewable energy sources respectively, while a BESS unit and EV fleets are also appropriately installed and connected with this MG. Note that EV fleets are connected with bus 3 in Figure 4.3, which only represents the initial position of EV fleets.

When an extreme event occurs, each MG switches into islanded mode and is connected with the rest of the MGs via tie-lines. The day-ahead scheduling method is employed to run the AC OPF algorithm and make decisions about power output of generators, power exchange and battery energy management. Conventional generators in all three MGs have capacities of 250 kW, 350 kW,

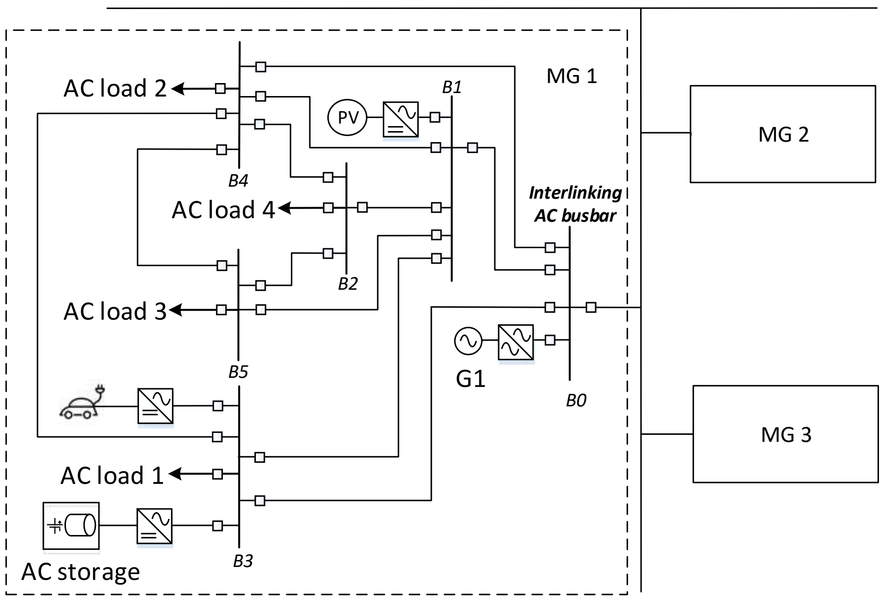

Figure 4.3: An AC MG utilised in simulations.

300 kW respectively, while the PV plant in each MG has a capacity of 100 kW. Each MG includes a low power-high energy battery (e.g., 50 kW/200 kWh) and EV fleets with a total of capacity 300 kWh. In the following case studies, the distinction between critical and non-critical loads is captured. For example, the critical loads could be lights and lift motors in a building-scale MG, and the non-critical loads could be kitchen and toilet appliances [98]. Similar to [71], the loads L_3 in the bus 3 of each MG (around 30%) are critical loads with high load shedding cost, while other types of loads are non-critical loads with low curtailment cost. Load profiles and PV profiles can be found in Figure 4.4, which are extracted and scaled from [98, 144].

4.3.1 Simulation I: Hierarchical control and centralised control

To verify the effectiveness of the proposed hierarchical control strategy, the comparison study between hierarchical control and centralised control is suggested in this subsection. A total of 10 scenarios are considered to represent uncertainties relating to renewable energy sources and loads. Furthermore, it is assumed that there are only limited generation resources (e.g., 3000 kWh energy reserve) in MG 1 and MG 3, which may lead to load shedding in these two MGs. All the simulations were run on Intel i7-8700u processor using 8 GB RAM.

Comparison results can be found in Table 4.2. Note that all comparison studies in this subsection do not consider the advantages of EV routing on tackling contingencies, because the centralised control method based on AC OPF cannot solve the proposed MINLP problem even under one

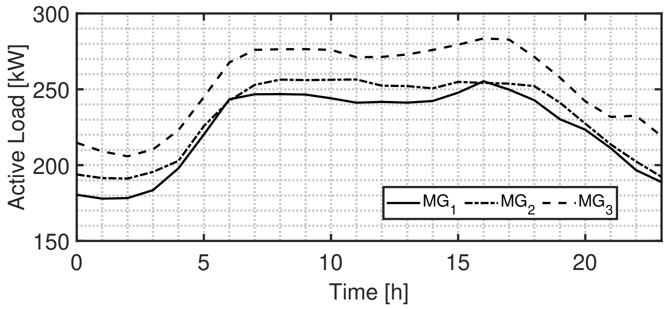

(a)

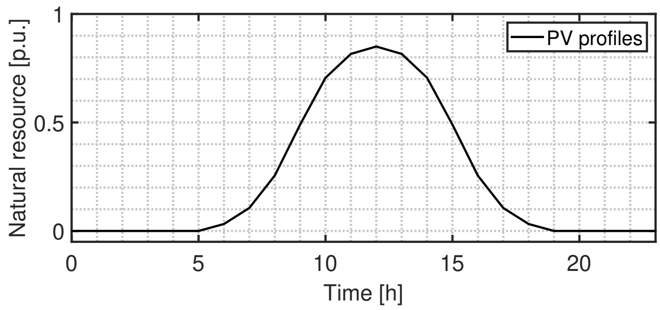

(b)

Figure 4.4: Simulation I: (a) Load profiles, (b) PV profiles.

single scenario. More details about the utilisation of EV fleets under hierarchical control can be found in the next subsection. RI in all three cases are very close, while the computation burden of the suggested hierarchical control method is much lower than that of the centralised method. The effectiveness of the suggested hierarchical control method has been clearly shown in this simulation. Note that computation burden under centralised control (CC) would significantly increase with the addition of more connected MGs, while the computing burden of hierarchical control (HC) shall not be largely increased because of the decentralised operation of each MG. This demonstrates that in a future setup, where tens or hundreds of MGs may be connected, a centralised control algorithm would struggle to provide a dispatch in time, while the proposed hierarchical control method would be well-placed to provide a quick response (even though it may be slightly sub-optimal).

Table 4.2: Comparison between hierarchical control and centralised control

Control methods	10 scenarios		5 scenarios		1 scenario	
	HC	CC	HC	CC	HC	CC
RI	97.56%	97.64%	97.57%	97.64%	97.72%	97.76%
Time	406.23s	3571.22s	208.54s	992.83s	12.95s	95.43s
Status	Optimal	Optimal	Optimal	Optimal	Optimal	Optimal

Figure 4.5(a) illustrates the result of load shedding based on the hierarchical control across the 24-hour horizon. In both cases, there is no load shedding in MG 2, while MG 1 and MG 3 have non-critical load shedding because of the limitation of generation resources. Power exchange results

can be found in Fig. 4.6, where the power sharing from MG 2 has reached the maximum in both cases. Fig. 4.5(b) shows that the total load shedding in MG 1 or MG 3 is less than their total power shortage, which means that more more power needs to be imported to avoid load shedding because of the existence of power loss. This is an important aspect of the proposed model, as hierarchical control strategies based on typical EMSs would neglect the influence of operational constraints and directly regard load shedding as equal to the power shortage, which can be inaccurate. The AC OPF algorithm utilised in this chapter can obtain more accurate solutions about power shortage and power surplus than EMS models. It can be anticipated that the total error between real power shortage and load shedding may become much larger with the increase of the number of MGs and the complexity of MG structure.

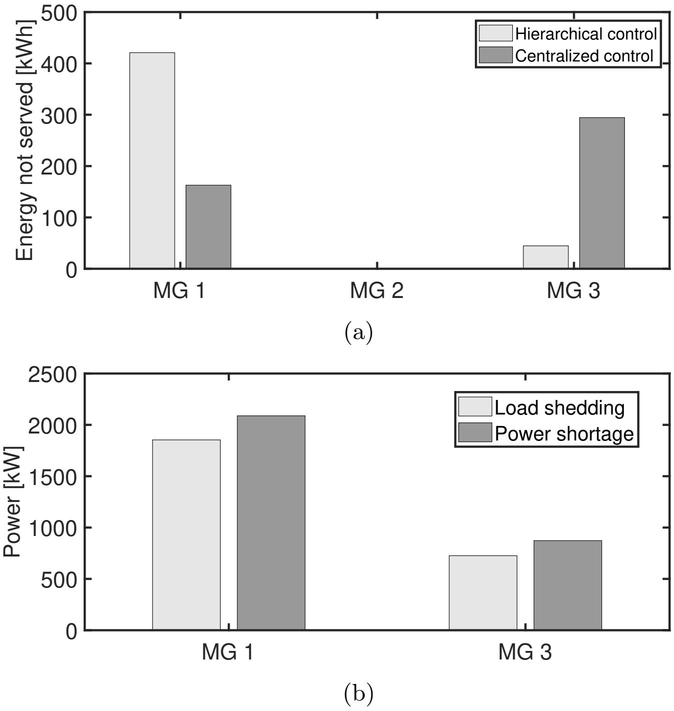

Figure 4.5: Simulation I: (a) Energy not served based on hierarchical control under one-scenario simulation (i.e., deterministic formulation), (b) Power shortage and load shedding in MG 1 and MG 3 based on hierarchical control under one-scenario simulation.

4.3.2 Simulation II: EV scheduling for contingencies

In this subsection, three different levels of contingencies are incorporated into the model to investigate the effect of EV routing on resilience enhancement. Faulted lines in the contingency set can be found in Table 4.3, where line 1-3 means that the line between bus 1 and bus 3 is damaged. As such, a total of 30 scenarios are considered to represent the impacts of uncertainties and contingencies.

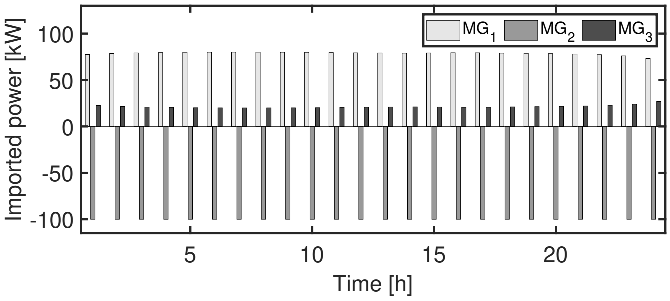

(a)

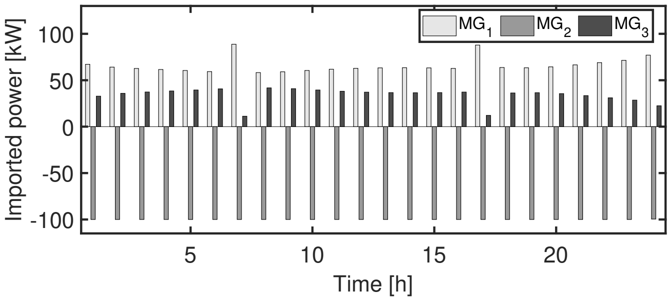

(b)

Figure 4.6: Simulation I: (a) Power exchange among MGs based on centralised control under one-scenario simulation, (b) Power exchange among MGs based on hierarchical control under one-scenario simulation.

To better present the advantages of mobile EV fleets, a comparison study considering two cases (mobile EVs and static EVs) is developed, where results can be found in Table 4.4. In general, considering the mobility aspect of EVs during extreme events obtains higher resilience levels than considering static EVs.

Table 4.3: Faulted lines under three different levels of contingencies

	Level 1	Level 2	Level 3
MG 1	line 1-3	line 1-5, line 2-5	line 0-3, line 1-3, line 3-4
MG 2	line 0-4	line 1-4, line 3-4	line 2-4, line 1-4, line 3-4
MG 3	line 2-4	line 3-4, line 4-5	line 2-5, line 3-4, line 4-5

EV routing under load profile 1 is illustrated in Table 4.5, where the number corresponds to a certain bus and “T” represents transportation. It can be found that all EVs connect with bus 3 at first and then travel to the bus with the need for power support. After EVs run out of energy, they may travel to bus 0 for charging and then move back to the bus requiring power support. It is worth noting that the critical load (load 3 in bus 3) in MG 1 has been entirely isolated under the level 3 contingency and EVs travel between bus 0 and bus 3 to support the critical load as well as enhancing resilience (RI 67.24%). For comparison, the RI of MG 1 using static EVs is 64.77%. It can be concluded that mobile units become much more important and effective than static ESSs when damage is caused on the system (e.g., entirely isolated loads).

Table 4.4: Comparison between mobile EVs and static EVs

	RI	Time	Status
Mobile EVs	94.98%	1380.05s	Optimal
Static EVs	92.92%	1179.98s	Optimal

Table 4.5: EV routing under different levels of contingencies for load profile 1.

Contingency	Time (h)														
	5	6	7	8	9	10	11	12	13	14	15	16	17	18	19
MG 1, level 1	3	3	T	5	T	2	2	T	3	T	1	T	2	2	2
MG 1, level 2	3	T	5	T	3	T	5	5	5	5	5	T	4	T	5
MG 1, level 3	3	3	3	3	T	0	0	0	0	T	3	3	3	3	3
MG 2, level 1	3	T	2	2	2	T	0	0	0	T	2	2	2	2	2
MG 2, level 2	3	3	T	0	0	T	2	2	2	2	2	2	2	T	4
MG 2, level 3	3	T	5	5	5	T	4	4	4	4	4	4	T	2	2
MG 3, level 1	3	3	T	2	2	T	5	T	1	T	3	T	5	T	4
MG 3, level 2	3	T	2	2	2	2	T	5	5	5	5	5	5	T	5
MG 3, level 3	3	T	5	5	T	0	0	T	5	5	5	5	5	5	5

4.4 Sensitivity analysis

Most research assumes that fully-charged EVs are utilised for resilience enhancement; nevertheless, uncertain event occurrence time may lead to a shorter EV charging duration (e.g., a shorter preventive stage), which means that EVs may not have enough time to be fully charged. A sensitivity analysis about event occurrence time is shown in Table 4.6, where fully-charged EVs correspond to a longer preparation duration in comparison with partially-charged EVs that represent a shorter preparation horizon. Table 4.6 illustrates that, even though marginal, fully-charged EVs obtain a higher resilience level than partially-charged EVs, because of the longer charging duration. Note that all the sensitivity studies are based on a total of 30 scenarios.

Table 4.6: Influence of event occurrence time

	Initial SoC (kWh)	RI
Fully-charged EVs	300	94.98%
Partially-charged EVs	200	94.31%

The capacity of tie lines has a significant influence on the power sharing between MGs, where larger capacity means larger power sharing between MGs. Figure 4.7(a) shows that a higher resilience level is achieved with the increase of power exchange limitation. The RI of MG 2 remains stable under different situations, while the resilience levels of MG 1 and MG 3 both increase largely when the capacity of tie lines is increased from 50 kW to 100 kW.

Additionally, the allowable EV scheduling horizon in each MG may be different during extreme events under different situations (e.g., different local policies). Another sensitivity analysis is suggested in Figure 4.7(b) to show the impacts of different allowable EV scheduling horizons on the resilience enhancement of each MG. A higher resilience level is achieved in each MG with the increase of EV charging duration.

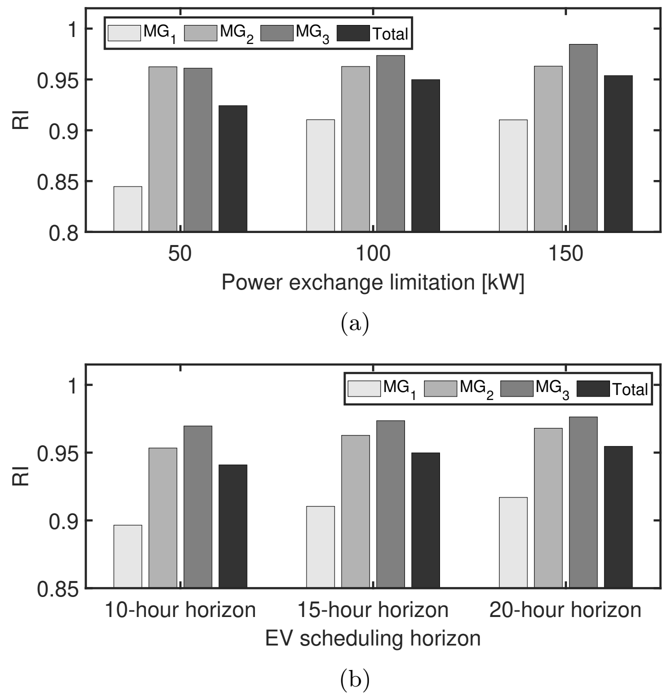

Figure 4.7: Sensitivity analysis: (a) Influence of power exchange limitation T_{ij}^{max}, (b) Influence of different EV scheduling horizons T_{ev}.

Chapter 5

A stochastic decentralised approach for load restoration

5.1 Introduction

Planning and operational strategies based on centralised control (e.g., [74, 95]) or hierarchical control (e.g., [136, 137]) have been widely developed for load restoration purposes of networked MGs. However, communication links between a central controller and local MGs may be interrupted after extreme events. In comparison with control approaches based on central controllers, distributed control approaches may not guarantee a globally optimal solution but can protect customer privacy and reduce the dependency of networked MGs on communication networks [132]. However, as mentioned in previous chapters, most papers on distributed control utilise EMSs to model MG operations which can only capture power balance equations of a MG model. Given the absence of detailed constraints for the network nodes/branches, it is impossible to use EMSs to model the spatial flexibilities of MESSs. Note that MESSs can introduce significant merits for resilience enhancement of power systems via delivering power and energy as backup power sources for critical load restoration [59]. Furthermore, the absence of technical constraints relating to voltage, angle and power loss may lead to unstable MG operations and inaccurate solutions, since power systems will be operated much closer to their stability limits under high uncertainties and severe contingencies.

Apart from EMS-based models, a stochastic bi-level optimisation model is developed in [88] to coordinate the power exchange between MGs and the utility grid in a decentralised way. However, this paper utilise a linearised distflow for MG operations, which ignores power losses through lines and can only be applied in radial networks. Note that MGs might have different network structures, other than traditional distribution systems [139]. Meshed networks include a more uniform power flow and can provide benefits for improving voltage profiles and reducing power losses; a feature that introduce stronger capabilities of meshed networks to withstand severe contingencies and improve resilience [145].

To summarise, there has been much research on distributed control of networked MGs; nevertheless, existing literature solves the optimisation problem on an hourly basis or ignores long timeframes, which cannot capture the flexibility of storage units, especially for mobile energy storage systems (MESSs). One of reasons for this is that consensus-based algorithms found in the literature (e.g., [63, 135]) address power sharing between MGs in independent time periods, which are inherently unable to capture any time-coupled flexibility [146]. It is necessary to develop a model to comprehensively consider such flexibility under distributed control. Additionally, existing literature tends to utilise linearised models for MG operations due to the need of reducing computing burden. There is little research focusing on control approaches, which can capture technical constraints relating to stability properties for accurate decision making and secure MG operations as well as ensuring computing efficiency. Furthermore, there is no significant amount of research focused on distributed control approaches capturing the merits of MESSs for resilience enhancement of networked MGs. Therefore, this chapter proposes a stochastic distributed control approach based on rolling optimisation for the resilience enhancement of networked MGs, which can effectively bridge a gap in this respective area. The contributions are summarised hereafter:

- A three-stage distributed control approach based on rolling optimisation is introduced for resilient scheduling of MGs. A time-coupled linearised AC OPF algorithm is used in the first stage to capture the flexibility of storage units and ensure computing efficiency.
- Time-coupled routing of MESSs inside each MG is modeled for load restoration, while transporting time of MESSs between different buses is appropriately incorporated in the model.
- A detailed AC OPF algorithm is utilised in the third stage to capture stability properties relating to voltage, angle and power loss to ensure no violation of technical constraints.
- Uncertainties with renewable energy sources and loads are captured in the first stage via a stochastic linearised OPF algorithm. Multiple line faults and load distinction are included in the case studies to capture a realistic scenario.

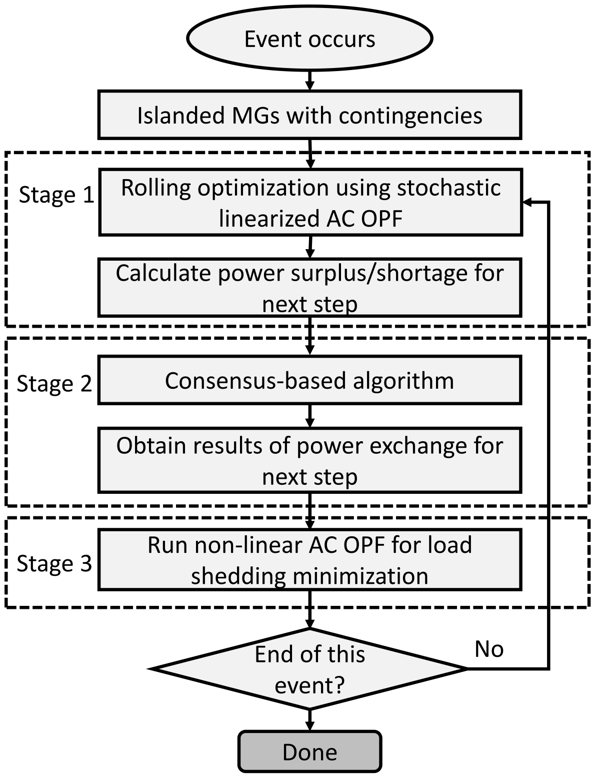

Figure 5.1: The proposed distributed control approach based on rolling optimisation.

5.2 Outline of the suggested distributed control approach

Extreme events are characterised by high impact and low probability, which cause high uncertainty and severe damages including: 1) uncertain event time and duration; 2) uncertain generation resources and load profiles; 3) severe damages (e.g., multiple line faults); 4) unavailable power resources; 5) unavailable central controllers; 6) MGs losing their connection to the utility grid. Considering the above mentioned properties, the suggested control approach should be decentralised and flexible enough against extreme events [65]. Uncertainties with renewable generation resources and load profiles, load distinction into critical and non-critical, and technical constraints relating to stability properties shall also be taken into account. As such, this chapter proposes a three-stage distributed control approach based on rolling optimisation to make decisions on power exchange among MGs for resilience enhancement, which is schematically represented by Figure 5.1. A more detailed description of the various elements coming together can be found hereafter:

5.2.1 Rolling optimisation

When an event occurs, MGs may switch into islanded mode (from grid-connected mode) due to intentional or unintentional islanding schemes. To minimise the influence of this event, MGs will

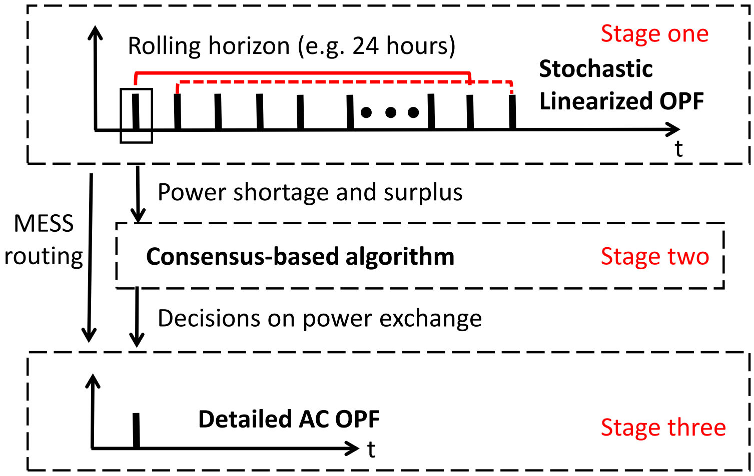

Figure 5.2: The proposed rolling optimisation approach.

choose to connect with nearby MGs through communication links, if communication resources between them are still available. According to Figure 5.1, each MG will schedule their resources based on the rolling optimisation method and calculate the power shortage and power surplus. Note that rolling optimisation is used to optimise the system operation for the next time slot while taking future time slots into account [65]. Figure 5.2 shows that the suggested approach utilizes a linearised AC OPF algorithm through a 24-hour scheduling horizon capturing uncertainties and time-coupled flexibility, while decisions (e.g., power exchange and MESS scheduling) on the first time step are implemented and eventually verified through a detailed AC OPF algorithm to ensure no violations of technical constraints.

As mentioned before, distributed control based on consensus algorithm is inherently time-independent, which cannot effectively capture the flexibility of MESSs and power sharing. However, the suggested rolling optimisation approach provides the advantage of handling unforeseen changes via appropriate operational measures as well as capture of the above flexibilities. Additionally, the influence of uncertain event time and duration on MG operations can be significantly reduced, since rolling optimisation methods are run in a hourly basis and have no dependence over the complete scheduling horizon. Furthermore, the computing efficiency increases due to the utilisation of linearised AC OPF in the first stage, compared with an entirely non-linear AC OPF algorithm.

5.2.2 Uncertainty modelling

Uncertainties relating to renewable energy sources (e.g., PVs) and load profiles shall be considered in rolling optimisation due to the high unpredictable nature of extreme events, since accurately updated forecasts over a long rolling horizon may be unavailable. This chapter utilises a scenario-based stochastic programming approach to capture these uncertainties. Monte-Carlo simulation is employed to initialize a large number of scenarios (e.g., 1000 scenarios) according to a normal distribution function, where PV and load profiles are associated with 5% and 3% errors respectively [138]. To ensure an appropriate trade-off between computing time and accuracy, the agglomerative hierarchical clustering method (bottom-up approach) with Ward's linkage is employed to group and reduce the number of scenarios [141]. Finally, an uncertain set containing several scenarios with different probabilities (e.g., 10 scenarios) are produced to represent the abovementioned uncertainties. Detailed information about this method can be found in the previous chapter.

5.2.3 MG operation based on distributed control

As shown in Figure 5.2, the suggested distributed control approach is divided into three distinct stages: 1) linearised stochastic AC OPF capturing time-coupled behaviours of MESSs; 2) a consensus-based algorithm calculating power exchange for the next time step; 3) a detailed AC OPF used to obtain accurate results and avoid the violation of technical constraints. Details of the suggested rolling optimisation approach can be found hereafter:

Stage 1 - Calculate power surplus/shortage

In the first stage, every MG runs a time-coupled linearised AC OPF algorithm in a stand-alone condition (i.e., not connected to other MGs) and calculates power shortage or power surplus (i.e., P^e) within the scheduling horizon. Note that only signals for one step will be sent to the second stage to calculate final results on power exchange. The objective function of one local MG in this stage can be found in (5.1). The first term corresponds to the real power surplus or power shortage, while the second term is related to the total load shedding cost capturing a set of uncertainties. In other words, the process of calculating power shortage/surplus for every MG is formulated as a scenario-based stochastic problem in which results are obtained according to a set of scenarios [138]. Variables on power shortage/surplus and the scheduling of MESSs are realised as here-and-now decision variables, while the others (e.g., load shedding or power output of generators) are wait-and-see variables depending on the realisation of each scenario.

$$F_1 = \sum_{t \in T} c^e P^e_t + \sum_{s \in S} p_s \sum_{t \in T} \sum_{b \in L_{bus}} c^{ls} P^{ls}_{b,t,s} \tag{5.1}$$

The incorporation of typical technical constraints and MESS routing makes the model become a MINLP problem, which is extremely difficult to solve with the consideration of time-coupled constraints and a set of uncertainties. In line with the requirements of resilience enhancement for computing efficiency, linearised techniques developed in [147] are used to simplify the non-linear OPF into a MILP formulation to obtain a trade-off between computing time and accuracy in the first stage. As such, the optimisation is posed as a minimisation problem, subject to linearised AC OPF constraints. The active power balance equation at the exchange bus b is shown in (5.2), while the reactive power balance equation is shown in (5.3). Classical equations pertaining to power flow problems are presented in (5.4) and (5.5). $P^{ex}_{b,t,s}$ and $Q^{ex}_{b,t,s}$ represent active and reactive power exchange between considered bus b and other buses at time t under scenario s respectively, while $\delta_{bp,t,s}$ corresponds to the voltage angle difference between buses b and p at time t under scenario s. Constraints (5.6)-(5.7) refer to the network model, where $P_{bp,t,s}$ and $Q_{bp,t,s}$ correspond to the active power and reactive power through the line from bus b to bus p. P^{L}_{bp} and Q^{L}_{bp} represent active and reactive power losses, which can be linearised via the loss factors suggested by [147], while equation (5.8) corresponds to the power exchange limit between the MG and nearby MGs. Note that T_{ij} means the tie-line capacity between two MGs (e.g., MG i and MG j).

$$P^{e}_{t} + \sum_{k\in N_{mes}} (P^{mes,d}_{b,k,t} - P^{mes,c}_{b,k,t}) + P^{ls}_{b,t,s} + \sum_{g\in NG_b} P_{g,t,s} = P^{ex}_{b,t,s} + P^{l}_{b,t,s} \tag{5.2}$$

$$\sum_{g\in NG_b} Q_{g,t,s} + Q^{ls}_{b,t,s} = Q^{ex}_{b,t,s} + Q^{l}_{b,t,s} \tag{5.3}$$

$$P^{ex}_{b,t,s} = \sum_{(b,p)\in N_{br}} P_{bp,t,s} + (\sum_{p\in N_{bus}} G_{bp})V^2_{b,t,s} \tag{5.4}$$

$$Q^{ex}_{b,t,s} = \sum_{(b,p)\in N_{br}} Q_{bp,t,s} - (\sum_{p\in N_{bus}} B_{bp})V^2_{b,t,s} \tag{5.5}$$

$$P_{bp,t,s} = G_{bp}(V^2_{b,t,s} - V^2_{p,t,s})/2 - B_{bp}\delta_{bp,t,s} + P^{L}_{bp}, \forall t \in T,\ \forall b \in N_{bus}, \forall s \in S \tag{5.6}$$

$$Q_{bp,t,s} = -B_{bp}(V^2_{b,t,s} - V^2_{p,t,s})/2 - G_{bp}\delta_{bp,t,s} + Q^{L}_{bp}, \forall t \in T,\ \forall b \in N_{bus}, \forall s \in S \tag{5.7}$$

$$-T^{max}_{ij} \le P^{e}_{t} \le T^{max}_{ij},\ \forall t \in T \tag{5.8}$$

Furthermore, events may cause potential damage on energy supply chains, such as gas networks and fuel networks, and therefore generation resources (e.g., fuel reserve) within one MG may be limited [15]. Therefore, it is reasonable to assume that each MG only has limited generation resources, which accounts for equations (5.9) and (5.10). GS_g^{Ini} corresponds to the initial energy reserve of a MG when an event occurs and generator g will fail to operate when GS_g^{Ini} reaches its minimum value GS_g^{min}.

$$GS_{g,t,s} = GS_{g,t-1,s} - P_{g,t,s}\Delta t \ \forall t \in T/\{1\}, \ \forall g \in N_g \tag{5.9}$$

$$GS_g^{min} \leq GS_{b,t,s} \leq GS_g^{Ini}, \ \forall t \in T, \ \forall g \in N_g, \ \forall s \in S \tag{5.10}$$

Equations (5.11)-(5.12) represent the operational constraints of voltage limit and line capacity, while equations (5.13)-(5.14) correspond to the power generation limit of conventional generators. These constraints capture the technical features of MGs and ensure the accuracy of obtained solutions. Note that $V_{b,t,s}^2$ can be treated as a variable in this linearised OPF. Constraint (5.12) is quadratic and defines a convex region, which can be linearised via the piecewise linearisation method suggested in [104]. As such, the typical AC OPF is linearised into an MILP formulation and can be solved efficiently via commercial softwares (e.g., CPLEX and GUROBI) [140]. Compared with EMS or DC OPF, this linearisation method takes reactive power and voltage into account. Compared with linearised Distflow, this approach can be utilised for both meshed and radial networks and effectively capture power losses through loss factors. However, there still exists risk for the linearised OPF to obtain solutions that do not satisfy power flow equations; hence, it is necessary to verify the practical feasibility of obtained solutions through a detailed AC OPF algorithm, which is introduced in the third stage.

$$V_{min}^2 \leq V_{b,t,s}^2 \leq V_{max}^2, \forall t \in T, \forall b \in N_{bus}, \forall s \in S \tag{5.11}$$

$$P_{bp,t,s}^2 + Q_{bp,t,s}^2 \leq S_i^{lim}, \forall t \in T, \forall i \in N_{br}, \forall s \in S \tag{5.12}$$

$$P_{g,min} \leq P_{g,t,s} \leq P_{g,max}, \forall t \in T, \forall g \in N_g, \forall s \in S \tag{5.13}$$

$$Q_{g,min} \leq Q_{g,t,s} \leq Q_{g,max}, \forall t \in T, \forall g \in N_g, \forall s \in S \tag{5.14}$$

MESS-related constraints are shown in equations (5.15)-(5.20). It is assumed that MESSs are transportable energy storage systems that can move between different buses within each MG. Inequalities (5.15) and (5.16) refer to the limits of charging and discharging power for MESS k. Integer variable $u_{b,k,t}^c$ and $u_{b,k,t}^d$ correspond to charging and discharging decisions of MESS k in bus b at time t. Constraint (5.17) ensures that power charging and discharging cannot occur simultaneously, while MESS k can only be connected with one bus at time t. Note that $u_{b,k,t}^c = 0$ and $u_{b,k,t}^d = 0$

mean that the MESS k does not connect with bus b at time t and vice versa. Constraint (5.18) corresponds to the transportation of MESS k within a MG, where T_{bp}^{trl} represents the travelling time of the MESS k from bus b to bus p [18]. Inequality (5.19) gives the limits with minimum energy storage and maximum energy storage of MESS k, while constraint (5.20) introduces the dependence of energy storage level at each time interval with the previous time step.

$$0 \leq P_{b,k,t}^{mes,c} \leq u_{b,k,t}^{c} \cdot P_{k}^{max}, \forall t \in T, \forall b \in N_{bus}, \forall k \in N_{mes} \tag{5.15}$$

$$0 \leq P_{b,k,t}^{mes,d} \leq u_{b,k,t}^{d} \cdot P_{k}^{max}, \forall t \in T, \forall b \in N_{bus}, \forall k \in N_{mes} \tag{5.16}$$

$$\sum_{b \in N_{bus}} u_{b,k,t}^{c} + u_{b,k,t}^{d} \leq 1, \forall t \in T, \forall k \in N_{mes} \tag{5.17}$$

$$\begin{gathered}[u_{b,k,t}^{c} + u_{b,k,t}^{d}] - [u_{b,k,t+1}^{c} + u_{b,k,t+1}^{d}] \leq 1 - [u_{p,k,t+h}^{c} + u_{p,k,t+h}^{d}],\\ \forall t \in T/\{1\},\ \forall k \in N_{mes}, b \neq p \in N_{bus}, h \in [1, ..., min(T_{bp}^{trl}, T - t)]\end{gathered} \tag{5.18}$$

$$ES_{k}^{min} \leq ES_{k,t} \leq ES_{k}^{max}, \forall t \in T, \forall k \in N_{mes} \tag{5.19}$$

$$ES_{k,t} = ES_{k,t-1} + (\eta_c \sum_{b \in N_{bus}} P_{b,k,t}^{mes,c} - \eta_d \sum_{b \in N_{bus}} P_{b,k,t}^{mes,d})\Delta t \tag{5.20}$$

Stage 2 - Consensus algorithm for power exchange

After extreme events, the main communication between central and local controllers in each MG may be unavailable. In this context, local controllers in each MG may connect with each other via available local communication resources, which renders the application of distributed control approaches valid for the decision making of power exchange between different MGs under emergency situations. In this chapter, a consensus-based algorithm is employed to optimise power sharing and reduce load shedding. Note that consensus algorithms have recently gained popularity in power dispatch problems because of their fast convergence and stability [63]. Given by the consideration of resilience, the incremental cost of load shedding $\lambda_{n,t}$ of each MG constitutes the consensus variables. Each MG estimates the values of their power shortage through Stage 1 and then update these estimates by exchanging information with their neighbouring MGs, where the communication network is represented by matrices P and Q. According to reference [63], these two matrices have the following properties:

- P is a row-stochastic matrix (summation of row entries is equal to one), while Q is a column-stochastic matrix and $Q = P^T$.

- $P_{mn} > 0$ means that MG m is connected to MG n.
- The values of P and Q can be free to choose, which will not influence the convergence rate.

The suggested consensus algorithm involves a four-step iterative process outlined below:

Step 1 (Initialisation) Using the results from Stage 1, the power shortage/surplus and power mismatches estimated by MG m are noted as below. Note that $P^{sho}_{m,t}$ and $P^{sur}_{m,t}$ will be derived from P^e of each MG.

$$P^{sho}_{m,t}, P^{sur}_{m,t}, P^{mis}_{m,t}, \ \forall m \in M, \ \forall t \in T \tag{5.21}$$

Regarding MG m, the power obtained from connected MGs is initialised as $P^{ob,0}_{m,t}$, where 0 means the first iteration. Note that $P^{ob,0}_{m,t}$ can be initialised as any feasible values. Additionally, the total available or required power P^{total}_t in the local network and the power mismatch $P^{mis,0}_{m,t}$ can be calculated as follows:

$$P^{total}_t = min[\sum_{m\in M} P^{sur}_{m,t}, \sum_{m\in M} P^{sho}_{m,t}] \tag{5.22}$$

$$P^{mis,0}_{m,t} = P^{total}_t/M - P^{ob,0}_{m,t} \tag{5.23}$$

Step 2 (Consensus variable update) At each iteration k, each MG m updates $\lambda_{m,t}$ and $P^{ob}_{m,t}$ based on the values of consensus variables obtained from connected MGs, which can be seen as (5.24). η is the learning gain constant, while α_m and β_m correspond to the parameters for load curtailment penalty cost.

$$\lambda^{k+1}_{m,t} = \sum_{n\in M} P_{mn}\lambda^{k}_{n,t} + \eta P^{mis,k}_{m,t} \tag{5.24}$$

$$P^{ob,k+1}_{m,t} = (\lambda^{k+1}_{m,t} - \beta_m)/(2\alpha_m) \tag{5.25}$$

Step 3 (Power mismatch update) Each MG m updates its power mismatch estimates based on i) its neighbouring MG estimates and ii) a correction term which is given by the difference between its optimal responses at the two most recent iterations.

$$P^{mis,k+1}_{m,t} = \sum_{n\in M} Q_{mn}P^{mis,k}_{n,t} - (P^{ob,k+1}_{m,t} - P^{ob,k}_{m,t}) \tag{5.26}$$

Step 4 (Convergence check) This process is repeated until the mismatch is within the acceptable range, e.g., less than ϵ. This condition assures the convergence of the algorithm. In general, the algorithm can converge within 50 iterations with a tolerance value of 0.01. However, to avoid any non-convergence, a slightly larger tolerance value can be applied for the iteration process.

$$P_{m,t}^{mis} \leq \epsilon, \ \forall m \in M \tag{5.27}$$

Stage 3 - Detailed AC OPF for feasible solutions

As mentioned before, MG operations may be much closer to stability limits due to the high-impact nature of extreme events, which leads to the necessity to ensure no violation of technical constraints relating to voltage, angle and power loss. Solutions obtained from the linearised AC OPF algorithm in the first stage may not satisfy classical non-linear power flow equations, even though computing efficiency can be guaranteed. As such, a detailed AC OPF algorithm capturing all the technical constraints is employed in this stage to obtain final results on load shedding for accurate decision making. Since only one time slot is considered, and the routing decisions of MESSs and power exchange results for the current step have been confirmed by the first stage and the second stage, the computing efficiency of using the detailed AC OPF can be ensured. The objective function can be found in (5.28), which includes one term relating to total load shedding cost in the current time step.

$$F_3 = \sum_{b \in L_{bus}} c^{ls} P_{b,t}^{ls} \tag{5.28}$$

Linearised power flow equations ((5.4)-(5.7)) are replaced by the typically non-linear power flow equations, which can be found in (5.29)-(5.30). The quadratic constraint (5.12) relating to line capacity can be verified, while other constraints relating to voltage limits, generation limits and power balance will be the same as those in the first stage. As such, the non-linear model of a detailed AC OPF is employed, which can be used for verification of decisions on power exchange and MESS routing. To ensure that solutions with good quality are found, a non-linear solver called 'IPOPT' is utilised to solve this operational problem [148].

$$P_{b,t}^{ex} = \sum_{p \in N_{bus}} V_{b,t} V_{p,t} (G_{bp} cos\delta_{bp,t} + B_{bp} sin\delta_{bp,t}), \ \forall t \in T, \ \forall b \in N_{bus} \tag{5.29}$$

$$Q_{b,t}^{ex} = \sum_{p \in N_{bus}} V_{b,t} V_{p,t} (G_{bp} sin\delta_{bp,t} - B_{bp} cos\delta_{bp,t}), \ \forall t \in T, \ \forall b \in N_{bus} \tag{5.30}$$

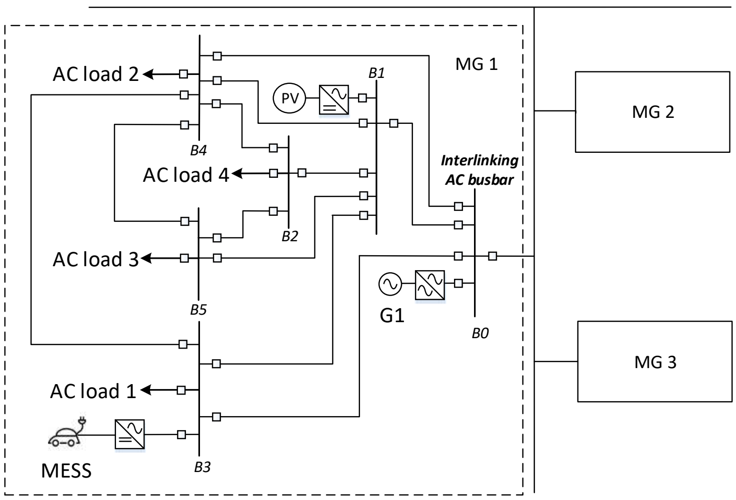

Figure 5.3: An AC MG utilised in simulations.

5.3 Case studies

The distributed control approach described in the previous section has been applied to the networked MGs illustrated in Figure 5.3; note that these MGs switch into islanded mode after extreme events and connect with each other for power sharing. Each MG includes a conventional generator (e.g., diesel generators), a photovoltaic array and a MESS as power sources. Solar irradiation and load profiles are illustrated in Figure 5.4, where the data are extracted from [98, 144]. Conventional generators in each MG have capacities of 150 kW, 350 kW and 100 kW respectively. As far as the MESSs are concerned, each MG includes one MESS containing a typical low energy-low power battery (e.g., 50 kW/200 kWh), which is placed on an initial location of bus 3. Through the extensive analysis of the following case studies, this chapter addresses fundamental modelling challenges pertaining to the operation of networked MGs with mobile units. All simulations have been run on Intel i7-8700u processor using 8 GB RAM.

As mentioned before, the key focus should be on critical load restoration during extreme events; hence, the discrimination of critical and non-critical loads is captured in following case studies. This chapter assumes that around 30% of the loads are critical with high curtailment cost, while other types of loads are non-critical with relatively low curtailment cost. Regarding uncertainty modelling, a total of 10 scenarios are generated to represent uncertainties relating to renewable energy sources and loads. The set of uncertainties in MG 1 has been illustrated in Figure 5.5. Additionally, the network status after the event (contingencies) can be found in Table 5.1. It is worth noting that this chapter assumes a severe damage in each MG to mimic the high impact nature of extreme events.

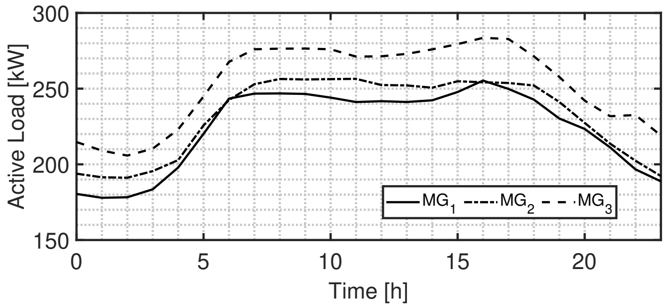

(a)

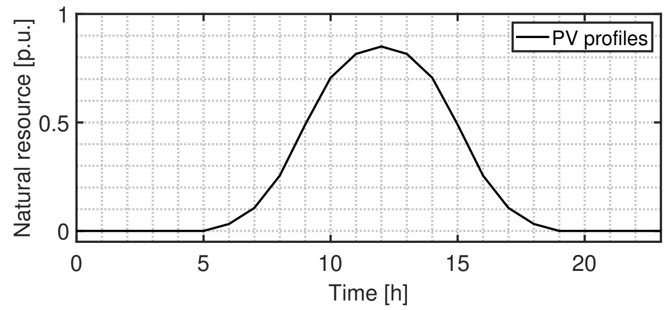

(b)

Figure 5.4: Data description: (a) Load profiles, (b) PV profiles.

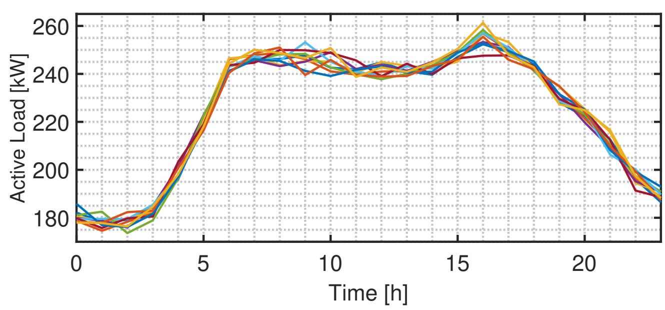

(a)

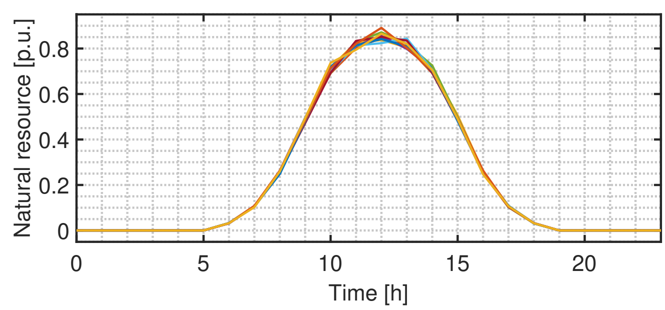

(b)

Figure 5.5: Uncertainty sets of : (a) load profiles, (b) PV profiles.

Table 5.1: Contingencies in networked MGs.

	MG 1	MG 2	MG 3
Line faults	line 1-3, 3-4	line 2-4, 2-5, 3-4	line 1-5, 3-4, 4-5

5.3.1 Simulation I: Results of MESS routing and distributed control

In this subsection, optimisation results using the suggested distributed control are demonstrated, where Table 5.2 illustrates the results of load shedding in each MG including both critical and non-critical load shedding. Note that there is only minimal critical load shedding in MG 1, while other MGs have no critical load shedding. Table 5.1 shows that line faults happening in MG 1 are both related to bus 3, which is connected with critical loads, while MG 2 and MG 3 only have one faulted line connected with bus 3; hence, critical load shedding is indeed expected in MG 1. As shown in Figure 5.4(a), MG 3 obtains the largest total load shedding due to the highest load level and the relatively low generator rating, while MG 2 has the lowest total load shedding due to the largest generator rating. Load shedding in an hourly basis is illustrated in Figure 5.6. More intensive load shedding is caused in networked MGs during the period of peak load level (e.g., 10-15 hours).

Table 5.2: Simulation I: Total load shedding in each MG.

	Critical load shedding (kW)	Total load shedding (kW)
MG 1	1.36439	210.783
MG 2	0	155.917
MG 3	0	1392.86

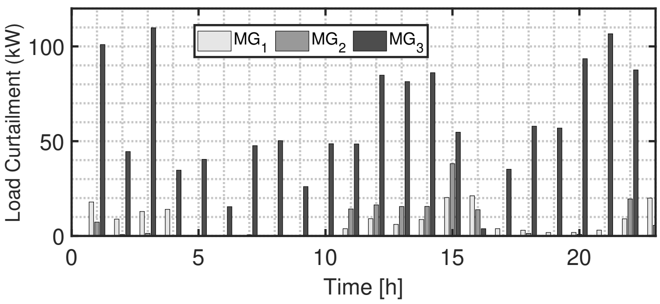

Figure 5.6: Simulation I: Hourly load curtailment of each MG

Regarding the 24-hour routing of MESSs in each MG, they can be found in Table 5.3. Generally, MESSs travel back and forth between bus 0 connecting the generator and other buses connecting loads towards load restoration. Note that the suggested rolling optimisation can consider the mobility of MESSs during a long scheduling horizon, compared with hourly resolutions which cannot capture the flexibility of MESSs. To further exhibit the merits of MESSs on load restoration, a comparison study between MESSs and ESSs is suggested here, where MESSs and ESSs have same power capacities and energy capacities. Table 5.4 reports optimal results on using MESSs and ESSs for resilience enhancement respectively. Obviously, MESSs obtain much less total load shedding cost due to the mobility merit. Additionally, much critical load shedding is avoided when MESSs are employed.

Table 5.3: Simulation I: MESS routing inside MGs for resilience enhancement.

MGs	Time (h)																						
	0	1	2	3	4	5	6	7	8	9	10	11	12	13	14	15	16	17	18	19	20	21	22	23
MG 1	3	3	3	T	5	5	5	5	5	5	T	0	0	0	0	T	5	5	5	5	5	5	T	0
MG 2	3	T	0	T	5	5	5	5	5	5	T	0	0	0	0	T	5	5	5	5	5	5	T	0
MG 3	3	T	0	0	T	5	5	5	5	T	0	0	0	0	T	5	5	5	5	T	0	0	T	5

Table 5.4: Discussion: Comparison between MESSs and ESSs including load shedding and cost.

	Critical load shedding (kW)	Total load shedding (kW)	Load shedding cost (k£)
MESSs	1.36	1759.56	264.07
ESSs	56.73	2257.04	344.23

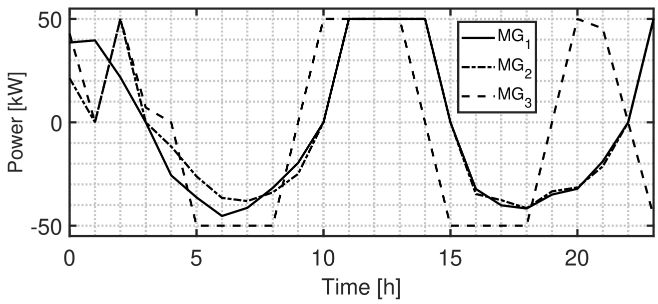

Figure 5.7: Simulation I: MESSs charging/discharging patterns during extreme events.

Figure 5.8(a) presents the power exchange results from the consensus algorithm, while Figure 5.8(b) shows the iteration of power mismatch between MGs for $t = 0$. After extreme events, all MGs switch into islanded mode and the generator in MG 2 has the largest capacity, which triggers the power flow from MG 2 to the other two MGs. Additionally, Figure 5.4(a) shows that MG 3 has the highest load level, therefore receives significantly more power from MG 2 than MG 1 does.

The advantage of the detailed OPF algorithm can be found in Figure 5.9. Voltage profiles of bus 3 in all three MGs are within the range of voltage limits (e.g., 0.9-1.1 p.u.). This is important, as typical energy management systems found in the literature would not capture the voltage constraints; this would lead to violation of technical requirements. Even though the voltage constraint of OPF may negatively impact on the operational cost for keeping voltages stable, it can capture realistic optimisation results and ensure safe MG operations; a highly important feature as we move in broad decentralisation.

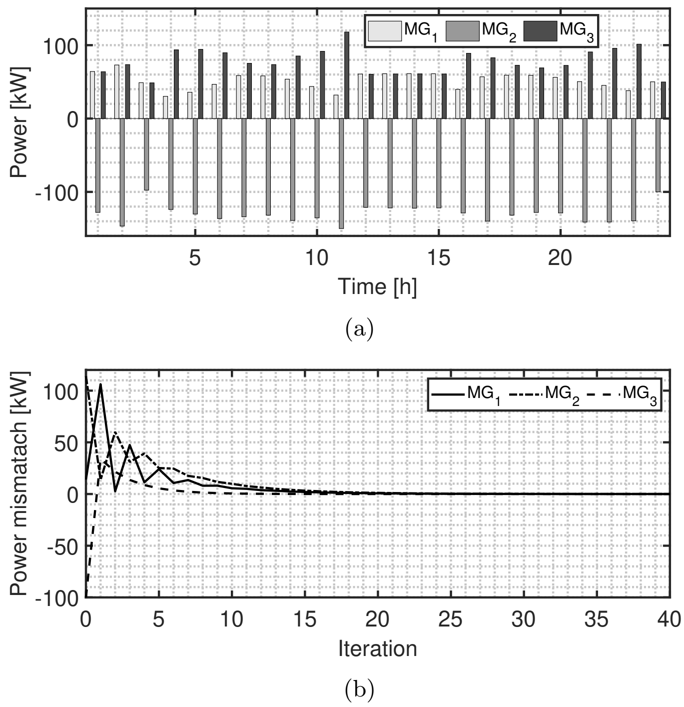

Figure 5.8: Simulation I: (a) Power exchange based on distributed control, (b) Power mismatch for $t = 0$.

5.3.2 Simulation II: Effect of limited generation resources

The above case study assumes that generation resources are unlimited, which is the reason that there is consistently power sharing between MGs as shown in Figure 5.8(a) and there is almost no critical load shedding in each MG. However, as mentioned before, the generation resources may be limited during extreme events, because of the potential disruption of the energy supply chain. In this case study, the effect of limited generation resources on optimal results is exhibited, where it is assumed that MG 1-3 only have 3500 kWh, 10000 kWh and 5000 kWh available resources during the event.

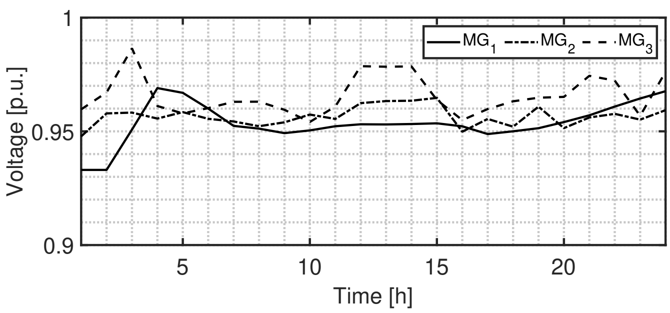

Figure 5.9: Simulation I: Voltage profiles of each MG in bus 3.

Results about final load shedding between MGs can be found in Table 5.5. It is shown that critical load shedding is caused in MG 1 and MG 3, while total load shedding in every MG has increased compared with results in the case study above. The reason can be found in Figure 5.10(a), which exhibits the final power sharing results between MGs. In the first 12 hours, there is a large amount of power supply from MG 2 to other MGs. However, after that, intensity and frequency of power sharing between MGs reduces a lot leading to larger load shedding in MG 1 and MG 3. This is because the suggested rolling optimisation method always considers a complete scheduling horizon (e.g., the next 24 hours). As such, after around 12 hours, MG 2 tends to distribute its generation resources for its own future usage (i.e., reducing load shedding) rather than using them for power sharing, which causes the reduced amount of power sharing during 15-20 hours. Figure 5.10(b) illustrates that there is much more load shedding caused in MG 1 and MG 3 in the last 10 hours.

Table 5.5: Simulation I: Load shedding in each MG under limited generation resources.

	Critical load shedding (kW)	Total load shedding (kW)
MG 1	56.18442	580.78514
MG 2	0	107.08655
MG 3	9.78499	1962.20392

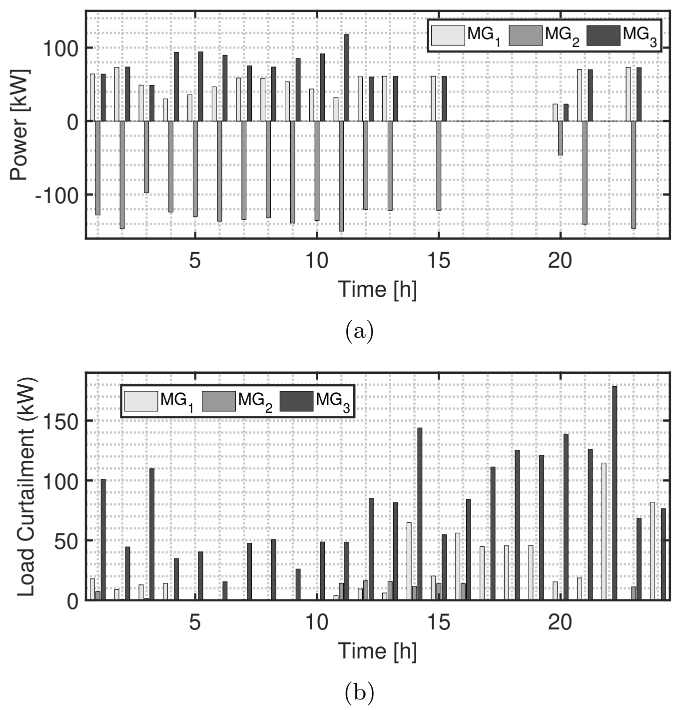

Figure 5.10: Simulation II: (a) Power exchange under limited generation resources, (b) Hourly load curtailment of each MG.

5.3.3 Simulation III: Non-cooperative behaviour of MGs

The main difference between networked MG systems under centralised control and distributed control is the protection of MG privacy and the localized decision making. As suggested in [135], MGs may try to manipulate certain parameters for further improving their own benefits (e.g., reducing operational cost), which is categorised as non-cooperative or dishonest behaviour. Especially during extreme events, it may be feasible for a certain MG to maintain higher levels of energy under its own territory for self-protection by reporting wrong values of parameters.

The model developed in this chapter can simulate the non-cooperative behaviour of MGs via a simple method explained hereafter. Let's assume that MG 2 may tend to reduce power export to the other MGs, since it has a conventional generator with a large rating and may be reluctant to share more energy to other MGs during an event. In this case, MG 2 may choose to reduce the value of parameter T_{ij}^{max} (e.g., from 150 kW to 100 kW or 50 kW), which will have a significant influence on optimal results of power exchange between MGs and final results of load shedding cost. As expected, Figure 5.11 illustrates that load shedding cost has largely increased when MG 2 reduces its power exchange limitation from 150 kW to 100 kW or 50 kW. Figure 5.12 corresponds to the power exchange under the non-cooperative behaviour of MG 2, which exhibits that less power can be imported into MG 1 and MG 3.

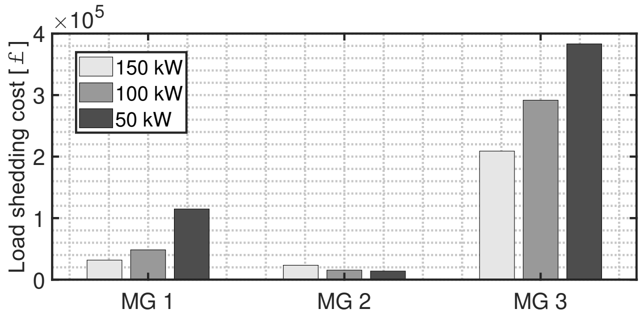

Figure 5.11: Simulation III: Load shedding cost under non-cooperative behaviours of MG 2.

5.4 Discussion

5.4.1 Sensitivity analysis investigating the influence of different rolling horizons

This section illustrates, through an appropriate sensitivity analysis, the influence of different rolling horizons on optimal results of the proposed scheme; refer to Table 5.6. On the one hand, selecting a very short horizon (e.g., 5 hours) would not sufficiently capture information regarding future uncertainties, which may lead to increased load shedding cost. On the other hand, if a long horizon (e.g., 24 hours) is selected, MGs may be convinced to share their resources conservatively which would cause slightly more load shedding, compared with a shorter horizon (e.g., 15 hours). All three

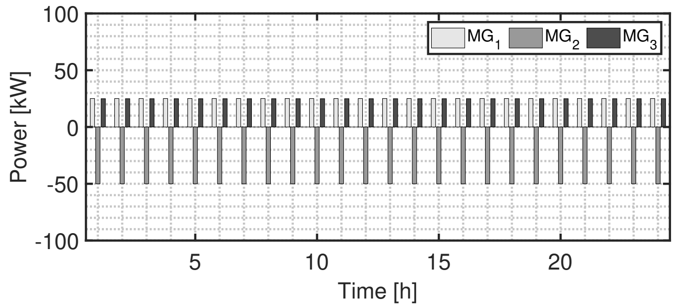

(a)

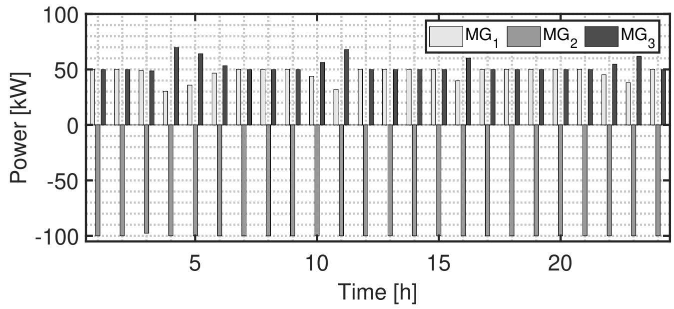

(b)

Figure 5.12: Simulation III: Power exchange between networked MGs (a) under 50 kW limit of MG 2, (b) under 100 kW limit of MG 2.

cases shown in Table 5.6 can be efficiently solved in an hourly basis via commercial softwares, while longer scheduling horizon would lead to longer computing time; note the exponential increase in computing time. Additionally, it shall be mentioned that the selection of the scheduling horizon is empirical and shall be appropriately decided according to realistic scenarios. For instance, a longer scheduling horizon could be used to better capture future uncertainties, if the event was to last for a long period (e.g., several days).

Table 5.6: Comparison between different scheduling horizons.

	Load shedding cost (k£)	Computing time for one step (s)
5 hours	283.02	0.76
15 hours	253.20	6.67
24 hours	264.07	29.04

5.4.2 A comparison of computing time between a typical centralised control and the distributed control approach

Table 5.7 illustrates that the computing time based on a centralised control approach is much longer than that based on the suggested distributed control approach under different scheduling horizons. The reason is that MG operations in the first and third stage of the suggested distributed control approach can be run in parallel, which largely reduces the computing burden. This comparative analysis demonstrates the merits of the proposed approach in terms of computing efficiency, which becomes significantly important in energy systems with high penetration of distributed energy sources that should be managed as close to real time as possible.

Table 5.7: Computing time of centralised control and distributed control under different scheduling horizons.

	distributed control	centralised control
5 hours	0.76s	5.58s
15 hours	6.67s	304.96s
24 hours	29.04s	3102.34s

5.4.3 Summary

To summarise, a three-stage stochastic distributed control approach based on rolling optimisation is suggested to enhance the resilience of networked MGs. Specifically, a stochastic linearised OPF is utilised in the first stage to capture the influence of uncertainties relating to renewable generation resources and load profiles as well as the flexibility of MESSs. A consensus-based algorithm is employed in the second stage to obtain results of power sharing between MGs, and finally a detailed AC OPF algorithm constitutes the third stage towards capturing technical constraints regarding stability properties and obtaining accurate solutions. Overall, the suggested approach provides benefits over other distributed control approaches found in the literature, as it can capture uncertainties, MESS routing and stability properties as well as ensuring computing efficiency. Additionally, this approach can be applied in different networked structures including both radial and meshed networks. Load distinction into critical and non-critical, the limitation of generation resources and the non-cooperative behaviours of MGs are appropriately considered in case studies to capture realistic scenarios and verify the effectiveness of the suggested rolling optimisation approach.

Chapter 6

A resilience-driven planning model for networked MGs

6.1 Introduction

As mentioned in the previous chapter, networked MGs can be utilised to decrease system cost in normal operation mode, while the energy sharing between MGs reduces load shedding during extreme events [44]. As such, networked MGs introduce further benefits for resilience enhancement than a standalone MG. Compared with the optimal sizing problem of a standalone MG, the planning problem of networked MGs is much more complicated due to more flexible operations, power exchange modelling and incorporation of more DERs [149]. There has been research focused on developing effective investment strategies for the normal operation of networked MGs (e.g., [150–152]). However, above papers only consider the internal uncertainties relating to generation resources and load profiles. External contingencies relating to potential extreme events, such as multiple line faults or power source damage, are ignored in above research.

In this context, resilience-driven planning problems of networked MGs have not been fully addressed in existing literature. One of the few papers that have considered resilience at planning stage (i.e., [64]) suggests an optimal sizing framework for energy storage units to enhance both resilience and reliability. However, this paper only considers the problem of battery sizing and utilises EMS to model the operation of networked MGs, which can lead to inaccurate solutions. Additionally, this paper considers single line fault as part of resilience modelling, which may be unrealistic; note that normally a resilience scenario should be based on $N-K$ contingencies. In [149], a two-stage chance constrained stochastic conic model is suggested to address the planning problem of networked MGs considering multi-site investment and dual-mode operations. In [153], a risk-averse mixed integer conic model is developed to design networked MGs considering reorganisation of the MGs boundaries. However, these two papers only consider MG islanding as the external contingency and [149] utilises a single-bus system to represent each MG, which may be unrealistic. Additionally, [149] considers several fixed capacities for the sizing problems of DERs, which can lead to over investment. To summarise, the research discussed above [64, 149, 153] simplifies OPF algorithms and utilises stochastic programming for uncertainty modelling, which makes it difficult to represent all possible scenarios ensuring the accuracy of the solution. When a detailed non-linear AC OPF is considered, computing efficiency and feasibility of solutions may not be guaranteed. As such, a robust-based method needs to be developed to ensure the required resilience level of networked MGs in the worst scenario, which is more realistic and efficient for planning problems considering both resilience and cost.

As far as the planning stage is concerned, there is no significant amount of research focusing on the optimal sizing problem of networked MGs capturing considerations both for resilience and cost, especially with the consideration of both internal uncertainties and external $N-K$ contingencies. In the operational level, all the literature tends to utilise EMS or linearised OPF to model MGs towards computational burden, however this may lead to inaccurate solutions. Additionally, linearised OPF algorithms utilised in several papers can only be suitable for radial networks, which limits its applications on other networks (e.g., meshed networks). Note that MGs might have different network structures, other than traditional distribution systems [139]. Meshed networks include a more uniform power flow and can provide benefits for improving voltage profiles and reducing power losses, which introduce stronger capabilities of meshed networks to withstand severe contingencies and improve resilience [145]. Therefore, this chapter proposes a three-level defender-attacker-defender model that can bridge a gap in this respective area. The key contributions of this chapter are summarised hereafter:

- A three-level model based on modified adaptive genetic algorithm (AGA) and non-dominated sorting genetic algorithm II (NSGA_II) is developed for the optimal sizing problem of networked MGs considering a trade-off between resilience and cost. AGA is utilised to obtain decisions for the normal planning problem in the first level and generate attacking plans in the second level, while NSGA_II is utilised to make a compromise between resilience and cost in the third level.

- Internal uncertainties relating to load profiles and external contingencies caused by extreme events including both multiple-line faults and power source damage are considered via the proposed AGA at the second level to mimic a realistic scenario and guarantee high reliability of the determined solutions. Note that there has been no research focusing on how to handle contingencies caused by power source damage and even further combining multiple types of contingencies.

- Detailed time-coupled AC OPF algorithm capturing technical constraints is utilised to model networked MGs for accurate solutions, which can capture the flexibility of ESSs and ensure the accuracy and efficiency of power sharing between MGs. A 96-hour scheduling horizon (i.e., 4 representative days) is utilised to represent a realistic scenario in the normal planning problem. An agglomerative hierarchical clustering method is utilised to group and select load data for the representative days and uncertainties relating to load profiles.

- The optimal sizing problem of both back-up generators and batteries is considered to demonstrate the effectiveness of the suggested three-level model on determining multiple parameters, while the approach is applied to a setup of networked MGs with a meshed structure and discrimination of loads into critical and non-critical.

6.2 Three-level model formulation

The optimal design and operation of networked MGs, as any other power system, is a notoriously hard problem because of the increased modelling complexity introduced by integer variables of sized assets and non-linear constraints pertaining to the AC power flow formulation [98]. It may be extremely time-consuming or impossible to directly solve this type of problems utilising current commercial software, especially when many parameters (e.g., over 3 parameters) need to be evaluated. Additionally, to address the requirement of resilience enhancement, a set of contingencies (e.g., multiple line faults and/or power source damage) shall be considered in the model to simulate emergency operations and ensure feasible solutions towards resilience, which largely increases the complexity of the suggested planning problem.

To solve this mixed integer non-linear problem (MINLP) with uncertainties and contingencies, a three-level planning model is designed in this chapter. The process can be found in Figure 6.1, while the input and output of each level have been presented in Figure 6.2. In the first level, the optimal sizing problem of networked MGs under normal operation is considered, while the second and third levels are formulated as a defender-attacker-defender model iteratively to capture a trade-off between resilience and cost [154]. A detailed explanation about the suggested three-level model can be found hereafter:

- In the first level, a meta-heuristic technique based on a modified AGA is utilised to tackle the normal optimal sizing problem of networked MGs (without the consideration of any contingency). After the AGA converges, the sizing results (e.g., capacities of generators and batteries) are sent to the second level.

- In the second level, different attacking plans are generated via the AGA to capture the influence of the worst event scenario on current sizing decisions and obtain the solution with the largest loss (i.e., load shedding). In this level, attacking plans will include power source damage, multiple line faults and be used towards maximising the load shedding cost of networked MGs. After the AGA converges, the attack plan that causes the largest load shedding cost will be sent to level three. If the selected attack plan still obtains a resilience level over the predefined target, current sizing results will be the final decisions and the iterative process ends. Note that attack plans to be determined in level two are based on the optimal sizing results obtained either from level one or level three (depending on the stage the algorithm has reached).

- In the third level, a multi-objective problem is formulated to consider the trade-off between investment cost and resilience as well as reducing the conservatism of final solutions. The problem is formulated via a NSGA_II algorithm, where two objective functions (cost minimisation and resilience maximisation) are considered. Both the normal operational problem and the operational problem incorporating the selected attacking plan from the second level are considered. Eventually, the NSGA_II will output several pareto solutions with different levels of cost and resilience. Then, according to the predefined resilience target (e.g., 65%), the solution that achieves the target (i.e., over 65%) and also obtains the lowest cost is selected and fed back to the second level for the next round of attack/verification.

To ensure that solutions with good quality are found, a non-linear solver called 'IPOPT' is utilised to solve the operational problem of networked MGs subject to the previously-obtained investment decisions [148].

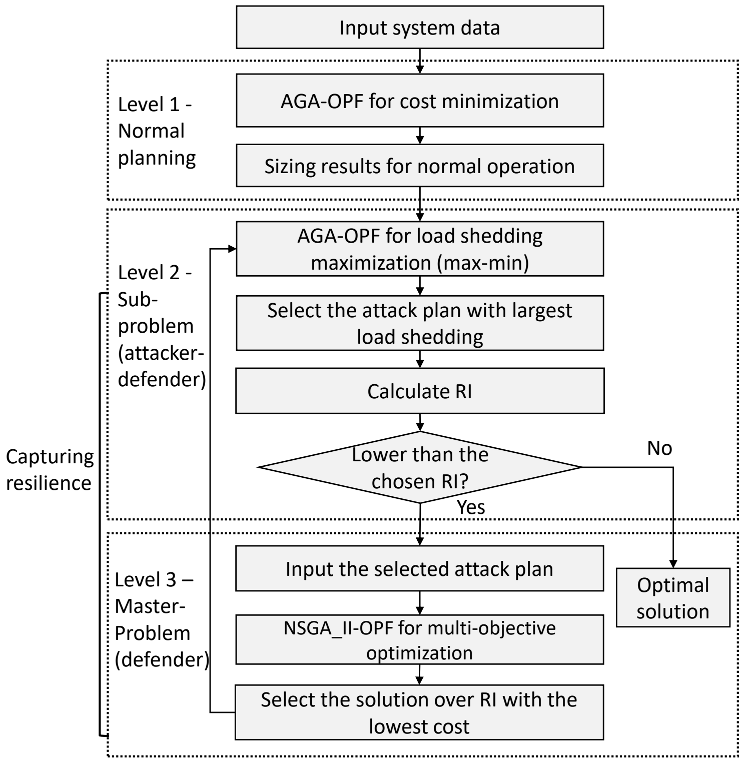

Figure 6.1: The flowchart of the three-level model.

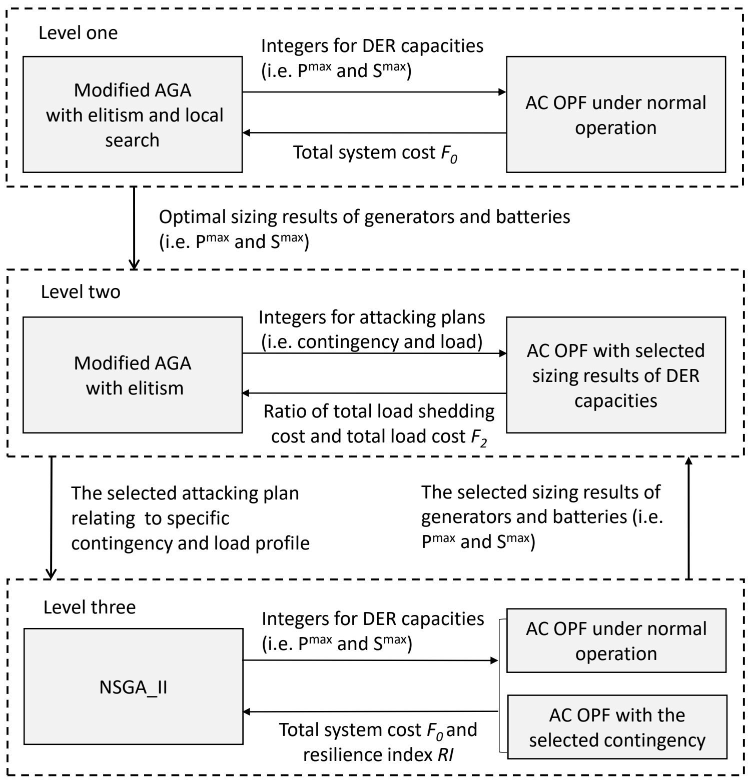

Figure 6.2: Input and output information of in each level.

As far as resilience assessment is concerned, the resilience trapezoid, a widely-used multi-phase resilience trapezoid approach has been suggested in [7]. Following this method, a resilience index (RI) corresponding to the percentage of weighted survived loads during extreme events is utilised in this chapter, which can be found in (6.1). $P^{ls}_{m,b,t}$ and $P^{l}_{m,b,t}$ correspond to load shedding and original load level in bus b of MG m at time t, while T_e refers to the scheduling horizon in emergency operation mode and c^{ls} is utilised to represent different weights of critical and non-critical loads.

$$RI = 1 - \frac{\sum_{m\in M}\sum_{t\in T_e}\sum_{b\in L_{bus}} c^{ls} P^{ls}_{m,b,t}}{\sum_{m\in M}\sum_{t\in T_e}\sum_{b\in L_{bus}} c^{ls} P^{l}_{m,b,t}} \tag{6.1}$$

6.2.1 First level-normal optimal sizing

The evaluation function for the normal planning of networked MGs is presented in (6.2), which includes the operational cost F_1 and the investment cost of back-up generators and ESSs. Note that the definition of F_1 has been given in equation (6.3) including generation cost, power exchange cost, load shedding cost and overslack cost, while C_{gen} and C_{ess} refer to investment costs of generators and batteries respectively. To meet the requirements of traditional power systems and mimic a realistic scenario, networked MGs utilised in this chapter will be operated via a centralized control method. The basic structure of isolated networked MGs is exhibited in Figure 6.3. MGs are connected with each other and are all managed by a central controller, which will make decisions on the power exchange among MGs. It is envisioned that this MG structure can capture the setting found in the MG of a so-called high-value building (e.g., hospitals, trading centres, etc.) within an urban centre.

$$min\ F_0 = F_1 + \sum_{b\in N_{gen}} C_{gen} + \sum_{d\in N_{ess}} C_{ess} \tag{6.2}$$

The AC OPF is utilised to assess the operational problem at hand, specifically for minimising the total system cost in both normal operation mode (without contingencies) and emergency operation mode (with contingencies), such as total generation cost and load shedding cost. The cost for load shedding shall be much larger than the cost for generation. Note that there should be no load shedding in normal operation, while the operator may need to curtail loads to guarantee the operation of networked MGs under emergency operation mode. In other words, the main target for resilience can be regarded as reducing load shedding. In mathematical terms, the objective function of the normal operation problem is given by (6.3). The first two terms involve the generation cost of conventional generators (e.g., diesel generators) and load shedding cost respectively. The third

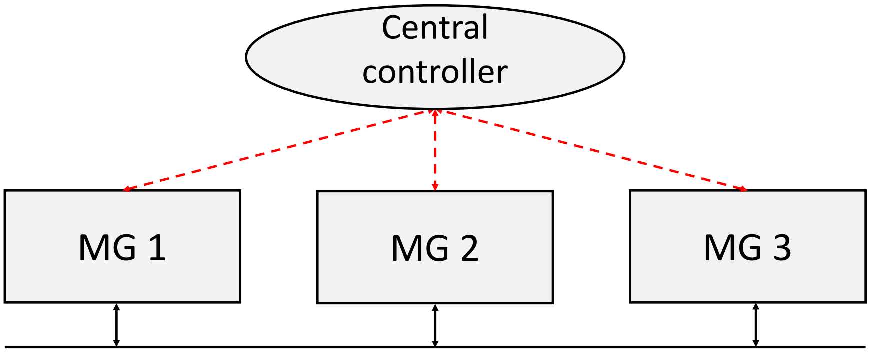

Figure 6.3: The structure of networked MGs.

term corresponds to the power exchange cost among different MGs and the fourth term is included to avoid infeasibilities, and in practice is modelled as a slack bus with a very high cost. The normal operational problem is posed as a minimisation problem, subject to the classical non-linear AC OPF constraints described in Chapter 3 and Chapter 4, while ESS-related constraints are also considered in the operational model.

$$\begin{aligned} min\ F_1 = \sum_{m\in M}\sum_{t\in T}[\sum_{g\in N_g} c^g P_{m,g,t} + \sum_{b\in L_{bus}} c^{ls} P^{ls}_{m,b,t}] \\ + \sum_{m\in M}\sum_{t\in T}\sum_{n\in M/m} c^e_{mn} \mid P^e_{mn,t} \mid + \sum_{m\in M}\sum_{t\in T}\sum_{b\in L_{bus}} c^{os} P^{os}_{m,b,t} \end{aligned} \tag{6.3}$$

6.2.2 Second level-event attacker

In this level, the main objective is to select the attacking plan that can cause the largest loss (i.e., load shedding) on current optimal sizing decisions, which can be formulated as a max-min problem. The objective function can be found in equation (6.4), which is calculated as the ratio of weighted load shedding cost over weighted load cost.

$$max\ min\ F_2 = \frac{\sum_{m\in M}\sum_{t\in T_e}\sum_{b\in L_{bus}} c^{ls} P^{ls}_{m,b,t}}{\sum_{m\in M}\sum_{t\in T_e}\sum_{b\in L_{bus}} c^{ls} P^{l}_{m,b,t}} \tag{6.4}$$

The classical equations pertaining to power flow problems have been provided in (6.5) and (6.6). Integer variables $x_{m,b,p}$ and $y_{m,g}$ are utilised to represent the influence of contingencies including both line faults and power source damage. $x_{m,b,p}$ represents the status of the line from bus b to bus p at MG m, where $x_{m,b,p} = 1$ corresponds to an intact line and $x_{m,b,p} = 0$ means the line has been damaged by extreme events. The power generation limit of conventional generators is modified as equation (6.7)-(6.8), where $y_{m,g} = 1$ represents the generator g is intact during emergency period and $y_{m,g} = 0$ means the generator g is damaged or tripped. Instead of T, T_e is utilised to represent the time scheduling horizon at emergency mode. Other constraints (e.g., power balance constraints) are the same as those in the first-level planning problem.

$$P^{ex}_{m,b,t} = \sum_{p \in N_{bus}} x_{m,b,p} V_{m,b,t} V_{m,p,t} (G_{bp} cos\delta_{bp,m,t} + B_{bp} sin\delta_{bp,m,t}),\ \forall t \in T_e,\ \forall b \in N_{bus} \tag{6.5}$$

$$Q^{ex}_{m,b,t} = \sum_{p \in N_{bus}} x_{m,b,p} V_{m,b,t} V_{m,p,t} (G_{bp} sin\delta_{bp,m,t} - B_{bp} cos\delta_{bp,m,t}),\ \forall t \in T_e,\ \forall b \in N_{bus} \tag{6.6}$$

$$y_{m,g} P^{min}_{m,g} \le P_{m,g,t} \le y_{m,g} P^{max}_{m,g},\ \forall t \in T_e,\ \forall g \in N_g \tag{6.7}$$

$$y_{m,g} Q^{min}_{m,g} \le Q_{m,g,t} \le y_{m,g} Q^{max}_{m,g},\ \forall t \in T_e,\ \forall g \in N_g \tag{6.8}$$

As such, the problem in the second level is still a MINLP problem because of the incorporation of contingency-related integer variables. To capture feasible and accurate operational solutions as well as to consider the influence of uncertainties and contingencies, the suggested AGA is utilised to handle integer variables and solve the level 2 problem. More details about the solving procedure can be found in Section 6.3.

6.2.3 Third level-defender

According to Figure 6.1, the third level is formulated as a multi-objective optimisation problem considering a trade-off between cost and resilience, where one objective relates to cost minimisation, which mainly considers reduction of investment cost in normal planning, and the other objective is to maximise the resilience level (i.e., reducing load shedding) under the selected attacking plan obtained from level 2, which may require more investment. Note that extreme events are featured by low probability and unpredictability, which means that it may not be appropriate to invest a lot for rare events. As such, a trade-off between cost and resilience is necessary for decision making at the planning stage. The two objective functions have been formulated in (6.9) and (6.10), where (6.9) is the same as the objective of the normal planning problem and (6.10) utilises the suggested RI as the objective. The constraints of F_{3_1} and F_{3_2} are the same as the normal planning problem, while F_{3_2} is based on the worst scenario s obtained in the second level.

$$\min\ F_{3\_1} = F_0 \tag{6.9}$$

$$\max \ F_{3\_2} = RI \tag{6.10}$$

Considering the incorporated integer variables relating to generator and battery ratings (MINLP formulation), the multi-objective optimisation problem will be solved by NSGA_II, which has the advantage to output several pareto solutions capturing both resilience and cost for decision makers' consideration. According to the requirement of decision makers, the solution over the required resilience level with the lowest system cost will be selected and sent back to the second level for next-round verification.

6.3 Problem solution procedure

6.3.1 Data preparation

As far as the normal planning problem is concerned, 4 representative days (96-hour scheduling horizon) are selected from one-year data to ensure that typical load profiles across different seasons are captured and the system is not oversized due to using a peak day. Note that the proposed optimal sizing model is closer to operational planning rather than long-term multi-year infrastructure planning. As such, this is a choice to capture realistic scenarios and also guarantee computing efficiency. Regarding uncertainties, 15 different load profiles are generated and employed to represent the load uncertainty, which aims to represent the uncertain fluctuations of load profiles across a year. Additionally, to ensure that a realistic scenario is captured, the data for both representative days and uncertainties are from real data.

It is worth noting that the use of four typical days can be considered representative in the following case studies, since there are four seasons in a year [155, 156]. Note that the suggested model deals with static planning, which means that the assets (i.e., generators and batteries) are to be sized once and the possibility for future load growth, additions/upgrades, and cascading failures is not considered. Even though utilising a greater number of typical days is good practice for a better approximation of total system cost, it is important to note that planning decisions are mostly made by a small number of operating points (e.g., peak load level) [98]. Utilising typical days for the representation of one-year duration is a common approach employed to reduce computing burden for planning research without compromising solution integrity [155]. Additionally, there has been research focusing on developing advanced approaches to select representative days more effectively, which can reduce the number of representative days while maintaining similar accuracy.

For instance, [157] has suggested an optimisation approach, which can ensure that the accuracy of planning models by selecting 4 days is similar to the accuracy of other approaches selecting 24 days.

The agglomerative hierarchical clustering method (bottom-up approach) with Ward's linkage is employed to establish different groups of load data and identify representative days or an uncertainty set from a different cluster [142]. After obtaining these clusters, medoid points of clusters are selected to represent final scenarios (i.e., 4 representative days or 15 uncertain load profiles). Given that each initial operating scenario has the same occurrence probability, the probability of each final scenario can be calculated as the ratio of the number of initial scenarios that belong to the cluster and the number of scenarios [141].

6.3.2 Modified adaptive genetic algorithm

Both the first and second level problems (*min* and *max min*) proposed in this chapter belong to MINLP problems, because of the introduction of numerous binary variables to determine asset sizing, attacking plans and non-linear constraints. To keep technical constraints under consideration, this chapter suggested a modified adaptive genetic algorithm (AGA) to solve these MINLP models. A genetic algorithm (GA), categorised as a global search meta-heuristic, mimics natural biological procedures via operators such as crossover and mutation. The advantages of the GA is that it does not suffer from the limitation of parameter numbers and is very efficient in terms of computational time and programming simplicity [98]. However, traditional GA, which normally utilises a small mutation rate (e.g., 0.01-0.1), may easily fall within a local minimum for the mathematical formulation suggested in this chapter, while a large mutation rate (e.g., over 0.3) can make the problem hard to converge. In this chapter, an AGA with local search and elitism [158] is developed to solve these MINLP problems. Adaptive crossover/mutation probabilities and local search are utilised to enhance the ability of the GA to avoid local optimum, while the application of elitism preserves good offsprings and speeds up the convergence of GA. The iterative process of the suggested AGA can be found in Figure 6.4.

The calculation rules of crossover probability (p^c) and mutation probability (p^m) are modified and shown in (6.11-6.14) [159]. f' represents the smaller fitness value in two children that is chosen for a crossover operation, while f^{ave} corresponds to the average fitness value of the whole population and f^{max} regarding the largest fitness value in the whole population. k_1, k_2, k_3, k_4 and α are constant, which can take different values for different optimisation problems. In [159],

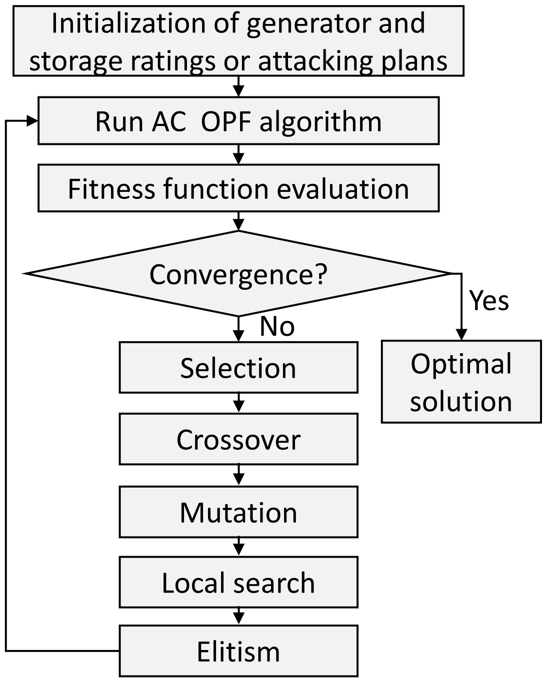

Figure 6.4: Flowchart of the suggested AGA.

a set of values [1, 0.5, 1, 0.5] is suggested for k_1, k_2, k_3 and k_4. However, the very large value of k_1 and low value of k_4 leads to non-convergence for the specific application. Since the first level is formulated as a minimization problem, the value of f' may be equal to f^{max}. Therefore, it is necessary to introduce the parameter α to avoid this problem, where α shall be slightly larger than 1. In this chapter, they take the values of 0.85, 0.5, 1, 1 and 2 respectively. Note that the criteria for choosing the constants k_1, k_2, k_3 and k_4 and α are empirical (i.e., through tens of trial-and-error simulations). In different optimization problems, they can take different values depending on the purposes they serve. An explanation of the elitism process can be found in [158].

$$p^c = k_1 \frac{\alpha f^{max} - f^{ave}}{\alpha f_{max} - f'}, \; when \; f' \leq f^{ave} \tag{6.11}$$

$$p^c = k_3, \; when \; f' > f^{ave} \tag{6.12}$$

$$p^m = k_2 \frac{\alpha f^{max} - f^{ave}}{\alpha f^{max} - f'}, \; when \; f' \leq f^{ave} \tag{6.13}$$

$$p^m = k_4, \; when \; f' > f^{ave} \tag{6.14}$$

Last but not least, the modified AGA has stronger ability to avoid local minimum than a generic GA; nevertheless, it still cannot utilise the nature of the problem to find and improve the optimal solution. The poor local search ability may need the AGA to generate a large scale of populations to find the optimal solution. To strengthen the local search ability of AGA, this chapter suggests a simple method to improve the qualities of solutions in every generation. The process of local search is as follows:

- Select the child with the worst fitness value from every generation and replace it with the best child;
- Randomly pick up one parameter from all determined ones and reduce the value of this parameter by x (e.g., 3);
- Calculate the fitness value of the new child and add it to the offspring list.

Regarding the first level problem, capacities of back-up generators and ESSs can be initialised as iterated generations (e.g., pairs of back-up generator ratings [200 kW, 200 kW, 200 kW] with the range of [0 kW, 400 kW] and pairs of ESS ratings [40 kW, 40 kW, 40 kW] within the range of [0 kW, 100 kW]. Note that it is considered that the energy content of each ESS can be as high as four times the selected capacity [98]. The fitness function is the total system cost provided iteratively for each chromosome through the utilised AC OPF. The algorithm is considered to have converged, when the optimal solution has not changed for more than a certain number of iterations (e.g., 20 or 30), or the maximum number of iterations has been reached (e.g., 100). Note that the suggested three-level model is characterised by a highly non-linear nature in each level, which introduces challenges in obtaining solutions with good quality. As such, this chapter has chosen a strict rule of convergence to ensure that the suggested AGA can find solutions with good quality and better avoid over investment. Particularly, the maximum number of iterations allowed is set to 100, while in case the fitness function does not change for 20 iterations, then algorithm finishes.

Regarding the second level problem, internal uncertainties and external contingencies need to be considered. As such, one chromosome has to include two different types of genes: i) the attack plan including power source damage and line faults; ii) selected load profile from uncertainty set. For instance, one attacking plan can be represented via a chromosome [2, 4, 5, 6, 1], which reflects generator 2 and three lines [4, 5, 6] from different MGs being damaged in this attack plan, while the load profile from cluster 1 is selected. Note that the local search technique is not utilised for the second level problem.

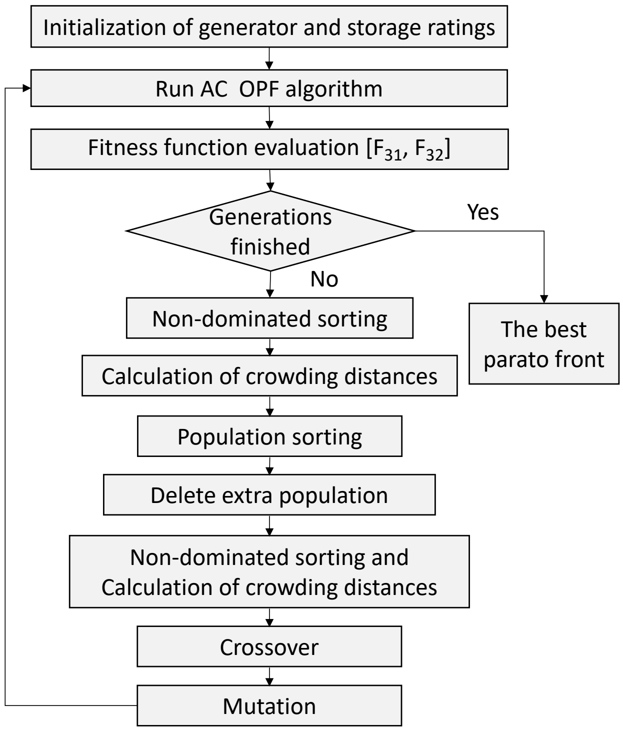

Figure 6.5: NSGA_II flowchart.

6.3.3 NSGA_II

The target of the third level problem is to obtain sizing solutions that can capture a trade-off between cost and resilience. Hence, a multi-objective evolutionary algorithm based on NSGA_II [160] is adopted to solve the problem. The most significant advantage of NSGA_II is that it can obtain an optimal solution set rather than a single optimal solution, which gives operators more options for decision making. Note that extreme events have a very low probability, even though the damage may be huge. As such, if the power system is located in an area with a higher probability of extreme events or decision makers have a low-risk tolerance, it may be necessary to invest more for a higher resilience level; otherwise, there may be no need for pursuing a very high resilience level under the worst scenario. The suggested multi-objective formulation at this level has the advantage of avoiding the conservatism of final solutions and provides several options for decision makers. The process of NSGA_II can be found in Figure 6.5.

According to Figure 6.1, all three levels are formulated in an iterative way. One challenge based on the suggested multi-objective formulation is how to guarantee the effectiveness of the current solution against attacks from previous iterations. To improve the solutions step by step, it is necessary to introduce a budget set for the initialisation of new offsprings. To make it clear, the process of the suggested DAD model in iteration k can be found hereafter:

1. Attack the current solution via AGA and select the attack plan with the largest loss.

2. Obtain the attack plan from level 2 and the previous sizing result of iteration $k-1$, where generator i is damaged and several lines are tripped. Assume the current budget group set is represented by B. More details about updating B can be found in step (5).

3. Initialize the ratings of generators and batteries according to the current budget set B, which guarantees the new solution will meet requirements of resilience against worst scenarios from previous iterations.

4. Run NSGA_II and obtain the pareto front. Select the solution with respect to the operators' requirements (i.e., achieve desired resilience level and also with the relatively lowest system cost). The solution is represented by $[G_1, G_2, ...G_n]$ and $[ES_1, ES_2, ...ES_n]$, where G and ES for generators and ESSs respectively.

5. To ensure that the updated solutions still meet the resilience requirement against the current attack, it is necessary to generate a new group of budget plans $\sum_{g\in G/i} P_g^{max} \geq \sum_{g\in N/i} G_g$ and $S_b^{max} \geq ES_b, \forall b \in E$ for following iterations.

6. Add the new budget plans into set B and send the solution back to step (1) for next round attack (i.e., iteration $k+1$) and verification.

6.4 Case studies

The following case studies are specifically focusing on isolated networked MGs, which is in alignment with other relevant research (e.g., [161]); hence a utility grid has not been included. The structure of a typical AC MG utilised in this chapter is presented in Figure 7.4; note that an urban centre composing of three MGs could have emergency backup generator(s) and ESSs (especially in the future system setting). That is why in each MG a conventional generator (e.g., diesel generator) is installed as a conventional energy resource, while an ESS unit is also installed and connected with this MG through power converters. All operational and investment data related to the electricity system are extracted from [144] and [98]. It is more realistic to assume that not all loads would be essential. Similar to [71], it is assumed that the loads L_3 in the bus 3 of each MG (around 30% of total loads) are critical loads with high curtailment cost, while other types of loads are

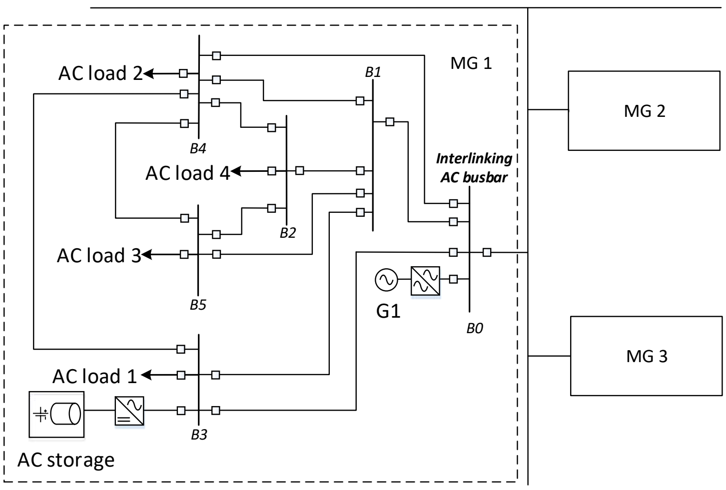

Figure 6.6: Networked MGs utilised for simulations.

non-critical loads with relatively lower curtailment cost. Additionally, a 96-hour scheduling horizon is formulated to capture the seasonal change of load profiles and the flexibility of ESSs.

6.4.1 Simulation I - Size generators under normal operation

In this case, three back-up generators are optimally sized via the AGA, while the sizing results in three stand-alone MGs are utilised for comparison. As far as the storage devices are concerned, each MG includes a low power-low energy battery (e.g., 50 kW/200 kWh). Figure 6.7(a) illustrates the evolution of the total system cost across the AGA evolution, which converged within 50 iterations. The lowest system cost and investment cost are £54464.20 and £45905.28 respectively, while the optimal design corresponds to capacities of [52 kW, 362 kW, 270 kW] for the three back-up generators respectively. Note that the total system cost includes both investment cost and operational cost.

When three stand-alone MGs are optimally sized separately with the solution [202 kW, 256 kW, 226 kW], the total system cost and investment cost are £110546.38 and £103090.56 respectively, which are much larger than the cost obtained from the optimal sizing of networked MGs under normal mode. Figure 6.7(b) exhibits that the optimal capacity of back-up generators in MG 1 (with the highest investment cost) has been significantly reduced because of the consideration of power sharing between MGs. It can be concluded that the power sharing between MGs can enhance the ability of each MG to supply loads and then reduce investment cost. The power exchange results in normal operation can be found in Figure 6.8(a), which show that MG 1 requires more power support from other MGs. Figure 6.8(b) indicates how ESSs in different MGs charge and discharge

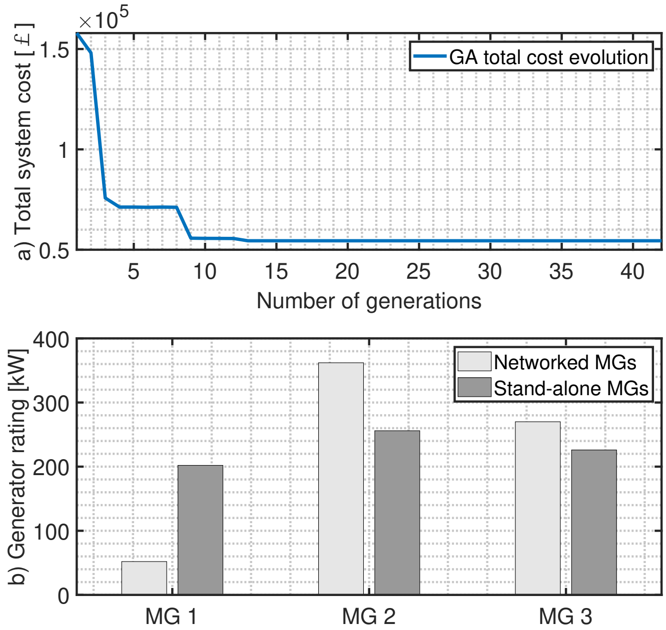

Figure 6.7: Simulation I: (a) GA total system cost evolution of networked MGs; (b) Back-up generator ratings in both cases.

when loads are significantly changed.

6.4.2 Simulation II - Trade-off between resilience and cost

As mentioned earlier, considering resilience at the planning stage is important for the normal operation of networked MGs. In this subsection, the suggested three-level approach is utilised to determine a trade-off between resilience and cost, and the results can be found in Figure 6.9. Figure 6.9(a) shows the pareto front of the NSGA_II in the first iteration, where the sizing results account for different combinations of cost and resilience. Generally, more investment cost leads to a higher resilience level. The suggested multi-objective formulation can meet different requirements and also avoid conservative results, which are normally caused by robust-based methods. Three groups of results including 'For RI 65 %', 'For RI 70 %', 'For RI 75 %' are utilised to represent the potential requirements of decision makers for resilience. Note that Figure 6.9(a) only exhibits the results of the first iteration. If the obtained result fails to get through the attacking verification of the second level, NSGA_II needs to run again considering the newest attacking set and solutions will also be updated.

Because the defender-attacker-defender model always considers the worst scenario, all three groups of final results for resilience-driven optimal sizing of back-up generators can be obtained within five iterations, which can be found in Figure 6.9(b). To achieve a higher resilience level,

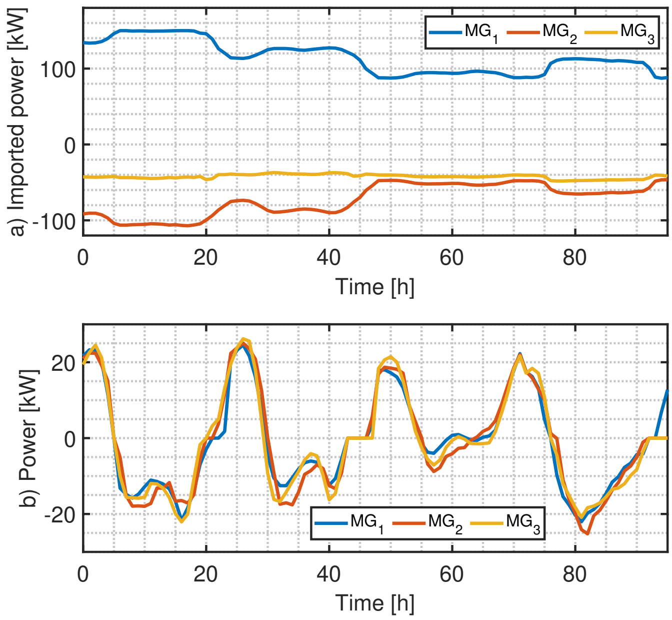

Figure 6.8: Simulation I: (a) Power exchange between MGs in normal operation; (b) Batteries charging/discharging patterns at normal operation.

the sizing results of MG 1 and MG 3 have been significantly increased. Compared with the system cost in normal planning problem, the system costs of all these three groups have increased, which accounts for £69856.84, £80462.92, £98872.44 respectively. It can be expected that the investment cost increases with the requirement of a higher resilience level. As mentioned earlier, the algorithm is effective and can obtain final solutions within several iterations. For instance, the improving process of the obtained solution for RI 65% is [52, 362, 270] → [73, 315, 296] → [88, 303, 309] → [89, 309, 308] with the worst loss accounting for 46.71% → 37.41% → 36.61% → 34.88%.

Additionally, the verification of final optimal results can be found in Figure 6.9(c) which shows that the results achieve the required resilience level, proving the effectiveness of the suggested approach. Note that achieving 75 % resilience is actually a very high standard for decision makers, because of the consideration of the worst scenario including both power source damage and line faults; nevertheless, the total system cost under RI 75% is still lower than the system cost of stand-alone MGs, and this is a significant result showing key direction for future operational and planning considerations of MGs found in a network.

6.4.3 Simulation III - Size both generators and batteries

To further exhibit the effectiveness of the suggested three-level model on deciding multiple parameters, ratings of both generators and batteries are considered in the optimal sizing problem. Figure 6.10(a) shows the sizing results under normal planning problem, where the results of stand-alone MGs are utilised for comparison. Compared with the battery settings [50 kW, 50 kW, 50 kW] used in previous simulations, battery ratings in all MGs reduce significantly to [24 kW, 20 kW, 20 kW], even though the sizing results of generators have been slightly increased to [77 kW, 365 kW, 272 kW]. It is proven that the suggested planning approach has the ability to size multiple parameters at the same time and avoid unnecessary oversizing issues. Regarding three stand-alone MGs optimally sized separately, the sizing results are [210 kW, 267 kW, 237 kW, 24 kW, 20 kW, 20 kW], while the total system cost and investment cost are £206149.92 and £198692.16 respectively, compared with networked MGs accounting for total system cost £156324.37 and investment cost £148003.20.

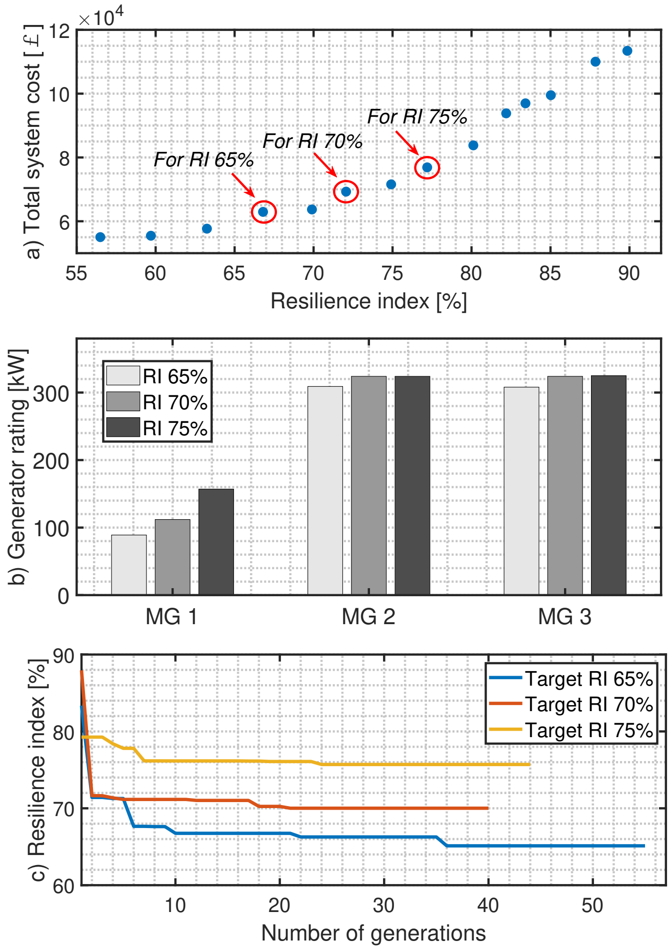

Figure 6.9: Simulation II: (a) Pareto front after the first iteration of NSGA_II; (b) Results considering both resilience and cost; (c) The final verification of the second stage attack.

Three groups of trade-off results between resilience and cost can be found in Figure 6.10(b). Sizing results of battery units are basically the same as the normal planning problem, while generator ratings slightly increased compared with the results of Simulation II. On the one hand, this illustrates the effectiveness of the suggested planning model on obtaining a trade-off between resilience and

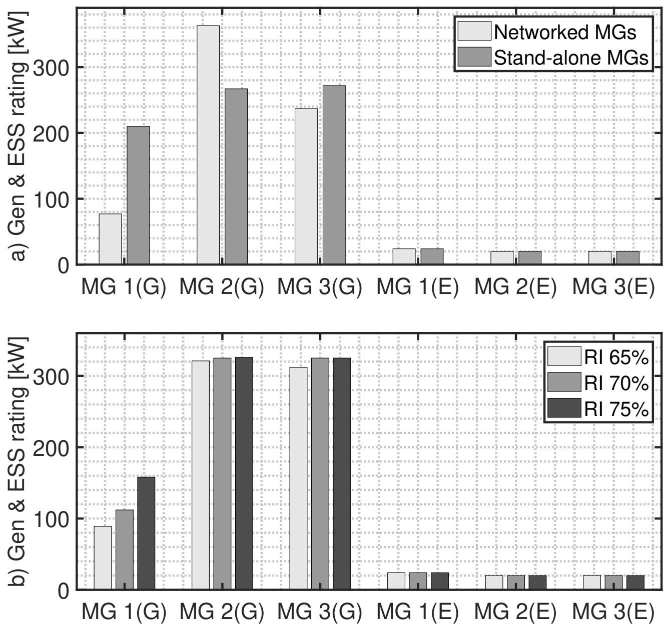

Figure 6.10: Simulation III: (a) Back-up generator ratings under normal planning problem; (b) Three groups of results considering both resilience and cost, where 'G' and 'E' account for generators and batteries respectively.

cost; on the other hand, it can be concluded that battery ratings are less sensitive to resilience level than generators, of which ratings directly influence the power & load balance. However, comparison results between Simulation II and Simulation III also show that it is necessary to consider both generators and batteries to avoid over investment and reduce system cost, because of the significantly higher price of battery units.

6.4.4 Simulation IV - Sizing results considering MG islanding

The connection between MGs may be interrupted due to unstable cyber links or faulted lines during extreme events; hence, it is necessary to consider the influence of MG islanding on sizing results of each MG, which can be captured through the following points: 1) it is possible for every MG to switch into islanded mode due to the interrupted connection or self-protection; 2) it anticipates that islanded MGs can still achieve the required resilience level. Note that the above two points are aligned with the suggested three-level model based on robust optimisation (i.e., capturing the worst scenario). As such, it is reasonable to firstly calculate the optimal sizing results of each MG in islanded mode and then regard these results as lower limits of the suggested three-level model.

To achieve this goal, the suggested model is firstly used to find the optimal sizing results for each islanded MG. Note that these results will consider cost minimisation as well as ensuring the expected resilience level of each MG under islanded mode. After that, these results will be treated as lower limits for the initialisation of DER ratings in the third level of the suggested model. For instance, optimal sizings of generators in each MG under islanded mode account for [118 kW, 137 kW, 119 kW] with a resilience level 65% respectively, which means that the initialisation of generator ratings in each MG at the third level shall not be lower than these values [118 kW, 137 kW, 119 kW]. If not, when one MG switches into islanded mode, it can not ensure the expected resilience level. Using this method, the influence of MG islanding is appropriately considered in final sizing results.

The optimal sizing results of DER ratings considering MG islanding have been updated to [118 kW, 286 kW, 280 kW] and [131 kW, 308 kW, 306 kW] for RI 65% and 70% respectively. Note that sizing results under RI 75% do not change, since the limit has no influence on the final results when RI 75% is expected. The comparison between sizing results with and without the consideration of MG islanding can be found in Figure 6.11. Figure 6.11(a) and 6.11(b) correspond to the difference of generator ratings on MG 1 and MG 2, while Figure 6.11(c) presents that total system costs for RI 65% and RI 70% have increased with islanding consideration. The reason is that the generator rating (the most expensive generator) in MG 1 has increased a lot to ensure the expected resilience level when it switches into islanded mode during extreme events, which accounts for much larger investment cost.

6.5 Cost comparison between case studies

This section serves as a cost comparison under normal operation between the previously presented acse studies. Figure 6.12 illustrates the total system cost split into investment and operational costs for each case investigated in the previous subsections. Obviously, sizing both generators and batteries will lead to higher investment cost than sizing only generators. Additionally, it is clearly demonstrated that under normal operation the majority of the costs are associated with the investment via the comparison between Figure 6.12(a) and Figure 6.12(b), while the investment cost increases when decision makers require higher resilience level across the networked MGs.

An interesting observation relates to the operational cost in Figure 6.12(b), which exhibits that the operational cost decreases a bit with the increase of investment cost or required resilience level. The reason for this is that decision makers tend to reduce investments in expensive generators (e.g., the generator in MG 1) under the normal planning problem and increase expenditure in more cost-effective generators (e.g., the generator in MG 2), which leads to higher energy exchange between MGs. However, when contingencies are considered, investment in expensive generators shall increase, which actually reduces the power exchange cost between MGs under normal operation mode.

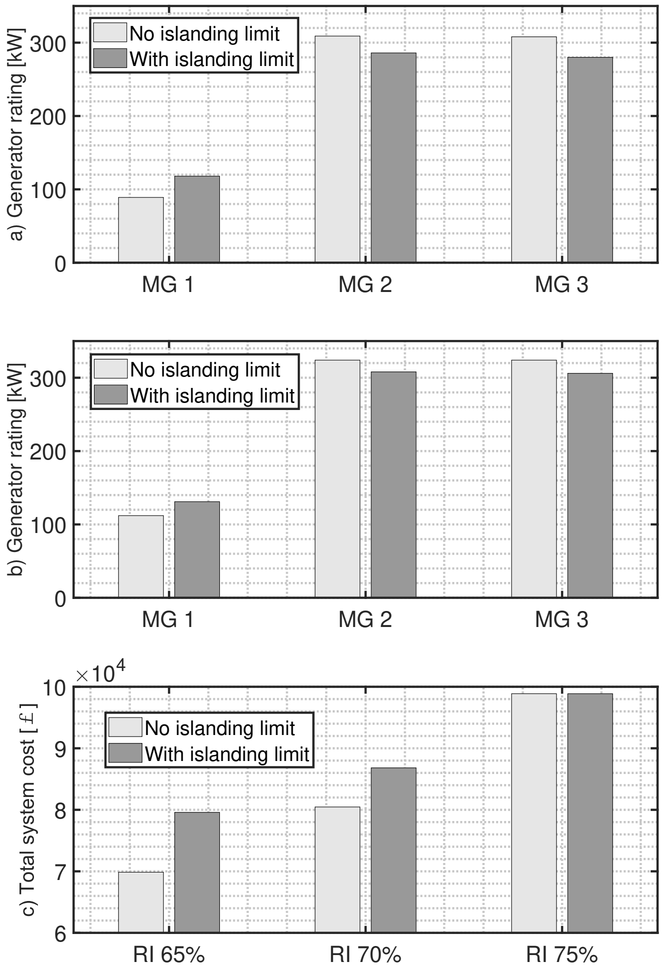

Figure 6.11: Simulation IV: (a) Comparison of optimal sizing results for RI 65%; (b) Comparison of optimal sizing results for RI 70%; (c) Cost comparison between sizing results with and without islanding limits.

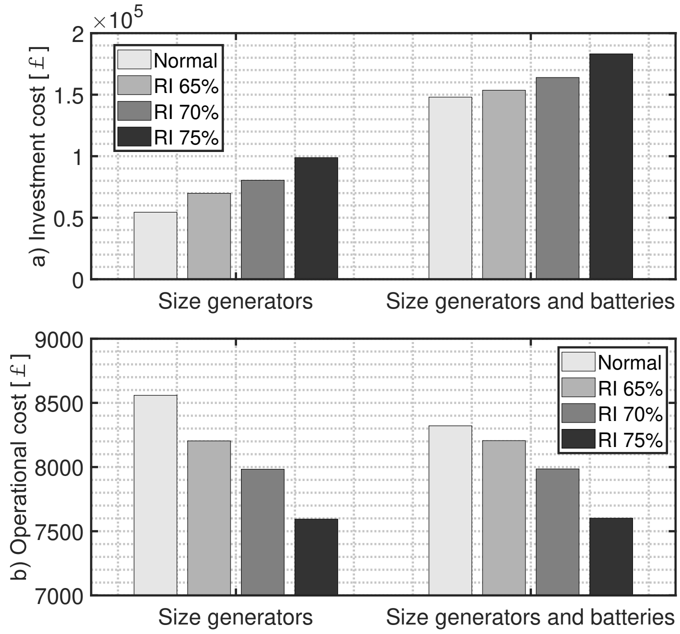

Figure 6.12: Total system cost breakdown of the investigated cases: (a) Investment cost; (b) Operational cost.

Chapter 7

Optimal sizing and pre-positioning of MESSs

7.1 Introduction

Networked MGs are widely used as an effective strategy for load restoration and cost minimisation during extreme events [44], while MPSs (e.g., MESSs) have attracted research interest due to their mobility and flexibility compared to static resources [162]. As such, this chapter aims to develop a resilience-driven planning model for optimal sizing and pre-positioning problems of MESSs in decentralised networked MGs, which is generic enough to capture main contingencies caused by both man-made events and natural disasters.

7.1.1 Networked MGs based on distributed control

Centralised control and hierarchical control have been employed for resilience-driven planning and operations of networked MGs [6, 149, 163]. However, operations of networked MGs considered in above research require central controllers for decision making, which might be unrealistic when an extreme event occurs. Compared to control approaches requiring central controllers, MG operations based on distributed control might not reach global optimum easily but can have faster response and less dependence of each MG on a central controller [135]. Recently, much research focuses on developing decentralised operation strategies for networked MGs, where linearised Distflow and EMSs are two main approaches for MG modelling. As mentioned in previous chapters, these two approaches have apparent limitations. Overall, operations of power systems can easily reach their stability limits during extreme events [164], which makes it a necessity to capture all the technical constraints for safe MG operations.

As far as planning problems capturing networked MGs with distributed control are concerned, there is not much research focused on this area. In [151], a planning model capturing cooperative behaviours of interconnected MGs has been developed to deploy renewable energy sources and minimise investment cost; nevertheless, only normal operations have been considered in this paper. In [150], a power dispatch framework based on a consensus algorithm is proposed for the planning and operation of networked MGs. However, this paper does not incorporate any uncertainties or contingencies into the model. It can be concluded that there is no research focused on resilience-driven planning problems of decentralised networked MGs capturing both uncertainties and contingencies. Additionally, existing planning approaches on networked MGs mainly focus on static DERs (e.g., generators and batteries). However, extreme events have the high-impact and low-probability nature, which may lead to the requirement for higher flexibility than normal planning problems [165]. In this context, the sizing and pre-positioning problems of MPSs (e.g., MEGs and MESSs) can be much more realistic and effective.

7.1.2 Mobile units for load restoration

Planning problems of distributed energy resources (e.g., storage systems) have attracted research interest due to the trend of highly electrified future and the appearance of economical storage options [166]. To better tackle the impact of severe contingencies, the incorporation of MPSs such as MESSs and mobile emergency generators (MEGs) in power systems has become more and more common for load restoration. For instance, in [16], a pre-hurricane resource allocation strategy is suggested to provide proactive preparedness for distribution systems against natural disasters. Generation resources such as diesel oil, transportable batteries and electric buses are considered for allocation. In [18], a two-stage pre-sizing and positioning model of MESSs is proposed to restore loads after extreme events. In [59], a two-stage pre-positioning framework is proposed to implement resilient routing and scheduling of MPSs. Both load survivability and recovery performance of the system are considered in the paper. In [69], a two-stage framework focusing on the pre-positioning and optimal dispatch of MEGs is suggested to dynamically formulate multiple MGs and restore critical loads after extreme events. However, the multi-period dynamic dispatch is ignored because the allocated MEGs stand still at the same place.

Except for the above pre-allocation problems, there has been much research focused on developing operational strategies of MESSs due to their mobility and flexibility for load restoration [167]. In [68], a co-optimisation model with the routing and scheduling of repair crews and MPSs is developed to restore distribution systems and enhance grid resilience. In [19], a post-disaster joint scheme incorporating multiple MGs, MESSs, network reconfiguration and generation scheduling is suggested for load restoration. In [168], a load restoration strategy based on rolling optimisation is proposed to coordinate the routing decisions of MESSs and the reconfiguration of distribution networks. However, the above papers only consider the operational level and do not include any uncertainty.

There are limitations in the above research: firstly, no uncertainties relating to renewable energy sources and load profiles are considered on the above planning models; secondly, external contingencies are handled via scenario-based stochastic programming, which may only be able to consider small number of scenarios due to large computing burden; thirdly, most papers only consider pre-positioning problems of MPSs (e.g., [16] and [59]) rather than both optimal sizing and pre-positioning, which cannot fully present the advantages of MPSs. Above limitations or simplifications are all related to the large computing burden brought by the modelling of MPSs (e.g., the introduction of large amounts of integer variables) and they will lead to inaccurate optimisation results. As such, it is necessary to develop a comprehensive planning model considering both optimal sizing and pre-positioning problems of mobile units as well as capturing both internal uncertainties and external contingencies via an appropriate approach. As mentioned before, different distributed control approaches for networked MGs can largely reduce computing burden, which brings opportunities for the application of MPSs. Additionally, approaches based on robust optimisation may be more appropriate for modelling severe contingencies [169].

To summarise, there is no significant amount of research focused on optimal sizing and pre-positioning problems of MESSs for the resilience enhancement of decentralised networked MGs. Additionally, direct mathematical programming approaches only featuring stochastic programming can be inappropriate for solving the suggested problem due to the consideration of distributed control, internal uncertainties and external contingencies. Therefore, this chapter proposes a novel resilience-driven planning model for the optimal sizing and pre-positioning problems of MESSs in decentralised networked MGs capturing both internal uncertainties and external contingencies, which can bridge a gap in this respective area. The contributions are summarized hereafter:

- A three-level defender-attacker-defender (DAD) model based on an adaptive genetic algorithm (GA) is developed to solve the optimal sizing and pre-positioning problem of MESSs capturing the main features of extreme events including both external contingencies and internal uncertainties.

- A three-stage distributed control approach based on a consensus algorithm is developed for the operational problem of networked MGs, while a linearised time-coupled AC OPF algorithm is utilised to capture network constraints, technical constraints relating to stability properties and the flexibility of MESSs.

- Internal uncertainties with renewable generation sources and load profiles are considered in the operational model via scenario-based stochastic programming, while external contingencies including multiple line outages are captured via the suggested DAD model.

- Extensive case studies considering different attack budgets, different scheduling horizons of MESSs and a comparison between mobile units and static units are developed to present the effectiveness of the suggested DAD model.

7.2 Outline of the suggested planning model

A typical DAD planning model includes three components, i.e., planner, attacker and operator, where the planner is formulated as the upper-level problem in this context to determine optimal resource allocation (e.g., MESS sizing and pre-positioning) against potential attacks [154]. The attacker corresponds to the middle-level problem aiming at maximising total load shedding via specific attack actions, while the operator is regarded as the lower-level problem representing the responsive actions of MG operator against attacks from the middle level. It is worth noting that decision variables in higher levels are treated as constants by lower-level problems [170].

To solve the suggested three-level optimisation problem, the first step is to merge the middle-level problem and lower-level problem into a single-level formulation, which is realised as a max-min subproblem to identify the worst-case scenario (e.g., the attack action causing most load shedding), while the upper-level problem is designed as a master problem to make decisions on MESS sizing and pre-positioning. The flowchart of the proposed three-level DAD model can be found in Figure 7.1. The subproblem and the master problem will be solved via a column-and-constraint generation (C&CG) method iteratively until convergence, where ϵ corresponds to the value of convergence tolerance [90]. Note that the C&CG algorithm has been widely used to efficiently solve various mathematical models featuring robust optimisation [171]. Additionally, both internal uncertainties and external contingencies are incorporated in the planning model. Uncertainties with renewable energy sources and load profiles are captured via a scenario-based stochastic programming approach in the decentralised operation of networked MGs, while the influence of contingencies including multiple line outages are considered via the suggested DAD model. Specifically, the subproblem can produce different attack actions relating to different line outages and select the attack action that can cause the largest load shedding cost. After obtaining the selected attack action, the master problem will update the current optimal sizing and pre-positioning results against this attack.

Important input and output information in the master problem and subproblem is illustrated in Figure 7.2. It is worth noting that the master problem and the subproblem are further divided into two levels. The upper level corresponds to the proposed adaptive genetic algorithm for handling integer variables with optimal sizing, pre-positioning and attack actions, while the lower level refers to the decentralised operation of networked MGs with uncertainties for load restoration. Distributed power sharing between MGs is achieved via a consensus-based algorithm, while the operation of each MG is formulated as a MILP problem and can be efficiently solved by commercial solvers. Detailed mathematic formulation of the subproblem and the master problem can be found in the next section.

As mentioned before, extreme events are featured by high impact and low probability, which may

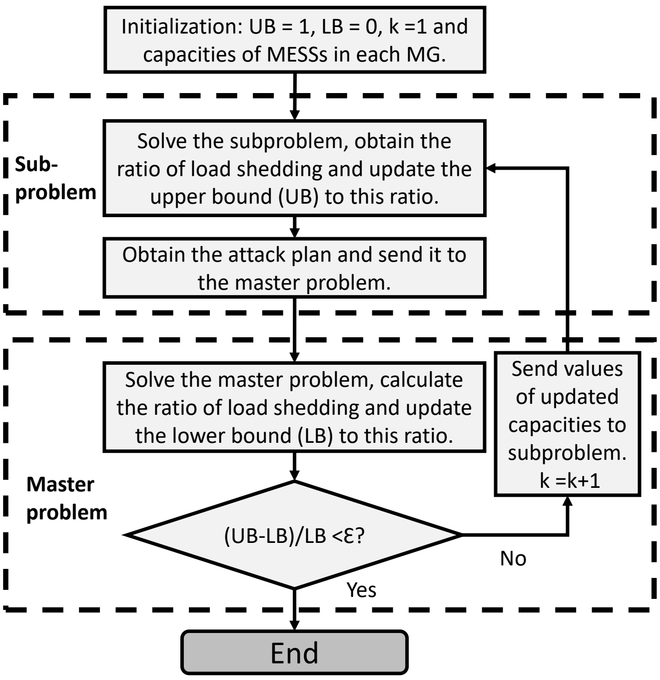

Figure 7.1: Outline of the suggested three-level DAD model.

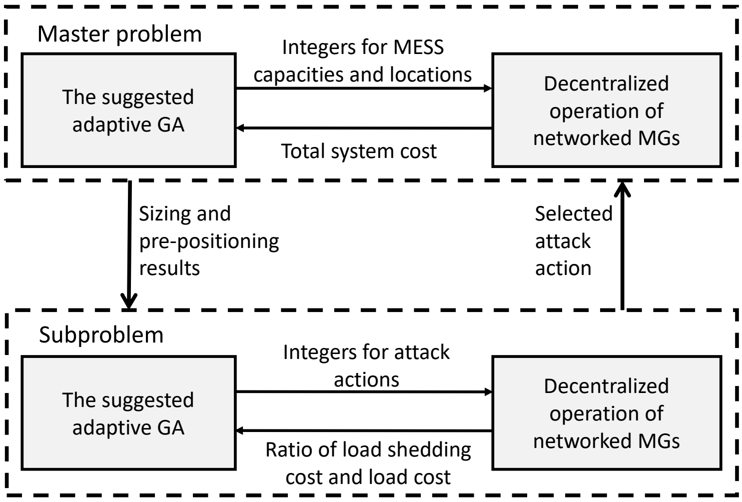

Figure 7.2: Information flow of the suggested DAD model.

cause temporary damage on central controllers or the communication between central and local controllers in each MG; nevertheless, local connections between MGs may still be reliable, which renders the application of distributed control approaches for the decision making of power exchange between different MGs under emergency situations. In this case, operations of MG clusters based on a distributed control approach is more realistic for the suggested resilience-driven planning problem. As such, a consensus-based algorithm is utilised in this chapter to decide the power exchange between networked MGs, which is featured by the fast convergence and stability [172].

7.3 Problem formulation

7.3.1 Master problem

To consider the trade-off between total system cost and resilience (e.g., total load shedding), the objective function at the planning level should include both MESS sizing cost and allocation cost (C_{mes}) and operational cost (F_{op}) of each MG, which is illustrated in (7.1).

$$F^{mas} = \sum_{m \in M} C^{mes} + \sum_{m \in M} F^{op} \tag{7.1}$$

where the operational cost of a certain MG corresponds to (7.2), which includes generation cost and load shedding cost across a set of scenarios. S represents the uncertainty set and p_s refers to the occurrence probability of scenario s, while c^g corresponds to generation costs of conventional generators.

$$F^{op} = \sum_{s \in S} p_s \sum_{t \in T} \sum_{g \in N_g} c^g P_{g,t,s} + \sum_{s \in S} p_s \sum_{t \in T} \sum_{b \in L_{bus}} c^{ls} P^{ls}_{b,t,s} \tag{7.2}$$

The proposed operational model based on distributed control can be divided into three stages: (a) Obtain results on power surplus or shortage of each MG through the linearised AC OPF algorithm capturing uncertainties; (b) Update decisions on power exchange using a consensus-based algorithm; (c) Run the linearised AC OPF again to re-schedule each MG according to updated power exchange results. Detailed information about each stage can be found hereafter:

Stage 1 - Calculate power surplus/shortage

In this stage, a time-coupled linearised AC OPF algorithm is run in each local MG allowing power surplus or power shortage results to be obtained, which is represented by the variable P^e. Specifically, $P^e > 0$ means power shortage, while $P^e < 0$ corresponds to power surplus. Note that the algorithm is run by each MG in a stand-alone condition (i.e., not connected to other MGs) during this stage. The objective function of one local MG in this stage can be found in (7.3), which includes the calculated power surplus or power shortage and the total load shedding cost across a set of uncertainties. Notably, a scenario-based stochastic problem is formulated to capture uncertainties pertaining to load profiles and renewable energy sources [138]. Variables relating to the scheduling of MESSs and power sharing are realised as here-and-now decisions, while other variables (e.g., active power output or load curtailment) are regarded as wait-and-see decisions, which are influenced by the scenario set.

$$F_1 = \sum_{t \in T} c^e P^e_t + \sum_{s \in S} p_s \sum_{t \in T} \sum_{b \in L_{bus}} c^{ls} P^{ls}_{b,t,s} \tag{7.3}$$

MG operations shall be realised as a cost minimisation problem capturing constraints pertaining to the AC OPF algorithm; nevertheless, the well-known classical AC OPF algorithm includes high non-linearity. If MESS routing decisions are further incorporated, the operational model becomes a MINLP problem, which is extremely difficult to solve with time-coupled constraints and a set of uncertainties. As such, linearised techniques developed in [147] are used to simplify the original MINLP problem into a MILP formulation. Constraints related to MESS routing and charging/discharging behaviours are also incorporated into the proposed operation model [18].

Stage 2 - Consensus algorithm for power exchange

In this stage, the consensus-based algorithm is used to optimise the power sharing and reduce load shedding because of its fast convergence and stability [63]. Given by the consideration of resilience, the incremental cost of load shedding $\lambda_{n,t}$ of each MG constitutes consensus variables. After estimating the values of their power shortage in stage 1, each MG updates these estimates by exchanging information with their neighbouring MGs, where the communication network of this MG cluster is represented by matrices P and Q [63]. The suggested consensus algorithms involve a four-step iterative process, which is can be found in Chapter 5 in more detail.

Stage 3 - Re-scheduling with updated power exchange results

After local controllers in each MG receive the updated decisions on power exchange from the second stage, these results are used to update MG operations and obtain final operational cost. As such, the final objective function of a certain MG m is similar to that in the first stage, which can be found in (7.4) including both generation cost and load shedding cost.

$$F_{op} = \sum_{s\in S} p_s \sum_{t\in T} \sum_{g\in N_g} c^g P_{g,t,s} + \sum_{s\in S} p_s \sum_{t\in T} \sum_{b\in N_{bus}} c^{ls} P^{ls}_{b,t,s} \tag{7.4}$$

The constraint relating to active power balance at a certain bus b is modified as per equation (7.5). Note that the first term represents the final power exchange result of MG m from nearby MGs, while the second and third terms correspond to MESS discharging and charging respectively. The rest of the terms have been described in previous chapters. Note that the rest of the constraints in Stage 1 (e.g., MESS-related constraints and technical constraints) are also considered in this stage.

$$P^{ob,final}_{m,t} + \sum_{k\in N_{mes}} P^{mes,d}_{b,k,t} - \sum_{k\in N_{mes}} P^{mes,c}_{b,k,t} + P^{ls}_{b,t,s} + \sum_{g\in NG_b} P_{g,t,s} = P^{ex}_{b,t,s} + P^{l}_{b,t,s} \tag{7.5}$$

7.3.2 Subproblem

In the subproblem, the main objective is to choose the attack that would cause the largest load curtailment on current planning decisions. Following this target, the optimisation problem is designed in a max-min structure, where the objective function is shown in (7.6) corresponding to the ratio of weighted cost of load curtailment over total weighted cost of loads across different scenarios.

$$\max \ \min \ F_{sub} = \frac{\sum_{m\in M}\sum_{t\in T}\sum_{b\in L_{bus}}\sum_{s\in S} p_s c^{ls} P^{ls}_{b,t,s}}{\sum_{m\in M}\sum_{t\in T}\sum_{b\in L_{bus}}\sum_{s\in S} p_s c^{ls} P^{l}_{b,t,s}} \tag{7.6}$$

Equations relating to power flow problems have been modified and provided in (7.7) and (7.8). Binary variables $x_{b,p}$ correspond to line status, where $x_{b,p} = 0$ represents line outage. The rest of the constraints (e.g., MESS-related and technical constraints) presented in Chapter 5 are also incorporated into the subproblem.

$$P^{ex}_{b,t,s} = \sum_{(b,p)\in N_{br}} x_{b,p} P_{bp,t,s} + \sum_{p\in N_{bus}} x_{b,p} G_{bp} V^2_{b,t,s}, \ \forall t \in T, \ \forall b \in N_{bus}, \ \forall s \in S \tag{7.7}$$

$$Q^{ex}_{b,t,s} = \sum_{(b,p)\in N_{br}} x_{b,p} Q_{bp,t,s} - \sum_{p\in N_{bus}} x_{b,p} B_{bp} V^2_{b,t,s}, \ \forall t \in T, \ \forall b \in N_{bus}, \ \forall s \in S \tag{7.8}$$

To summarise, the subproblem is a complicated max-min problem with a decentralised structure capturing a set of scenarios. To effectively solve this problem, an adaptive GA is proposed to deal with binary variables representing potential attacks, while a MILP solver is employed to solve the lower-level minimisation problem. Details about the suggested adaptive GA are presented in the next section.

7.4 Problem solving procedure

Regarding solving methodologies, approaches based on linear and mixed-integer mathematic programming have been widely employed to solve different types of optimal sizing or pre-positioning problems [129]; nevertheless, these approaches can be only employed in planning models based on centralised control, since decentralised models normally include many different entities with their own objective functions. Additionally, the subproblem is a two-level max-min problem, which cannot be effectively solved via a direct mathematic programming approach. Furthermore, the suggested model involves numerous binary variables to determine capacities, initial locations and routing decisions of MESSs and potential contingencies, which causes significant increase of computing time. As such, it is necessary to further divide the master problem and subproblem into two stages. As such, a meta-heuristic approach based on an adaptive GA is employed to solve the suggested model through handling integer variables relating to MESS capacities, locations and potential contingencies, while routing decisions of MESSs are decided by the operational model.

GA is utilised as a global search technique for optimisation problems due to its feature of imitating natural biological procedures and programming simplicity [129]. With adaptive crossover/mutation probabilities, the GA can have the ability to utilise a large mutation rate and better avoid local optimum. As such, an adaptive GA is more suitable to solve the mathematic formulation suggested in this chapter. Furthermore, a technique called elitism is incorporated into the suggested adaptive GA to preserve offsprings with good quality and enhance the ability of convergence [158]. Figure 7.3 illustrates the detailed process of the suggested adaptive GA. The suggested adaptive GA starts from the initialization of chromosomes that represent MESS ratings and positions. These chromosomes are sent to the operational problem of decentralised networked MGs for calculating the fitness function. Afterwards, the results are fed back to the adaptive GA for evaluation. Then, the best candidates are selected through a tournament, while adaptive crossover and mutation are applied to these candidates and alter their composition according to related probabilities of crossover and mutation. Finally, the next generations or offsprings are produced for the next-round iteration.

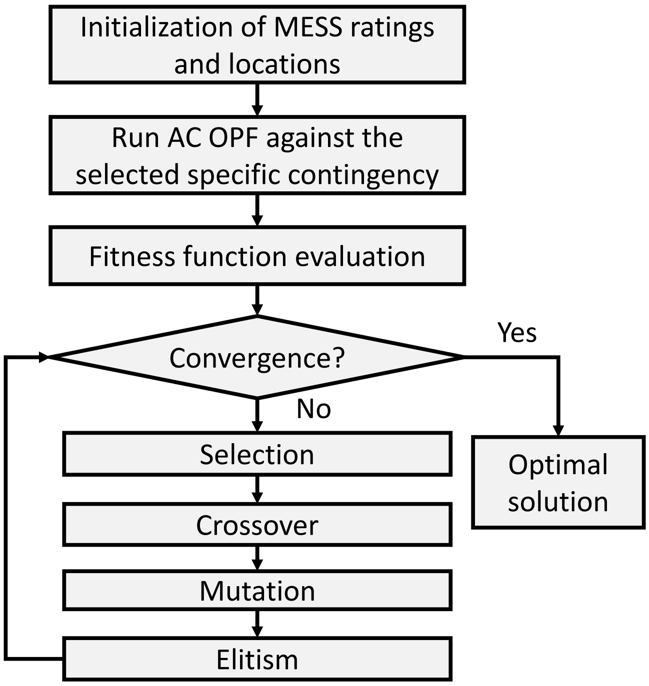

Figure 7.3: Flowchart of the suggested adaptive GA.

Regarding the master problem, capacities and locations of MESSs are initialised as iterated generations (e.g., [100 kW, 3]), where 100 kW and 3 represent the capacity and initial position of the chosen MESS respectively. It is assumed that the MESS energy content is equal to four times the selected capacity [129], while it is worth noting that both energy and power capacities can also be optimised as variables. The total system cost including both investment cost and operational cost is employed to represent the fitness function of each chromosome. Similarly to the master problem, various contingencies can be initialised to represent locations of faulted lines with the range of [0,10] for each MG. For example, one attack in the subproblem corresponds to a certain chromosome (e.g., [2, 3, 5, 4, 1, 3]), which means that lines represented by those numbers are attacked and impacted by the investigated event.

7.5 Case studies

Figure 7.4 illustrates the network structure of an AC MG utilised in this chapter. In each MG, conventional generators (e.g., diesel generators) are installed as conventional generation resources with capacities of 100 kW, 300 kW and 150 kW, while PV devices and MESS units are deployed in each MG through power converters. Note that MESSs are connected with bus 3 as shown in Figure 7.4, which is only for presentation, since the final location of each MESS will be decided via the DAD model. Additionally, MESSs employed in the model belong to utility-owned units as suggested in [16,59]. Data relating to load and PV profiles are extracted from [144] and [129], where load profiles in each MG are illustrated in Figure 7.5. Uncertainties with load profiles and renewable energy sources are represented via 10 scenarios obtained from the stochastic programming approach suggested in [138].

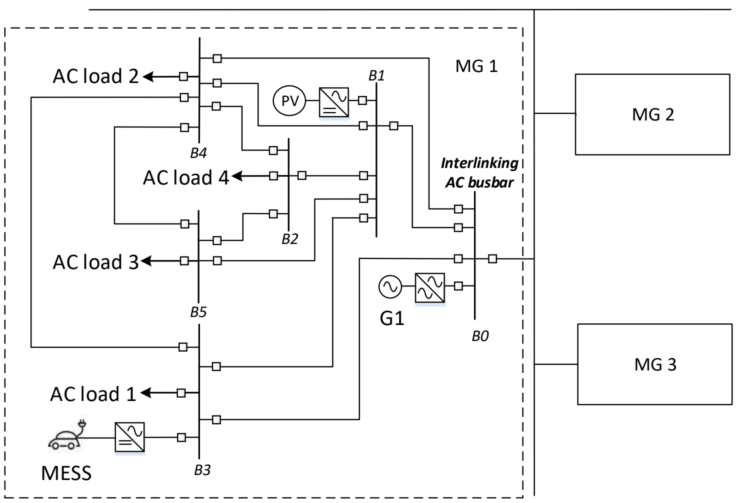

Figure 7.4: Networked MGs used in case studies.

Additionally, to capture the main focus of MGs during an extreme event (e.g., essential load restoration), the case studies presented hereafter consider the discrimination of essential and non-essential loads. As suggested in [71], around 30% of total loads in each MG is regarded as essential

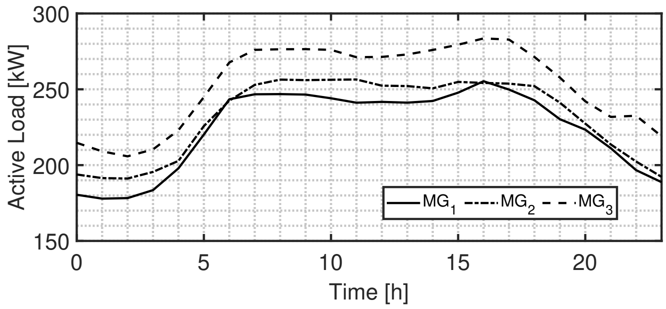

Figure 7.5: Data illustration of load profiles in networked MGs.

loads with large shedding cost, while other loads are assumed to be non-essential loads with relatively lower shedding cost.

7.5.1 Optimal sizing and pre-positioning of MESSs

Results on optimal sizing and pre-positioning of MESSs can be found in Table 7.1 under two sets of attack budgets, where $AB = 6$ and $AB = 3$ represent that the event can cause at most 6 and 3 line outages, respectively. Regarding power capacities, the MESS in MG 2 obtains the largest capacity, while the MESS in MG 1 owns the smallest capacity. The reason is that the conventional generator in MG 2 has the largest rating, which requires much larger MESS capacity for more effective energy transmitting. Compared to MG 2, MG 1 has a generator with small rating and a relatively low load level, which both reduce the need for a large MESS capacity. Table 7.1 also shows that much larger MESS capacities are required with the increase of attack budgets from $AB = 3$ and $AB = 6$. Regarding initial locations of MESSs, it seems that bus 3 and bus 0 in each MG are the most common chosen locations. The potential reason is that these buses are more important than other buses in each MG. For instance, bus 3 is connected with essential loads, while bus 0 is connected with the conventional generator in each MG.

Table 7.1: Optimal sizing and pre-positioning results of MESSs in each MG under different attack budgets.

Attack Budget	No. of MG	MESS Capacity	Initial Location
AB = 6	MG 1	118 kW	Bus 3
	MG 2	212 kW	Bus 5
	MG 3	197 kW	Bus 0
AB = 3	MG 1	97 kW	Bus 3
	MG 2	115 kW	Bus 0
	MG 3	108 kW	Bus 4

Behaviours of MESS routing in each MG against the worst contingency can be found in Table 7.2, where 'T' corresponds to transportation. It can be found that all MESSs move back and forth between bus 0 and other buses (e.g., bus 3 and bus 5) for charging and discharging. In other words, when the energy content of a MESS is low, it can move to bus 0 for charging and then travel to one bus that needs power supply. Additionally, it can be found that average travelling times of MESSs inside each MG are reduced with the increase of MESS capacities or attack budgets. In other words, MESSs with large capacities may require fewer travelling times due to the stronger ability of charging and discharging. When attack budgets are increased, the MG system tends to increase the capacity of MESSs against more severe contingency. Larger capacities allow much higher energy content and relatively longer discharging durations for load restoration, which leads to decrease of average travelling times (i.e., due to being connected to the grid). Charging/discharging behaviours of MESSs in each MG under the worst contingency are illustrated in Figure 7.6. It is worth noting that the value of final energy content of each MESS equals to the initial value, which corresponds to the cycling constraint of battery units for realistic simulations. Except for the influence of severe contingencies, it can also be found that load and PV profiles have influence on charging/discharging patterns of MESSs, especially when the attack budget is low. For instance, Figure 7.6(b) illustrates that all the storage devices charge during the hours of high sunshine (e.g., around 10-15 h). Additionally, MESSs charge when the load level is relatively low and discharge when the load level has significantly increased (e.g., during 5-10 h).

Table 7.2: MESS routing decisions inside MGs against the final worst contingency.

Attack Budget	No. of MG	Time (h)																							
		0	1	2	3	4	5	6	7	8	9	10	11	12	13	14	15	16	17	18	19	20	21	22	23
AB = 6	MG 1	3	T	0	0	0	T	3	3	3	3	3	3	T	0	0	0	0	T	3	3	3	3	3	3
	MG 2	5	T	0	0	0	0	T	4	4	4	4	4	T	0	0	0	0	T	5	5	5	5	5	5
	MG 3	0	0	0	T	5	5	5	5	T	0	0	0	0	T	4	4	4	4	T	0	0	T	2	2
AB = 3	MG 1	3	T	0	0	0	T	5	5	5	5	T	0	0	0	0	T	3	3	T	5	5	5	T	0
	MG 2	0	0	0	0	T	5	5	5	5	5	T	0	0	0	0	T	5	5	5	5	T	0	T	5
	MG 3	4	T	0	0	0	0	T	3	3	3	3	3	T	0	0	0	0	T	5	5	5	5	T	0

7.5.2 Results of distributed control based on linearised AC OPF

As mentioned before, a distributed control approach based on a consensus-based algorithm is utilised to formulate the operational problem of networked MGs, while a linearised AC OPF algorithm is employed to capture stability properties relating to voltage and power losses. Figure 7.7 presents the

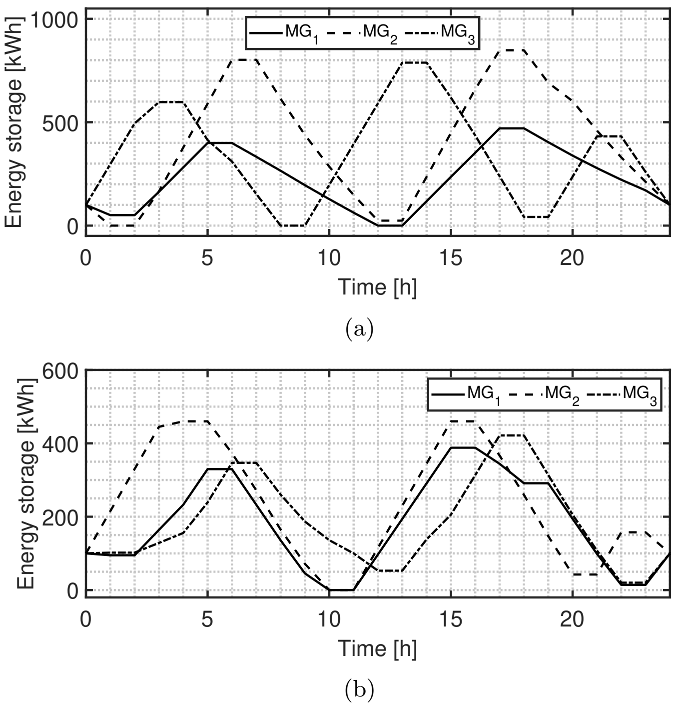

Figure 7.6: Charging/discharging patterns of MESSs in each MG: (a) AB = 6, (b) AB = 3.

power exchange results from the suggested control approach under the worst contingency. During extreme events, MGs lose the connection to the main grid and MG 2 owns the most generation resources, which triggers more power flow from MG 2 to two other MGs.

The advantage of the used linearised AC OPF algorithm can be found in Figure 7.8, which illustrates voltage profiles of MG 2. Note that voltage in bus 3 reaches the minimum value (e.g., 0.9 p.u.) at most time snapshots, which shows that MGs need to operate very close to their stability limits under severe contingencies. As mentioned before, typical EMS-based models fail to capture all the technical constraints relating to voltage profiles, which can cause unstable MG operations. Although considering these constraints to ensure stable voltage profiles in the operational model may have a negative influence on the total operational cost, they can lead to realistic optimisation results and reliable decision making (e.g., reasonable sizing and positioning results of MESSs).

7.5.3 Comparative case studies

When it comes to mobile units, it might be unrealistic to consider a 24-hour scheduling horizon of MESSs. In other words, the scheduling horizon of MESSs might be different from MGs. As such, the first comparison is conducted to show the influence of a shorter MESS scheduling horizon on final optimal sizing and pre-positioning results. Table. 7.3 illustrates the planning results of MESSs

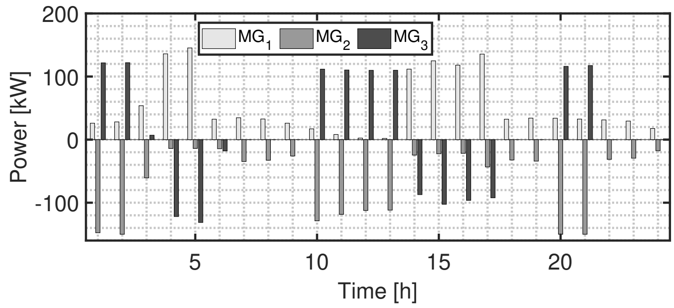

(a)

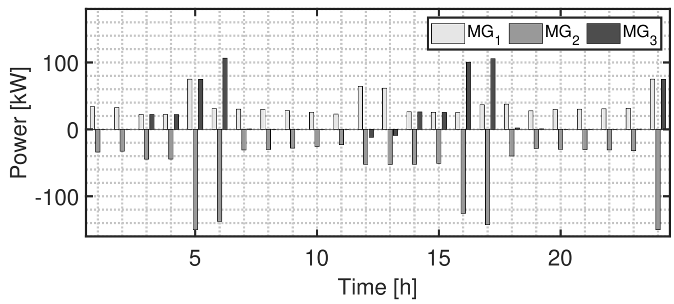

(b)

Figure 7.7: Power exchange based on distributed control: (a) AB = 6, (b) AB = 3.

under a 15-hour scheduling horizon. It can be found that the final power capacities of MESSs significantly increase, compared with the sizing results in the previous case study. The reason is that MESSs have to consider shorter travelling time with a much shorter scheduling horizon, which leads to larger power capacities for more efficient charging and discharging so that the number of moving between different buses can be reduced. However, it can also be anticipated that larger capacities lead to larger investment, while a shorter scheduling horizon of MESSs will cause larger potential load shedding. Detailed information on cost and load shedding can be found in the next section. Figure 7.9 corresponds to the charging and discharging process of MESSs in each MG under two types of attack budgets. Note that the initial energy content of MESSs is the same as the final energy content of MESSs, which reduces the influence of MESS initial energy on optimisation results so that the effectiveness of mobility of MESSs can be shown significantly.

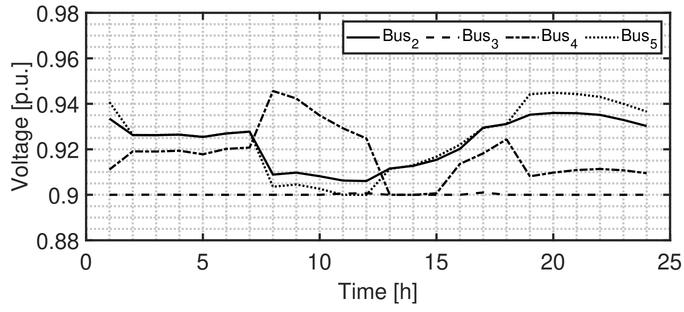

Figure 7.8: Voltage profiles of MG 2 when AB = 6.

Table 7.3: Optimal sizing and pre-positioning results of MESSs in each MG with a 15-hour scheduling horizon.

Attack Budget	No. of MG	MESS Capacity	Initial Location
AB = 6	MG 1	176 kW	Bus 0
	MG 2	326 kW	Bus 5
	MG 3	235 kW	Bus 0
AB = 3	MG 1	114 kW	Bus 5
	MG 2	149 kW	Bus 0
	MG 3	123 kW	Bus 3

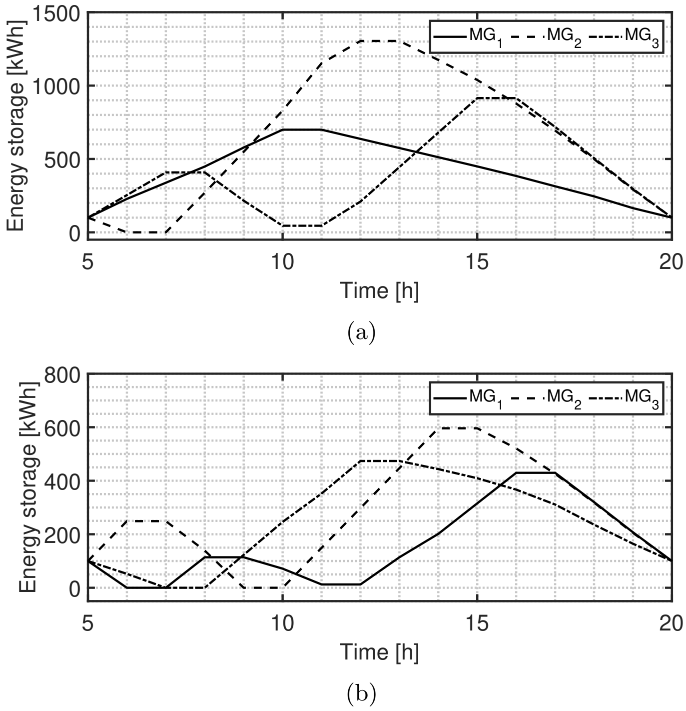

Figure 7.9: Charging/discharging patterns of MESSs in each MG: (a) AB = 6, (b) AB = 3.

The second comparison aims to present the advantages of utilising MESSs for resilience enhancement compared to static ESSs. As such, extra cases focusing on the optimal sizing and pre-positioning of ESSs are done via the suggested approach, where the results under two types of attack budgets can be found in Table 7.4. On the one hand, it can be found that final power capacities of ESSs (around 30 kW) are significantly lower than those of MESSs. It is because ESS units can only be located in one fixed bus and the charging/discharing behaviors are influenced by related line thermal capacities. Even though larger capacities are arranged for these ESS units, these capacities can not be fully used due to the lack of mobility. On the other hand, all three ESSs are located in bus 3 in each MG according to final positioning results. The potential reason is that bus 3 is connected with essential loads, which are much more important than non-essential loads. Additionally, it seems that the final sizing results of ESSs under different attack budgets are very similar. In other words, the capacities of ESSs are not improved significantly when attack budgets increase from 3 to 6, which implies that using ESSs against contingencies during an event may not be as effective as MESSs. It is obvious to consider that much larger load shedding can be caused when using ESSs against the worst contingency. Detailed discussion on cost and load shedding can be found in the next section. Furthermore, Figure 7.10 corresponds to the charging and discharging process of static ESSs in each MG under different attack budgets.

Table 7.4: Optimal sizing and pre-positioning results of ESSs in each MG.

Attack Budget	No. of MG	ESS Capacity	Location
AB = 6	MG 1	26 kW	Bus 3
	MG 2	26 kW	Bus 3
	MG 3	33 kW	Bus 3
AB = 3	MG 1	25 kW	Bus 3
	MG 2	25 kW	Bus 3
	MG 3	28 kW	Bus 3

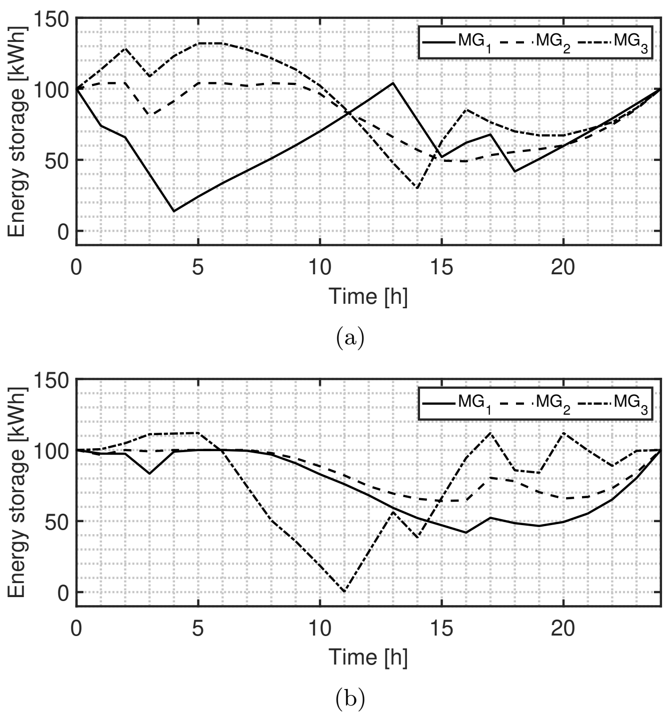

Figure 7.10: Charging/discharging patterns of ESSs in each MG: (a) AB = 6, (b) AB = 3.

7.5.4 Performance testing in a larger system

The MG system used in the previous section considers 3 MGs, which might be not enough to validate the scalability of the suggested DAD model and the adaptive GA. As such, a larger system including 6 MGs fully modelled via the linearised AC OPF algorithm as well as capturing uncertainties and contingencies is employed in this subsection to prove the effectiveness of the proposed algorithm. The optimal sizing and pre-positioning results of this larger system can be found in Table 7.5.

The MESS in MG 2 has the largest capacity because of the largest rating of conventional generation and the high load level, while MG 1 and MG 4 receive relatively small MESS capacities due to the small generation rating and low load level. Specifically, when the attack budget increases from $AB = 3$ to $AB = 6$, MESS capacities in each MG are enlarged against more severe contingencies. These findings are aligned with previous case studies. As such, it can be concluded that the suggested three-level model still achieves good performance in obtaining realistic sizing and pre-positioning results, even though a larger system with more parameters is under consideration. The reason is that GA is featured by the ability to effectively consider multiple parameters or decision variables for optimisation problems [129], while distributed control approaches also have the advantages of high scalability and relatively low communication burden.

Table 7.5: Optimal sizing and pre-positioning results of MESSs in each MG.

Attack Budget	No. of MG	MESS Capacity	Location
AB = 6	MG 1	157 kW	Bus 3
	MG 2	267 kW	Bus 0
	MG 3	205 kW	Bus 5
	MG 4	140 kW	Bus 3
	MG 5	194 kW	Bus 0
	MG 6	191 kW	Bus 0
AB = 3	MG 1	94 kW	Bus 4
	MG 2	119 kW	Bus 0
	MG 3	113 kW	Bus 3
	MG 4	60 kW	Bus 0
	MG 5	102 kW	Bus 3
	MG 6	98 kW	Bus 0

7.6 Discussion

Results on system cost and load shedding under different case studies are discussed in this section. Several additional case studies considering a larger attack budget ($AB = 9$) and ESSs with a 15-hour scheduling horizon are included to conduct a comprehensive comparison. Figure 7.11(a) illustrates the investment cost of MESSs and ESSs in this MG system under three different types of attack budgets. The investment cost of MESSs has been significantly increased when more severe contingencies are considered, while investment of ESSs does not change much due to the lack of mobility and the incorporated cycling constraint. Figure 7.11(b) corresponds to the ratio of weighted curtailed loads on total demands under the worst contingency, which presents that using MESSs for resilience enhancement leads to significantly lower load shedding than using ESSs, while a longer scheduling horizon of MESSs or ESSs leads to much lower total load shedding.

Figure 7.11(c) shows that total system costs including both investment cost and load shedding cost under each case significantly increase when more severe contingencies are caused. It can be found that using ESSs to reduce load shedding obtains the worst performance (highest total system cost), even though the investment cost of ESSs is much lower than that of MESSs (shown in Figure 7.11(a)). Additionally, MESSs with a 24-hour scheduling horizon achieves considerably cost savings compared to other cases.

To summarise, a three-level DAD model focusing on the influence of the worst scenarios is suggested to solve an optimal sizing and pre-positioning problem of MESSs for resilience enhancement of networked MGs. At the planning level, a tailor-made adaptive genetic algorithm is employed to optimally size and locate MESSs in each MG as well as producing potential attack actions; at the operational level, a three-stage distributed control approach based on consensus algorithm is utilised to obtain the power sharing results between MGs, while a linearised AC optimal power flow algorithm incorporating technical constraints relating to voltage and power losses is employed to model MG operations for more accurate optimisation results. Uncertainties relating to load profiles and renewable energy sources are captured in the model via a scenario-based stochastic programming approach. It is concluded that MESSs can be more effective for load restoration than static ESSs when extreme events occur, while capacities of MESSs increase when larger attack budgets are considered.

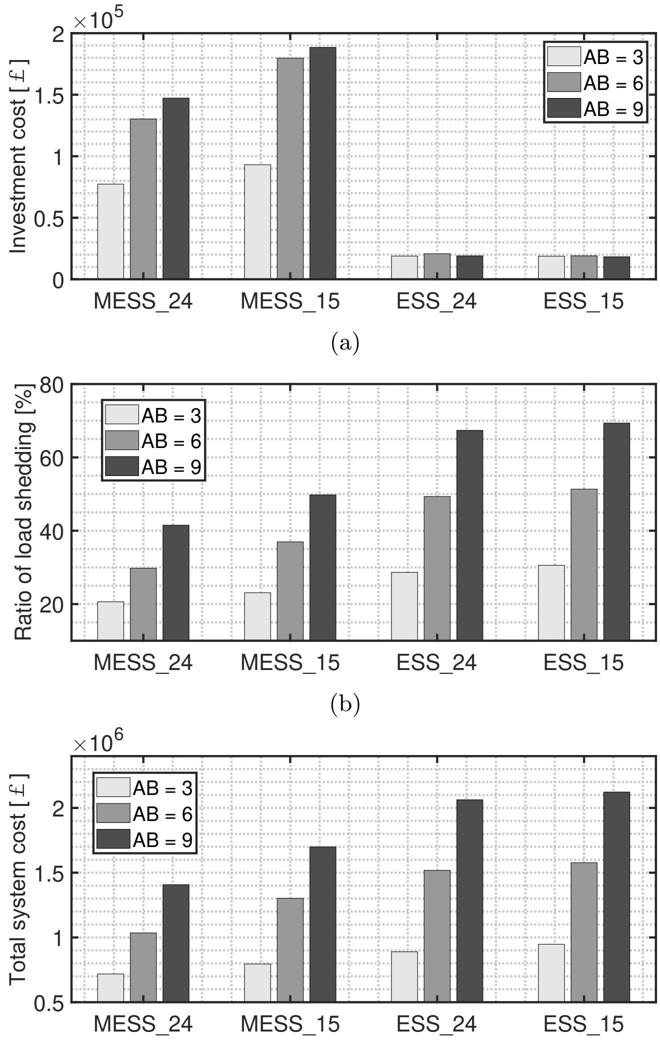

(a) (b) (c)

Figure 7.11: Cost analysis with different attack budgets: (a) Investment cost, (b) Ratio of load shedding, (c) Total system cost.

Chapter 8

MARL for MESS routing and scheduling

8.1 Introduction

The energy industry has undergone major transformations in various sectors because of a number of economic, environmental and technical factors over the last few decades. Among them, the most important one is the significant increasing penetration of DERs including both static and mobile units to the energy mix, especially renewable energy sources [173]. Model-based optimisation approaches have been developed to model the routing and scheduling process of MPSs towards resilience enhancement of power networks [162], which are better summarised in previous chapters, e.g., two-stage pre-allocation problems of MPSs [16, 18, 59] and operation problems of MESSs [19, 68, 168, 174–176].

8.1.1 Research limitations of model-based approaches

It can be concluded that extensive efforts have been made to study the MESS routing and scheduling problems in terms of their flexibility and mobility against extreme events [167]. However, the limitations of research above cannot be erased and are summarised hereafter. First, no optimisation models comprehensively consider the uncertainties related to both renewable energy sources and load profiles; second, uncertainties are handled via scenario-based stochastic programming approaches, which may only be able to capture small number of representative scenarios. Both these limitations or simplifications are due to the large computational burden caused by the modelling of MESSs (e.g., the incorporation of large amounts of integer variables and time-coupled characteristics), which can lead to inaccurate and unrealistic optimisation results. Additionally, resilience-driven operations normally require fast response due to their high-impact nature; nevertheless, above approaches may not be able to provide timely services for the damaged system. Furthermore, the model-based optimisation problem discussed above assumes that the MESSs require the complete knowledge of the experiment environment, e.g., power networks, transportation statuses, accurate uncertain parameters. However, such assumptions are normally impractical considering the highly stochastic and dynamic real-world environment.

To this end, compared to approaches featuring mathematical programming, *reinforcement learning* (RL) [117], as a data-driven and model-free approach, is suitable for resilience-driven operations because of its ability to provide fast response and incorporate uncertainties and contingencies. However, there is not much research focused on RL approaches for resilience-driven MESS routing problems. The only research comes from [177], which formulates the routing problem of MESSs as a *Markov decision process* (MDP) for load restoration and resource dispatching of MGs. However, this paper regards each MG as a single node without detailed network structure, which can be unrealistic. The high-impact nature of extreme events on power networks is not captured in this approach. As such, it is necessary to investigate the research of coordinated MESS routing and scheduling problem capturing both transportation and power networks. Regarding RL approaches for resilience-driven operations of power systems, a model-free approach based on *deep reinforcement learning* (DRL) is developed in [178] to reschedule DERs for the resilience enhancement of a distribution system. However, this paper does not aim at the optimisation of MESS routing decisions, which can be much more complicated due to the hybrid action space including both continuous (scheduling) and discrete (routing) actions.

8.1.2 State-of-the-art RL methods

The application of RL on demand response problems has been increasingly recognised, as reviewed in [179]. In general, the applied RL methods can be divided into two categories: 1) discrete action space; and 2) continuous action space. In discrete action space, the conventional *Q-learning* (QL) is regarded as the fundamental RL method that has been applied to various areas. In [180], a QL method augmented with Monte-Carlo tree search is proposed to dispatch the BESS in MGs incorporating uncertainty of PV generation and demand. In [181], a QL-based operation strategy is proposed for optimal operation of BESS in both grid-connected and islanded modes under MG concept. The objective of BESS in grid-connected mode is to maximise its profit, while the objective of BESS in islanded mode is to minimise the load shedding amount in the entire system by cooperating with the MG. For multi-agent setup, QL is used to help home energy management system (HEMS) optimally control the various smart devices with the objective of reducing energy cost [182]. A framework for residential MG energy scheduling mechanism with V2G system is built under the concept of multi-agent QL [183], while the fuzzy QL is used for a multi-agent decentralised energy management in MGs to address power balancing problem between production and consumption units [184]. However, QL relies on a look-up table to represent the Q-value function for each possible state-action pair and thus suffers severely from the curse of dimensionality. The discretisation of both state and action spaces may distort the feedback that the agent receives on the impact of its actions on the environment and adversely affect the feasible action space, resulting in sub-optimal control policies.

In view of the limitations above, *deep Q-network* (DQN), combining deep learning with RL, recently has been explored in developing more complex control problems, driven by its ability in handling high-dimensional continuous state space. In [185], a DQN method is proposed to learn an optimal policy for carbon storage reservoir management problem. In [186], a DQN-based energy management of hybrid electric bus is proposed to achieve 5.6% fuel economy better than QL. In [187], authors develop a DQN-based flexible and scalable smart charging strategy for electric vehicles (EVs) that reduce the grid congestion and increase user comfort. However, in empirical experiments, much research found that the conventional DQN suffers from its Q-value overestimates since the weight values are used for both selection and evaluation of an action [188]. To resolve this issue, authors in [188] propose a variant of DQN, named double deep Q-network (DDQN), that decouples selections from the evaluation. In DDQN, a primary network is used to choose the action and a target network is used to generate the target Q-value for that action. In [189], authors propose a distributed operation strategy for a BESS using DDQN method in both grid-connected and islanded modes. The results show that the proposed DDQN method can perform better in case of a longer time span and a larger MG system. In [190], a DDQN method is implemented to learn the optimised control actions for battery storage under very complex environment with price uncertainty. In [191], a DDQN method is proposed to control the charging/discharging schedule of a BESS and the reserve purchase schedule of a wind power producer in electricity markets under the uncertainties of wind generation and electricity price. On the other hand, DQN and DDQN are also widely used for multi-agent setup. In [192], a multi-agent DQN method is proposed to solve an automatic peer-to-peer (P2P) energy trading problem among multiple prosumers with PV and storage systems. In [193], a multi-agent DQN method is adopted to optimise the distributed energy management and strategy in a MG market. Although DQN and its variant DDQN employ a *deep neural network* (DNN) to approximate the Q-value function, generalizing well to high-dimensional continuous state space, it performs poorly in problems with continuous action space because the employed DNN is trained to produce discrete Q-value estimates rather than continuous actions.

In this regard, the second category is characterised by *policy gradient* (PG) theorem [117] that can directly optimise the probability of taking an action or the action value rather than estimating the Q-value function. In [194], authors develop a *stochastic policy gradient* (SPG) method with capability of handling multiple actions simultaneously to optimise the building energy management consumption and cost. The proposed SPG method is able to efficiently cope with the inherent uncertainty and variability in PV generation, and users energy behaviors. In [195], authors successfully develop a SPG method to optimise the energy consumption of a single household considering multiple smart devices. The experiments find that SPG converges at a faster convergence rate but results in an unstable policy. This is because SPG generally suffers from low sampling efficiency and high variance in its gradient estimates which result in a lower performance evaluation. To resolve this issue, a *deterministic policy gradient (DPG)* is proposed in [196] that directly computes action values in a deterministic manner. In [197], authors use a continuous DPG method to manage the state-of-the-charge (SoC) of a BESS providing the enhanced frequency response. In [198], a DPG method is proposed to design an optimal energy management algorithm for BESS in smart homes. The numerical results demonstrate that the proposed method can save energy cost by more than 10% without sacrificing user's comfort with respect to the system without BESS. Furthermore, PG theorem has been adopted to many multi-agent environments in demand response problems. In [199], a *multi-agent deep deterministic policy gradient* (MADDPG) method is adopted to obtain the optimal schedule for different machines in a discrete manufacturing systems energy management. In [200], authors use an improved MADDPG method based on double-side auction market to formulate an automated P2P energy trading problem among multiple consumers and prosumers. In [201], a combination of MADDPG method and *parameter sharing* (PS) technique is proposed to enhance the scalability of a large-scale multi-agent system with privacy perseverance.

The above literature has successfully applied different kinds of RL and DRL methods to many promising single-agent and multi-agent research problems. Nevertheless, both of two categories are incapable of handling hybrid discrete-continuous action space, which means the method can simultaneously generate discrete and continuous actions at the same time step. This drawback is particular in the setting of the examined problem, since the action domains model both the discrete (routing) and continuous (charge/discharge schedules) action spaces.

8.1.3 Contributions

This chapter aims at addressing the real-time routing and scheduling problem of multiple MESSs in the context of both power and transportation networks towards resilience enhancement, which can effectively bridge research gaps discussed above. A novel multi-agent deep reinforcement learning (MADRL) method based on parameterised double deep Q-network (P-DDQN) and PS technique is employed to implement routing decisions of the studied MESSs in transportation network and also determine their corresponding charging/discharging schedules in power network, while uncertainties associated with renewable energy sources, demand patterns, line outages, and traffic volumes are incorporated into the proposed framework. The novel contributions of this chapter are described as follows:

(1) A *Partially Observable Markov Game* (POMG) is proposed to formulate the coordination effect of the real-time automatic MESSs routing and scheduling problem for the load restoration of power networks after extreme events. As such, both the spatial and temporal flexibility of MESSs can be fully exploited.

(2) A novel MADRL method, namely P-MADDQN, is proposed to efficiently solve this MESSs routing and scheduling coordination problem by integrating the parameterised policy to model the hybrid discrete-continuous action space, introducing the double deep Q-networks (DDQN) [188] to stabilise the training performance, abstracting a collective index to represent the system dynamics, and using a PS framework to enhance the training efficiency.

(3) Both the structures of transportation networks and power networks are formulated into the environment of the proposed MADRL method for realistic decision making process. A traffic network model is proposed to capture the impact of traffic time and congestion, while a linearised AC-OPF algorithm capturing dynamic network reconfiguration is employed to incorporate all the technical constraints relating to stability properties and coordinate with MESS routing and scheduling decisions.

(4) Extensive case studies are developed to evaluate the superior performance of the proposed P-MADDQN method in achieving resilience enhancement and reducing computational time, and is capable of adapting to various uncertainties of renewable energy sources, load profiles, line outages and traffic volumes. Finally, the proposed P-MADDQN method demonstrates its scalability to different environments related to the MESS number and the power-transportation network size.

8.2 Mathematical models of MESS routing and system operations

8.2.1 Problem setting

As an emerging technology, MESSs have been gradually deployed in power networks for emergency considerations due to their mobility and flexibility, compared to the static ESSs. This chapter focuses on the routing process of a group number of MESSs incorporated with the charging/discharging behaviours in the context of power networks incorporated with transportation networks. These MESSs are allowed to move between different buses towards load restoration after extreme events, while the traffic time and congestion impact between different nodes are also captured through the proposed transportation network. Note that severe damage caused by extreme events may significantly exacerbate traffic congestion, leading to much longer commuting time. Regarding the power network, DERs are appropriately deployed, including conventional generations (e.g., diesel generators (DGs)) and renewable energy sources (e.g., photovoltaics (PVs)), while the electric demand including both essential and non-essential loads is reasonably assigned to certain buses. Additionally, MESSs are connected to the power network through charging stations. The routing and scheduling process of MESSs and the context of power-transportation networks are schematically represented in Figure 8.1.

Some related works consider that MESSs are utility-owned and scheduled by the system operator [19,59,174]. However, it might be time consuming to make a fast-responding decision accounting for the complex power-transportation network and the vast system uncertainties. Furthermore, MESSs have their own travelling plans and operation characteristics [202]. Therefore, system operator may not acquire the accurate mathematical models and parameters of MESSs to solve a centralised control problem. Such perspectives are also discussed in [59]. In order to address the above issues, decentralised approach is becoming a future trend for next-generation resilient distribution system

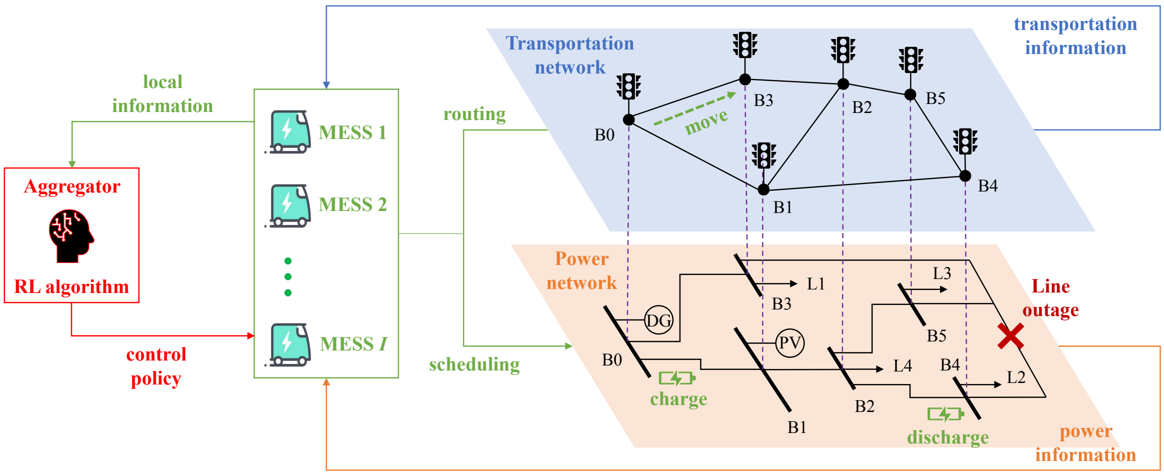

Figure 8.1: The scheme of routing and scheduling processes of multiple MESSs in a coupled power-transportation network.

[1]. This chapter thus assumes that all MESSs are from independent owners that can operate in a distributed manner without a central controller, thereby preserving their private information [203]. However, an aggregator is still introduced to communicate with each MESS and provide for MESSs proper incentives to reach a cooperative fashion. In this setting, MESSs can make their own routing and scheduling decisions without the operator's commands, but also ensure the control optimality via the incentive signals. More specifically, the operation time step is $\Delta t = 30$ mins, where $t \in [1, T]$ and $T = 48$ is the total number of time steps during the daily horizon. At each time step t, after 1) reading the local information of line status (outage or not); 2) observing the local power information of electric demand, PV generation and the local transportation information of map location and traffic volume; and 3) measuring the MESS information of battery SoC, each MESS with a smart automatic control algorithm that can optimally manage 1) the route selections in transportation network; and 2) the charging/discharging power rates of battery storage in power network.

On the other hand, once the route selections and power rates of all MESSs are determined, the power network equips a *microgrid central controller* (MGCC) that can optimally manage the energy schedules of each controllable component (DGs and loads) to minimise the load shedding cost towards resilience enhancement. The system is fully modelled by a linearised AC-OPF algorithm capturing all the network constraints and technical constraints related to stability properties, which ensures accurate optimisation results and secure system operations compared with DC OPF or linearised Distflow models. However, it is worth noting that a non-linear OPF algorithm can also be used here for more accurate optimisation results, while the training time will significantly increase due to its non-linear nature. Additionally, dynamic network reconfiguration [204] is performed to coordinate with the routing and scheduling behaviours of MESSs via the smart switch operations. This section presents the details of the proposed mathematical models including the MESS routing and charge/discharge scheduling, transportation network models, and the AC-OPF algorithm for power system operations.

8.2.2 MESS routing and scheduling

In the context of mathematical programming, the routing and scheduling behaviors of MESSs can be formulated as equations (8.1)-(8.6). In detail, constraints (8.1) and (8.2) limit the charging power $P_{i,b,t}^{mes,c}$ and discharging power $P_{i,b,t}^{mes,d}$ of MESS i, where integer variables $u_{i,b,t}^{c}$ and $u_{i,b,t}^{d}$ represent the charging and discharging decisions of MESS i in bus b at time t respectively. Equation (8.3) ensures that the power charging and discharging patterns cannot be triggered simultaneously, while MESS i can only be connected with at most one bus per time step t. When both $u_{i,b,t}^{c}$ and $u_{i,b,t}^{d}$ equal to 0, the MESS i is not connected to bus b at time step t and vice versa. Constraint (8.4) represents the moving actions of MESS i within the power network, where $T_{bp,t}^{trl}$ represents the travelling time of MESSs from bus b to bus p at time step t [18]. The detailed explanations and calculations of travelling time $T_{bp,t}^{trl}$ are discussed in Section 8.2.3. Constraint (8.5) restricts the minimum and maximum energy storage levels $E_{i,t}^{mes}$ of MESS i, while the time-coupling constraint of energy storage level between two consecutive time steps is presented in (8.6).

$$0 \le P_{i,b,t}^{mes,c} \le u_{i,b,t}^{c} \cdot P_{i}^{max},\ \forall i \in I,\ \forall b \in B,\ \forall t \in T \tag{8.1}$$

$$-u_{i,b,t}^{d} \cdot P_{i}^{max} \le P_{i,b,t}^{mes,d} \le 0,\ \forall i \in I,\ \forall b \in B,\ \forall t \in T \tag{8.2}$$

$$\sum_{b \in B} u_{i,b,t}^{c} + u_{i,b,t}^{d} \le 1,\ \forall i \in I,\ \forall t \in T \tag{8.3}$$

$$\begin{gathered}(u_{i,b,t}^{c} + u_{i,b,t}^{d}) - (u_{i,b,t+1}^{c} + u_{i,b,t+1}^{d}) \le 1 - (u_{i,p,t+h}^{c} + u_{i,p,t+h}^{d}),\\ \forall i \in I,\ b \neq p \in B,\ \forall t \in T - \{1\},\ \forall h \in [1, ..., min(T_{bp,t}^{trl}, T - t)]\end{gathered} \tag{8.4}$$

$$E_{i}^{min} \le E_{i,t}^{mes} \le E_{i}^{max},\ \forall i \in I,\ \forall t \in T \tag{8.5}$$

$$E_{i,t}^{mes} = E_{i,t-1}^{mes} + (\eta_{i}^{c} \sum_{b \in B} P_{i,b,t}^{mes,c} + \sum_{b \in B} P_{i,b,t}^{mes,d} / \eta_{i}^{d})\Delta t,\ \forall i \in I,\ \forall t \in T - \{1\} \tag{8.6}$$

8.2.3 Transportation network modelling

The transportation network consists of several pairs of original and destination nodes (O-D pairs) designed for these MESSs to connect with. Each O-D pair is connected by a set of routes (Ro) through the network, while each route consists of several transportation roads (R) [204]. MESSs commute through the routes of each O-D pair to connect with certain nodes for charging and discharging power towards resilience enhancement.

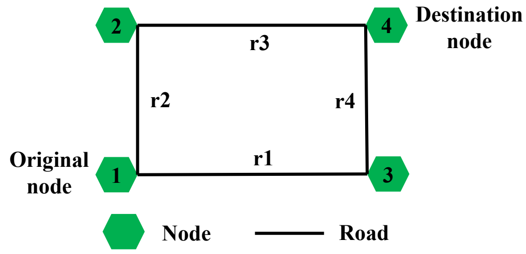

Figure 8.2: The route combinations of one O-D pair.

As shown in Figure 8.2, there are several routes consisting of different roads (e.g., $r_1 - r_4$) between one O-D pair, while each road r has different commuting time $T^{trl}_{r,t}$ at different time point t due to the dynamics of traffic volumes represented by $V^{trl}_{r,t}$. As such, the travelling time $T^{trl}_{r,t}$ may be influenced by traffic congestion, which can be calculated by (8.7) according to the U.S. Bureau of Public Roads [205]. $T^{trl,0}_{r}$ is the driving time in the state of free prevailing driving, while C_r, α^{rd} and β^{rd} correspond to the capacity of road r and the retardation coefficients, respectively. Note that this function can describe the relationship between travel time and traffic volume but also reflect the road impedance from the characteristics of traffic flow itself. The travelling time of an O-D pair (route) k is defined as (8.8), where $\Theta_{r,k}$ is used to indicate whether road r is part of route k. Thus, if congestion happens on road r, the travelling time on route k will also increase accordingly.

$$T^{trl}_{r,t} = T^{trl,0}_{r}[1 + \alpha^{rd}(\frac{V^{rd}_{r,t}}{C_r})^{\beta^{rd}}],\ \forall t \in T,\ \forall r \in R \tag{8.7}$$

$$T^{trl}_{k,t} = \sum_{r \in R} T^{trl}_{r,t}\Theta_{r,k},\ \forall t \in T,\ \forall k \in Ro \tag{8.8}$$

The real-time traffic volume $V^{trl}_{r,t}$ on road r at time step t can be calculated by (8.9), which is determined by the base flow $d^{rd}_{r,t}$ [206] (other types of vehicles in the transportation network with specific daily patterns) and the number of MESSs on the road r at time step t (represented by the sum of $u^{rd}_{i,r,t}$).

$$V^{rd}_{r,t} = d^{rd}_{r,t} + \sum_{i \in I} u^{rd}_{i,r,t}, \ \forall t \in T, \ \forall r \in R \tag{8.9}$$

Finally, given the travelling time $T^{trl}_{r,t}$, the average speed $V^{avg}_{r,t}$ of road r at time step t can be calculated by (8.10), where L_r is the commuting distance of road r.

$$V^{avg}_{r,t} = \frac{L_r}{T^{trl}_{r,t}}, \ \forall t \in T, \ \forall r \in R \tag{8.10}$$

8.2.4 Power network modelling

To ensure secure operations and incorporate MESS routing, this subsection introduces the linearised AC-OPF algorithm for resilience-driven operations. Maintaining the continuity of essential loads (e.g., police stations and data centres) during extreme events is the main driver of resilience-driven operations. Hence, the widely-used objective function is to minimise the expectation of the weighted load shedding cost capturing load distinction into essential and non-essential, which can be found hereafter:

$$\sum_{t \in T} \sum_{d \in N_{load}} \mathbb{E}\{c^{ls}_d P^{ls}_{d,t} \Delta t\} \tag{8.11}$$

where the expectation operator $\mathbb{E}$ is taken over the randomness of system uncertainty parameters (e.g., electric demand, PV generation, and line outages), and corresponding stochastic decision variables (e.g., power flows, DG power outputs, and voltage angles), c^{ls}_d and $P^{ls}_{d,t}$ refer to the load shedding cost and the quantity of load shedding for load d respectively. Note that high uncertainties shall be captured in resilience-driven operations due to the high-impact nature. Stochastic programming and robust optimisation are two-commonly employed approaches to deal with the influence of uncertainties; nevertheless, both of them have obvious limitations, i.e., suffering from computing burden or inherent conservativeness of optimisation results respectively. In this regard, the data-driven nature of RL approaches allows encapsulating uncertainties in various input scenarios, which is convenient and efficient.

The original optimisation problem is posed as a cost-minimisation problem, subject to the following linearised AC-OPF constraints [147]. The active power balance at the exchange bus b is presented in (8.12), while the reactive power balance corresponds to (8.13). The sets B_{ed}, B_{dg}, B_{pv} and B_{mes} correspond to the nodal demand, DG, PV and MESS located at bus b, respectively. Notably, the charging/discharging characteristics of MESSs (i.e., $P^{mes,c}_{i,b,t}$ and $P^{mes,d}_{i,b,t}$) have been incorporated into (8.12) for ensuring active power balance. Classical equations pertaining to power flow problems and operational constraints are linearised and incorporated into the model.

$$\sum_{d\in B_{ed}} P^{ls}_{d,t}+\sum_{g\in B_{dg}} P^{dg}_{g,t}+\sum_{g\in B_{pv}} P^{pv}_{g,t}=\sum_{i\in B_{mes}}(P^{mes,d}_{i,b,t}+P^{mes,c}_{i,b,t})+P^{ex}_{b,t}+\sum_{d\in B_{ed}} P^{ed}_{d,t},\ \forall b\in B,\forall t\in T \quad (8.12)$$

$$\sum_{g\in B_{dg}} Q^{dg}_{g,t}+\sum_{d\in B_{ed}} Q^{ls}_{d,t}=Q^{ex}_{b,t}+\sum_{d\in B_{ed}} Q^{ed}_{d,t},\ \forall b\in B,\forall t\in T \quad (8.13)$$

In addition, if the utilised power network follows a radial structure, the system radiality should be maintained in the network reconfiguration process, subject to the following constraints (8.14)-(8.17) [68]. However, it is worth noting that other network structures (e.g., meshed networks) can also be utilised for MG modelling. Specifically, constraints (8.14)-(8.16) introduce a fictitious network with the same structure as the power network, ensuring that 1) the fictitious network has $|N_e|-1$ closed branches where N_e is the number of electric buses, 2) all fictitious nodes are connected [207]. Constraint (8.17) restricts the real power network to close a subset of closed branches in the fictitious network. $e_{bp,t}$ corresponds to the connection status of line (b,p) in the fictitious network (1 if closed, 0 if open), while g and M refer to the fictitious substation node and a big enough number respectively. Detailed information of this network reconfiguration scheme can be found in [68].

$$\sum_{(b,p)\in L} e_{bp,t}\le |N_e|-1,\forall(b,p)\in L,\forall t\in T, \quad (8.14)$$

$$\sum_{(p,b)\in L} f_{pb,t}-\sum_{(b,p)\in L} f_{bp,t}=1,\forall b\in B/g,\forall t\in T, \quad (8.15)$$

$$-e_{bp,t}\cdot M\le f_{bp,t}\le e_{bp,t}\cdot M,\forall(b,p)\in L,\forall t\in T, \quad (8.16)$$

$$y_{bp,t}\le e_{bp,t},\forall(b,p)\in L,\forall t\in T, \quad (8.17)$$

8.2.5 Challenges

It is worth noting that solving the above MESS routing and scheduling problems (Section 8.2.1) in this coupled power-transportation network (Sections 8.2.2-8.2.3) is very challenging. First, MESSs are independently owned that cannot acquire the explicit mathematical models and technical parameters of transportation network and AC-OPF algorithm. Similarly, MGCC cannot make the centralised decisions for MESSs if they are not utility-owned. Second, a vast number of system uncertainties and dynamics (renewable, demand, line outages, and traffic volumes) need to be handled by MESSs in the complicated power-transportation network. Although scenario-based stochastic optimisation approaches have been widely applied for many applications to deal with uncertainties, the large computation burden cannot be ignored when requiring fast-responding time to resilience enhancement problem. In order to address the above two issues, this chapter proposes an alternative solution method and reformulates the above model-based mathematical optimisation problem into a model-free MADRL-based problem without a *prior* knowledge. Additionally, MADRL eliminates the need to solve an optimisation problem in a time-coupled fashion and enables the MESS agents to provide an adaptive control scheme for various system dynamics and state conditions without the knowledge of uncertain parameters.

8.3 MESSs reformulation as a markov game

8.3.1 Markov game

Specifically, a RL setup is utilised to reformulate the coordination of MESS routing and scheduling problem following a finite *Partially Observable Markov Game* (POMG) with discrete time steps. The POMG is defined by a set of agents (MESSs) $i \in I$ interacting with the environment $\mathcal{E}$ (i.e., the coupled power-transportation network) [117], including: a set of environment states $s \in \mathcal{S}$; a set of local observation space $\{o_i \in \mathcal{O}_{1:I}\}$; a set of action space $a_i \in \mathcal{A}_{1:I}$; a set of immediate scalar reward function $r(o, a) \in \mathcal{R}_{1:I} : \mathcal{O} \times \mathcal{A} \rightarrow \mathbb{R}$; and a state transition $\mathcal{T}(s, a_{i:I}, \omega) : \mathcal{S} \times \mathcal{A}_{1:I} \times \mathcal{W} \rightarrow \mathcal{S}$ following a probability function $P(s'|s, a_{i:I}, \omega) : \mathcal{S} \times \mathcal{A}_{i:I} \times \mathcal{W} \times \mathcal{S} \rightarrow \mathbb{R}$ conditioned on the environment global state s, the all agents' actions $a_{i:I}$, and the environment stochasticity $\omega \in \mathcal{W}$ (e.g., renewable, demand, line outages, and traffic volumes). The time interval between two consecutive time steps $\Delta t = 30$ mins following the same setup in Section 8.2. MESS agent i employs a policy π_i to interact with POMG and emits a set of trajectories integrating with all agents' observations, actions, and rewards: $\{o_{i,1}, a_{i,1}, r_{i,1}, o_{i,2}, ..., r_{i,T}\}_{i=1}^{I}$ over $\mathcal{O}_{i:I} \times \mathcal{A}_{i:I} \times \mathcal{O}_{i:I} \rightarrow \mathbb{R}$. In detail, at each time step t, each MESS agent i chooses an action $a_{i,t}$ according to its control policy $\pi_i(a_i|o_i) : \mathcal{O}_i \rightarrow P(\mathcal{A}_i, \mathcal{W})$ based on its local observation $o_{i,t}$. The environment then moves into the next state according to the state transition function $\mathcal{T}(s, a_{1:I}, \omega)$. Each MESS agent then obtains a reward $r_{i,t}$ and a new local observation $o_{i,t+1}$. The objective of each MESS agent is maximising its cumulative discounted reward $R_i = \sum_{t=0}^{T} \gamma^t r_{i,t}$, where $\gamma \in [0, 1)$ is the discount factor and $T = 48$ is the time horizon of the operation problem. The POMG formulation of the proposed coordinated MESSs routing and scheduling problem is detailed as the following subsections:

8.3.2 Observation

The local observation $o_{i,t}$ observed by each MESS agent i at each time step t is defined as a 6-dimensional vector:

$$o_{i,t} = [S_{i,t}^{line}, P_{i,t}^{ed}, P_{i,t}^{pv}, E_{i,t}^{mes}, N_{i,t}^{loc}, V_{i,t}^{trl}] \in \mathcal{O}_i, \ \forall i \in I \tag{8.18}$$

which consists of two parts: 1) the exogenous state features which represents the local information unaffected by the action, including the line status (e.g., outage or not) $S_{i,t}^{line}$, the local demand $P_{i,t}^{ed}$ or PV generation $P_{i,t}^{pv}$, and the bus number where the MESS agent i is located at; and 2) the endogenous state serving as the feedback signals of its executed routing and scheduling actions, including the current battery SoC $E_{i,t}^{mes}$, the transportation information of node index $N_{i,t}^{loc}$ and traffic volume $V_{i,t}^{trl}$ of EV i. As such, each MESS agent only requires partial information from the environment rather than the complete system knowledge.

8.3.3 Action

The action $a_{i,t}$ executed by each MESS agent i at each time step t is defined as a 2-dimensional vector:

$$a_{i,t} = [a_{i,t}^{loc}, a_{i,t}^{pow}] \in \mathcal{A}_i, \ \forall i \in I \tag{8.19}$$

which consists of two parts: 1) the discrete routing action $a_{i,t}^{loc} \in \{0, 1, ..., N^{rd}\}$ is selected from the set of available routes upon the transportation node, where 0 indicates the idle status without any routing behavior and N^{rd} indicates the number of potential routes at transportation node $N_{i,t}^{loc}$, as discussed in [208–210]; and 2) the continuous scheduling action $a_{i,t}^{pow} \in [-1, 1]$ represents the magnitude of charging (positive) and discharging (negative) power of MESS agent i as a percentage of its battery power capacity $[-P_i^{max}, P_i^{max}]$.

8.3.4 State transition

The state transition from time step t to $t+1$ is governed by $s_{t+1} = \mathcal{T}(s_t, a_{1:I,t}, \omega_t)$ with a probability function $P(s_{t+1}|s_t, a_{1:I,t}, \omega_t)$. It is noted that the transition is influenced partly by the environment state s_t, the all agents' actions $a_{1:I,t}$, and partly by the environment stochasticity ω_t. In the examined problem, this corresponds to the exogenous state features $\omega_t = [P_t^{ed}, P_t^{pv}, S_t^{line}, V_t^{trl}]$ which are decoupled from the agent's action and are characterised by inherent variability and uncertainty. In this context, it presents significant challenges to identify suitable probabilistic models which can fully capture such randomness since it is influenced by many exogenous factors, such as energy usage behaviors, solar radiation, line status, and traffic volumes. RL remedies this problem in a data-driven approach which does not rely on accurate models of the underlying uncertainties but learning the characteristics through the constructed dataset via the machine learning techniques [117].

By contrast, the state transitions for endogenous features $N_{i,t}^{loc}$, $E_{i,t}^{mes}$, and $P_{i,t}^{ls}$ are determined by actions $a_{i,t}^{loc}$ and $a_{i,t}^{pow}$ of MESS agent i at time step t. More specifically, the control actions $a_{i,t}$ executed to the environment are assumed as the inputs to determine the routing and charging/discharging power of MESS agent i as well as the AC-OPF algorithm outcomes. On the one hand, N_t^{loc} is determined by $a_{i,t}^{loc}$, which corresponds to the route selections at network topology with the consideration of transportation network, such as travelling time and traffic volumes. On the other hand, the mutually exclusive quantities $P_{i,t}^{mes,c}$ and $P_{i,t}^{mes,d}$ (as a storage cannot charge and discharge simultaneously) are managed by action $a_{i,t}^{pow}$, limited by its minimum and maximum SoC levels E_i^{min}, E_i^{max} and charging and discharging efficiencies η_i^c, η_i^d.

$$P_{i,t}^{mes,c} = [\min(a_{i,t}^{pow} P_i^{max},\ (E_i^{max} - E_{i,t}^{mes})/(\eta_i^c \Delta t))]^+,\ \forall i \in I, \forall t \in T \tag{8.20}$$

$$P_{i,t}^{mes,d} = [\max(a_{i,t}^{pow} P_i^{max},\ (E_i^{min} - E_{i,t}^{mes})\eta_i^d/\Delta t)]^-,\ \forall i \in I, \forall t \in T \tag{8.21}$$

where $[\cdot]^{+/-} = \max/\min\{\cdot, 0\}$. Given the charging and discharging power $P_{i,t}^{mes,c}, P_{i,t}^{mes,d}$ and the energy efficiency η_i^c, η_i^d, the state transition of $E_{i,t}^{mes}$ from time step t to $t+1$ can be expressed in (8.22) that captures the time-series characteristics of storage energy levels, which is also aligned with equation (8.6).

$$E_{i,t+1}^{mes} = E_{i,t}^{mes} + (\eta_i^c P_{i,t}^{mes,c} + P_{i,t}^{mes,d}/\eta_i^d)\Delta t,\ \forall i \in I, \forall t \in T \tag{8.22}$$

Once the locations and charging/discharging power schedules of all MESS agents are determined, this information is an input into the AC-OPF algorithm as known quantities replacing MESS-related variables (i.e., $u_{i,b,t}^c$, $u_{i,b,t}^d$, $P_{i,b,t}^{mes,c}$, and $P_{i,b,t}^{mes,d}$). Afterwards, MGCC solves the linearised AC-OPF, each MESS agent i then can obtain the load shedding quantity $P_{i,t}^{ls}$. It is notable that the operation constraints of MESS in (8.1)-(8.5) are not violated through the $[\cdot]^{+/-}$ and $\min[\cdot]/\max[\cdot]$ operators expressed in (8.20)-(8.21), while the operation constraints of AC-OPF algorithm are also not violated, since (8.11)-(8.17) (environment) is an independent optimisation problem that all the constraints should be satisfied once an optimal solution is obtained. However, some scenarios may occur if the charging/discharging power of MESS agents are extremely high or low, which results in infeasible solutions of AC-OPF algorithm (8.11)-(8.17) when an extreme event occurs.

8.3.5 Reward

At the end of time step t, each agent i obtains its reward $r_{i,t}$. The objective of the studied problem is to reduce the system overall load shedding cost (8.11), where c_d^{ls} corresponds to the load shedding cost of load d. However, each agent is difficult to acquire the system global load shedding condition, the reward function for each agent i at time step t thus can be designed as the negativity of its nodal load shedding cost. In addition, once the AC-OPF algorithm becomes infeasible by the MESSs' actions (as discussed above in Section 8.3.4), a penalty is required to avoid such actions in the future states. However, it is difficult to design a proper penalty function. A relatively large value may break the learning policy while a relatively small value may not be strong enough to penalise such actions. To make a balance, the penalty function is designed, which is similar to the reward function but uses the original load $P_{d,t}^{ed}$ as the baseline. As a result, the integrated reward function of MESS agent i at time step t can be expressed as:

$$r_{i,t} = \begin{cases} -c_d^{ls} P_{d,t}^{ls} & \text{if AC-OPF is optimal} \\ -c_d^{ls} P_{d,t}^{ed} & \text{if AC-OPF is infeasible} \end{cases}, \ d = N_{i,t}^{loc}, \ \forall i \in I, \ \forall t \in T. \tag{8.23}$$

8.4 Multi-agent deep reinforcement learning method for hybrid action space

8.4.1 State-of-the-art RL methods

Before introducing the proposed P-MADDQN method, a comprehensive review of the state-of-the-art RL methods is provided for both discrete and continuous action spaces and their limitations are analysed when applied to the proposed hybrid continuous-discrete (routing-scheduling) action space problem.

Discrete action space

The valued-based method is the fundamental RL method that first estimates a value function and then outputs the greedy policy with respect to that estimate. *Q-learning* (QL) is one of the popular value-based RL methods that learns the value of executing action a in state s in form of the expected Q-value function $Q^{\pi}(s,a) = \mathbb{E}[R|s_t = s, a_t = a]$, which can be recursively updated as the Bellman equation:

$$Q^{\pi}(s,a) = \mathbb{E}_{s'}[r(s,a) + \gamma \mathbb{E}_{a' \sim \pi}[Q^{\pi}(s',a')]] \tag{8.24}$$

Deep Q-network (DQN) is another value-based method combing deep learning and QL that approximates the Q-value function with *deep neural networks* (DNN) parameterised by θ:

$$\mathcal{L}(\theta) = \mathbb{E}\big[(r + \gamma \max_{a'} Q'(s',a') - Q(s,a))^2\big] \tag{8.25}$$

where $Q'(\cdot)$ is the target network whose parameters θ' slowly follow θ, to give consistent target during *temporal-difference* (TD) learning. In addition, the network being trained off-policy with samples from a replay buffer $(s,a,r,s') \sim \mathcal{D}$ further stabilises the training performance.

However, the value-based QL and DQN both suffer from the discrete action space, which can not be practically applied to the RL setup defined in Section 8.3. Although the continuous action space (i.e., MESS charging/discharging schedules) can be discretised into finite intervals, the executed actions are inaccurate, leading to the sub-optimal energy scheduling decisions. Furthermore, the conventional DQN method exhibits the unstable evolution, since the learned Q-value function may overestimate the Q-values, which then leads to the sub-optimal policies, as it exploits errors in the Q-value function [188].

Continuous action space

In addition to the value-based methods, the policy-based methods directly models the optimal actions. *Stochastic policy gradient* (SPG) [117] employs a DNN (parameterised by ϕ) which takes as input a continuous state s, and outputs a continuous action sampling from the stochastic policy $a \sim \pi_{\phi}(a|s)$ (action selection probability). The main idea is directly adjusting the parameter ϕ of the policy in order to maximise the objective $J(\theta) = \mathbb{E}_{s \sim \rho^{\pi}, a \sim \pi_{\phi}}[R(s,a)]$ by taking steps in the direction of $\nabla_{\phi} J(\phi)$. Using the Q-value function as the expected return, the gradient of the stochastic policy can be written as:

$$\nabla_\phi J(\pi_\phi) = \mathbb{E}_{s\sim\rho^\pi, a\sim\pi_\phi}\big[\nabla_\phi \log\pi_\phi(a|s) Q^\pi(s,a)\big] \tag{8.26}$$

where ρ^π is the state distribution. Moving a in the direction indicated by this gradient $\nabla_\phi J(\phi)$ can increase the log-probability of choosing that a proportionate to the associated state-action value function $Q^\pi(s,a)$. To model continuous control, we represent the probability distribution of agent's action with a Normal distribution $\mathcal{N}(\mu, \sigma^2)$, and predict the mean μ and the variance σ^2 of it with a DNN, referred to as a *Gaussian Policy* [196]. However, the training of SPG is inefficient with low sampling performance as both state and action spaces are required to be computed in the policy gradient theorem. Furthermore, SPG normally has high training variance and slow convergence speed without making use of the past experiences.

Moreover, it is also possible to adopt policy-based methods to continuous action space by considering the deterministic policies $\mu_\phi(s)$. Similar as (8.26), the *deterministic policy gradient* (DPG) theorem [117] states that:

$$\nabla_\phi J(\mu_\phi) = \mathbb{E}_{s\sim\rho^\pi}\big[\nabla_\phi \mu_\phi(s) Q^\pi(s,a)\big] \tag{8.27}$$

Instead of optimising the distribution parameters in SPG, DPG directly outputs the action values, thereby constituting a more efficient policy. However, similar as SPG, DPG is also incapable of handling discrete action space for MESS routing selections in the investigated problem.

8.4.2 Proposed P-MADDQN method

In order to handle the hybrid continuous-discrete action space and further address the overestimates of conventional value-based methods in a multi-agent setup, we propose a parameterised and stable MADRL method based on parameterised action space and double DQN method, namely P-MADDQN as depicted in Figure 8.3. In detail, P-MADDQN consists of three parts: 1) two separate networks applied to construct the continuous and discrete action spaces, respectively; 2) two separate Q-value networks applied to construct the target Q-values in order to reduce the bias in updating the network weights; 3) an collective index to represent the system dynamics so as to stabilise the training performance with privacy protection of each individual agent.

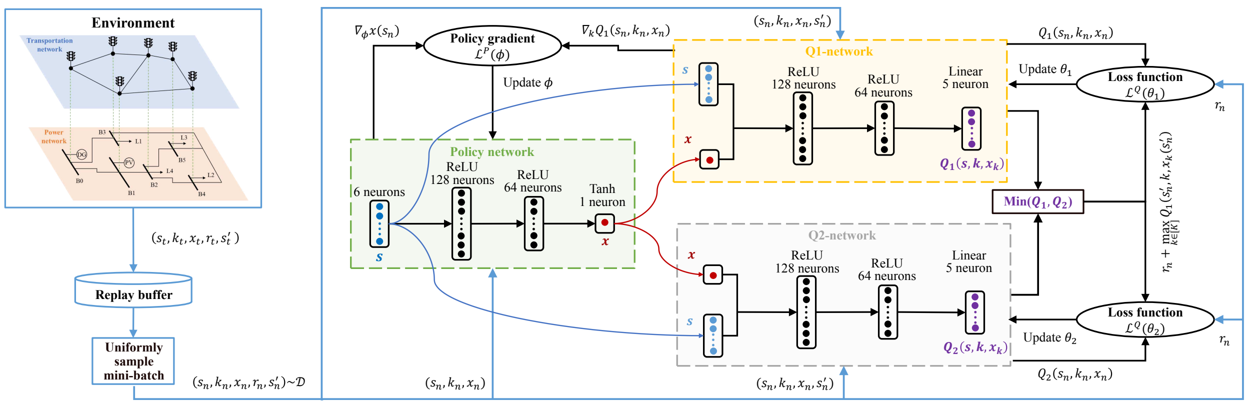

Figure 8.3: Architecture of the proposed P-MADDQN method.

Parameterised Q-value function

This section introduces the proposed framework to handle the application with hybrid continuous-discrete action space. We reconsider a POMG with a parametrised action space $\mathcal{A}_i$ for each agent i, which consists of K discrete actions each associated with a continuous parameter x^k. In specific, any action $a_i \in \mathcal{A}_i$ can be written as $a_i = (k_i, x_i^k)$, where $k_i \in \{1, ..., K_i\}$ is the discrete action, and $x_i^k \in \mathcal{X}_i$ is a continuous parameter associated with the k-th discrete action. Thus action $a_{i,t}$ is a hybrid of discrete and continuous components with the value of the continuous action determined after the discrete action is chosen. Then the parameterised action space $\mathcal{A}_i$ can be written as:

$$\mathcal{A}_i = \left\{ (k_i, x_i^k) \,|\, x_i^k \in \mathcal{X}_i, \ \forall k \in \{1, ..., K_i\} \right\}, \ \forall i \in I \tag{8.28}$$

In the sequel, $\{1, ..., K_i\}$ is denoted by $[K_i]$ for short. For the action space $\mathcal{A}_i$ in (8.28), the action value function is denoted by $Q_i(o_i, a_i) = Q_i(o_i, k_i, x_i^k)$ where $o_i \in \mathcal{O}_i$, $k_i \in [K_i]$, and $x_i^k \in \mathcal{X}_i$. Then the Bellman equation becomes:

$$Q_i(o_i, k_i, x_i^k) = \mathbb{E}_{r_i, o_i'} \left[r_i + \gamma \max_{k_i \in [K_i]} \sup_{x_i^k \in \mathcal{X}_i} Q_i(o_i', k_i, x_i^k) \right], \ \forall i \in I \tag{8.29}$$

Here inside the conditional expectation on the right-hand side of (8.29), we first solve $x_i^{k*} = \text{argsup}_{x_i^k \in \mathcal{X}_i} Q_i(o_i', k_i, x_i^k)$ for each $k_i \in [K_i]$, and then take the largest $Q_i(o_i', k_i, x_i^{k*})$. Note that taking supremum over continuous space $\mathcal{X}_i$ is computationally intractable. However, the right-hand side of (8.29) can be evaluated efficiently providing x_i^{k*} is given.

To elaborate this idea, first note that, when the Q_i function is fixed, for any $o_i \in \mathcal{O}_i$ and

$k_i \in [K_i]$, it can be viewed that

$$x_i^{k,Q}(o_i) = \operatorname{argsup}_{x_i^k \in \mathcal{X}_i} Q_i(o_i, k_i, x_i^k), \ \forall i \in I \tag{8.30}$$

as a function of local observation o_i. That is, we identify (8.30) as a function $x_i^{k,Q} : \mathcal{O}_i \to \mathcal{X}_i$. Then, the Bellman equation in (8.29) can be rewritten as:

$$Q_i(o_i, k_i, x_i^k) = \mathbb{E}_{r_i, o_i'}\Big[r_i + \gamma \max_{k_i \in [K_i]} Q_i\big(o_i', k_i, x_i^{k,Q}(o_i')\big)\Big], \ \forall i \in I \tag{8.31}$$

Note that this new Bellman equation resembles the classical Bellman equation in (8.24) with $A = [K]$. Similar to DQN, a DNN $Q_i(o_i, k_i, x_i^k|\theta_i)$ parameterised by θ_i is used to approximate $Q_i(o_i, k_i, x_i^k)$ for agent i. Moreover, for such a parameterised $Q_i(o_i, k_i, x_i^k|\theta_i)$, $x_i^{k,Q}(o)$ in (8.30) is approximated with a deterministic policy network $x_i^k(\cdot|\phi_i) : \mathcal{O}_i \to \mathcal{X}_i$, where ϕ_i denotes the network weights of the policy network for agent i. When θ_i is fixed, it is expected to find ϕ_i such that

$$Q_i(o_i, k_i, x_i^k(o_i|\phi_i) \,|\, \theta_i) = \sup_{x_i^k \in \mathcal{X}_i} Q_i(o_i, k_i, x_i^k \,|\, \theta_i), \ \forall i \in I, \ \forall k_i \in [K_i] \tag{8.32}$$

Double Q-value function

Inspired by the technique in *Double Q-learning* [188] using a separate target Q-value function to estimate the current Q-value, thus reducing the bias, two separate online Q-value networks $(Q_{i,1}, Q_{i,2})$ parameterised by $\theta_{i,1}, \theta_{i,2}$ are introduced for each agent i, along with two target Q-value networks $(Q_{i,1}', Q_{i,2}')$ parameterised by $\theta_{i,1}', \theta_{i,2}'$. Then the two target values used to update the online Q-value can be written as:

$$\begin{aligned} y_{i,1} &= r_i + \gamma \max_{k_i \in [K_i]} Q_{i,1}\Big(o_i', k_i, x_i^k(o_i'|\phi_i) \,|\, \theta_{i,1}\Big), \ \forall i \in I \\ y_{i,2} &= r_i + \gamma \max_{k_i \in [K_i]} Q_{i,2}\Big(o_i', k_i, x_i^k(o_i'|\phi_i) \,|\, \theta_{i,2}\Big), \ \forall i \in I \end{aligned} \tag{8.33}$$

However, the values of $Q_{i,1}$ and $Q_{i,2}$ cannot be equal, and it is inevitable that the high value may be overestimated. Therefore, we make a slight change on the basis of *Double Q-learning*, and take the minimum value between these two estimates to get the target Q-value:

$$y_i = r_i + \gamma \min_{j=1,2} \max_{k_i \in [K_i]} Q_{i,j}(o_i', k_i, x_i^k(o_i'|\phi_i) \,|\, \theta_{i,j}), \ \forall i \in I \tag{8.34}$$

With this improvement, P-MADDQN can simultaneously train two Q-value networks and pick the minimum value of them, thus alleviating the overestimation phenomenon.

Collective index

As discussed in Section 8.1.2, independent RL acquiring only local observations without others' information may suffer from the instability issue, even though the Double Q-learning is adopted. Furthermore, it is impractical to acquire and incorporate all other agents' local observations into the centralised Q-value networks, mainly driven by the privacy challenge and curse-of-dimensionality of Q-value networks' inputs increasing proportionally with the agent size and observation space. To this end, this chapter assumes the MESS aggregator as a trusted third party who can provide the utilised MESSs with system critical signals that reflect the collective behavior of all agents in the training process. To this effect, the Q-value function (8.32) of each agent i is reformulated as:

$$Q_i(o_i, k_i, x_i^k \mid \theta_i) = Q_i(h_i, o_i, k_i, x_i^k \mid \theta_i), \ \forall i \in I \tag{8.35}$$

where $h_i = \sum_{d \in N_{mes}} (P_{d,t}^{ed} - P_{d,t}^{ls}) / \sum_{d \in N_{load}} (P_{d,t}^{ed} - P_{d,t}^{ls}) \in [0,1]$ denotes the contribution of agent i to the system overall load restoration. It can be observed that h_i is an embedded function that not only abstracts all other agents' local observations (e.g., $P_{i-,t}^{ed}, P_{i-,t}^{pv}, S_{i,t}^{ln}, \forall i- \in \mathcal{I}(i-)$, where $\mathcal{I}(i-)$ donates the set of all other agents $i-$ apart from i), but also reflects the status of agent i providing the system resilience (the higher value of h_i indicates the better performance of contributing to resilience enhancement, and vice versa). As a result, this function provides a good approximation of all other agents' local observations as well as the overall system dynamics. Incorporating h_i into the Q-value function estimations, each agent can make acquainted decisions on the basis of the impact of self and all other agents' observations and actions, albeit not knowing their power-transportation local information and control activities, thereby protecting the MESSs' privacy and also improving the training stability in multi-agent setup.

Training process

Similar as DQN, P-MADDQN is also an off-policy MADRL method that requires the past experiences to update the networks. Since a POMG of I agents with the same observation, action and reward function is considered, their policies can be trained with enhanced efficiency by using a PS framework [201]. PS allows all agents to share the parameters of a single control policy. This enables the shared policy to be trained with the sample experiences gathered by all agents, while still allowing different behaviors among different agents, since each agent receives different local observations. In order to realise this framework, it can be assumed that the experiences acquired from the environment of all local MESS agents are transmitted to the central aggregator for updating the shared hybrid policy parameterised by $\{\theta_1, \theta_2, \phi\} = \{\theta_{i,1}, \theta_{i,2}, \phi_i\}, \forall i \in \mathcal{I}$. This shared policy is then broadcast to all local MESS agents to compute actions executed to the environment. To this end, a shared experience replay buffer $\mathcal{D}$ is also employed to store the past experiences of all agents, where the buffer is a cache storing the past experiences of all agents acquired from the environment (an experience is a transition tuple $(s_{i,t}, k_{i,t}, x_{i,t}, r_{i,t}, h_{i,t}, s'_{i,t})$. For each time step t, a minibatch of N experiences are uniformly sampled from the replay buffer $\{(s_n, k_n, x_n, r_n, h_n, s'_n)\}_{n=1}^{N} \sim \mathcal{D}$ to compute the mean-squared TD error of two online Q-value networks:

$$\mathcal{L}^Q(\theta_1) = \frac{1}{N}\sum_{n=1}^{N}\left[\left(y_n - Q_1(h_n, o_n, k_n, x_n \,|\, \theta_1)\right)^2\right] \tag{8.36}$$

$$\mathcal{L}^Q(\theta_2) = \frac{1}{N}\sum_{n=1}^{N}\left[\left(y_n - Q_2(h_n, o_n, k_n, x_n \,|\, \theta_2)\right)^2\right] \tag{8.37}$$

$$y_n = \begin{cases} r_n & \text{if } o'_n \text{ is the terminal state} \\ r_n + \gamma \min\limits_{j=1,2} \max\limits_{k\in[K]} Q_j\Big(h'_n, o'_n, k, x_k(o'_n|\phi) \,|\, \theta_j\Big) & \text{otherwise} \end{cases}, \ \forall n \in N \tag{8.38}$$

Moreover, since the target is to find ϕ that maximises $Q(h, o, k, x_k(o|\phi) \,|\, \theta)$ with θ fixed, the loss function for ϕ is presented as following:

$$\mathcal{L}^P(\phi) = -\frac{1}{N}\sum_{n=1}^{N} Q_1(h_n, o_n, k_n, x_n|\theta_1) \tag{8.39}$$

The network parameters of two Q-value networks and one policy network can be then written as:

$$\theta_1 \leftarrow \theta_1 - \alpha^{\theta_1}\nabla_{\theta_1}\mathcal{L}^Q(\theta_1) \tag{8.40}$$

$$\theta_2 \leftarrow \theta_2 - \alpha^{\theta_2}\nabla_{\theta_2}\mathcal{L}^Q(\theta_2) \tag{8.41}$$

$$\phi \leftarrow \phi - \alpha^{\phi}\nabla_{\phi}\mathcal{L}^P(\phi) \tag{8.42}$$

where α^{θ_1}, α^{θ_2}, and α^{ϕ} are the learning rates of the gradient descent algorithm for the two online Q-networks and one policy network, respectively.

Algorithm 1 Training process of P-MADDQN

Initialise weights θ_1, θ_2, and ϕ for two Q-value networks and one policy network, respectively.
Initialise a replay buffer $\mathcal{D}$, time-dependent exploration parameters σ_t, ϵ_t.
for episode (i.e., day) $= 1 : M$ **do**
  Initialise the global state s_0
  for time step $t = 1 : T$ **do**
    For each agent i, receives local observation $o_{i,t}$
    For each agent i, selects action $a_{i,t} = \{k_{i,t}, \hat{x}^k_{i,t}\}$ in (8.44) and (8.43) according to the current local observation $o_{i,t}$
    Execute all agents' actions $a_{i:I,t}$ to the environment
    MGCC solves AC-OPF algorithm (8.11)-(8.17)
    For each agent i, observes reward $r_{i,t}$ and next local observation $o'_{i,t}$
    For each agent i, transits local experience $(o_{i,t}, k_{i,t}, x_{i,t}, r_{i,t}, h_{i,t}, o'_{i,t})$ to aggregator
    Aggregator stores all experience $\{(o_{i,t}, k_{i,t}, x_{i,t}, r_{i,t}, h_{i,t}, o'_{i,t})\}_{i=1}^{I}$ to replay buffer $\mathcal{D}$
    Sample a random minibatch of N experiences from reply buffer $\{(o_n, k_n, x_n, r_n, h_n, o'_n)\}_{n=1}^{N} \sim \mathcal{D}$
    Update two Q-value networks and one policy network using (8.40)-(8.42)
    Exponentially decay exploration parameters σ_t, ϵ_t
    Update the environment state $s_t \leftarrow s'_t$ and new local observations $o_{i,t} \leftarrow o'_{i,t}$
  end for
end for

In order to assist the agent in exploring the environment and acquire more valuable experiences, two separate exploration noises are applied to the online policy. More specifically, a random Gaussian noise $\mathcal{N}(0, \sigma_t^2)$ is added to the parameterised network output $x(o_{i,t}|\phi)$, constructing an exploration parameterised policy:

$$\hat{x}(o_{i,t}) = x(o_{i,t}|\phi) + \mathcal{N}(0, \sigma_t^2), \ \forall i \in I, \forall t \in T \tag{8.43}$$

On the other hand, the exploration for discrete action follows the same ϵ-greedy policy in DQN:

$$k_{i,t}(o_{i,t}) = \begin{cases} \max\limits_{k_i \in [K]} Q_1(h_{i,t}, o_{i,t}, k_i, x_i^k(o_{i,t})) & \text{with probability } 1-\epsilon_t \\ \text{a random sample from [K]} & \text{with probability } \epsilon_t \end{cases}, \ \forall i \in I, \forall t \in T \tag{8.44}$$

Finally, the training process of the proposed P-MADDQN method for the coordinated MESS routing and scheduling problem is presented in Algorithm 1.

Test process

The training process lasts for M episodes until the trained policy is being converged. Once in the test process, we firstly collect the weight parameters ϕ^* of policy network and θ_1^* of the first Q-value network respectively trained in Algorithm 1. For each time step in the test days D, each MESS agent i observes the current local observation $o_{i,t}$ and accordingly executes control actions $a_{i,t} = \{k_{i,t}, x_{i,t}\}$ (with the outputs of policy network and first Q-value network) to the environment. The actions are then mapped to the operation models of power-transportation network (environment), transiting to the next state and time step (Section 8.3.4).

Algorithm 2 Test process of P-MADDQN

```
Load the weight parameters φ* and θ*_1 trained by Algorithm 1
for test day = 1 : D do
  Receive the initial state s_0 of the test day.
  for time step = 1 : T do
    For each agent i, receives local observation o_{i,t}
    For each agent i, selects action a_{i,t} = {k_{i,t}, x̂^k_{i,t}} according to the local observation o_{i,t}
    Execute all agents' actions a_{i:I,t} to the environment
    MGCC solves AC-OPF algorithm (8.11)-(8.17)
    For each agent i, observes reward r_{i,t} and next local observation o'_{i,t}
    Update the environment state s_t ← s_{t+1} and new local observations o_{i,t} ← o'_{i,t}
  end for
end for
```

8.5 Input data and experiment setup

8.5.1 Experiment setup

The case studies evaluates the routing and scheduling process of 3 MESSs on a 6-bus power network located in a 6-node transportation network, which are illustrated in Figures 8.4 and 8.5, respectively. Red dotted lines in Figure 8.4 correspond to tie lines that can be closed against extreme events, while four lines (branch $2-5$, $1-2$, $3-4$ and $4-5$) are equipped with smart switches towards dynamic network reconfiguration [68]. Note that radial distribution networks are normally operated with a number of tie switches for the potential network reconfiguration in fault conditions. When extreme events occur, load restoration can be performed by utilising these normally-open tie switches. More specifically, this chapter focuses on an isolated power network supported by DERs including both conventional generation resources (e.g., DGs) and renewable energy sources (e.g., PVs), while 3 MESS agents are connected with the network for load restoration. All the operation data related to the power system (e.g., PV and load patterns) are extracted from [144], which can be found in Figures 8.6 and 8.7. The line data of the 6-bus power system can be found in Table 8.1, while the parameters of important components are presented in Table 8.3. As mentioned before, it is necessary to capture the load distinction into essential and non-essential for realistic decision making; hence, around 30% of total loads are regarded as essential loads with high curtailment cost, while other loads are realised as non-essential loads with low curtailment cost.

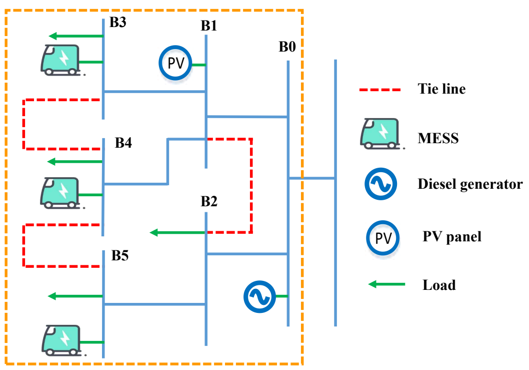

Figure 8.4: Power network of 6-bus system.

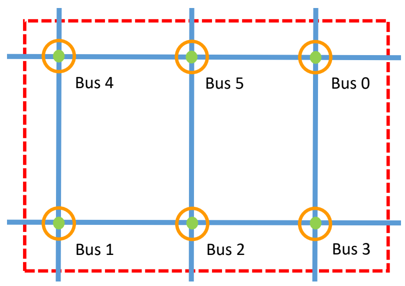

Figure 8.5: Transportation network with electrical buses in 6-bus system.

In order to capture uncertainties associated with renewable energy sources and load profiles, a Monte-Carlo simulation is used to output various scenarios (e.g., 10000) initially following a normal distribution function with 5% and 3% errors in PVs and load profiles to mimic the inevitable forecasting errors since accurate updated forecasts might be unavailable in the context of resilience-driven operations. Regarding the severe contingency caused by the event, it is assumed that random

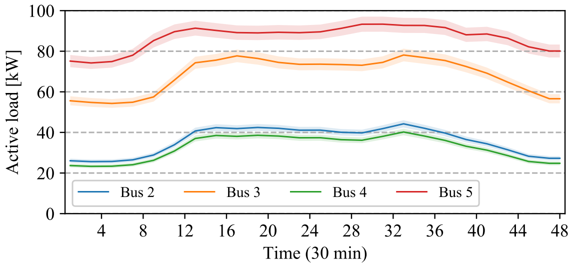

Figure 8.6: Load profiles.

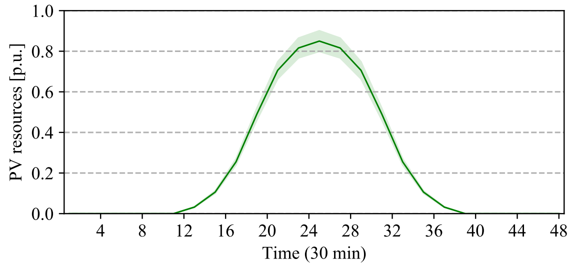

Figure 8.7: PV profile.

Table 8.1: Line data corresponding to the power network

Line between two buses	Reactance ($X_{bp}[p.u.]$)	Resistance ($R_{bp}[p.u.]$)	Capacitance ($C_{bp}[p.u.]$)	Maximum flow ($S_{bp}^{lim}[kVA]$)
$0 \to 1$	0.200	0.100	0.040	100
$0 \to 2$	0.200	0.050	0.040	100
$1 \to 3$	0.300	0.080	0.060	100
$1 \to 4$	0.250	0.050	0.060	60
$2 \to 5$	0.100	0.050	0.020	60
$1 \to 2$	0.300	0.100	0.040	60
$3 \to 4$	0.200	0.070	0.050	60
$4 \to 5$	0.260	0.120	0.050	60

line outages (maximum 2 lines per day) can occur in this power network, including the entire isolation from the upper grid. On the one hand, it is worth noting that the choice of generated scenario number is empirical, while the scenario number shall be large enough to capture the fluctuating nature of renewable energy resources and load profiles. On the other hand, 2 line outages can be regarded as severe damage in the small 6-bus system, while it can be expected that more load shedding will be caused if more line outages occur.

With regards to the transportation network, it is assumed that each electric bus is located at one specific road node, of which its traffic network data is presented in Table 8.2. More specifically, the transportation time between two road nodes is half an hour and different electric buses are settled in different road nodes. According to this routing scheme, the least travelling time between different buses is 0.5 hr; nevertheless, some buses may need more time to reach (e.g., 1 hour from bus 0 to bus 2), as illustrated in Figure 8.5. Additionally, road congestion may cause longer travelling time, as described in equation (8.7). For instance, 10 min congestion happens between bus 5 and bus 0. If the MESS agent still chooses the route $5 \to 0$, the travelling time will be 28.6 min. In order to model the uncertainties of such traffic volumes, 5% errors are added in base flow of each route. In this regard, it can be anticipated that MESS agents may tend to choose a routing scheme with short transporting time in order to allow more hours for connecting with the grid and restoring demand during a daily charging/discharging cycle.

Table 8.2: Road data of 6-node 7-edge transportation network

Route between two nodes	Capacity ($C_r[\#]$)	Free flow travel time ($T_r^{trl,0}[Min]$)	coefficients (α^{rd}, β^{rd})
$0 \to 5$	1000	20.0	4, 0.15
$0 \to 3$	1000	16.8	4, 0.15
$1 \to 2$	1000	17.6	4, 0.15
$1 \to 4$	1000	19.9	4, 0.15
$2 \to 5$	1000	18.6	4, 0.15
$2 \to 3$	600	23.7	4, 0.15
$4 \to 5$	600	27.4	4, 0.15

Table 8.3: Characteristics of components in the electrical system

Component	Parameters
DG	Min-Max Capacity: 0-150 kW
PV	Capacity: 50 kW
MESS	Max power/energy capacity: 50 kW/200 kWh; Initial SoC: 0.5
Essential load	Curtailment cost: 250 £ / kW
Non-essential load	Curtailment cost: 150 £ / kW

8.5.2 Implementations of proposed P-MADDQN method

The network structure of the proposed P-MADDQN method for this experiment is shown in Figure 8.3 and explained as follows: the input data of the policy network is a 2-dimensional data vector $(None, 6)$, where $None$ is the batch size of the training data, and 6 is input dimension of the extracted state features defined in Section 8.3.2. The policy network outputs a $(None, 1)$ vector with a `tanh` activation function bounded by $[-1, 1]$, representing the continuous action of MESS charging/discharging decision a^{pow}. The two Q-value networks inputs the combination of continuous action (i.e., policy network output) and the certain state features, and outputs a 5-dimensional vector $(None, 5)$ with a `linear` activation function, representing the Q-values of 5-dimensional route actions. Note that the examined transportation network in Figure 8.5 is characterised by the regular intersection with 4 potential routes per traffic node. If the investigated case includes more direction choices, the action dimension can also be easily extended. The policy network and two Q-value networks are formulated via the multilayer perceptrons (MLPs) with two hidden layers containing 128 and 64 units, respectively.

During the training process, the RMSProp optimiser is used with a learning rate $\alpha^{\theta_1} = 1 \times 10^{-3}$, $\alpha^{\theta_2} = 1 \times 10^{-3}$, and $\alpha^{\phi} = 1 \times 10^{-4}$, respectively. The discount rate expecting a long-term return within one episode $\gamma = 0.99$, while a replay buffer $\mathcal{D} = 1 \times 10^5$ and a minibatch $N = 64$ are employed, respectively. For the RL exploration, a Gaussian noise process is added to the policy network for continuous action, the standard deviation decreases exponentially from 2 to 0.05 within the first

1,000 episodes and stays unchanged until to end in all experiments. Furthermore, the MESS agents apply the $\epsilon-greedy$ policy for discrete action, with probability ϵ sampling a random action from $[K]$ or taking the greedy action with respect to the current Q-value function otherwise. The ϵ decreases from 1 to 0.05 within 1,000 episodes as well. Finally, the proposed P-MADDQN method has been implemented in Python with Tensorflow v2.6.0 [211], and the linearised AC-OPF algorithm of the environment (Section 8.2.2) has been implemented in Pyomo with Gurobi solver [212].

8.5.3 Implementations of benchmark control methods

In order to validate the superior performance of the proposed P-MADDQN method in the coordinated MESSs routing and scheduling problem, and to test how close the proposed method is to the theoretical benchmark, we compare it against the various model-based optimisation and model-free MADRL methods:

(1) Perfect-MILP: the MGCC solves a model-based deterministic MILP for the daily optimisation problem with the objective function (8.11) and constraints (8.1)-(8.10), (8.12)-(8.17), which assumes the perfect information of MESSs and AC-OPF mathematical models, technical parameters, and system uncertainties. More specifically, the demand and PV profiles are selected as their mean illustrated in Figures 8.6 and 8.7, outage scenario includes two lines ($0-2$ and $1-4$), and serious congestion on route $4-5$ (around 0.4 hr). Free flow travel time for each traffic route used to calculate traffic volume is collected from Table 8.2. It is also mentioned that the solutions under Perfect-MILP are considered as the theoretical benchmark of the coordinated MESS routing and scheduling problem.

(2) Stochastic-MILP: the MGCC solves a scenario-based stochastic MILP for the daily optimisation with the objective function (8.11) and constraints (8.1)-(8.10), (8.12)-(8.17), which assumes the perfect information of MESSs and AC-OPF mathematical models and technical parameters, but considers the stochasticity of system uncertainties. More specifically, we uniformly sample 10 scenarios for each uncertainty parameter of electric demand, PV generation, traffic volume, and line outages, thereby generating 10^4 scenarios in the constructed uncertainty set. In order to make the optimisation computable, we use scenario reduction technique [213] to obtain the most representative 10 scenario sets as the input of Stochastic-MILP.

(3) DQN: each MESS agent adopts a model-free independent-MADRL method with the employment of DQN method, discretising the continuous action space into 3 dimensions. In this setting, the action space becomes 15 (3×5) dimensions. The control decisions (routing and scheduling) are made by selecting the maximise Q-value with respect to the 15 discrete action dimensions. The Q-value network is constructed by two hidden MLP layers with 128 and 64 units, respectively. The output layer is a linear activation function with 15 dimensions. The other hyperparameters (e.g., learning rates, discount factor, buffer and batch size, $\epsilon - greedy$ policy) are the same as the proposed P-MADDQN method in Section 8.5.2.

(4) P-MADQN: each MESS agent adopts a model-free MADRL method with the employment of P-MADQN method, which is based on the proposed hybrid action space and PS framework. But instead of using double Q-value function, P-MADQN directly adopts the conventional DQN method for the parameterised Q-value network. As a result, there are only two networks, one for the policy network and the other one for the Q-network. The network structures and hyperparameters are the the same as the proposed P-MADDQN method in Section 8.5.2.

In order to make the experiments comparable, we run 5,000 episodes with the same 10 random seeds and DNN weights initialisation for all three (including the proposed P-MADDQN) MADRL methods.

8.6 Case Studies

8.6.1 Training performance

This section aims at comparing the training performance and the computational time of three examined MADRL methods. Figure 8.8 illustrates the evolution of episodic total reward (i.e., minus system load shedding costs and penalty values) of all 3 MESS agents over 5,000 episodes for different MADRL methods during the training process. More specifically, their corresponding values are also collected in Table 8.4. Furthermore, their episodic training time as well as the number of episodes and total training time required to reach convergence are summarised in Table 8.5.

The first observation is that all three MADRL methods show an upward trend and their policies are being improved. This is because the MESS agents are in the status of exploring the environment without an optimised policy during the initial learning stage. However, as the learning process

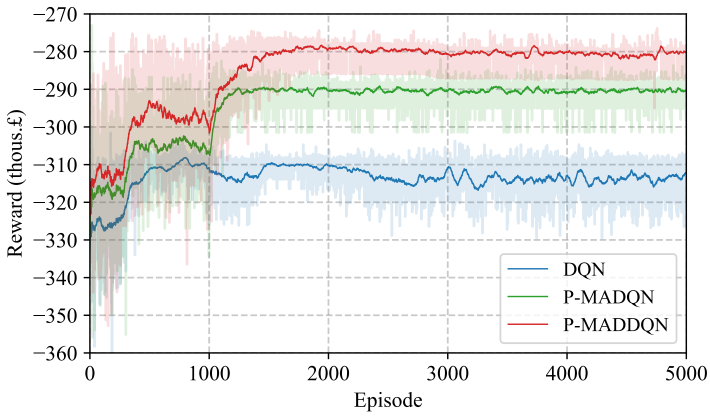

Figure 8.8: Episodic total reward of 3 MESS agents over 5,000 episodes for different MADRL methods.

Table 8.4: The value of episodic total reward of 3 MESS agents over 5,000 episodes for different MADRL methods

Method	Episode						
	1	200	500	1,000	2,000	3,000	5,000
DQN	-333.98	-324.94	-311.26	-310.98	-310.26	-310.80	-312.00
P-MADQN	-339.47	-318.38	-304.31	-306.83	-290.36	-290.25	-290.26
P-MADDQN	-322.47	-314.43	-293.49	-300.95	-279.25	-280.69	-280.25

continues and more valuable experiences are acquired for updating the networks, the policies are being improved and the rewards keep increasing for all three MADRL methods. More specifically, it can be observed that DQN (blue) as the most fundamental MADRL method converges to the lowest reward level among three methods. This is because the naive discritization of action space significantly hinders its effectiveness in addressing the continuous charging/discharging behaviors of MESS, leading to the sub-optimal policy. In order to effectively deal with the hybrid continuous-discrete action space, P-MADQN (green) owing to its parameterised action space algorithm exhibits a superior training performance. It can be further observed that P-MADQN (converges around 1,200 episodes) exhibits a much more stable performance with respect to the independent DQN (relatively stable around 3,400 episodes), this is because P-MADQN using PS framework and collective index that can address the non-stationary issue of multi-agent environment. These advantages of PS framework and collective index can be achieved in P-MADDQN (red) as well. Furthermore, compared to P-MADQN, P-MADDQN using double Q-value networks learns a higher reward, as illustrated in Figure 8.8. In relative terms, the proposed P-MADDQN achieves 10.18% / 3.45% higher average reward over MADQN / P-MADQN, respectively (Table 8.4).

Go further, we analyse their computational performance in the training process. It can be

Table 8.5: Computational performance for different MADRL methods

Method	Episodic training time (sec)	Number of episodes	Total training time (hr)
DQN	1.96	3,400	1.85
P-MADQN	2.51	1,200	0.84
P-MADDQN	2.97	1,800	1.49

observed from Table 8.5 that the episodic training time is the lowest in DQN (since this method only needs to train one Q-value network to compute both routing and scheduling actions), higher in P-MADQN (since this method trains an independent policy network to execute the scheduling action), and the highest in P-MADDQN (since this methods additionally involves another Q-value network and a collective index to stabilise the training performance). Furthermore, we can observe that P-MADQN is the fastest method to reach convergence (around 1,200 episodes), this is owing to the PS framework that all agents' experiences are used to update one policy on every training iteration. Furthermore, without double Q-network, the policy in P-MADQN is easier to be trained. P-MADDQN exhibits a relatively slower training speed (around 1,800 episodes) due to the extra training requirement of double Q-network. DQN results in the slowest training speed (around 3,400 episodes) due to the instability issue of independent learning algorithm. Finally, given the above discussions and the presented value in Table 8.5, the proposed P-MADDQN costs 1.49 hr training time to reach convergence.

8.6.2 Test evaluation

To test the performance evaluation of the proposed P-MADDQN method in the examined MESSs routing and scheduling problem, we first uniformly pick up (sample) 7 days' data from the uncertainty distributions as the test set, then freeze and load the weight parameters of policy network and online Q-value network, and finally apply them to respectively determine the automatic routing and scheduling decisions for 3 MESS agents in the test data (Algorithm 2). In this section, the proposed P-MADDQN is also compared with the four benchmark methods as introduced in Section 8.5.3, where their daily load shedding quantities and costs as well as the actions execution time over the 7 test days for different control methods are presented in Table 8.6.

It can be observed that Perfect-MILP obtains the theoretic solutions of the averaged daily load shedding quantity at 1,799 kWh and cost at 275 thous. £. Although the proposed P-MADDQN cannot reach to the theoretic benchmark, such differences of quantity at 3.80% and cost at 2.43% can be acceptable, which are also assumed as the reasonable solutions. However, theproposed

Table 8.6: Averaged daily load shedding quantity, load shedding cost and execution time over 7 test days for different control methods

Method	Load shedding (kWh)	Load shedding cost (thous.£)	Execution time (sec)
DQN	2,104.02	322.97	0.0901
P-MADQN	1,954.31	296.41	0.1342
P-MADDQN	1,867.10	281.68	0.1163
Stochastic-MILP	1,901.78	288.89	486.6523
Perfect-MILP	1,798.84	275.01	42.6531

P-MADDQN is more efficient to handle the system uncertainties compared to the model-based Stochastic-MILP and exhibits a lower daily load shedding quantity and cost. Moreover, for the other two model-free MADRL methods (DQN, P-MADQN), both of them do not exhibit good performance on the test set of the coordinated MESSs routing and scheduling problem, respectively achieving 19.97% / 8.64% higher daily load shedding quantity and 17.44% / 7.78% higher daily load shedding cost over Perfect-MILP.

The computational performance of the proposed P-MADDQN and the other benchmark methods is also compared in the last column of Table 8.6. It can be observed that the control scheme of all three MADRL methods can be delivered in real-time around 0.1 sec averaged per day. However, the computational time is slightly higher in P-MADQN and P-MADDQN, since the network structures are more complex when the policy network is involved. On the other hand, Perfect-MILP (around 43 sec) and Stochastic-MILP (around 487 sec) exhibit much higher computational time than MADRL methods by solving a model-based daily optimisation problem, because of the introduction of a large number of integer variables. It is noted that control policies of MADRL methods can adapt to various state scenarios (including renewable energies, demand patterns, line outages, and traffic volumes) in the test set, since the policies have been well trained during the training process, while the model-based approaches have to run individual optimisation for each test day. Furthermore, although the training time of MADRL methods in Section 8.6.1 is higher than the optimisation time of model-based methods in Section 8.6.2, their hybrid control policies can be deployed to make the practical MESSs routing and scheduling decisions in 0.1 sec. More importantly, MADRL methods is a model-free approach that does not require any knowledge of the studied power-transportation systems. And in practice, these knowledge is normally not obtained.

The above results demonstrate that 1) the proposed P-MADDQN achieves a good performance evaluation for the examined problem; 2) the proposed P-MADDQN is able to learn an effective policy that can generalise to variable state information in different test days; 3) the MADRL methods exhibit a more favorable computational performance, rendering it the most efficient tool in addressing the proposed real-time automatic MESS routing and scheduling problem, and also destroy the impractical assumptions on acquiring the knowledge of power-transportation systems and system uncertainties in model-based optimisation approaches.

8.6.3 MESS routing and scheduling analysis

To verify the learned hybrid policy in the P-MADDQN method, this section aims at analysing the MESS routing process and charging/discharging characteristics in the examined 6-bus test system, which are illustrated in Figure 8.9. One outage scenario (selected from the above 7 test days) including two line outages (line $0-2$ and line $1-4$) and the isolation from the upper grid is appropriately selected for presentation, as depicted in Figure 8.9. Additionally, the most serious traffic congestion happens on the route $4-5$, which can cause around 0.4 hr travelling delay of MESS agents. The bar in Figure 8.10 presents the active power of charging/discharging and the purple line with asterisks corresponding to the right Y-axis indicates the routing process of 3 MESS agents. Furthermore, we also compare the load patterns before and after load shedding for different buses in Figure 8.11. Finally, it may be interesting to analyse the voltage changes at different buses, which are illustrated in Figure 8.12.

It can be observed from Figure 8.10 that 3 MESSs are initially connected with buses 3, 4 and 5 respectively, and discharge for restoring loads in the first few time steps. After fully or partly discharging power, MESS agents will move to bus 0 for charging, since the conventional generator is located at bus 0. After fully or partly charging power, MESS agents moves back to buses connected with load (e.g., bus 5) for discharging power, since bus 5 has the highest load level. Following this routing pattern, MESSs move to bus 0 for charging when the SoC level is low; then, they move back and stays at buses connected with load after charging power. Note that all the MESS agents move to bus 5 for discharging power due to the large load shedding occurring on bus 5, as depicted in Figure 8.11. Additionally, Figure 8.10 illustrates that different MESS agents choose to charge or discharge power in different time periods to reach a coordinated control fashion. Furthermore, it can be found that it takes about 1 hour for MESS 2 to move from bus 4 to bus 5 in the first few time steps; nevertheless, the ideal travelling time is around 0.5 h. This is because road congestion happens on the road between bus 4 and bus 5 delaying the MESS travel. The advantages of MESSs on reducing load shedding, the coordinated control of multiple MESSs and the impact of road congestion have been clearly shown in Figure 8.10.

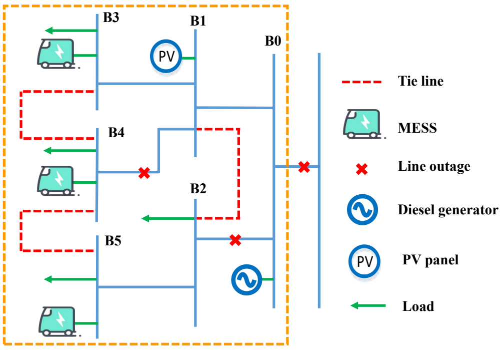

Figure 8.9: The 6-bus power system with line outages for presentation.

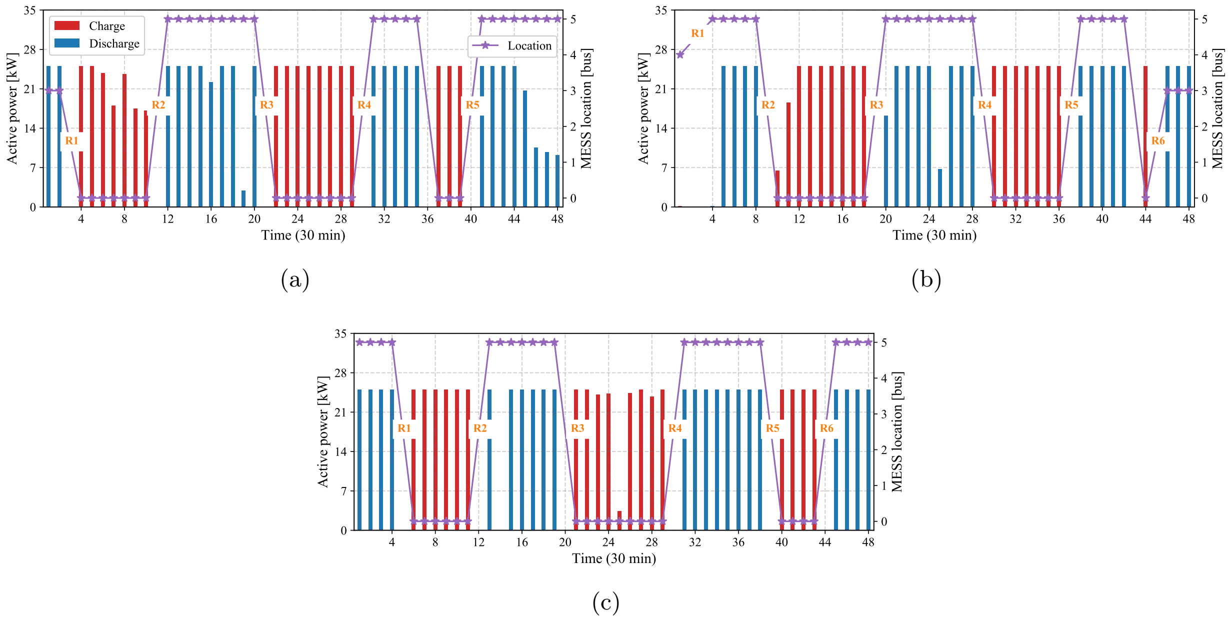

Figure 8.10: Daily routing and scheduling decisions of 3 MESS agents.

Table 8.7: Switch operations of the 6-bus system for network reconfiguration during the restoration process

Time period (hr)	1	1.5	3.5	10
Switch actions	close 1-2, 3-4	close 4-5 and open 2-5	close 2-5 and open 1-2	open 2-5 and close 1-2

Switch operations accounting for the dynamic network reconfiguration are described in Table 8.7. Specifically, tie line $1-2$ and $3-4$ are closed to restore the connection with bus 2 and bus 4 in the first time step after the damage happens; hence, most demand in bus 2 can be restored by the power flow provided through tie lines and MESS agents can focus on other buses with power shortage (e.g., bus 5). Additionally, tie line $4-5$ is closed in the second time step to ensure the power supply to the demand in bus 5, while line $2-5$ is open to ensure the radial structure of

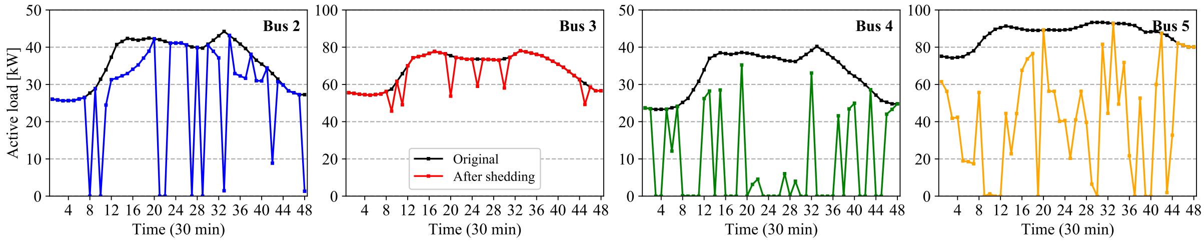

Figure 8.11: Comparison between the original daily load and the daily load level after shedding for different buses.

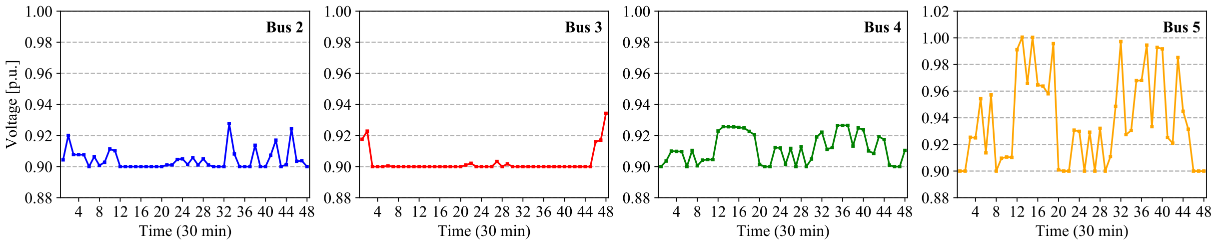

Figure 8.12: Daily voltage profiles for different buses.

the power network. Through smart switch operations, the coordination scheme between dynamic network reconfiguration and MESS routing has been shown clearly.

Furthermore, Figure 8.11 corresponds to the load changes while indicating the amount of load shedding at each bus. It can be found that there is essential load shedding at bus 3, since the severe contingency caused in the power network; nevertheless, the amount of load shedding is very limited due to the importance of supporting essential loads. On the other hand, large load shedding is caused at buses 2, 4 and 5, since these three buses are connected with non-essential loads and close to the faulted lines. Specifically, bus 4 and bus 5 receive much larger load shedding than bus 2 due to the severe contingency occurring at the line between bus 1 and bus 4, bus 0 and bus 2, respectively. More specifically, bus 5 obtains the largest non-essential load shedding, because of the highest load level compared to bus 2 and bus 4.

The voltage changes at 4 buses are illustrated in Figure 8.12. It can be observed that all the voltage levels are limited within the operational range (e.g., 0.9-1.1 p.u.) because of the incorporation of technical constraints. In addition, severe contingencies may require the electrical system to operate very close to its stability limits. More specifically, the voltage level at bus 3 hits the minimum value in most time steps due to the severe contingency caused by the event, while load shedding is caused during these hours to ensure that the voltage level is within the reasonable range. On the other hand, when large amount of non-essential demand is curtailed at buses 2, 4 and 5, voltage levels are significantly raised. As discussed in Section 8.2.2, operation models based on EMS or DC-OPF are incapable of including all the technical constraints relating to stability properties, which increase the risk of insecure system operations, especially when extreme events happen. Even though the value of optimal solutions may be negatively influenced by these constraints since more limitations are required in the operation model, the reality and reliability of the final optimisation results can be guaranteed.

Table 8.8: Performance for different load types in 6-bus system

Performance	Essential load	Non-essential load	Total
	Bus 3	Bus 4, 5, 2	
Quantity (kWh)	45.93	1858.72	1904.65
Cost (thous.£)	11.48	278.81	290.29

Finally, the quantity and cost of both essential and non-essential loads are summarised in Table 8.8. As discussed above, there is not much essential load shedding due to its large curtailment cost, while large amount of non-essential loads have been curtailed for stable and safe operations of the system. In relative terms, the non-essential loads (at buses 4, 5, 2) achieve 40 times load shedding quantity and 24 times load shedding cost over the essential loads (at bus 3).

8.6.4 Test results in the IEEE modified 33-bus system

To further prove the scalability of the proposed P-MADDQN, a larger power network (i.e., a modified 33-bus system) is utilised in this section, as depicted in Figure 8.13. Several DGs and PVs are appropriately installed, while 6 MESSs are initially located at different buses. It is assumed that branches 7-20, 8-14, 11-21, 17-32, 24-28, 15-16, 20-21 and 25-26 are equipped with remote-controlled switches [68]. The associated transportation network is illustrated in Figure 8.14, where MESSs are allowed to move positions within 9 specified buses equipped with charging stations. To capture the severe damage caused by extreme weather events, uncertain multiple line outages are assumed to occur in this system, including the isolation from the main grid or substations. As such, there might be no power supply from main grid and the system can only obtain power from local DERs. Load profiles and PV profiles are extracted from [144], while a power/energy capacity of 100 kW/400 kWh has been used in these MESSs due to the large network size. As discussed in Section 8.6.2, once P-MADDQN is well-trained, its policy can be deployed in the test set and has shown its effectiveness of resilience enhancement in 6-bus system. For 33-bus system, we use the same policy trained in 6-bus system (Section 8.6.1) and increase the number of MESS agents from 3 to 6, since the MDP properties remains the same. However, it is worth noting that retraining or transfer learning can also be applied to achieve better training performance [214]. In other words, the 6 MESS agents in 33-bus system share the same policy trained in P-MADDQN. As a result, both system size and agent numbers are increased in this section to investigate the scalability of theproposed P-MADDQN.

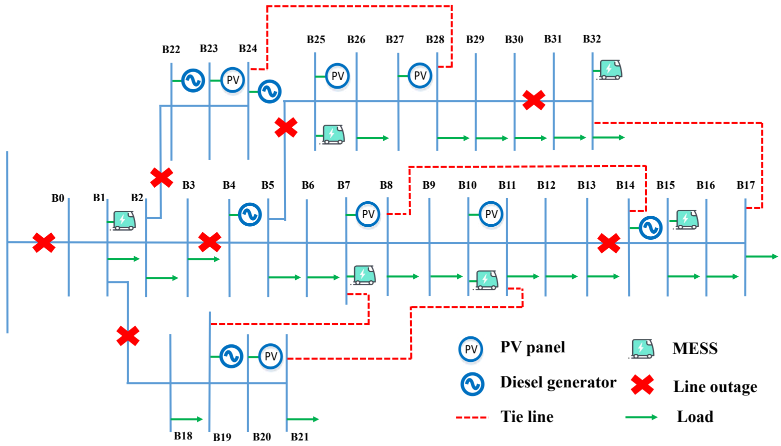

Figure 8.13: Power network in 33-bus system.

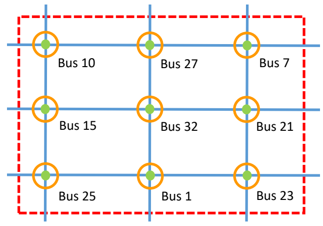

Figure 8.14: Transportation network with electrical buses.

In order to verify the performance of the proposed MADRL method, a scenario with 7 branches damaged by the natural disaster is randomly selected for the distribution system to analyse the routing and scheduling characteristics of these MESS agents and the coordination with dynamic network reconfiguration, as illustrated in Figure 8.13. Additionally, serious traffic congestion mainly happens on routes $7-21$ and $1-25$. Detailed charging/discharging behaviors are also illustrated in Figure 8.15, showing that 6 MESS agents moves back and forth between buses connected with loads (e.g., bus 1, bus 15 and bus 32) and buses connected with generation resources (e.g., bus 23 and bus 25). Note that, the demand at bus 1, bus 2 and bus 3 has been entirely isolated from the rest of the network and obtains no power supply due to severe line outages shown in Figure 8.13, while bus 1 is connected with essential loads. As such, MESS agents (e.g., agent 2, 4 and 5) tend to discharge more power at bus 1 to supply as much demand as possible through reasonable routing and scheduling. Following this routing and scheduling pattern shown in Figure 8.15, most essential demand at bus 1 is restored. On the other hand, it can be found that another half an hour time period is required for the MESS agent 4 to route from initial position (bus 25) to bus 1 due to the serious congestion occurring at route $1-25$. Meanwhile, MESS agent 5 chooses to acquire energy from bus 23 connected with DERs rather than bus 25 due to the congestion between bus 1 and bus 25. The advantages of MESS routing and scheduling on load restoration and the impact of road congestion on MESS routing decisions have been shown clearly.

Switch operations accounting for the dynamic network reconfiguration can be found in Table

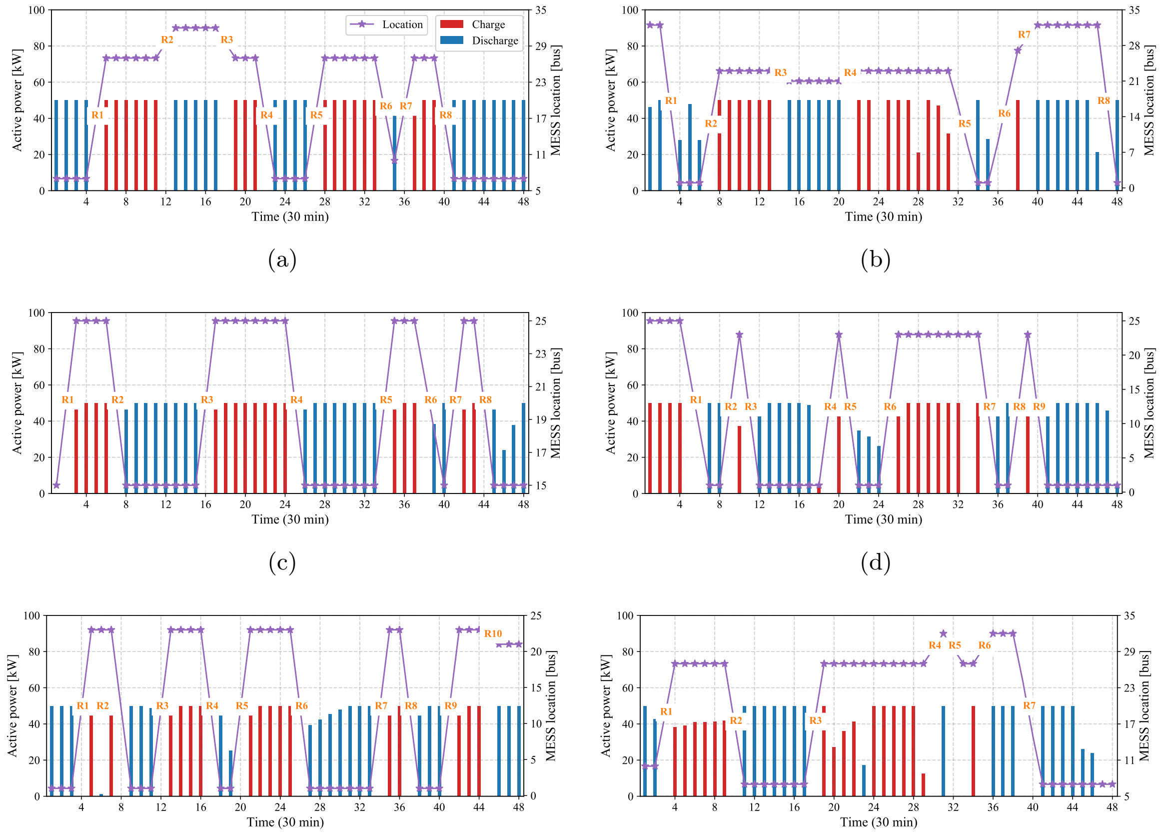

(a) (b) (c) (d) (e) (f)

Figure 8.15: Daily routing and scheduling decisions of 6 MESS agents in 33-bus system.

Table 8.9: Switch operations of the 33 bus system for network reconfiguration

Time period	1 hr	1.5 hr	22 hr
Switch actions	close 7-20, 8-14, 17-32 and 24-28	close 11-21	open 20-21

8.9. Four tie lines including branch $17-32$, $24-28$, $8-14$ and $7-19$ are closed to provide energy supply for areas with power shortage. For instance, after the severe damage happens, the demand connected to bus 31 and bus 32 has been isolated from the power network; nevertheless, power supply to this area is restored by closing the tie line $17-32$. Both bus 31 and bus 32 are connected with essential loads, while there is no load shedding occurring on these two buses. It is worth noting that large amounts of essential loads may be curtailed, if there is no tie line between $17-32$. Also, MESS agents have to focus on this area for load restoration considering the significant importance of essential loads. However, MESS agents can choose to connect with other important areas suffering power shortage due to the existence of tie line $17-32$. As such, the effective coordination between MESS routing and network reconfiguration has been shown appropriately.

In addition, we present the detailed load shedding information in Figure 8.16. Most buses

Table 8.10: Performance for different load types in 33-bus system

Performance	Essential load	Non-essential load	Total
Quantity (kWh)	40.37	5748.74	5789.11
Cost (thous.£)	10.10	862.31	872.41

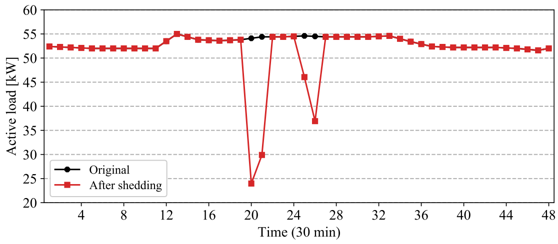

(a)

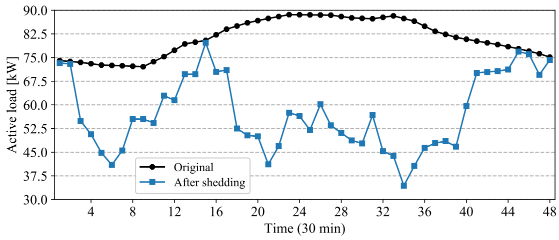

(b)

Figure 8.16: Comparison between original load and the load level after shedding at buses having load shedding: (a) Essential load at bus 1, (b) Averaged non-essential loads at buses 2, 3, 5, 6, 11-13, 17, 18, 21.

connected with essential loads have no load shedding except for bus 1, while large amount of non-essential load shedding is caused at other 10 buses. The only essential load shedding comes from bus 1 due to the isolation of bus 1 with the left power network; nevertheless, it can be found that most essential load at bus 1 is restored by the coordinated routing and scheduling of the MESS agents. Notably, if static battery systems are utilised to supply the essential load at bus 1, it can be predicted that large amount of essential load shedding will be caused due to the lack of mobility. As a result, the advantages of MESSs have been further proven clearly in this case study. Finally, we also compare the load shedding quantities and costs between the essential and non-essential loads in Table 8.10, and also quantify their total values. Similar as the results obtained in the 6-bus system (Table 8.8), there is a large amount of load shedding quantity occurred at the buses with non-essential loads, resulting in serious costs with respect to the essential loads.

Chapter 9

Conclusions and future work

This research firstly reviews recent literature on resilience-oriented planning and operational models and strategies based on MGs. Modelling details are appropriately presented across four dimensions: objectives and metrics, resilience scenarios, control methods and strategies. Among these, load restoration or survivability, cost minimisation, and frequency and voltage stabilities are three main considerations for the selected objective functions, while uncertainty information, contingencies, generation resources and interdependencies between different networks are four basic factors to capture the main features of resilience. Based on three control methods (OPF, EMS and dynamic control), four types of network topologies (including utilisation of existing MGs for network resilience, dynamic formation of MGs, islanding schemes of MGs and networked MGs for resilience enhancement) are presented with their advantages and disadvantages discussed in detail. Based on the suggested framework for resilience enhancement, the following research on developing appropriate resilience-driven planning and operational models has been done:

- An operational model considering preventive power importing and demand response is proposed to enhance the resilience of AC/DC hybrid MGs during extreme events. Both grid-connected and islanded modes are considered in the presented model. Preventive power importing is used to prepare the MG for future events, while demand response is employed to reduce load shedding and operational cost during emergency mode. Detailed OPF algorithm capturing technical constraints is adopted to formulate the non-linear problem. The impact of limited generation resources, the discrimination of loads into critical and non-critical, demand shifting and contingencies on load survivability are appropriately illustrated.
- A hierarchical control strategy based on detailed AC OPF is proposed to deal with the power

sharing problem between networked MGs for accurate solutions, while stochastic programming is utilised to model uncertainties relating to renewable energy sources and load profiles. Technical constraints relating to voltage, angle and power loss are appropriately captured in the model, while the suggested approach can be applied on both meshed and radial networks. Routing of EV fleets in each MG is employed to provide power support and reduce load shedding. Three different levels of contingencies and the limitation of generation resources are also incorporated into the model to mimic a realistic scenario.

- A three-stage distributed control approach based on rolling optimisation is developed for the resilience-driven operation problem of networked MGs after extreme events. In the first stage, a linearised AC OPF algorithm featuring stochastic programming is utilised to capture uncertainties associated with renewable energy sources and load profiles and ensure fast response to extreme events. In the second stage, a consensus-based algorithm is employed for the power sharing between MGs. Note that the routing and scheduling decisions of MESSs in the first stage and power sharing results in the second stage are sent to the third stage; after receiving these results, the MG cluster runs a detailed AC OPF algorithm in the third stage to ensure the feasibility of final optimal solutions.

- A three-level model is suggested for the optimal sizing problem of networked MGs considering a trade-off between resilience and cost. A normal optimal sizing problem is considered in the first level, while the second and third levels are combined as a defender-attacker-defender model to capture resilience. An AGA is developed to consider the normal planing problem in the first level and generate attacking actions in the second level. A detailed AC OPF algorithm capturing technical constraints such as voltage, angle and power loss is utilised in the operation of each MG to obtain accurate solutions, which is suitable both for meshed and radial networks. A multi-objective optimisation problem based on NSGA_II algorithm considering resilience budgets is utilised to capture the trade-off between cost and resilience in the third level. Two types of contingencies including power source damage and multiple line faults and uncertainties with load profiles are incorporated into the model to represent the highly uncertain nature of extreme events.

- The three-level defender-attacker-defender model developed in above chapter is employed to solve an optimal sizing and pre-position problem of MESSs in the context of decentralised networked MGs. The three-level structure is firstly reformulated as a master problem and a subproblem, where the subproblem is used to generate attack actions that can cause the most severe contingency and the master problem is designed to produce optimal results against the worst contingency. The master problem and the subproblem are run in an iterative way until the pre-defined resilience level is achieved. Extensive case studies are developed to prove the optimality, stability and scalability of the proposed planning model on realistic decision making.

- A model-free real-time multi-agent deep reinforcement learning approach featuring parameterised double deep Q-networks is proposed to reformulate the coordination effect of MESSs routing and scheduling process as a Partially Observable Markov Game, which is capable of capturing a hybrid policy including both discrete and continuous actions. A coupled transportation network and linearised AC OPF algorithm are realised as the environment, while the internal uncertainties associated with renewable energy sources, load profiles, line outages, and traffic volumes are incorporated into the proposed data-driven approach through the learning procedure. Extensive case studies including both 6-bus and 33-bus power networks are developed to evaluate the effectiveness of the proposed approach. Specifically, a detailed comparison between different multi-agent reinforcement learning and model-based optimization approaches is conducted to present the superior performance of the proposed approach.

9.1 Future Work

Even though a large amount of literature has focused on developing appropriate and effective resilience models and strategies, several challenges still need to be further considered and incorporated into planning and operation models to better estimate and achieve the desired level of resilience during extreme events. Future research directions, as indicated through the extensive literature review, are summarised hereafter:

9.1.1 Dynamic model for frequency and voltage stabilities

Resilience-oriented models that combine static operational constraints and dynamic differential constraints can lead to more accurate solutions. Uncertainties introduced by extreme events make power systems reach their operating limits more frequently and increase the risk of system failure, which highlights the importance of considering power dynamics in a resilience scenario. However, current resilience-driven modelling approaches for MGs are mainly based on EMS, unit commitment (UC), or various linearised AC OPF algorithms, which focus only on steady-state driven control of MGs and could make final optimisation results dynamically unstable. Hence, there is not much research focused on the application of transient-stability constrained OPF on providing optimal dispatch decisions for the stability properties of the MG.

Future work can concentrate on a novel dynamic model that can assist operators to make real-time dynamic decisions on MG operations. More specifically, a dynamic model including both static AC OPF constraints and differential equations relating to DERs can be developed to capture potential frequency deviations and enhance resilience. Various battery storage systems can also be integrated into the proposed model to investigate the benefits of enhanced voltage and frequency control in MGs. In addition to energy storage, the vehicle-to-grid ($V2G$) concept in supporting real-time dynamic management of MGs might be included in the dynamic OPF. It can be anticipated that this novel model will be capable of capturing realistic frequency and voltage deviations and used for different resilience scenarios.

9.1.2 Realistic power system representation

Renewable energy sources are normally used to deal with the challenges of climate change. According to recent research, it seems to be irreversible to increase the penetration of renewable energy sources on power systems. However, renewable energy sources have lower capabilities in shock absorption and their penetration may cause the system to fail under transient conditions [215], which highlights the importance of developing more stable and robust power systems. To reduce the risk, the proportion of renewable energy sources has to be carefully determined and the control challenges caused by the intermittency characterizing renewable resources have to be tackled in the future. Energy storage systems (e.g., mobile storage units and static storage units) can be employed to reduce the impact of the fluctuating renewable energy resources [98].

Additionally, scenario-based optimization and robust optimization approaches are widely used to tackle the uncertainties associated with renewable energy resources, which may only be able to capture a small number of representative scenarios or lead to very conservative optimization results. In this context, more advanced approaches, such as risk-averse, approaches and learning approaches, shall be developed to ensure realistic model formulation while capturing the stochastic nature of renewable generation.

Furthermore, distribution systems are inherently unbalanced because of the random change of load demands on each phase [13]. The existence of multiple uncertainties may cause a larger unbalance in distribution networks. However, most literature assumes three-phase balanced distribution networks for modelling purposes, which may be unrealistic [28]. Resilience-oriented models based on unbalanced distribution networks need to be developed and the unbalanced dynamic control of voltage and frequency can also be further researched to lead to more accurate results.

9.1.3 Interdependencies between different network structures

Except for power networks, other infrastructures, such as natural gas networks and district heating networks, can also be influenced or even damaged by extreme events, and meanwhile, these systems have very close interconnections among each other, which can introduce further challenges for the resilience enhancement process. In this case, to achieve a higher overall resilience level, MGs can even integrate multiple energy styles as multi-energy microgrids (MEMGs) for more effective energy integration and coordination, which can be more beneficial for resilience enhancement. In detail, MEMGs can be a combination of multiple conversion, distribution, and storage technologies that are controlled to benefit from the synergy of various carriers, thereby electricity, heat, natural gas, and so on optimally interact with each other to meet a higher-level resilience target, e.g., providing energy supply for the critical loads in different energy sectors including electrical loads, gas loads, and heat loads, etc. [216].

Additionally, since the energy sharing among MEMGs can drive more efficient use of various energy styles, several MEMGs can use their higher controllability to further connect with each other as interconnected MEMGs against extreme weather events after switching into islanded mode. These interconnections of many localized MEMGs can better enable the resilience-driven operation and real-time network control of integrated multi-energy systems at both the national level and the local level through the appropriate information and communication technologies (ICT) infrastructure. In this context, multiple interconnected MEMGs can facilitate the paradigm shift in delivering resilience and security of supply from redundancy in assets and preventive control to more intelligent operation through real-time corrective control actions [11]. To achieve real-time corrective control, efficient MEMG operation frameworks featured by distributed control and privacy protection are highlighted in the future.

Furthermore, based on the multi-energy system mentioned above, transportation systems and communication systems are also closely related to power systems. When the network structures of these systems are damaged by extreme events, the resilience of power systems will also be influenced, e.g., more load shedding, slower recovery, etc. On one hand, mobile power sources may not be fully utilised or even unavailable, if transportation networks are damaged. On the other hand, interconnected MEMGs may not connect and exchange power with each other for resilience enhancement, if extreme events destroy the communication infrastructures inside the MG cluster. A possible solution to address the above issue is to further enable cooperation among different network operators as integrated systems, which may be able to mobilise all available resources in a short period for overall resilience enhancement.

9.1.4 Grid-connected MGs for resilience enhancement

As aforementioned in the introduction, MGs or MEMGs can integrate DERs (e.g., DGs, WTs, and PVs) for load restoration at the local level via effective islanding schemes, while they can also stay in grid-connected mode and assist the main grid in restoring critical loads, when the severe damage is caused by extreme events. This thesis particularly deals with the problem of optimal planning and operation for networked MGs based on islanding schemes towards resilience enhancement; nevertheless, how to employ grid-connected MGs or MEMGs for grid load restoration via active and reactive power support is not investigated in this work.

Future work can focus on developing effective control strategies for the active and reactive power scheduling of multiple grid-connected MGs towards the overall resilience enhancement of power networks. It is worth noting that MGs normally have fixed boundaries and self-controllability due to the considerations of customer privacy, load and power balance, and frequency and voltage control. In this context, distributed control approaches featuring privacy protection and fast response time can be more appropriate for the resilience-driven scheduling problem of multiple grid-connected MGs. Additionally, the advantages of different types of MGs (e.g., DC MGs or AC/DC MGs) are worth investigation, since DC MGs normally have low cable losses and simplified control strategies that can offer a more economical power delivery and higher resilience compared with AC MGs [30].

9.1.5 Advanced planning and operation strategies for resilience enhancement

Transportable generation resources are more flexible and effective than static distributed generation resources when extreme events occur. In this thesis, EVs and MESSs have been employed for the resilience enhancement of networked MGs due to their significant mobility and flexibility; nevertheless, other mobile resources, such as mobile emergency generators (MEGs) and repair crews, are not investigated in this thesis. As such, it is necessary to develop comprehensive operational strategies for the coordinated routing and scheduling characteristics of these mobile generation and repairing resources. It can be anticipated that the combination of these mobile resources can introduce more benefits for resilience enhancement than a single type of resources. However, the combination of multi-type resources (e.g., MEGs, MESSs, EVs, repair crews, etc.) can also bring challenges to resilience-oriented modelling because of the incorporation of large amounts of integer variables [24]. In this context, machine learning based techniques and reinforcement learning approaches have the potential in solving large-scale optimisation problems incorporating multi-type mobile resources.

On the other hand, the advantages of operational strategies are influenced and limited by the decision-making at the planning stage (e.g., battery capacities and generator capacities), which leads to the need for developing effective and economical planning strategies incorporating resilience modelling [91]. To address this issue, planning models have been developed in this thesis, while these models mainly focus on the optimal sizing problems of static and mobile DERs in the context of networked MGs. It is necessary to develop a comprehensive planning model capturing elements relating not only to optimal sizing but also optimal network reconfiguration and demand growth for achieving enhanced levels of resilience in the presence of extreme events. Additionally, future work can focus on developing advanced day-selecting approaches that capture all the operational interactions between representative days and the variance in occurrence probability between different scenarios. Furthermore, most planning models are based on traditional mathematical programming methods, which are not very suitable for various power systems featuring distributed control. As such, advanced planning approaches capable of decentralised optimisation need to be further investigated in the future.

Bibliography

[1] Y. Wang, C. Chen, J. Wang, and R. Baldick, “Research on resilience of power systems under natural disasters-a review,” *IEEE Transactions on Power Systems*, vol. 31, no. 2, pp. 1604–1613, 2015.

[2] Z. Yang, H. Zhong, Q. Xia, and C. Kang, “Fundamental review of the opf problem: Challenges, solutions, and state-of-the-art algorithms,” *Journal of Energy Engineering*, vol. 144, no. 1, p. 04017075, 2018.

[3] A. Hussain, V.-H. Bui, and H.-M. Kim, “A resilient and privacy-preserving energy management strategy for networked microgrids,” *IEEE Transactions on Smart Grid*, vol. 9, no. 3, pp. 2127–2139, 2016.

[4] M. Panteli and P. Mancarella, “The grid: Stronger bigger smarter?: Presenting a conceptual framework of power system resilience,” *IEEE Power and Energy Magazine*, vol. 13, no. 3, pp. 58–66, 2015.

[5] N. Hatziargyriou, *Microgrids: architectures and control*. John Wiley & Sons, 2014.

[6] A. Hussain, V.-H. Bui, and H.-M. Kim, “Microgrids as a resilience resource and strategies used by microgrids for enhancing resilience,” *Applied energy*, vol. 240, pp. 56–72, 2019.

[7] M. Panteli, P. Mancarella, D. N. Trakas, E. Kyriakides, and N. D. Hatziargyriou, “Metrics and quantification of operational and infrastructure resilience in power systems,” *IEEE Transactions on Power Systems*, vol. 32, no. 6, pp. 4732–4742, 2017.

[8] A. Clark-Ginsberg, “What’s the difference between reliability and resilience?,” *Stanford University, Tech. Rep*, 2016.

[9] M. J. Ghadi, A. Rajabi, S. Ghavidel, A. Azizivahed, L. Li, and J. Zhang, "From active distribution systems to decentralized microgrids: A review on regulations and planning approaches based on operational factors," *Applied Energy*, vol. 253, p. 113543, 2019.

[10] A. Khodaei, "Provisional microgrids," *IEEE Transactions on Smart Grid*, vol. 6, no. 3, pp. 1107–1115, 2014.

[11] G. Strbac, N. Hatziargyriou, J. P. Lopes, C. Moreira, A. Dimeas, and D. Papadaskalopoulos, "Microgrids: Enhancing the resilience of the european megagrid," *IEEE Power and Energy Magazine*, vol. 13, no. 3, pp. 35–43, 2015.

[12] R. H. Lasseter and P. Piagi, "Microgrid: A conceptual solution," in *IEEE Power Electronics Specialists Conference*, vol. 6, pp. 4285–4291, Citeseer, 2004.

[13] K. P. Schneider, F. K. Tuffner, M. A. Elizondo, C.-C. Liu, Y. Xu, and D. Ton, "Evaluating the feasibility to use microgrids as a resiliency resource," *IEEE Transactions on Smart Grid*, vol. 8, no. 2, pp. 687–696, 2016.

[14] Y. Xu, C.-C. Liu, K. P. Schneider, F. K. Tuffner, and D. T. Ton, "Microgrids for service restoration to critical load in a resilient distribution system," *IEEE Transactions on Smart Grid*, vol. 9, no. 1, pp. 426–437, 2016.

[15] H. Gao, Y. Chen, Y. Xu, and C.-C. Liu, "Resilience-oriented critical load restoration using microgrids in distribution systems," *IEEE Transactions on Smart Grid*, vol. 7, no. 6, pp. 2837–2848, 2016.

[16] H. Gao, Y. Chen, S. Mei, S. Huang, and Y. Xu, "Resilience-oriented pre-hurricane resource allocation in distribution systems considering electric buses," *Proceedings of the IEEE*, vol. 105, no. 7, pp. 1214–1233, 2017.

[17] X. Liu, M. Shahidehpour, Z. Li, X. Liu, Y. Cao, and Z. Bie, "Microgrids for enhancing the power grid resilience in extreme conditions," *IEEE Transactions on Smart Grid*, vol. 8, no. 2, pp. 589–597, 2016.

[18] J. Kim and Y. Dvorkin, "Enhancing distribution system resilience with mobile energy storage and microgrids," *IEEE Transactions on Smart Grid*, vol. 10, no. 5, pp. 4996–5006, 2018.

[19] S. Yao, P. Wang, and T. Zhao, "Transportable energy storage for more resilient distribution systems with multiple microgrids," *IEEE Transactions on Smart Grid*, vol. 10, no. 3, pp. 3331–3341, 2018.

[20] S. Mohagheghi and S. Rebennack, "Optimal resilient power grid operation during the course of a progressing wildfire," *International Journal of Electrical Power & Energy Systems*, vol. 73, pp. 843–852, 2015.

[21] Y. Zhou, M. Panteli, R. Moreno, and P. Mancarella, "System-level assessment of reliability and resilience provision from microgrids," *Applied energy*, vol. 230, pp. 374–392, 2018.

[22] S. Chanda and A. K. Srivastava, "Defining and enabling resiliency of electric distribution systems with multiple microgrids," *IEEE Transactions on Smart Grid*, vol. 7, no. 6, pp. 2859–2868, 2016.

[23] M. Panteli, C. Pickering, S. Wilkinson, R. Dawson, and P. Mancarella, "Power system resilience to extreme weather: fragility modeling, probabilistic impact assessment, and adaptation measures," *IEEE Transactions on Power Systems*, vol. 32, no. 5, pp. 3747–3757, 2016.

[24] Y. Wang, Y. Xu, J. He, C.-C. Liu, K. P. Schneider, M. Hong, and D. T. Ton, "Coordinating multiple sources for service restoration to enhance resilience of distribution systems," *IEEE Transactions on Smart Grid*, 2019.

[25] J. Najafi, A. Peiravi, A. Anvari-Moghaddam, and J. M. Guerrero, "Resilience improvement planning of power-water distribution systems with multiple microgrids against hurricanes using clean strategies," *Journal of Cleaner Production*, vol. 223, pp. 109–126, 2019.

[26] C. Chen, J. Wang, F. Qiu, and D. Zhao, "Resilient distribution system by microgrids formation after natural disasters," *IEEE Transactions on smart grid*, vol. 7, no. 2, pp. 958–966, 2015.

[27] T. Ding, Y. Lin, Z. Bie, and C. Chen, "A resilient microgrid formation strategy for load restoration considering master-slave distributed generators and topology reconfiguration," *Applied energy*, vol. 199, pp. 205–216, 2017.

[28] B. Chen, C. Chen, J. Wang, and K. L. Butler-Purry, "Sequential service restoration for unbalanced distribution systems and microgrids," *IEEE Transactions on Power Systems*, vol. 33, no. 2, pp. 1507–1520, 2017.

[29] C. Gouveia, J. Moreira, C. Moreira, and J. P. Lopes, "Coordinating storage and demand response for microgrid emergency operation," *IEEE transactions on smart grid*, vol. 4, no. 4, pp. 1898–1908, 2013.

[30] L. Che and M. Shahidehpour, "Dc microgrids: Economic operation and enhancement of resilience by hierarchical control," *IEEE Transactions on Smart Grid*, vol. 5, no. 5, pp. 2517–2526, 2014.

[31] K. P. Schneider, F. K. Tuffner, M. A. Elizondo, C.-C. Liu, Y. Xu, S. Backhaus, and D. Ton, "Enabling resiliency operations across multiple microgrids with grid friendly appliance controllers," *IEEE Transactions on Smart Grid*, vol. 9, no. 5, pp. 4755–4764, 2017.

[32] Q. Zhou, Z. Li, Q. Wu, and M. Shahidehpour, "Two-stage load shedding for secondary control in hierarchical operation of islanded microgrids," *IEEE Transactions on Smart Grid*, vol. 10, no. 3, pp. 3103–3111, 2018.

[33] M. Chen, X. Xiao, and J. M. Guerrero, "Secondary restoration control of islanded microgrids with a decentralized event-triggered strategy," *IEEE Transactions on Industrial Informatics*, vol. 14, no. 9, pp. 3870–3880, 2017.

[34] Q. Zhou, M. Shahidehpour, A. Alabdulwahab, and A. Abusorrah, "Flexible division and unification control strategies for resilience enhancement in networked microgrids," *IEEE Transactions on Power Systems*, vol. 35, no. 1, pp. 474–486, 2019.

[35] K. P. Schneider, N. Radhakrishnan, Y. Tang, F. K. Tuffner, C.-C. Liu, J. Xie, and D. Ton, "Improving primary frequency response to support networked microgrid operations," *IEEE Transactions on Power Systems*, vol. 34, no. 1, pp. 659–667, 2018.

[36] M. Ouyang and L. Duenas-Osorio, "Multi-dimensional hurricane resilience assessment of electric power systems," *Structural Safety*, vol. 48, pp. 15–24, 2014.

[37] M. Panteli, D. N. Trakas, P. Mancarella, and N. D. Hatziargyriou, "Power systems resilience assessment: Hardening and smart operational enhancement strategies," *Proceedings of the IEEE*, vol. 105, no. 7, pp. 1202–1213, 2017.

[38] M. Amirioun, F. Aminifar, H. Lesani, and M. Shahidehpour, "Metrics and quantitative framework for assessing microgrid resilience against windstorms," *International Journal of Electrical Power & Energy Systems*, vol. 104, pp. 716–723, 2019.

[39] M. H. Amirioun, F. Aminifar, and M. Shahidehpour, "Resilience-promoting proactive scheduling against hurricanes in multiple energy carrier microgrids," *IEEE Transactions on Power Systems*, vol. 34, no. 3, pp. 2160–2168, 2018.

[40] S. D. Manshadi and M. E. Khodayar, "Resilient operation of multiple energy carrier microgrids," *IEEE Transactions on Smart Grid*, vol. 6, no. 5, pp. 2283–2292, 2015.

[41] A. Hussain, A. O. Rousis, I. Konstantelos, G. Strbac, J. Jeon, and H.-M. Kim, "Impact of uncertainties on resilient operation of microgrids: A data-driven approach," *IEEE Access*, vol. 7, pp. 14924–14937, 2019.

[42] H. Lee, G.-S. Byeon, J.-H. Jeon, A. Hussain, H.-M. Kim, A. O. Rousis, and G. Strbac, "An energy management system with optimum reserve power procurement function for microgrid resilience improvement," *IEEE Access*, vol. 7, pp. 42577–42585, 2019.

[43] J. Wang, X. Zheng, N. Tai, W. Wei, and L. Li, "Resilience-oriented optimal operation strategy of active distribution network," *Energies*, vol. 12, no. 17, p. 3380, 2019.

[44] Z. Li, M. Shahidehpour, F. Aminifar, A. Alabdulwahab, and Y. Al-Turki, "Networked microgrids for enhancing the power system resilience," *Proceedings of the IEEE*, vol. 105, no. 7, pp. 1289–1310, 2017.

[45] S. Mousavizadeh, M.-R. Haghifam, and M.-H. Shariatkhah, "A linear two-stage method for resiliency analysis in distribution systems considering renewable energy and demand response resources," *Applied energy*, vol. 211, pp. 443–460, 2018.

[46] J. Najafi, A. Peiravi, and J. M. Guerrero, "Power distribution system improvement planning under hurricanes based on a new resilience index," *Sustainable cities and society*, vol. 39, pp. 592–604, 2018.

[47] M. Panteli, D. N. Trakas, P. Mancarella, and N. D. Hatziargyriou, "Boosting the power grid resilience to extreme weather events using defensive islanding," *IEEE Transactions on Smart Grid*, vol. 7, no. 6, pp. 2913–2922, 2016.

[48] L. Che and M. Shahidehpour, "Adaptive formation of microgrids with mobile emergency resources for critical service restoration in extreme conditions," *IEEE Transactions on Power Systems*, vol. 34, no. 1, pp. 742–753, 2018.

[49] L. Che, M. Khodayar, and M. Shahidehpour, “Only connect: Microgrids for distribution system restoration,” *IEEE Power and Energy Magazine*, vol. 12, no. 1, pp. 70–81, 2013.

[50] A. Hussain, V.-H. Bui, and H.-M. Kim, “Robust optimal operation of ac/dc hybrid microgrids under market price uncertainties,” *IEEE Access*, vol. 6, pp. 2654–2667, 2017.

[51] Z. Wang, C. Shen, Y. Xu, F. Liu, X. Wu, and C.-C. Liu, “Risk-limiting load restoration for resilience enhancement with intermittent energy resources,” *IEEE Transactions on Smart Grid*, vol. 10, no. 3, pp. 2507–2522, 2018.

[52] M. Tavakoli, F. Shokridehaki, M. F. Akorede, M. Marzband, I. Vechiu, and E. Pouresmaeil, “Cvar-based energy management scheme for optimal resilience and operational cost in commercial building microgrids,” *International Journal of Electrical Power & Energy Systems*, vol. 100, pp. 1–9, 2018.

[53] Z. Liang, Q. Alsafasfeh, and W. Su, “Proactive resilient scheduling for networked microgrids with extreme events,” *IEEE Access*, vol. 7, pp. 112639–112652, 2019.

[54] W. Lin, J. Zhu, Y. Yuan, and H. Wu, “Robust optimization for island partition of distribution system considering load forecasting error,” *IEEE Access*, vol. 7, pp. 64247–64255, 2019.

[55] J. Chen and Q. Zhu, “A game-theoretic framework for resilient and distributed generation control of renewable energies in microgrids,” *IEEE Transactions on Smart Grid*, vol. 8, no. 1, pp. 285–295, 2016.

[56] D. R. Shang, “Pricing of emergency dynamic microgrid power service for distribution resilience enhancement,” *Energy Policy*, vol. 111, pp. 321–335, 2017.

[57] J. C. Bedoya, J. Xie, Y. Wang, X. Zhang, and C.-C. Liu, “Resiliency of distribution systems incorporating asynchronous information for system restoration,” *IEEE Access*, vol. 7, pp. 101471–101482, 2019.

[58] J. Li, X.-Y. Ma, C.-C. Liu, and K. P. Schneider, “Distribution system restoration with microgrids using spanning tree search,” *IEEE Transactions on Power Systems*, vol. 29, no. 6, pp. 3021–3029, 2014.

[59] S. Lei, C. Chen, H. Zhou, and Y. Hou, “Routing and scheduling of mobile power sources for distribution system resilience enhancement,” *IEEE Transactions on Smart Grid*, vol. 10, no. 5, pp. 5650–5662, 2018.

[60] Z. Bie, Y. Lin, G. Li, and F. Li, “Battling the extreme: A study on the power system resilience,” *Proceedings of the IEEE*, vol. 105, no. 7, pp. 1253–1266, 2017.

[61] H. Lei, S. Huang, Y. Liu, and T. Zhang, “Robust optimization for microgrid defense resource planning and allocation against multi-period attacks,” *IEEE Transactions on Smart Grid*, vol. 10, no. 5, pp. 5841–5850, 2019.

[62] S. Yao, P. Wang, X. Liu, H. Zhang, and T. Zhao, “Rolling optimization of mobile energy storage fleets for resilient service restoration,” *IEEE Transactions on Smart Grid*, vol. 11, no. 2, pp. 1030–1043, 2019.

[63] A. Hussain, V.-H. Bui, and H.-M. Kim, “Resilience-oriented optimal operation of networked hybrid microgrids,” *IEEE Transactions on Smart Grid*, vol. 10, no. 1, pp. 204–215, 2017.

[64] H. Xie, X. Teng, Y. Xu, and Y. Wang, “Optimal energy storage sizing for networked microgrids considering reliability and resilience,” *IEEE Access*, vol. 7, pp. 86336–86348, 2019.

[65] H. Farzin, M. Fotuhi-Firuzabad, and M. Moeini-Aghtaie, “Enhancing power system resilience through hierarchical outage management in multi-microgrids,” *IEEE Transactions on Smart Grid*, vol. 7, no. 6, pp. 2869–2879, 2016.

[66] Z. Wang, B. Chen, J. Wang, and C. Chen, “Networked microgrids for self-healing power systems,” *IEEE Transactions on smart grid*, vol. 7, no. 1, pp. 310–319, 2015.

[67] A. Kavousi-Fard, M. Wang, and W. Su, “Stochastic resilient post-hurricane power system recovery based on mobile emergency resources and reconfigurable networked microgrids,” *IEEE Access*, vol. 6, pp. 72311–72326, 2018.

[68] S. Lei, C. Chen, Y. Li, and Y. Hou, “Resilient disaster recovery logistics of distribution systems: Co-optimize service restoration with repair crew and mobile power source dispatch,” *IEEE Transactions on Smart Grid*, vol. 10, no. 6, pp. 6187–6202, 2019.

[69] S. Lei, J. Wang, C. Chen, and Y. Hou, “Mobile emergency generator pre-positioning and real-time allocation for resilient response to natural disasters,” *IEEE Transactions on Smart Grid*, vol. 9, no. 3, pp. 2030–2041, 2016.

[70] A. Gholami, T. Shekari, F. Aminifar, and M. Shahidehpour, “Microgrid scheduling with uncertainty: The quest for resilience,” *IEEE Transactions on Smart Grid*, vol. 7, no. 6, pp. 2849–2858, 2016.

[71] A. Hussain, V.-H. Bui, and H.-M. Kim, "Optimal operation of hybrid microgrids for enhancing resiliency considering feasible islanding and survivability," *IET Renewable Power Generation*, vol. 11, no. 6, pp. 846–857, 2017.

[72] M. Amirioun, F. Aminifar, and H. Lesani, "Resilience-oriented proactive management of microgrids against windstorms," *IEEE Transactions on Power Systems*, vol. 33, no. 4, pp. 4275–4284, 2017.

[73] K. Balasubramaniam, P. Saraf, R. Hadidi, and E. B. Makram, "Energy management system for enhanced resiliency of microgrids during islanded operation," *Electric Power Systems Research*, vol. 137, pp. 133–141, 2016.

[74] Z. Wang and J. Wang, "Self-healing resilient distribution systems based on sectionalization into microgrids," *IEEE Transactions on Power Systems*, vol. 30, no. 6, pp. 3139–3149, 2015.

[75] A. Arif and Z. Wang, "Networked microgrids for service restoration in resilient distribution systems," *IET Generation, Transmission & Distribution*, vol. 11, no. 14, pp. 3612–3619, 2017.

[76] A. Hussain, V.-H. Bui, and H.-M. Kim, "A proactive and survivability-constrained operation strategy for enhancing resilience of microgrids using energy storage system," *IEEE Access*, vol. 6, pp. 75495–75507, 2018.

[77] M. H. Amirioun, F. Aminifar, and H. Lesani, "Towards proactive scheduling of microgrids against extreme floods," *IEEE Transactions on Smart Grid*, vol. 9, no. 4, pp. 3900–3902, 2017.

[78] A. Khodaei, "Resiliency-oriented microgrid optimal scheduling," *IEEE Transactions on Smart Grid*, vol. 5, no. 4, pp. 1584–1591, 2014.

[79] E. Rosales-Asensio, M. de Simón-Martín, D. Borge-Diez, J. J. Blanes-Peiró, and A. Colmenar-Santos, "Microgrids with energy storage systems as a means to increase power resilience: An application to office buildings," *Energy*, vol. 172, pp. 1005–1015, 2019.

[80] H. Gao, Y. Chen, Y. Xu, and C.-C. Liu, "Dynamic load shedding for an islanded microgrid with limited generation resources," *IET Generation, Transmission & Distribution*, vol. 10, no. 12, pp. 2953–2961, 2016.

[81] A. Gholami, T. Shekari, and S. Grijalva, "Proactive management of microgrids for resiliency enhancement: An adaptive robust approach," *IEEE Transactions on Sustainable Energy*, vol. 10, no. 1, pp. 470–480, 2017.

[82] A. Hussain, V.-H. Bui, and H.-M. Kim, "Fuzzy logic-based operation of battery energy storage systems (besss) for enhancing the resiliency of hybrid microgrids," *Energies*, vol. 10, no. 3, p. 271, 2017.

[83] H. Farzin, M. Fotuhi-Firuzabad, and M. Moeini-Aghtaie, "Stochastic energy management of microgrids during unscheduled islanding period," *IEEE Transactions on Industrial Informatics*, vol. 13, no. 3, pp. 1079–1087, 2016.

[84] A. Khodaei, "Microgrid optimal scheduling with multi-period islanding constraints," *IEEE Transactions on Power Systems*, vol. 29, no. 3, pp. 1383–1392, 2013.

[85] H. Qiu, W. Gu, Z. Wu, S. Zhou, G. Pan, X. Yang, X. Yuan, and X. Ding, "Resilience-directional robust power dispatching of microgrids under meteorological disasters," *IET Renewable Power Generation*, vol. 13, no. 12, pp. 2084–2093, 2019.

[86] M. U. Shahid, M. M. Khan, K. Hashmi, R. Boudina, A. Khan, J. Yuning, and H. Tang, "Renewable energy source (res) based islanded dc microgrid with enhanced resilient control," *International Journal of Electrical Power & Energy Systems*, vol. 113, pp. 461–471, 2019.

[87] D. Neves, A. Pina, and C. A. Silva, "Comparison of different demand response optimization goals on an isolated microgrid," *Sustainable Energy Technologies and Assessments*, vol. 30, pp. 209–215, 2018.

[88] Z. Wang, B. Chen, J. Wang, *et al.*, "Decentralized energy management system for networked microgrids in grid-connected and islanded modes," *IEEE Transactions on Smart Grid*, vol. 7, no. 2, pp. 1097–1105, 2015.

[89] L. Liang, Y. Hou, D. J. Hill, and S. Y. R. Hui, "Enhancing resilience of microgrids with electric springs," *IEEE Transactions on Smart Grid*, vol. 9, no. 3, pp. 2235–2247, 2016.

[90] Y. Lin and Z. Bie, "Tri-level optimal hardening plan for a resilient distribution system considering reconfiguration and dg islanding," *Applied Energy*, vol. 210, pp. 1266–1279, 2018.

[91] W. Yuan, J. Wang, F. Qiu, C. Chen, C. Kang, and B. Zeng, "Robust optimization-based resilient distribution network planning against natural disasters," *IEEE Transactions on Smart Grid*, vol. 7, no. 6, pp. 2817–2826, 2016.

[92] C. Yuan, M. S. Illindala, and A. S. Khalsa, "Modified viterbi algorithm based distribution system restoration strategy for grid resiliency," *IEEE Transactions on Power Delivery*, vol. 32, no. 1, pp. 310–319, 2016.

[93] F. Wang, C. Chen, C. Li, Y. Cao, Y. Li, B. Zhou, and X. Dong, "A multi-stage restoration method for medium-voltage distribution system with dgs," *IEEE Transactions on Smart Grid*, vol. 8, no. 6, pp. 2627–2636, 2016.

[94] T. Ding, Y. Lin, G. Li, and Z. Bie, "A new model for resilient distribution systems by microgrids formation," *IEEE Transactions on Power Systems*, vol. 32, no. 5, pp. 4145–4147, 2017.

[95] A. Barnes, H. Nagarajan, E. Yamangil, R. Bent, and S. Backhaus, "Resilient design of large-scale distribution feeders with networked microgrids," *Electric Power Systems Research*, vol. 171, pp. 150–157, 2019.

[96] Y.-J. Kim, J. Wang, and X. Lu, "A framework for load service restoration using dynamic change in boundaries of advanced microgrids with synchronous-machine dgs," *IEEE Transactions on Smart Grid*, vol. 9, no. 4, pp. 3676–3690, 2016.

[97] J. Liu, X. Lu, and J. Wang, "Resilience analysis of dc microgrids under denial of service threats," *IEEE Transactions on Power Systems*, vol. 34, no. 4, pp. 3199–3208, 2019.

[98] A. O. Rousis, I. Konstantelos, and G. Strbac, "A planning model for a hybrid ac–dc microgrid using a novel ga/ac opf algorithm," *IEEE Transactions on Power Systems*, vol. 35, no. 1, pp. 227–237, 2019.

[99] F. Capitanescu, "Critical review of recent advances and further developments needed in ac optimal power flow," *Electric Power Systems Research*, vol. 136, pp. 57–68, 2016.

[100] A. J. Wood, B. F. Wollenberg, and G. B. Sheblé, *Power generation, operation, and control*. John Wiley & Sons, 2013.

[101] Z. Yang, H. Zhong, Q. Xia, and C. Kang, "A novel network model for optimal power flow with reactive power and network losses," *Electric Power Systems Research*, vol. 144, pp. 63–71, 2017.

[102] J. Lavaei and S. H. Low, "Zero duality gap in optimal power flow problem," *IEEE Transactions on Power Systems*, vol. 27, no. 1, pp. 92–107, 2011.

[103] B. Stott, J. Jardim, and O. Alsaç, "Dc power flow revisited," *IEEE Transactions on Power Systems*, vol. 24, no. 3, pp. 1290–1300, 2009.

[104] Z. Yang, H. Zhong, Q. Xia, A. Bose, and C. Kang, "Optimal power flow based on successive linear approximation of power flow equations," *IET Generation, Transmission & Distribution*, vol. 10, no. 14, pp. 3654–3662, 2016.

[105] S. Xia, Z. Ding, M. Shahidehpour, K. W. Chan, S. Bu, and G. Li, "Transient stability-constrained optimal power flow calculation with extremely unstable conditions using energy sensitivity method," *IEEE Transactions on Power Systems*, vol. 36, no. 1, pp. 355–365, 2020.

[106] Q. Jiang and Z. Huang, "An enhanced numerical discretization method for transient stability constrained optimal power flow," *IEEE Transactions on Power Systems*, vol. 25, no. 4, pp. 1790–1797, 2010.

[107] N. Zhang, C. Kang, Q. Xia, Y. Ding, Y. Huang, R. Sun, J. Huang, and J. Bai, "A convex model of risk-based unit commitment for day-ahead market clearing considering wind power uncertainty," *IEEE Transactions on Power Systems*, vol. 30, no. 3, pp. 1582–1592, 2014.

[108] J. M. Morales, A. J. Conejo, and J. Pérez-Ruiz, "Economic valuation of reserves in power systems with high penetration of wind power," *IEEE Transactions on Power Systems*, vol. 24, no. 2, pp. 900–910, 2009.

[109] J. Yan, B. Hu, K. Xie, J. Tang, and H.-M. Tai, "Data-driven transmission defense planning against extreme weather events," *IEEE Transactions on Smart Grid*, vol. 11, no. 3, pp. 2257–2270, 2019.

[110] P. Panciatici, Y. Hassaine, S. Fliscounakis, L. Platbrood, M. Ortega-Vazquez, J. Martinez-Ramos, and L. Wehenkel, "Security management under uncertainty: From day-ahead planning to intraday operation," in *2010 IREP Symposium Bulk Power System Dynamics and Control-VIII (IREP)*, pp. 1–8, IEEE, 2010.

[111] S. Karagiannopoulos, L. Roald, P. Aristidou, and G. Hug, "Operational planning of active distribution grids under uncertainty," in *IREP 2017, X Bulk Power Systems Dynamics and Control Symposium*, 2017.

[112] E. DallAnese, K. Baker, and T. Summers, "Chance-constrained ac optimal power flow for distribution systems with renewables," *IEEE Transactions on Power Systems*, vol. 32, no. 5, pp. 3427–3438, 2017.

[113] J. Schmidli, L. Roald, S. Chatzivasileiadis, and G. Andersson, "Stochastic ac optimal power flow with approximate chance-constraints," in *2016 IEEE Power and Energy Society General Meeting (PESGM)*, pp. 1–5, IEEE, 2016.

[114] D. Pozo and J. Contreras, "A chance-constrained unit commitment with an nk security criterion and significant wind generation," *IEEE Transactions on Power systems*, vol. 28, no. 3, pp. 2842–2851, 2012.

[115] B. Venkatesh, P. Yu, H. Gooi, and D. Choling, "Fuzzy milp unit commitment incorporating wind generators," *IEEE transactions on power systems*, vol. 23, no. 4, pp. 1738–1746, 2008.

[116] N. Zhang, C. Kang, Q. Xia, Y. Ding, Y. Huang, R. Sun, J. Huang, and J. Bai, "A convex model of risk-based unit commitment for day-ahead market clearing considering wind power uncertainty," *IEEE Transactions on Power Systems*, vol. 30, no. 3, pp. 1582–1592, 2015.

[117] R. S. Sutton and A. G. Barto, *Reinforcement learning: An introduction.* MIT press, 2018.

[118] A. O'Connell, J. Taylor, J. Smith, and L. Rogers, "Distributed energy resources takes center stage: A renewed spotlight on the distribution planning process," *IEEE Power and Energy Magazine*, vol. 16, no. 6, pp. 42–51, 2018.

[119] G. Strbac, D. Pudjianto, M. Aunedi, D. Papadaskalopoulos, P. Djapic, Y. Ye, R. Moreira, H. Karimi, and Y. Fan, "Cost-effective decarbonization in a decentralized market: The benefits of using flexible technologies and resources," *IEEE Power and Energy Magazine*, vol. 17, no. 2, pp. 25–36, 2019.

[120] A. R. Sayed, C. Wang, and T. Bi, "Resilient operational strategies for power systems considering the interactions with natural gas systems," *Applied Energy*, vol. 241, pp. 548–566, 2019.

[121] A. O. Rousis, P. Boonsiri, and G. Strbac, "Utilization of an urban ac microgrid for improving voltages across a distribution system," in *2019 International Conference on Smart Energy Systems and Technologies (SEST)*, pp. 1–6, IEEE, 2019.

[122] A. Hirsch, Y. Parag, and J. Guerrero, "Microgrids: A review of technologies, key drivers, and outstanding issues," *Renewable and sustainable Energy reviews*, vol. 90, pp. 402–411, 2018.

[123] D. Kumar, F. Zare, and A. Ghosh, "Dc microgrid technology: System architectures, ac grid interfaces, grounding schemes, power quality, communication networks, applications, and standardizations aspects," *IEEE Access*, vol. 5, pp. 12230–12256, 2017.

[124] P. Wang, L. Goel, X. Liu, and F. H. Choo, "Harmonizing ac and dc: A hybrid ac/dc future grid solution," *IEEE Power and Energy Magazine*, vol. 11, no. 3, pp. 76–83, 2013.

[125] Y. Wang, A. O. Rousis, and G. Strbac, "On microgrids and resilience: A comprehensive review on modeling and operational strategies," *Renewable and Sustainable Energy Reviews*, vol. 134, p. 110313, 2020.

[126] M. S. Mahmoud, M. S. U. Rahman, and M.-S. Fouad, "Review of microgrid architectures–a system of systems perspective," *IET Renewable Power Generation*, vol. 9, no. 8, pp. 1064–1078, 2015.

[127] Z. Wang, B. Chen, J. Wang, M. M. Begovic, and C. Chen, "Coordinated energy management of networked microgrids in distribution systems," *IEEE Transactions on Smart Grid*, vol. 6, no. 1, pp. 45–53, 2014.

[128] M. Hosseinzadeh and F. R. Salmasi, "Power management of an isolated hybrid ac/dc microgrid with fuzzy control of battery banks," *IET Renewable Power Generation*, vol. 9, no. 5, pp. 484–493, 2015.

[129] A. O. Rousis, I. Konstantelos, and G. Strbac, "A planning model for a hybrid ac–dc microgrid using a novel ga/ac opf algorithm," *IEEE Transactions on Power Systems*, vol. 35, no. 1, pp. 227–237, 2019.

[130] A. Eajal, M. A. Abdelwahed, E. El-Saadany, and K. Ponnambalam, "A unified approach to the power flow analysis of ac/dc hybrid microgrids," *IEEE Transactions on Sustainable Energy*, vol. 7, no. 3, pp. 1145–1158, 2016.

[131] Y. Wang, A. O. Rousis, and G. Strbac, "Resilience-driven modeling, operation and assessment for a hybrid ac/dc microgrid," *IEEE Access*, vol. 8, pp. 139756–139770, 2020.

[132] J. Wang and X. Lu, "Sustainable and resilient distribution systems with networked microgrids," *Proceedings of the IEEE*, vol. 108, no. 2, pp. 238–241, 2020.

[133] S. E. Ahmadi, N. Rezaei, and H. Khayyam, "Energy management system of networked microgrids through optimal reliability-oriented day-ahead self-healing scheduling," *Sustainable Energy, Grids and Networks*, p. 100387, 2020.

[134] P. L. Querini, O. Chiotti, and E. Fernádez, "Cooperative energy management system for networked microgrids," *Sustainable Energy, Grids and Networks*, vol. 23, p. 100371, 2020.

[135] M. M. Arsoon and S. M. Moghaddas-Tafreshi, "Peer-to-peer energy bartering for the resilience response enhancement of networked microgrids," *Applied Energy*, vol. 261, p. 114413, 2020.

[136] N. Bazmohammadi, A. Tahsiri, A. Anvari-Moghaddam, and J. M. Guerrero, "A hierarchical energy management strategy for interconnected microgrids considering uncertainty," *International Journal of Electrical Power & Energy Systems*, vol. 109, pp. 597–608, 2019.

[137] S. E. Ahmadi and N. Rezaei, "A new isolated renewable based multi microgrid optimal energy management system considering uncertainty and demand response," *International Journal of Electrical Power & Energy Systems*, vol. 118, p. 105760, 2020.

[138] J. Najafi, A. Peiravi, A. Anvari-Moghaddam, and J. M. Guerrero, "An efficient interactive framework for improving resilience of power-water distribution systems with multiple privately-owned microgrids," *International Journal of Electrical Power & Energy Systems*, vol. 116, p. 105550, 2020.

[139] T. Ding, Z. Wang, W. Jia, B. Chen, C. Chen, and M. Shahidehpour, "Multiperiod distribution system restoration with routing repair crews, mobile electric vehicles, and soft-open-point networked microgrids," *IEEE Transactions on Smart Grid*, vol. 11, no. 6, pp. 4795–4808, 2020.

[140] J. Kronqvist, D. E. Bernal, A. Lundell, and I. E. Grossmann, "A review and comparison of solvers for convex minlp," *Optimization and Engineering*, vol. 20, no. 2, pp. 397–455, 2019.

[141] M. Sun, F. Teng, X. Zhang, G. Strbac, and D. Pudjianto, "Data-driven representative day selection for investment decisions: A cost-oriented approach," *IEEE Transactions on Power Systems*, vol. 34, no. 4, pp. 2925–2936, 2019.

[142] S. C. Johnson, "Hierarchical clustering schemes," *Psychometrika*, vol. 32, no. 3, pp. 241–254, 1967.

[143] K.-F. Liu, J. Liang, and Y.-B. Yang, "Variance reduction and cluster decomposition," *Physical Review D*, vol. 97, no. 3, p. 034507, 2018.

[144] X. Zhang, G. Strbac, N. Shah, F. Teng, and D. Pudjianto, "Whole-system assessment of the benefits of integrated electricity and heat system," *IEEE Transactions on Smart Grid*, vol. 10, no. 1, pp. 1132–1145, 2018.

[145] Y. Liu, J. Li, and L. Wu, "Coordinated optimal network reconfiguration and voltage regulator/der control for unbalanced distribution systems," *IEEE Transactions on Smart Grid*, vol. 10, no. 3, pp. 2912–2922, 2018.

[146] J. Li, Y. Ye, D. Papadaskalopoulos, and G. Strbac, "Consensus-based coordination of time-shiftable flexible demand," in *2019 International Conference on Smart Energy Systems and Technologies (SEST)*, pp. 1–6, IEEE, 2019.

[147] Z. Yang, H. Zhong, A. Bose, T. Zheng, Q. Xia, and C. Kang, "A linearized opf model with reactive power and voltage magnitude: A pathway to improve the mw-only dc opf," *IEEE Transactions on Power Systems*, vol. 33, no. 2, pp. 1734–1745, 2017.

[148] A. Wächter and L. T. Biegler, "On the implementation of an interior-point filter line-search algorithm for large-scale nonlinear programming," *Mathematical programming*, vol. 106, no. 1, pp. 25–57, 2006.

[149] X. Cao, J. Wang, and B. Zeng, "Networked microgrids planning through chance constrained stochastic conic programming," *IEEE Transactions on Smart Grid*, vol. 10, no. 6, pp. 6619–6628, 2019.

[150] Z. Liu, Y. Yi, J. Yang, W. Tang, Y. Zhang, X. Xie, and T. Ji, "Optimal planning and operation of dispatchable active power resources for islanded multi-microgrids under decentralised collaborative dispatch framework," *IET Generation, Transmission & Distribution*, vol. 14, no. 3, pp. 408–422, 2019.

[151] H. Wang and J. Huang, "Cooperative planning of renewable generations for interconnected microgrids," *IEEE Transactions on Smart Grid*, vol. 7, no. 5, pp. 2486–2496, 2016.

[152] F. S. Gazijahani and J. Salehi, "Stochastic multi-objective framework for optimal dynamic planning of interconnected microgrids," *IET Renewable Power Generation*, vol. 11, no. 14, pp. 1749–1759, 2017.

[153] X. Cao, J. Wang, J. Wang, and B. Zeng, "A risk-averse conic model for networked microgrids planning with reconfiguration and reorganizations," *IEEE Transactions on Smart Grid*, vol. 11, no. 1, pp. 696–709, 2019.

[154] K. Lai, M. Illindala, and K. Subramaniam, "A tri-level optimization model to mitigate coordinated attacks on electric power systems in a cyber-physical environment," *Applied energy*, vol. 235, pp. 204–218, 2019.

[155] I. Konstantelos, S. Giannelos, and G. Strbac, "Strategic valuation of smart grid technology options in distribution networks," *IEEE Transactions on Power Systems*, vol. 32, no. 2, pp. 1293–1303, 2016.

[156] T. M. Masaud and E. F. El-Saadany, "Correlating optimal size, cycle life estimation, and technology selection of batteries: A two-stage approach for microgrid applications," *IEEE Transactions on Sustainable Energy*, vol. 11, no. 3, pp. 1257–1267, 2020.

[157] K. Poncelet, H. Höschle, E. Delarue, A. Virag, and W. Dhaeseleer, "Selecting representative days for capturing the implications of integrating intermittent renewables in generation expansion planning problems," *IEEE Transactions on Power Systems*, vol. 32, no. 3, pp. 1936–1948, 2016.

[158] S. S. Moghaddasi and N. Faraji, "A hybrid algorithm based on particle filter and genetic algorithm for target tracking," *Expert Systems with Applications*, p. 113188, 2020.

[159] M. Srinivas and L. M. Patnaik, "Adaptive probabilities of crossover and mutation in genetic algorithms," *IEEE Transactions on Systems, Man, and Cybernetics*, vol. 24, no. 4, pp. 656–667, 1994.

[160] K. Deb, A. Pratap, S. Agarwal, and T. Meyarivan, "A fast and elitist multiobjective genetic algorithm: Nsga-ii," *IEEE transactions on evolutionary computation*, vol. 6, no. 2, pp. 182–197, 2002.

[161] T. Alharbi, K. Bhattacharya, and M. Kazerani, "Planning and operation of isolated microgrids based on repurposed electric vehicle batteries," *IEEE Transactions on Industrial Informatics*, vol. 15, no. 7, pp. 4319–4331, 2019.

[162] C. Dong, Q. Gao, Q. Xiao, R. Chu, and H. Jia, "Spectrum-domain stability assessment and intrinsic oscillation for aggregated mobile energy storage in grid frequency regulation," *Applied Energy*, vol. 276, p. 115434, 2020.

[163] D. Wang, J. Qiu, L. Reedman, K. Meng, and L. L. Lai, "Two-stage energy management for networked microgrids with high renewable penetration," *Applied Energy*, vol. 226, pp. 39–48, 2018.

[164] D. Thomas, G. D'Hoop, O. Deblecker, K. N. Genikomsakis, and C. S. Ioakimidis, "An integrated tool for optimal energy scheduling and power quality improvement of a microgrid under multiple demand response schemes," *Appl. Energy*, vol. 260, p. 114314, 2020.

[165] Y. Zhou, M. Panteli, R. Moreno, and P. Mancarella, "System-level assessment of reliability and resilience provision from microgrids," *Applied Energy*, vol. 230, pp. 374–392, 2018.

[166] S. Tsianikas, N. Yousefi, J. Zhou, M. D. Rodgers, and D. Coit, "A storage expansion planning framework using reinforcement learning and simulation-based optimization," *Applied Energy*, vol. 290, p. 116778, 2021.

[167] G. Han, Y. Kwon, J. B. Kim, S. Lee, J. Bae, E. Cho, B. J. Lee, S. Cho, and J. Park, "Development of a high-energy-density portable/mobile hydrogen energy storage system incorporating an electrolyzer, a metal hydride and a fuel cell," *Applied Energy*, vol. 259, p. 114175, 2020.

[168] S. Yao, P. Wang, X. Liu, H. Zhang, and T. Zhao, "Rolling optimization of mobile energy storage fleets for resilient service restoration," *IEEE Transactions on Smart Grid*, vol. 11, no. 2, pp. 1030–1043, 2020.

[169] X. Lu, Z. Liu, L. Ma, L. Wang, K. Zhou, and N. Feng, "A robust optimization approach for optimal load dispatch of community energy hub," *Applied Energy*, vol. 259, p. 114195, 2020.

[170] X. Wu and A. J. Conejo, "An efficient tri-level optimization model for electric grid defense planning," *IEEE Transactions on Power Systems*, vol. 32, no. 4, pp. 2984–2994, 2017.

[171] B. Zeng and L. Zhao, "Solving two-stage robust optimization problems using a column-and-constraint generation method," *Operations Research Letters*, vol. 41, no. 5, pp. 457–461, 2013.

[172] L. Yin and Z. Sun, "Multi-layer distributed multi-objective consensus algorithm for multi-objective economic dispatch of large-scale multi-area interconnected power systems," *Applied Energy*, vol. 300, p. 117391, 2021.

[173] W. Gan, M. Yan, W. Yao, and J. Wen, "Peer to peer transactive energy for multiple energy hub with the penetration of high-level renewable energy," *Applied Energy*, vol. 295, p. 117027, 2021.

[174] T. Ding, Z. Wang, W. Jia, B. Chen, C. Chen, and M. Shahidehpour, "Multiperiod distribution system restoration with routing repair crews, mobile electric vehicles, and soft-open-point networked microgrids," *IEEE Transactions on Smart Grid*, vol. 11, no. 6, pp. 4795–4808, 2020.

[175] S. Xie, Z. Hu, J. Wang, and Y. Chen, "The optimal planning of smart multi-energy systems incorporating transportation, natural gas and active distribution networks," *Applied Energy*, vol. 269, p. 115006, 2020.

[176] Z. Yang, P. Dehghanian, and M. Nazemi, "Seismic-resilient electric power distribution systems: Harnessing the mobility of power sources," *IEEE Transactions on Industry Applications*, vol. 56, no. 3, pp. 2304–2313, 2020.

[177] S. Yao, J. Gu, H. Zhang, P. Wang, X. Liu, and T. Zhao, "Resilient load restoration in microgrids considering mobile energy storage fleets: A deep reinforcement learning approach," in *2020 IEEE Power Energy Society General Meeting (PESGM)*, pp. 1–5, 2020.

[178] Z. chen Zhou, Z. Wu, and T. Jin, "Deep reinforcement learning framework for resilience enhancement of distribution systems under extreme weather events," *International Journal of Electrical Power & Energy Systems*, vol. 128, p. 106676, 2021.

[179] J. R. Vázquez-Canteli and Z. Nagy, "Reinforcement learning for demand response: A review of algorithms and modeling techniques," *Applied Energy*, vol. 235, pp. 1072–1089, 2019.

[180] Y. Shang, W. Wu, J. Guo, Z. Ma, W. Sheng, Z. Lv, and C. Fu, "Stochastic dispatch of energy storage in microgrids: An augmented reinforcement learning approach," *Applied Energy*, vol. 261, p. 114423, 2020.

[181] V.-H. Bui, A. Hussain, and H.-M. Kim, "Q-learning-based operation strategy for community battery energy storage system (cbess) in microgrid system," *Energies*, vol. 12, no. 9, p. 1789, 2019.

[182] X. Xu, Y. Jia, Y. Xu, Z. Xu, S. Chai, and C. S. Lai, "A multi-agent reinforcement learning-based data-driven method for home energy management," *IEEE transactions on Smart Grid*, vol. 11, no. 4, pp. 3201–3211, 2020.

[183] X. Fang, J. Wang, G. Song, Y. Han, Q. Zhao, and Z. Cao, "Multi-agent reinforcement learning approach for residential microgrid energy scheduling," *Energies*, vol. 13, no. 1, p. 123, 2020.

[184] P. Kofinas, A. Dounis, and G. Vouros, "Fuzzy q-learning for multi-agent decentralized energy management in microgrids," *Applied Energy*, vol. 219, pp. 53–67, 2018.

[185] A. Y. Sun, "Optimal carbon storage reservoir management through deep reinforcement learning," *Applied Energy*, vol. 278, p. 115660, 2020.

[186] J. Wu, H. He, J. Peng, Y. Li, and Z. Li, "Continuous reinforcement learning of energy management with deep q network for a power split hybrid electric bus," *Applied Energy*, vol. 222, pp. 799–811, 2018.

[187] F. Tuchnitz, N. Ebell, J. Schlund, and M. Pruckner, "Development and evaluation of a smart charging strategy for an electric vehicle fleet based on reinforcement learning," *Applied Energy*, vol. 285, p. 116382, 2021.

[188] H. Van Hasselt, A. Guez, and D. Silver, "Deep reinforcement learning with double q-learning," in *Proceedings of the AAAI conference on artificial intelligence*, vol. 30, 2016.

[189] V.-H. Bui, A. Hussain, and H.-M. Kim, "Double deep q-learning-based distributed operation of battery energy storage system considering uncertainties," *IEEE Transactions on Smart Grid*, vol. 11, no. 1, pp. 457–469, 2019.

[190] J. Cao, D. Harrold, Z. Fan, T. Morstyn, D. Healey, and K. Li, "Deep reinforcement learning-based energy storage arbitrage with accurate lithium-ion battery degradation model," *IEEE Transactions on Smart Grid*, vol. 11, no. 5, pp. 4513–4521, 2020.

[191] J. Yang, M. Yang, M. Wang, P. Du, and Y. Yu, "A deep reinforcement learning method for managing wind farm uncertainties through energy storage system control and external reserve

purchasing," *International Journal of Electrical Power & Energy Systems*, vol. 119, p. 105928, 2020.

[192] J.-G. Kim and B. Lee, "Automatic p2p energy trading model based on reinforcement learning using long short-term delayed reward," *Energies*, vol. 13, no. 20, p. 5359, 2020.

[193] X. Fang, Q. Zhao, J. Wang, Y. Han, and Y. Li, "Multi-agent deep reinforcement learning for distributed energy management and strategy optimization of microgrid market," *Sustainable Cities and Society*, vol. 74, p. 103163, 2021.

[194] E. Mocanu, D. C. Mocanu, P. H. Nguyen, A. Liotta, M. E. Webber, M. Gibescu, and J. G. Slootweg, "On-line building energy optimization using deep reinforcement learning," *IEEE Transactions on Smart Grid*, vol. 10, no. 4, pp. 3698–3708, Jul. 2019.

[195] N. Tsang, C. Cao, S. Wu, Z. Yan, A. Yousefi, A. Fred-Ojala, and I. Sidhu, "Autonomous household energy management using deep reinforcement learning," in *Proc. 25th IEEE Int Conf Eng Technol Innov (ICE/ITMC)*, pp. 1–7, IEEE, 2019.

[196] T. P. Lillicrap, J. J. Hunt, A. Pritzel, N. Heess, T. Erez, Y. Tassa, D. Silver, and D. Wierstra, "Continuous control with deep reinforcement learning," in *Proc. 4th Int. Conf. Learn. Represent. (ICLR)*, (San Juan, Puerto Rico), pp. 1–14, May. 2016.

[197] F. S. Gorostiza and F. M. Gonzalez-Longatt, "Deep reinforcement learning-based controller for soc management of multi-electrical energy storage system," *IEEE Transactions on Smart Grid*, vol. 11, no. 6, pp. 5039–5050, 2020.

[198] L. Yu, W. Xie, D. Xie, Y. Zou, D. Zhang, Z. Sun, L. Zhang, Y. Zhang, and T. Jiang, "Deep reinforcement learning for smart home energy management," *IEEE Internet Things J*, vol. 7, no. 4, pp. 2751–2762, 2019.

[199] R. Lu, Y.-C. Li, Y. Li, J. Jiang, and Y. Ding, "Multi-agent deep reinforcement learning based demand response for discrete manufacturing systems energy management," *Applied Energy*, vol. 276, p. 115473, 2020.

[200] D. Qiu, J. Wang, J. Wang, and G. Strbac, "Multi-agent reinforcement learning for automated peer-to-peer energy trading in double-side auction market," in *Proceedings of the Thirtieth International Joint Conference on Artificial Intelligence, IJCAI*, pp. 2913–2920, 2021.

[201] D. Qiu, Y. Ye, D. Papadaskalopoulos, and G. Strbac, "Scalable coordinated management of peer-to-peer energy trading: A multi-cluster deep reinforcement learning approach," *Applied Energy*, vol. 292, p. 116940, 2021.

[202] N. Chen, M. Li, M. Wang, J. Ma, and X. Shen, "Compensation of charging station overload via on-road mobile energy storage scheduling," in *2019 IEEE Global Communications Conference (GLOBECOM)*, pp. 1–6, IEEE, 2019.

[203] M. Yan, M. Shahidehpour, A. Alabdulwahab, A. Abusorrah, N. Gurung, H. Zheng, O. Ogunnubi, A. Vukojevic, and E. A. Paaso, "Blockchain for transacting energy and carbon allowance in networked microgrids," *IEEE Transactions on Smart Grid*, vol. 12, no. 6, pp. 4702–4714, 2021.

[204] M. Yan, M. Shahidehpour, A. Paaso, L. Zhang, A. Alabdulwahab, and A. Abusorrah, "Distribution system resilience in ice storms by optimal routing of mobile devices on congested roads," *IEEE Transactions on Smart Grid*, vol. 12, no. 2, pp. 1314–1328, 2020.

[205] W. Yuanqing, Z. Wei, and L. Lianen, "Theory and application study of the road traffic impedance function," *Journal of Highway and Transportation Research and Development*, vol. 21, no. 9, pp. 82–85, 2004.

[206] Y. Sun, Z. Chen, Z. Li, W. Tian, and M. Shahidehpour, "Ev charging schedule in coupled constrained networks of transportation and power system," *IEEE Transactions on Smart Grid*, vol. 10, no. 5, pp. 4706–4716, 2018.

[207] D. K. Smith, "Network flows: theory, algorithms, and applications," *Journal of the Operational Research Society*, vol. 45, no. 11, pp. 1340–1340, 1994.

[208] B. Zhou, Q. Song, Z. Zhao, and T. Liu, "A reinforcement learning scheme for the equilibrium of the in-vehicle route choice problem based on congestion game," *Applied Mathematics and Computation*, vol. 371, p. 124895, 2020.

[209] J. Zhao, M. Mao, X. Zhao, and J. Zou, "A hybrid of deep reinforcement learning and local search for the vehicle routing problems," *IEEE Transactions on Intelligent Transportation Systems*, vol. 22, no. 11, pp. 7208–7218, 2021.

[210] J. Li, Y. Ma, R. Gao, Z. Cao, A. Lim, W. Song, and J. Zhang, "Deep reinforcement learning for solving the heterogeneous capacitated vehicle routing problem," *IEEE Transactions on Cybernetics*, pp. 1–14, 2021.

[211] M. Abadi and *et al.*, "TensorFlow: Large-scale machine learning on heterogeneous systems," 2015. Software available from tensorflow.org.

[212] M. L. Bynum, G. A. Hackebeil, W. E. Hart, C. D. Laird, B. L. Nicholson, J. D. Siirola, J.-P. Watson, and D. L. Woodruff, *Pyomo–optimization modeling in python*, vol. 67. Springer Science & Business Media, third ed., 2021.

[213] J. Dupačová, N. Gröwe-Kuska, and W. Römisch, "Scenario reduction in stochastic programming," *Mathematical programming*, vol. 95, no. 3, pp. 493–511, 2003.

[214] F. Zhuang, Z. Qi, K. Duan, D. Xi, Y. Zhu, H. Zhu, H. Xiong, and Q. He, "A comprehensive survey on transfer learning," *Proceedings of the IEEE*, vol. 109, no. 1, pp. 43–76, 2020.

[215] Y. Xu, C.-C. Liu, Z. Wang, K. Mo, K. P. Schneider, F. K. Tuffner, and D. T. Ton, "Dgs for service restoration to critical loads in a secondary network," *IEEE Transactions on Smart Grid*, vol. 10, no. 1, pp. 435–447, 2017.

[216] Q. Sun, Z. Wu, Z. Ma, W. Gu, X.-P. Zhang, Y. Lu, and P. Liu, "Resilience enhancement strategy for multi-energy systems considering multi-stage recovery process and multi-energy coordination," *Energy*, vol. 241, p. 122834, 2022.